UCRL-ID-114972-4
CONF-9505323--

SERS Internship Spring 1995 Abstracts and Research Papers

Beverly Davis

November 1995

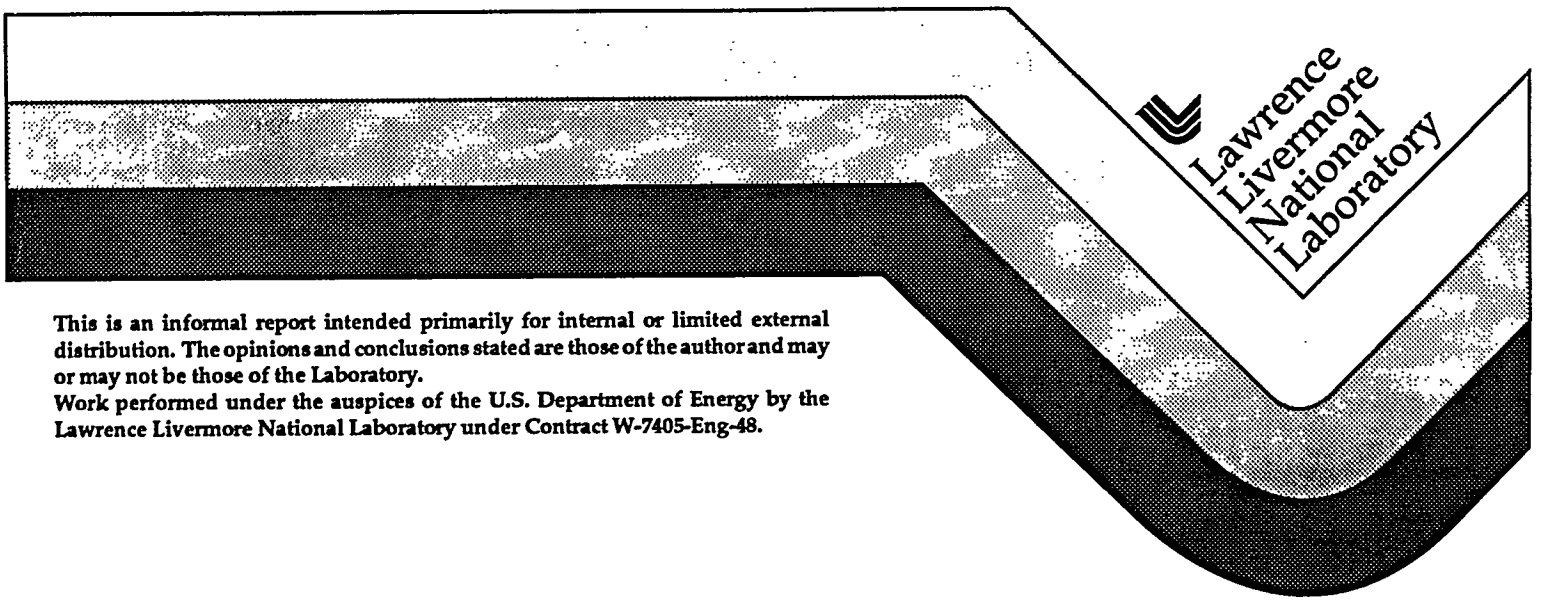

SCIENCE & ENGINEERING

SERS

RESEARCH SEMESTER

Spring 1995 Symposium Abstracts

Table of Contents

STUDENT REPORTS

SCIENCE & ENGINEERING

SERS

RESEARCH SEMESTER

Lawrence Livermore National Laboratory
Spring 1995

ABSTRACTS FOR STUDENT SYMPOSIUM

Sponsored by:

The U.S. Department of Energy
Office of Energy Research

Competitive Neighborhoods and the Use of Interference Indices to Assist in the Restoration of *Amsinckia Grandiflora*

Peter Beesley
San Francisco State University
Environmental Restoration Division

ABSTRACT

As part of the on-going efforts to reintroduce the large-flowered fiddleneck (*Amsinckia grandiflora*) into California native perennial bunch grass communities, we developed indices of competitive interference to predict the fecundity of individuals in populations of this rare annual forb. These indices, developed from aspects of the spatial distribution of neighboring competitors, are used as independent variables in linear regressions to predict plant fecundity of *A. grandiflora* individuals within a *Poa secunda* bunch grass population. This was accomplished by examining the distance to each competitor along with the number, basal area, and angular dispersion of competitors within a fixed radius about *A. grandiflora* individuals. The data was taken from individuals planted within naturally occurring bunch grass populations and within transplanted bunch grass plots controlled for density and distribution. Density, spatial pattern, and basal area all had significant effects upon *A. grandiflora* individuals within controlled plots. As number of competitors increases within the competitive neighborhood of *A. grandiflora* individuals, seed (nutlet) output declines. A similar relationship holds true for increasing competitor basal areas. Distance to competitors also influences nutlet output with fecundity falling as more competitors become closer to focal individuals. Complex interactions of the above factors were also significant with the overall trend being reduced nutlet output with increasing dispersion of competitors. Although the above regressions are highly significant ($p < 0.01$), the variation each describes is low. Density and an indice of distance to competitors were the only significant predictors ($p < 0.05$) of plant fecundity for *A. grandiflora* individuals found in naturally occurring *Poa secunda* populations. These relationships show similar trends as those found for controlled plots. Continued research and the development of further interference indices to better assess individual variation are currently being investigated in the hopes that we can better predict *A. grandiflora* fecundity in natural bunch grass communities.

Real-Time, Face Recognition Technology

Shane Brady
University of Missouri-Rolla
Computations Department

ABSTRACT

The Institute for Scientific Computing Research (ISCR) at Lawrence Livermore National Laboratory recently developed the real-time, face recognition technology KEN. KEN uses novel imaging devices such as silicon retinas developed at Caltech or off-the-shelf CCD cameras to acquire images of a face and to compare them to a database of known faces in a robust fashion. The KEN-Online project makes that recognition technology accessible through the World Wide Web (WWW), an internet service that has recently seen explosive growth. A WWW client can submit face images, add them to the database of known faces and submit other pictures that the system tries to recognize. KEN-Online serves to evaluate the recognition technology and grow a large face database. KEN-Online includes the use of public domain tools such as mSQL for its name-database and perl scripts to assist the uploading of images.

Corrosion Studies by Use of the Thermogravimetric Analyzer

Gregory M. Brinker
Michigan State University
Earth Sciences Division

ABSTRACT

A series of tests have been performed by use of the thermogravimetric analyzer. Weight gain vs. time graphs have been generated by exposing one inch by two inch by sixty five hundredths of an inch low carbon (1020) steel specimens to a range of relative humidities (65% - 90%) and temperatures (50 - 70C). Data collected from these studies will give insight to both the kinetics of oxide formation and the material's critical relative humidity. It has been observed that two separate rates and mechanisms for oxide formation exist. It is believed that dry oxidation is prevalent at low relative humidities, while aqueos electrochemical corrosion persists at high relative humidities. The relative humidity(s) and temperature(s) that oxidation formation transforms from one rate and mechanism to the other is of interest. The critical relative humidity is defined as the relative humidity at which oxide formation will become highly accelerated with respect to its normal growth rate. Hence, a better understanding of 1020 steel's oxide formation kinetics and the alloy's critical relative humidity will aid in waste package designs for use in conjunction with the proposed nuclear waste containment center at Yucca Mountain.

Finite Element Modeling of the Human Pelvis

Bethany Carlson
Clemson University
Mechanical Engineering Department

ABSTRACT

A finite element model of the human pelvis was created using a commercial wire frame image as a template. To test the final mesh, the model's mechanical behavior was analyzed through finite element analysis and the results were displayed graphically as stress concentrations. In the future, this grid of the pelvis will be integrated with a full leg model and used in side-impact car collision simulations.

Purification of Mammalian DNA Repair Protein XRCC1

Ingrid Chen
University of California, Berkeley
Biology and Biotechnology Research Program

ABSTRACT

Malfunctioning DNA repair systems lead to cancer mutations, and cell death. XRCC1 (X-ray Repair Cross Complementing) is a human DNA repair gene that has been found to fully correct the *x-ray* repair defect in Chinese hamster ovary (CHO) cell mutant EM9. The corresponding protein (XRCC1) encoded by this gene has been linked to a DNA repair pathway known as base excision repair, and affects the activity of DNA ligase III (Caldecott et al. 1992). Previously, an XRCC1 cDNA minigene (consisting of the uninterrupted coding sequence for XRCC1 protein followed by a decahistidine tag) was constructed and cloned into vector pET-16b for the purpose of: 1) overproduction of XRCC1 in both prokaryotic and eukaryotic cells; and, 2) to facilitate rapid purification of XRCC1 from these systems (Caldecott et al. 1994). A vector is basically a DNA carrier that allows recombinant protein to be cloned and overexpressed in host cells. In this study, XRCC1 protein was overexpressed in E. *coli* and purified by immobilized metal affinity chromatography. Currently, the XRCC1 minigene is being inserted into a new vector [pET-26b(+)] in hopes to increase overexpression and improve purification. Once purified XRCC1 can be crystallized for structural studies, or studied in vitro for its biological function.

Study of Chemical and Radiation Induced Carcinogenesis

Albert Chmura
State University of New York
Health and Ecological Assessment Division

ABSTRACT

The study of chemical and radiation induced carcinogenesis has up to now based many of its results on the detection of genetic aberrations using the fluorescent *in situ* hybridization (FISH) technique. FISH is time consuming and this tends to hinder its use for looking at large numbers of samples. We are currently developing new technological advances which will increase the speed, clarity and functionality of the FISH technique. These advances include multi-labeled probes, amplification techniques, and separation techniques.

Production of Hydrogen from Municipal Solid Waste

Sherrell L. Coleman
Tuskegee University
Chemistry & Material Science Division

ABSTRACT

The Gasification of Municipal Solid Waste (MSW) includes gasification and the process for producing a gasificable slurry from raw MSW by using high pressures of steam. A potential energy source, MSW is a composite of organic materials such as: paper, wood, food waste, etc. There are different paper grades producing different results with low-quality paper forming better slurries than high-quality papers; making MSW a difficult feedstock for gasification. The objective of the bench-scale laboratory work has been to establish operating conditions for a hydrothermal pre-processing scheme for municipal solid waste (MSW) that produces a good slurry product that can be pumped and atomized to the gasifier for the production of hydrogen. Batch reactors are used to determine product yields as a function of hydrothermal treatment conditions. Various ratios of water-to-paper were used to find out solid product, gas product, and soluble product yields of MSW. Experimental conditions covered were temperature, time, and water to feed ratio. Temperature had the strongest effect on product yields.

Total On-Line Purchasing System (TOPS)

Nicholas Collins
Louisiana State University
Information Management Division

ABSTRACT

The Information Management Division (IMD) at LLNL is developing a new purchasing system for the Procurement Department. The first major development of this new system is called, "Total On-Line Purchasing System" (TOPS). TOPS will help speed up the requisitioning process by having requisitions electronically entered by requesters and electronically sent to buyers to be put on Purchase Orders. The new purchasing system will use Electronic Commerce (EC)/Electronic Data Interchange (EDI), to help increase transaction flows for shipping notices, RFQs, Quotes, Purchase Orders, and Invoices. ANSI X.12 is the EDI standard that this new EC will use.

Micropower Impulse Radar Imaging

Michael S. Hall
New Jersey Institute of Technology
Lasers

ABSTRACT

From designs developed at the Lawrence Livermore National Laboratory (LLNL) in radar and imaging technologies, there exists the potential for a variety of applications in both public and private sectors. Presently tests are being conducted for the detection of buried mines and the analysis of civil structures. These new systems use a patented ultra-wide band (impulse) radar technology known as Micropower Impulse Radar (GPR) imaging systems. LLNL has also developed signal processing software capable of producing 2-D and 3-D images of objects embedded in materials such as soil, wood and concrete. My assignment while at LLNL has focused on the testing of different radar configurations and applications, as well as assisting in the creation of computer algorithms which enable the radar to scan target areas of different geometeries.

Automobile Accessories: Assessment and Improvement

Marvin Jackson
University of Nevada Las Vegas
Electrical Engineering Department

ABSTRACT

With mandates and regulatory policies to meet both the California Air Resources Board (CARB) and the Partnership for a New Generation of Vehicles (PNGV), designing vehicles of the future will become a difficult task. As we look into the use of electric and hybrid vehicles, reduction of the required power demand by influential automobile components is necessary in order to obtain performance and range goals. Among those automobile components are accessories. Accessories have a profound impact on the range and mileage of future vehicles with limited amounts of energy or without power generating capabilities such as conventional vehicles. Careful assessment of major power consuming accessories helps us focus on those that need improvement and contributes to attainment of mileage and range goals for electric and hybrid vehicles.

Designing an Effective Gateway for Documentation Search Through a WWW Server

Vinh Nguyen
George Mason University
Computer Science Department

ABSTRACT

Lookup, a NERSC's utility, searches several documentation databases to find exact as well as approximate matches for the user's search term. However, it is only available for those who run it directly on NERSC's machines. To provide a wider access to a large audience, I developed a gateway which handles information requests and returns the appropriated documents.

Finite Element Analysis of Thumb Carpometacarpal Joint Implants

Cheri Nielsen
Johns Hopkins University
Medical Department

ABSTRACTS

The thumb carpometacarpal joint is frequently replaced in women who have developed severe osteoarthritis of the hand. A new, privately developed implant design consists of two components, trapezial and metacarpal, each with a saddle-shaped articulating surface. A three dimensional finite element model of this implant has been developed to analyze stresses on the device. The first simulations using the model involve loading the implant with forces normal to the trapezial component. Preliminary results show contact stress distributions at the articulating surfaces of the implant.

Software Interface and Data Acquisition Package for the LakeShore Cryogenics Vibrating Sample Magnetometer

Benjamin H. O'Dell
Guilbord College
Chemistry & Material Science Division

ABSTRACT

A software package was developed to replace the software provided by LakeShore for their model 7300 vibrating sample magnetometer (VSM). Several problems with the original software's functionality caused this group to seek a new software package. The new software utilizes many features that were unsupported in the LakeShore software, including a more functional step mode, point averaging mode, vector moment measurements, and calibration for field offset. The developed software interfaces the VSM through a menu driven graphical user interface, and bypasses the VSM's on board processor leaving control of the VSM up to the software. The source code for this software is readily available to any one. By having the source, the experimentalist has full control of data acquisition and can add routines specific to their experiment. The source code can be obtained by e-mailing odell8@llnl.gov.

Shooting Stars: Our Guide to the Early Solar System's Formation

Jennifer O'Reilly
Kean College of New Jersey
Chemistry & Material Science Division

ABSTRACT

Plagioclase grains were studied from the Allende meteorite, sample 916, to determine a chronology of events that occurred within the first ten million years of the solar system's formation. Radiometric dating of the ^{26}-Al--^{26}Mg* system was accomplished on the ion microprobe mass spectromer. The excess ^{26}-Mg* in core plagioclase grains of calcium-aluminum rich inclusions (CAIs) provided a time of original condensation for ^{26}-Al of ~4.55 million years ago, a hundred million years prior to the formation of the planets. This data has been found to correlate with other excess ^{26}-Mg* samples. Measurements of plagioclase in the CAI's periphery dated 1.52 million years later, suggesting an interesting history of collision and melting.

Groundwater Contaminant by Hexavalent Chromium

Christopher Parsons
University of Texas, Austin
Environmental Protection Department

ABSTRACT

Oxidation of trivalent chromium to hexavalent chromium has been investigated as a function of total manganese in soils as well as various incubation conditions. Chromium and manganese contents were analyzed by atomic absorption (graphite furnace and flame emission respectively) following acid digestion. Total hexavalent chromium generation capacity was determined by addition of 0.001 M CrCL3, incubation, and analysis by s-diphenyl carbazide (Bartlett and James, 1979). Samples were then leached with CaSO4 and MgSO4 and incubated in various environments (oven, freeze-drier, field moist, ultrafreeze) to test for geogenic generation of Cr(IV). The degree of geogenic generation of hexavalent chromium was compared with total Mn and Cr content as well as hexavalent generational capacity.

DCSP Hardware Maintenance System

Melissa Pazmino
St. Andrews Presbyterian College
Computation Division

ABSTRACT

This paper discusses the necessary changes to be implemented on the hardware side of the DCSP database. DCSP is currently tracking hardware maintenance costs in six separate databases. The goal is to develop a system that combines all data and works off a single database. Some of the tasks that will be discussed in this paper include adding the capability for report generation, creating a help package and preparing a users guide, testing the executable file, and populating the new database with data taken from the old database. A brief description of the basic process used in developing the system will also be discussed. Conclusions about the future of the database and the delivery of the final product are then addressed, based on research and the desired use of the system.

Post-Rehabilitation Evaluation of the Sanitary Sewer System at Lawrence Livermore National Laboratory

Delano Royal
Clark Atlanta University
Biology and Biotechnology Research Program

ABSTRACT

We are updating a CH2M Hill study which found that the sanitary sewer system is sufficient to transport peak dry weather flow. However, under peak wet weather conditions, the system has insufficient capacity to transport the projected flows for existing and future development. This is due to the amount of infiltration/inflow (I/I) that enters the sewer system when it rains.

Our goal is to examine the existing system to determine its adequacy to accommodate present and future peak flows, and also to further update and improve the CH2M Hill study. A set of alternatives was also developed to address deficiencies of the existing system.

The Numerical Modelling of a Driven Nonlinear Oscillator

Cindy Shew
Murray State University
Earth Sciences Division

ABSTRACT

The torsional oscillator in the Earth Sciences Division was developed at Lawrence Livermore National Laboratory and is the only one of its kind. It was developed to study the way rocks damp vibrations. Small rock samples are tested to determine the seismic properties of rocks, but unlike other traditional methods that propagate high frequency waves through small samples, this machine forces the sample to vibrate at low frequencies, which better models real-life properties of large masses. In this particular case, the rock sample is tested with a small crack in its middle. This forces the rock to twist against itself, causing a "stick-slip" friction, known as stiction. A numerical model that simulates the forced torsional osillations of the machine is currently being developed.

The computer simulation implements the graphical language LabVIEW, and is looking at the nonlinear spring effects, the frictional forces, and the changes in amplitude and frequency of the forced vibration. Using LabVIEW allows for quick prototyping and greatly reduces the "time to product" factor. LabVIEW's graphical environment allows scientists and engineers to use familiar terminology and icons (e.g. knobs, switches, graphs, etc.). Unlike other programming systems that use *text-based* languages, such as C and Basic, LabVIEW uses a *graphical* programming language to create programs in block diagram form.

Computing Environment for the ASSIST Data Warehouse at Lawrence Livermore National Laboratory

Kevin Shuk
Milwaukee School of Enginering
Administrative Information Systems Division

ABSTRACT

The current computing environment for the ASSIST data warehouse at Lawrence Livermore National Laboratory is that of a central server that is accessed by a terminal or terminal emulator. The initiative to move to a client/server environment is strong, backed by desktop machines becoming more and more powerful. The desktop machines can now take on parts of tasks once run entirely on the central server, making the whole environment computationally more efficient as a result.

Services are tasks that are repeated throughout the environment such that it makes sense to share them; tasks such as email, user authentication and file transfer are services. The new client/;server environment needs to determine which services must be included in the environment for basic functionality. These services then unify the computing environment, not only for the forthcoming ASSIST+, but for Administrative Information Systems as a whole, joining various server platforms with heterogeneous desktop computing platforms.

Photosynthetic Acclimation to Enriched CO_2 Concentrations in *Pinus Ponderosa*

Matthew P. Torres
California State University at Humbolt
Environmental Science Department

ABSTRACT

By the middle of the 21st century earth's ambient CO_2 level is expected to increase two-fold (~350 umol/L). Higher levels of CO_2 are expected to cause major changes in the morphological, physiological, and biochemical traits of the world's vegetation. Therefore, we constructed an experiment designed to measure the long-term acclimation processes of *Pinus Ponderosa*. As a prominent forest conifer, *Pinus Ponderosa* is useful when assessing a large scale global carbon budget.

Eighteen genetically variable families were exposed to 3 different levels of CO_2 (350 umol/L, 525 umol/L, 700 umol/L), for three years (April 1992 to April 1995). Acclimation responses were quantified by assays of photosynthetic rate, chlorophyll fluorescence, and chllorophyll pigment concentrations.

A Heterogeneous Chemistry Model for Acid Rain's Effect on Ozone

Tao Ye
University of New York, Stonybrook
Physics Department

ABSTRACT

A computer model for simulating heterogeneous reactions in cloud is developed to determine the S(IV) species' effect on ozone. Crutzen claims that NOx, HOx families and H2CO in the troposphere can decrease ozone by 5 to 10%. However, is this claim valid for a SOx polluted atmosphere? The SOx family reacts with the ozone destroyers. These reactions seem to be significant enough to reduce the H2CO's destructive effect on ozone.

STUDENT REPORTS

The use of non-destructive indices of competitive interference to assist in the restoration of *Amsinckia grandiflora.*

Peter Beesley
San Francisco State University
Environmental Restoration Division

Abstract

As part of the on-going efforts to reintroduce the large-flowered fiddleneck (*Amsinckia grandiflora*) into California native perennial bunch grass communities, we developed non-destructive indices of competitive interference to predict the fecundity of individuals in populations of this rare annual forb. These indices, developed from aspects of the spatial distribution of neighboring competitors, are used as independent variables in linear regressions to predict plant fecundity of *A. grandiflora* individuals within a *Poa secunda* bunch grass population. This was accomplished by examining the distance to each competitor along with the number, basal area, and angular dispersion of competitors within a fixed radius about *A. grandiflora* individuals. The data was taken from individuals planted within naturally occurring bunch grass populations and within transplanted bunch grass plots controlled for density and distribution. Density, spatial pattern, and basal area all had significant effects upon *A. grandiflora* individuals within controlled plots. As number of competitors increases within the competitive neighborhood of *A. grandiflora*, individuals, seed (nutlet) output declines. A similar relationship holds true for increasing competitor basal areas. Distance to competitors also influences nutlet output with fecundity falling as more competitors become closer to focal individuals. Complex interactions of the above factors were also significant with the overall trend being reduced nutlet output with increasing dispersion of competitors. Although the above regressions are highly significant ($p < 0.01$), the variation each describes is low. Density and an index of distance to competitors were the only significant predictors ($p < 0.05$) of plant fecundity for *A. grandiflora* individuals found in naturally occurring *Poa secunda* populations. These relationships show similar trends as those found for controlled plots. Continued research and the development of further interference indices to better assess individual variation are currently being investigated in the hopes that we can better predict *A. grandiflora* fecundity in natural bunch grass communities.

Introduction

Amsinckia grandiflora is considered one of the most endangered plants in California (Pavlik, 1990). We are currently investigating whether a native perennial bunch grass community can provide the spatial and/or temporal niche for this annual forb (Carlsen, 1993). The restoration effort has focused on understanding both the reproductive ecology of *A. grandiflora* as well as competitive effects on *A. grandiflora* within California grassland communities. The aim of the project is "to develop techniques for the restoration of a perennial bunch grass and large-flowered fiddleneck community" (Carlsen, 1993). Integral to these efforts is the ability to accurately predict fecundity of *A. grandiflora* within various bunch grass densities, and from this to evaluate bunch grass communities to determine the potential success of reintroduction efforts. Previous results show a clear

relationship between *A. grandiflora* nutlet (seed) production and the number of branches of individual plants (nutlet# = 16.808branch # -36.764; R^2=0.92; Carlsen, 1994). However, accurate predictors of individual branch number have yet to be developed. Earlier results do show a relationship between total branch number and total bunch grass biomass on a per plot basis, but this trend does not describe individual response. In order to improve these methods and to better examine individual response, we have modified our analysis to examine more closely the spatial distribution of competitors within a fixed radius around focal *A. grandiflora* individuals. These new techniques should better describe individual response within a competitive neighborhood, and, if so, may be utilized in a non-destructive manner to assess potential reintroduction sites for *A. grandiflora*.

Several studies investigating the effects of competitive interference based on the density and spatial distribution of competitors on focal individuals have been conducted (see Silander and Pacala 1985, Mack and Harper 1977, and Fowler 1984), but none have been developed to be eventually used in restoration efforts of rare plants. Along with this, many of these studies use methods that alter site vegetation by harvesting plant biomass (see Fowler 1984 and Mack and Harper 1977) which may in turn effect individual growth and thus influence community dynamics. This net result could affect restoration efforts for a *A. grandiflora*-perennial bunch grass community by enhancing growth of bunch grass competitors (Edwards 1994) and altering community dynamics. The methods described here are meant to minimize site impact during surveys of potential reintroduction sites.

Methods

In October of 1992, competition plots were designed on a west facing slope at Site 300 in San Joaquin county, California. The design consisted of 15 pre-existing (PE) or naturally occurring bunch grass plots and 15 planted (PP) bunch grass plots. PE plots were subjectively chosen for high, medium, and low density of *Poa secunda* populations within a 0.64 m^2 area. PP plots of the same area were planted with 45, 22, and 11 evenly distributed *Poa secunda* plants (approximately 2 inches of shoot and 2 inches of root) representing high, medium, and low density plots. These various densities for both PE and PP had 5 replicates each with the PP plots being randomly distributed in rows along the hillside.

A. grandiflora nutlets were placed in petri dishes on moistened filter paper on November 27, 1993 and left in the dark at about 21 C until germination occurred. Once cotyledons emerged, the germinules were transplanted into 17 cm stuewe tubes and placed in the greenhouse at Lawrence Livermore National Laboratory. Approximately 10 days later these seedlings were removed from the tubes and precision sewn, 4 to a plot, in a 30 cm by 30 cm square centered at each site. A final count of branch number was taken for each plant upon senescence.

After senescence of *A. grandiflora* individuals, mylar tracings were used to map competitor basal area and distribution within each plot. Using these tracings, data was collected on the number of *Poa secunda* that lie within a 25 cm radius of each *A. grandiflora* individual. These grasses are considered within the competitive neighborhood of a focal plant and data was then collected on their distance from this plant along with their angular dispersion (figure 1.0). Subsequent analysis following the methods of Silander and Pacala (1985) was used to determine whether branch number can be accurately predicted from this data. This involved the calculation of interference indices (Table 1) which were then used as independent variables in a linear regression to predict *A. grandiflora* fecundity.

Results

Density, spatial pattern, and basal area all had highly significant effects ($p < 0.01$) upon *A. grandiflora* fecundity within controlled (PP) plots while density and an index of distance to competitors were the only significant predictors ($p < 0.05$) in PE plots.

The average number of competitors for each individual within PP plots was six while the average for PE plots was three. As the number of *Poa secunda* grasses within the competitive neighborhood of focal individuals increases, fecundity decreases in both PP (figure 1.1) and PE (figure 1.2) plots. Fecundity also decreases with increasing size or basal area of bunch grass competitors in PP plots (figure 2).

The effect of distance to competitors was also important in influencing plant fecundity for both PP and PE plots. As competitor distance from target individuals decreases, interference increases and fecundity declines. For PP plots (figure 3.1), the weighted crowding coefficient equals two indicating "overdispersed neighbors are weighted more in relation to clumped neighbors (Silander and Pacala 1985)." For PE plots (figure 3.2), there is no weighting for clumped or dispersed neighbors.

Complex interactions of competitor density, dispersion, and distance also influenced individual *A. grandiflora* fecundity in PP plots. Using these parameters, about 34% of the variation seen in individual branch number can be described (figure 4). The overall trend was decreased fecundity with increasing neighborhood effects.

Although all the regressions described above are significant at or below the $p = 0.05$ level, the variance each describes is low.

Discussion

Clearly the influence of competitor density, spatial pattern, and size are all important factors in influencing *A. grandiflora* success within a perennial bunch grass community. These factors account for approximately 30% of the variation seen in plant fecundity in PP plots, but only about 8% of the

variation in PE plots indicating important differences that need to be considered.

Although I am not positive as to why we were not able to better predict plant response in the naturally occurring bunch grass plots, two important factors may have contributed to these differences. These include differences in the overall density of competitors in PE plots versus PP plots and differences between the general distribution patterns seen in PE plots compared to PP plots.

When considering the effects of density, one must examine how the experimental design may have influenced other factors, besides competitive ability, that can contribute to an individuals success. In particular, the influence of abiotic factors may be very different for PP and PE treatments when considering that individuals in the controlled plots had on average twice as many competitors as did the individuals in the naturally occurring plots. Goldberg (1987) suggests that higher densities should reduce variation in abiotic factors over the density gradient of a single neighbor species. By reducing this variation, one may enhance the importance of individualistic response under these conditions and increase the predictability of the indices in PP pots.

Along these same lines, predictability in PE plots could have been reduced since the "natural density gradient could indicate variation in some underlying abiotic factor, which in turn could directly affect target plant growth (Goldberg 1987)." A possible result is that the influence of abiotic factors may be of differential importance in the two cases. Further study into micro-environmental variation would be needed to support this hypothesis.

Another important contributing factor that may have influenced the differences between the fecundity predictions in PP and PE plots, is the differences in the general distribution patterns of each.

PP plots were controlled for density and distribution resulting in a quite dispersed population of competitors in all cases. In the naturally occurring plots, there was considerably more clumping of *Poa secunda* competitors. Some studies have suggested that a focal individuals response may actually be enhanced by some individuals within a competitive neighborhood (see Fowler 1984). This response is due to the fact that a focal plant's neighborhood may "incorporate individuals that actually have a positive effect on the focal plant by depressing growth of other closer neighbors (Fowler 1987)." This is not only important when determining the appropriate neighborhood radius to use, but it would also be important when considering clumped individuals in PE plots. It is quite likely that competitive interference on target individuals may be less when there is a greater degree of clumping in a neighborhood compared to sites with more dispersed competitors. These clumped individuals would tend to depress the growth of one another and may thus be less influential than the more dispersed neighbors in PP plots. The result could be less variation attributable to competition and greater variation in fecundity in response to other factors. A closer examination of the effects of individuals with clumped distribution

patterns may suggest that they be considered as a whole rather than as discreet individuals.

Since the variation described for both PP and PE plots was lower than expected, and because the influence of some neighbors on focal individuals may actually be positive, further investigations are needed. One current way being explored, is the use of other interference indices that rely on the same data set. Another suggested option is to examine more closely the size of the neighborhood radius used. Due to the constraint of the plot size, we can only decrease the current radius used. This would suggest a smaller zone of neighbor influence. The results could possibly give better fits to the above regressions, but if not, the process would still be valuable and give insight into the breadth of competitor influence.

Acknowledgements

I would like to thank my mentor Tina Carlsen for developing such an exciting project and for her assistance in interpreting the results. I would also like to thank Erin Espeland for her assistance in gathering all of the data and for her guidance throughout this project and semester.

Table 1 Calculated interference indices used as independent variables in a linear regression to predict individual plant fecundity. ϕ = the weighted crowding coefficient. When $\phi = 1$ there is no weighting between clumped or dispersed individuals. When $\phi = 2$ dispersed neighbors are weighted more than clumped neighbors.

Index of competitive interference		Description
(1)	$W_1^{\phi} = \Sigma(N) \times (1\text{-}d/25\ cm)^{\phi}$	An index based on competitor distance.
(2)	$W_4^{\phi} = \Sigma(\text{total competitors d}) \times (1\text{-}[\sqrt{(\Sigma \sin a)^2 \times (\cos a)^2}]/N)^{\phi}$	An index based on competitor distance, dispersion, and density

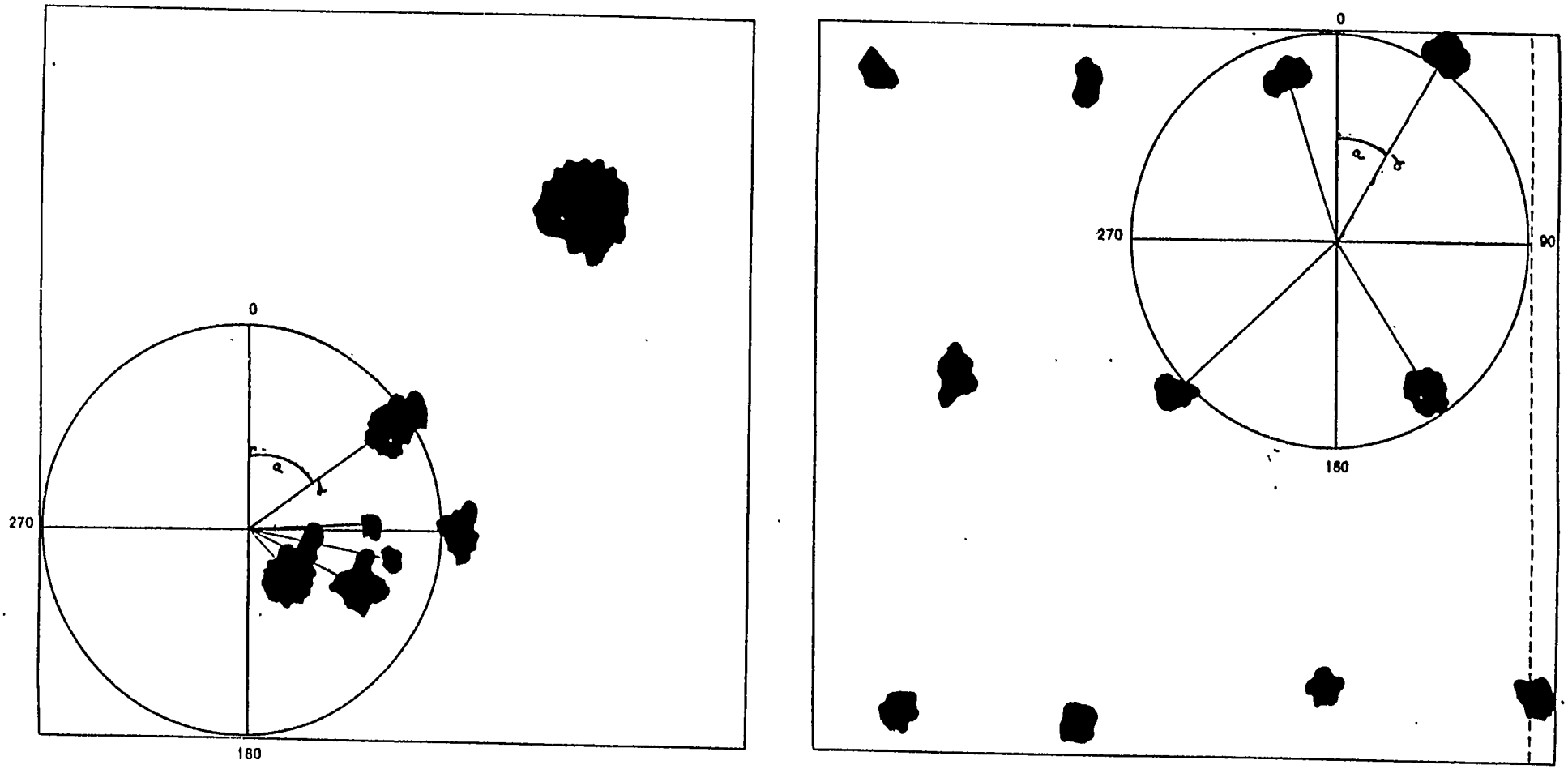

Figure 1.0 The competitive neighborhoods of two *A. grandiflora* individuals in a PE plot (left) and a PP plot (right). Each plot shows the competitive neighborhood of one focal individual. Data was collected on the number (N) of *Poa secunda* competitors, the distance (d) to each, their angular dispersion (a), and their area (A).

Figure 1.1 Neighborhood interference within PP plots showing competitor influence on Amsinckia grandiflora branch number. Fecundity decreases with an increase in number of competitors ($p < 0.01$).

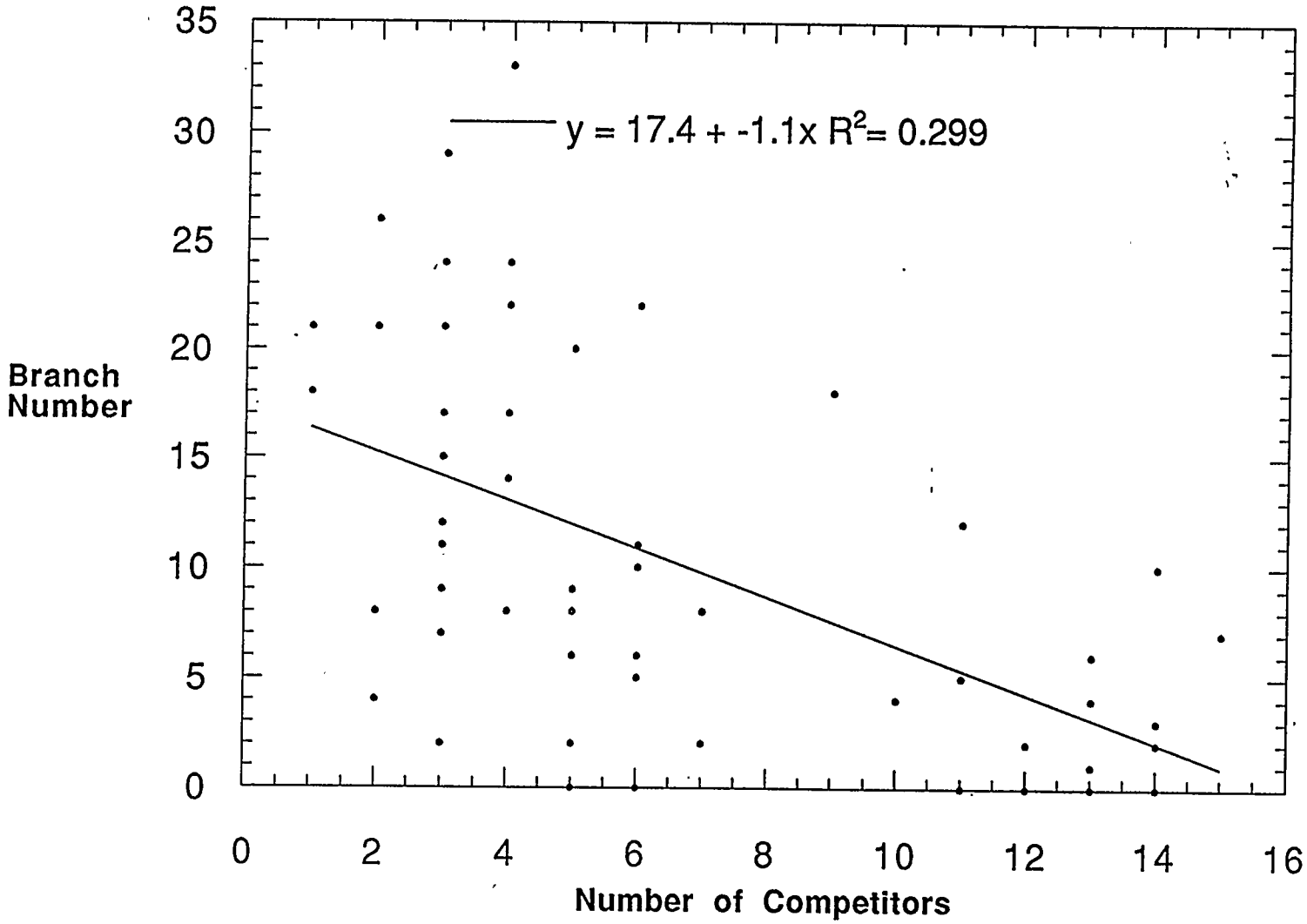

Figure 1.2 Neighborhood interference within PE plots showing competitor influence on A. grandiflora branch number. Fecundity decreases with an increase in number of competitors (p = 0.039).

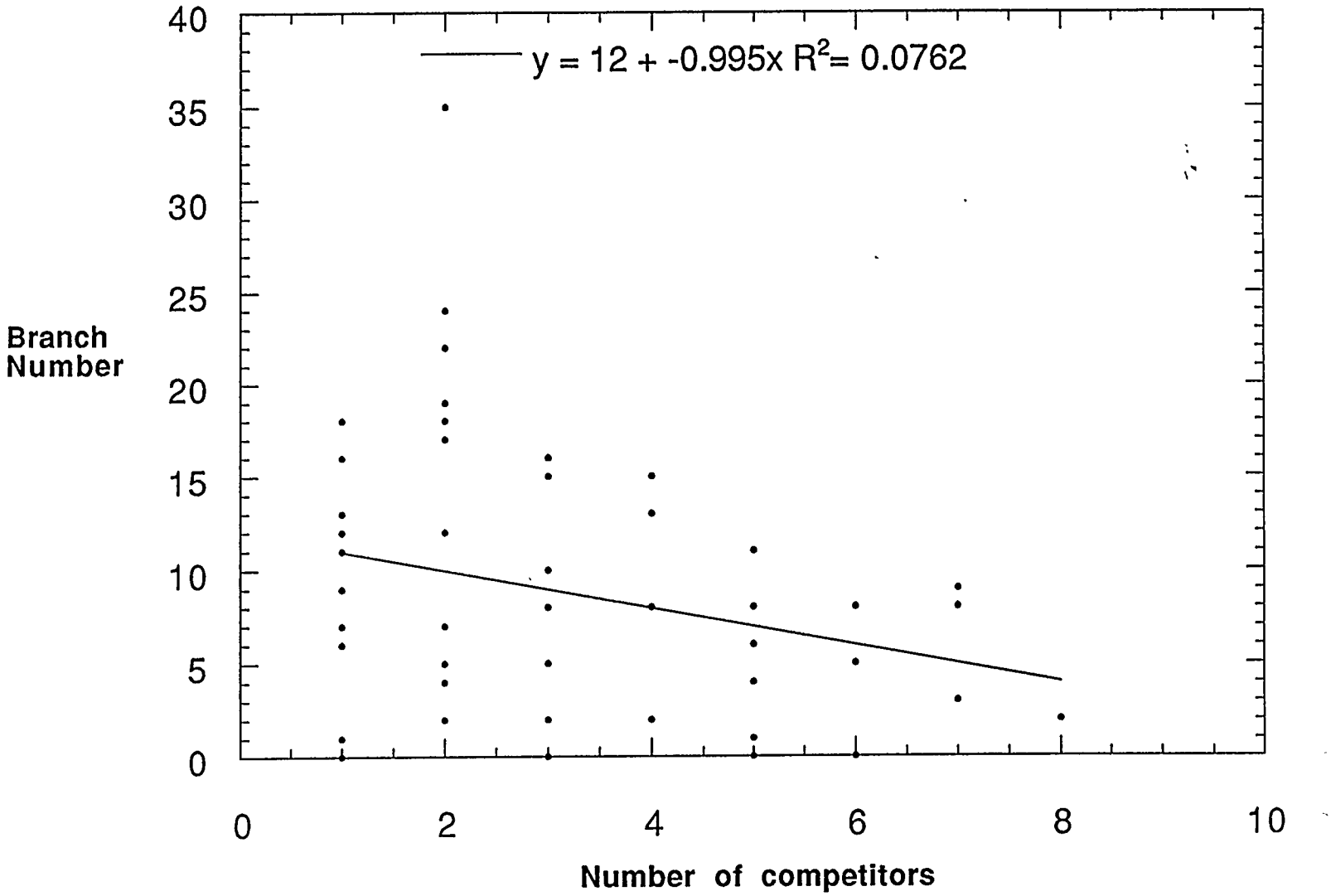

Figure 2 Neighborhood interference within PP plots: influence of competitor size on Amsinckia grandiflora branch number. As total competitor area increases in an individuals neighborhood, fecundity decreases ($p < 0.01$).

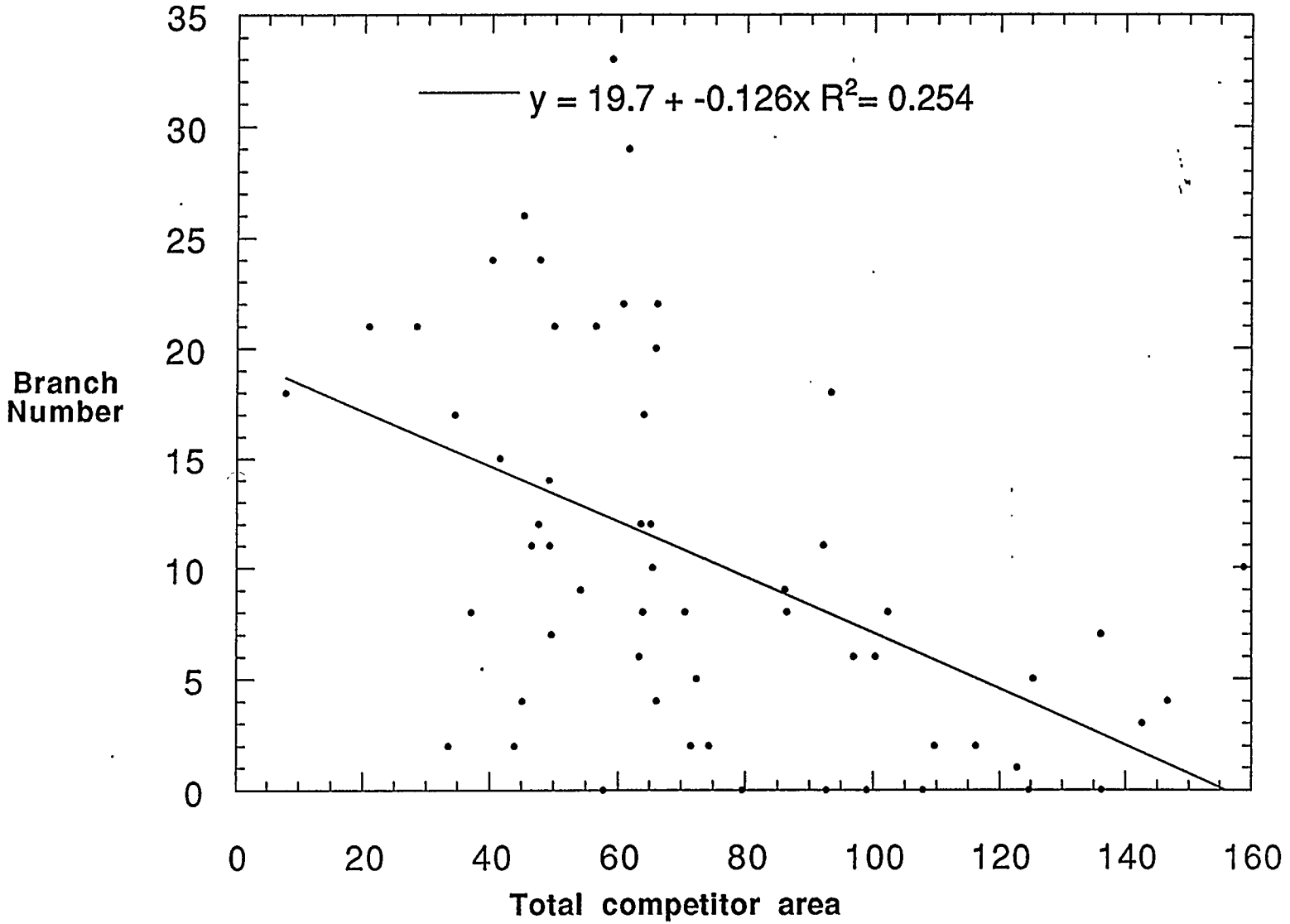

Figure 3.1 Neighborhood interference within PP plots showing influence of competitor proximity on A. grandiflora branch number. As competitor distance from target individuals decreases, fecundity declines ($p < 0.01$).

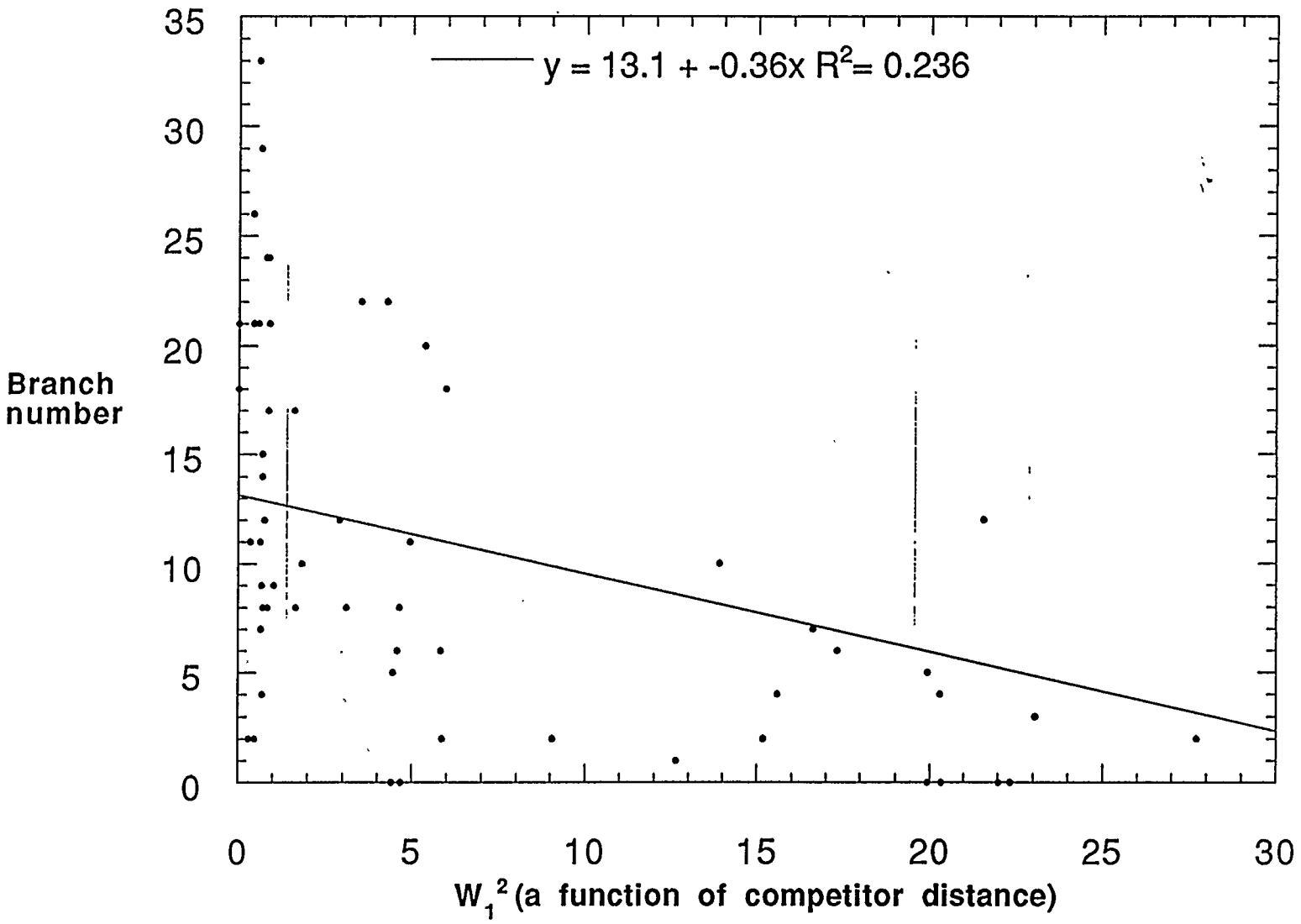

Figure 3.2 Neighborhood interference within PE plots showing influence of competitor proximity on A. grandiflora branch number. As competitor distance from target individuals decreases, fecundity decreases (p = 0.027).

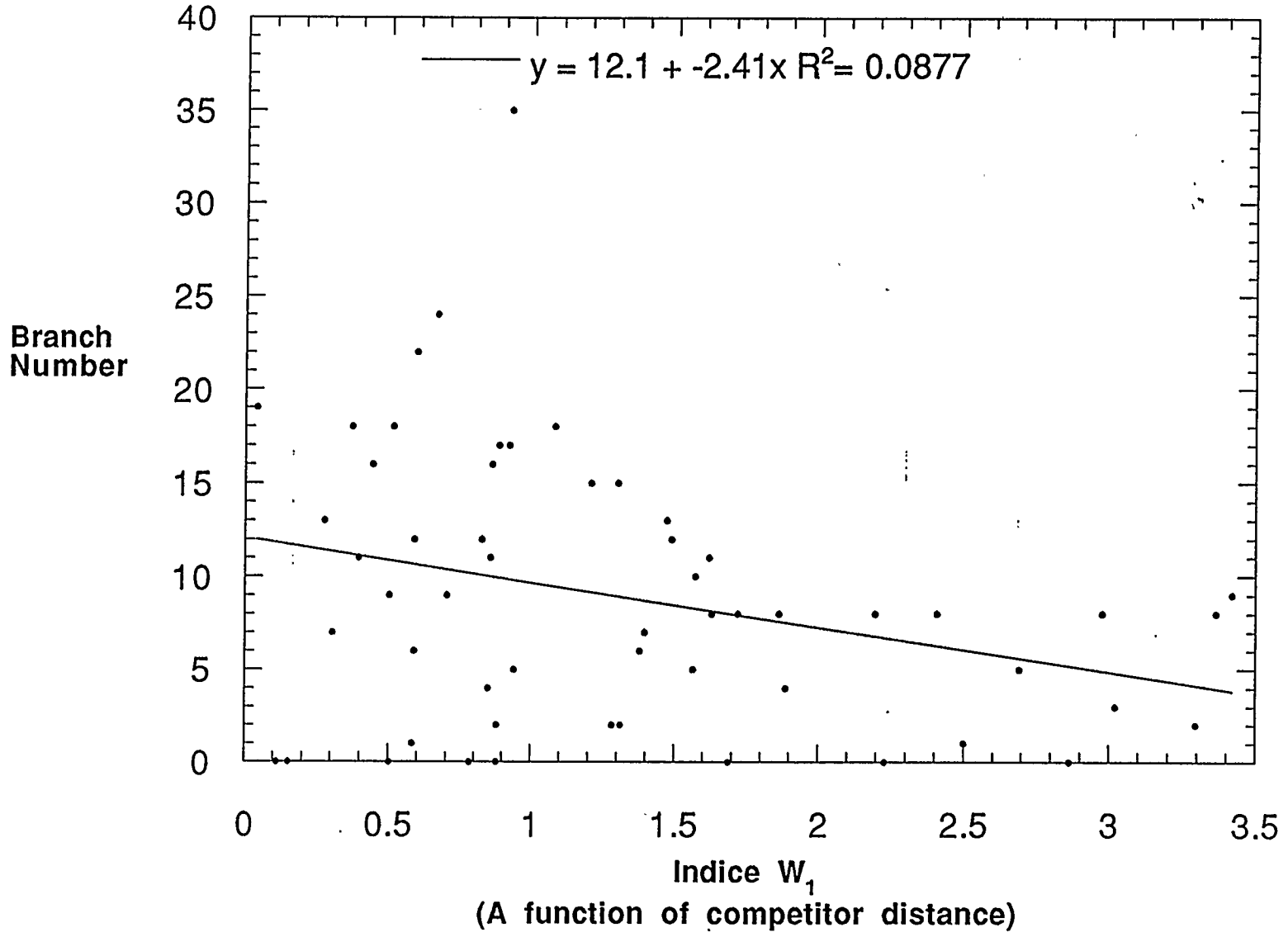

Figure 4 Neighborhood interference within PP plots showing influence of competitor distance (D), number (N), and dispersion on A. grandiflora branch number. As competitor dispersion increases, fecundity declines ($p<0.01$).

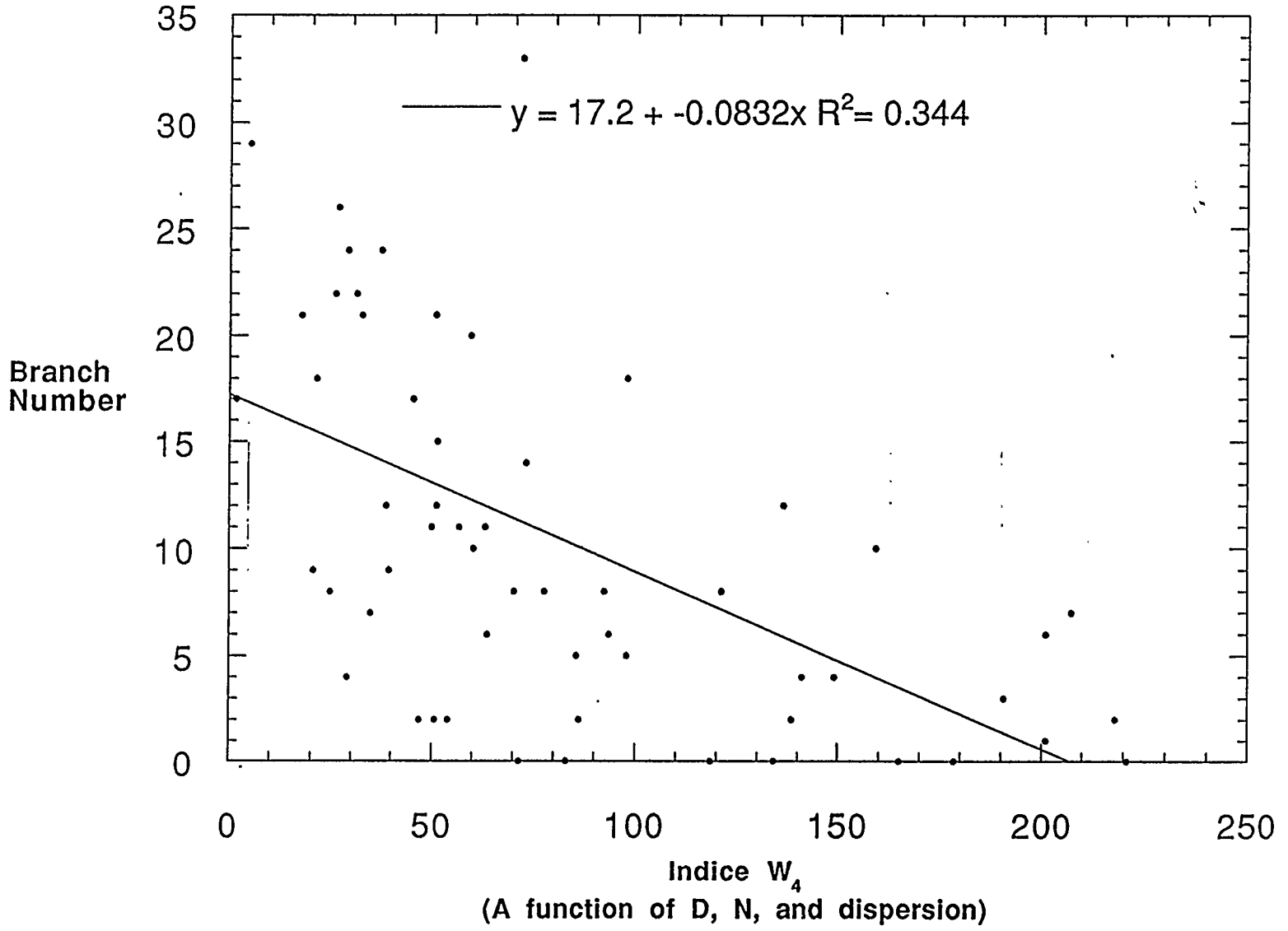

References

Carlsen, T.M. 1993. Scientific Summary. Habitat and Environmental Restoration: A proposal to investigate techniques to restore California native perennial grasses and the endangered *Amsinckia grandiflora*. Proposal 93-LW-101.

Carlsen, T.M. 1994. Scientific Summary. Habitat and Environmental Restoration: A proposal to investigate techniques to restore California native perennial grasses and the endangered *Amsinckia grandiflora*. Proposal 93-LW-101.

Edwards, S.W. 1994. Creating an Authentic California Meadow. *Four Seasons* 9(4):5-16.

Fowler, N.L. 1984. The role of germination date, spatial arrangement, and neighbourhood effects in competitive interactions in *Linum*. *Journal of Ecology*. 72:307-318.

Goldberg, D.E. 1987. Neighborhood competition in an old-field plant community. *Ecology*. 68(5):1211-1223.

Mack, R.N., Harper, J.L. 1977. Interference in dune annuals: Spatial pattern and neighbourhood effects. *Journal of Ecology*. 65:345-363.

Pavlik, B.M. 1990. *Reintroduction of Amsinckia grandiflora to Stewartville*. California Department of Fish and Game.

Silander, J.A., Pacala, S.W. 1985. Neighborhood predictors of plant performance. *Oecologia*. 66:256-263.

KEN-Online *

Shane Brady
University of Missouri-Rolla

Martin Lades
Lawrence Livermore National Laboratory

May 12, 1995

Abstract

The Institute for Scientific Computing Research (ISCR) at Lawrence Livermore National Laboratory (LLNL) recently developed the real-time, face recognition technology KEN. KEN uses novel imaging devices such as silicon retinas developed at Caltech or off-the-shelf CCD cameras to acquire images of a face and to compare them to a database of known faces in a robust fashion. The KEN-Online project makes that recognition technology accessible through the World Wide Web (WWW), an Internet service that has recently seen explosive growth. A WWW client can submit face images, add them to the database of known faces and submit other pictures that the system tries to recognize. KEN-Online serves to evaluate the recognition technology and grow a large face database. KEN-Online includes the use of public domain tools such as mSQL for its name-database and perl scripts to assist the uploading of images.

1 Introduction

Face recognition recently developed into a research field of its own merits. Many vision laboratories started to conduct research into possible strate-

*http://www-iscr.llnl.gov/KEN/KEN-Online/start.html

gies for mug shot recognition. KEN is a near real-time technology that was recently implemented at the Institute for Scientific Computing Research (ISCR) at the Lawrence Livermore National Laboratory (LLNL). The KEN-Online system brings this technology to the WWW for the benefit of its Cyber-denizens. KEN-Online allows a Web-User to upload an image of a face and either insert it in a database or match it against a database of people known to the system. Many computer users now have cameras on their systems and are able to provide image material right from their desktops. Images are uploaded under the understanding that they may be used for scientific evaluation and in publications.

The KEN-Online system serves two functions: first, it provides a service on the network for associative storage of faces (mugshots, store a face and see if you can find the person later); second, it helps us in the continuous improvement of the face recognition software by providing a growing set of test data. The test data consist of the growing collection of face images, statistics on recognition performance, and the feedback of many users testing the system. Please send us mail about what you think (hml@llnl.gov).

KEN-Online consists of several components: the mini Structured Query Language (mSQL, a database system implementing a subset of SQL); the World Wide Web (WWW) and the Hypertext Markup Language (HTML, soon version 3 for easier submission of images from net clients); the image conversion utilities ImageMagick and Portable Bitmap (PBM); the face recognition software written in C++ available as libraries for licensing; and perl version 5.0 to interface the components.

This paper contains three modules describing the function of each major software component of KEN-Online and modules describing the use of perl to develop an integrated system, the conclusions of the work, and possible improvements.

2 The KEN Face Recognition Software

The KEN recognition software performs the face-matching in the KEN-Online system. The KEN software uses three steps to recognize faces: first, it builds a face graph of a submitted face; then, it compares this graph model to previously submitted images; finally, it classifies the faces according to statistics collected in the comparison stage.

Figure 1: A face graph before and after elastic distortion.

First the software builds a model of the face. This model is based on the location of features in the face. To identify these features, the software performs a convolution on the image with Fourier transforms. The Fourier transform of the image is multiplied by a shifted Gaussian function. The inverse Fourier transform of this product results in a spatially filtered image. This process is repeated for several magnitudes and orientations of the shift vector for the Gaussian filter functions. A vector is formed through the resultant images with coefficients representing the intensities of points in the image. This identifies edges which indicate facial features. These features are represented by nodes that identify both a feature and its location. These nodes are linked together in a graph which is used for the recognition process.[1]

First, the new graph is compared to graphs of images previously modeled by the system. The new graph is positioned over an existing graph and is normalized in size and orientation with the other graph. Then, the graph is elastically distorted to match as many feature nodes as possible. This is done by constructing vectors from nodes in one image to matching nodes in the other. The vector lengths are contrast dependent and are discarded to make the system robust against differing lighting conditions. The vector directions measure the relative position distortion of the matching nodes.[1]

Each image is then statistically classified in similarity to the new submis-

sion. The system computes the angle between the vectors connecting nodes and vectors normal to the graph. Cost values are assigned to the positional distortions. The cost values for each image is compared with the others to determine which images are most similar to the submission.[1]

Interfacing with KEN's recognition software requires the image to be a square eight-bit greyscale image with a power of two pixels on a side. The recognition software stores all match criteria and file locations in a parameter file which is specified from the command line. Upon completion, the software returns a list of lines, ordered from best match to worst match, numerically describing each comparison. The perl script analyzes the first six listings and uses the returned statistics to identify the images to identify as matches.

3 The World Wide Web

The World Wide Web matches the two requirements for the KEN Online interface: it is widely available, and it is easy to use. To use the World Wide Web in my project, I needed to work the two software components used in the Web: the web-viewer and the web-server. Using these two components for the its interface, KEN-Online meets the interface requirements.

The web-viewer, or web-browser, displays the web-page that the user sees when using the World Wide Web. The viewers, such as Mosaic and Netscape, interpret tags in a file for how to display the contents. These tags are described by the hyper-text mark-up language (HTML) definition. With KEN-Online, all interaction with the user is through web-viewer.

The web-server is responsible for passing information to and from viewers. For the KEN-Online system, the information received from the viewer is processed and the results are printed on a new web-page. The web-server provides this processing capability by allowing certain files to be executed instead of being displayed in a viewer.

The HTML 2.0 specification defines input form capability through tags that direct the viewer to display input fields that users can fill in. Input fields are grouped together into an HTML form. The input in a form is passed to the specified executable when the submit button, which is defined by a tag, is pressed by the user.[2]

When an executable is invoked by the server, it receives all the information in the form as an encoded string. The server provides two methods of

passing this information. If the data passing method is specified as HTML GET, all the input from the form is passed to the program through the command line; with HTML POST, the form input is passed to the program by using the standard input stream. Anything written to the standard output stream is passed to the viewer.

For the viewer to display the information appropriately, it needs two pieces of information: what type of data it is receiving and the actual data. The data type is passed to the viewer in a header, which is followed by the data to be displayed. Depending on the header description of the data, the viewer displays the data, saves the data as a file, or passes it to a helper application for interpretation.

With KEN-Online, the user input is passed to the Facematch script via HTML POST. This script decodes the information and coordinates the various KEN-Online components, such as the KEN recognition software, the image decoder and converter, and the database engine, in processing the data. The results are passed to the viewer declared as type text/html and displayed as a new web-page.

The only major difficulty I encountered interfacing with the Web was with the web-server specifying paths from a different root directory than the machine on which it is running. The KEN-Online system uses directories through the web-server and through the standard Unix file system. Because the same directories have two different names under the two different systems, the KEN-Online system maintains two variables to access the same directories through the Unix system and the web-server.

4 Database Software

The database contains information about each image and the number of submissions made. Because of this, choosing the right database system was important. Of the three systems were considered, ACeDB, freeWAIS, and mSQL, I decided on mSQL for its simple interface and easy use.

The first database system I considered was ACeDB, an object-oriented system. In an object-oriented system, all data is stored in objects. Each object contains instance variables whose values describe the object. These systems use a hierarchical data model. The data is organized into classes in the hierarchy. Each class defines a data type and the operations that can be

done on its data. Descendants classes of a class are considered to be more specific definitions of the more general ancestor class. The benefit of this is that generalization of data is made possible.[3]

I considered ACeDB because it had been used in other projects and there is an extension that provided direct interaction with the World Wide Web. With the extension, however, ACeDB would not compile, and there was little documentation on the installation procedure, so I was unable to use ACeDB.

The second system I considered was freeWAIS, and indexing system. With this type of system, an index of all the words in all the files in specified directories is built. Queries to this system consist of words to look for in the index, and return the names of all the files containing these words[4]. For KEN-Online, a possible solution would be to keep all the information on an image in a file. In this system, there is no rigid record structure, which would allow the format of information stored about submitted images to be changed without changing past submission files. This solution, however, stipulates that a small file be kept for each submission, which would result in a large number of files to manage, and each matching image would require a separate file to be opened when reporting the match results.

The freeWAIS system did not function correctly either. A binary was available for the computer system I was using, so I did not have to compile it. Included was a program that built the index. When I tried to use the program, it crashed. I thought there might be incompatibilities with the binary and my system, so I downloaded the source code and compiled the indexing program. This also crashed when I tried to use it. There was little documentation describing possible problems, so I decided against using the program.

The final option was mSQL, a record based system. In this system, a table definition of the types of data to be stored in a record is made. Information fitting this definition can then be stored in the table.[3] Because these definitions must be made before data is entered, if a change in the record structure is needed, all the records must be rewritten.

The mSQL program uses the structured query language, SQL. This provides for compatibility with other database programs. mSQL compiled on the first attempt and did not crash when I used it. The distribution came with a complete manual on installation and use. The manual referred to a adaptor to perl. This adaptor, Msql.pm, required perl 5, so I installed it. Once I had installed perl 5, I had no problems accessing mSQL from perl

scripts. Although mSQL only supports characters, integers, and reals as data types and implements only a subset of SQL, this posed no problem as my design for KEN-Online did not need these features. Because mSQL proved to be the easiest database system to use, I chose to use it.

The database is responsible for maintaining a record for each submitted image. To manage all the data, KEN-Online uses two separate tables. One table contains information about the image file: the filename without an extension, the nickname of the person in it, how it was made, where it was retrieved from, and the sender. The filename is unique to an image, so it is used to identify separate images. The other table defines a counter that is incremented with each submissions, which counts the number of submissions and provides a simple way to give each new image a unique name.

Access to the database is needed for three steps: naming a new image, recording data about the image, and retrieving nicknames of matching images. For each step, a string containing a SQL query statement is built and submitted to the database engine. Any results from the query are returned through a second function call. The interface to mSQL from perl is done with Msql.pm, a perl 5 package, which translates calls in perl to calls in C on the mSQL library.

The need to manage all the data about submitted images is met by mSQL. With the Msql.pm package, the interface is made available in perl. Because mSQL uses a common query language, access to other database programs is possible with only minor modifications to the perl script.

5 The Facematch Script

The Facematch script coordinates the separate software components of KEN-Online. This modularity allows one component to be changed without requiring modification to other modules. It is written in perl[1] 5 because of perl's broad set of string-handling functions and excellent diagnostic messages.

The script includes three files—get-pict, match-pict, and print-page—which provide the functions defining how to do the work. Get-pict defines the functions that prepare the data for the matching and result printing. Match-pict interfaces with the KEN face-recognition software and retrieves

[1]Written by Larry Wall

information on matching images. Print-page defines how to print these results for the user.

When the "begin" button is pressed on the form, the Facematch script is invoked and all the information in the form is passed to it. This information is decoded and loaded into an associative array. A query is made on the database for the next filename to use for submissions. Then, either the image is fetched from the remote computer using lynx, a text-based web-browser, or is uudecoded from the data from the form. The new image is given a name unique to the images in the database.

The submitted image is converted into specific formats using the ImageMagick or Portable Bitmap conversion utilities for use with the matcher and display on the web. For the matcher, a copy of the submission is made as a 64 pixel by 64 pixel, greyscale, tiff file. For the web-browser, a 128 pixel wide, gif file is made. These copies are put in the appropriate directories and the original image is deleted. If the conversions are successful, all the submission data except the actual picture and the filename of the image are added to the mSQL database, and the submission counter is incremented to insure a unique name for the next submission.

The modified image is then passed to the KEN recognition software, which compares the new image to images in its database. It returns a list of matches, ordered from best match to worst with numerical descriptions of the similarity of each image to the submission. The Facematch script selects the best six matches and examines their numerical descriptions to determine which meet the match criteria.

To use KEN-Online, one needs only a digital image of a face, and a graphical web browser supporting HTML 2.0. The first two fields are used to obtain the image. Selecting the first option allows submission by specifying universal resource location (URL) of the image; selecting the second allows submission of an image as uuencoded text. The next field holds the nickname of the person in the image. The next set of options ask how the image was made. If it was not made using the first two methods, a CCD camera or silicon retina, the third option can be selected and a short description of the image source can be typed in. The forth field holds the e-mail address of the person submitting the image. The final set of check-boxes allows one to select whether to match the image against our database or just submit an image.

When the process is completed, the user will see the matching images

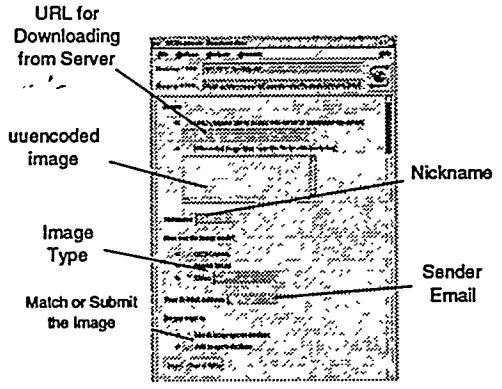

Figure 2: The KEN-Online submission form.

and their nicknames. From there, one can follow a link to a description of the KEN system.

6 Conclusion

KEN-Online gives the world access to the KEN face-recognition software by allowing users to upload an image and either insert it in a database or match it against a database. KEN is a near real-time recognition technology recently developed at the Institute for Scientific Computing Research at the Lawrence Livermore National Laboratory. It is available for licensing as C++ libraries.

KEN-Online integrates several components: the mini Structured Query Language (mSQL), the World Wide Web (WWW) and the Hypertext Markup Language (HTML), the image conversion utilities ImageMagick and Portable Bitmap, and the KEN face recognition software.

The KEN-Online system serves to both provide a service on the World Wide Web for associative face storage (mugshots, storing an image and matching it later) and aid in the continuous improvement of the face recognition software by providing it a growing data set. We encourage the use of the system and hope to receive feedback.

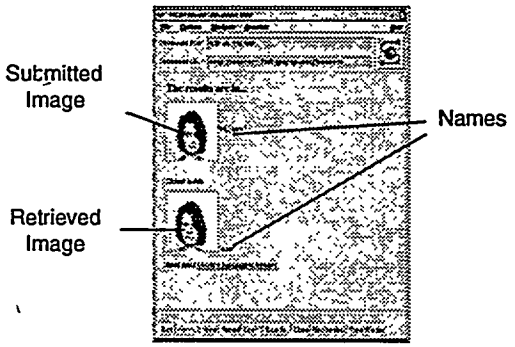

Figure 3: The results of a match.

7 Further Work

Further development of KEN-Online could be improvement of the image transfer and addition user control over the matching. The current method of using a URL or uuencoded image requires access to a web-server's directory tree or a windowing system allowing cutting and pasting on a client. Using HTML 3.0, which will support binary data transfer from a client, will allow direct image submission from both clients and servers. Currently, the matching criteria are fixed in the program and cannot be changed by a user. The system could allow configuration of the image-matching criteria for each submission to allow experimentation on what the best parameters are for accurate matching.

References

[1] Martin Lades Invariant Object Recognition with Dynamical Links, Robust to Variations in Illumination. University of Bochum, 1994.

[2] Mosaic for X version 2.0 Fill-Out Form Support. http://www.ncsa.uiuc.edu/SDG/Software/Mosaic/Docs/fill-out-forms/overview.html. NCSA 1994.

[3] Rajiv Gupta and Ellis Horowitz. Object-Oriented Databases with Applications to Case, Networks, and VLSI CAD. pp. 12-14. Prentice-Hall, 1991.

[4] Jason Ng. Installing Doc Finder—a tutorial. http://www.ncsa.uiuc.edu/SDG/docfinder/docf/docfind.tut.html NCSA 1994.

OXIDATION CHARACTERISTICS OF MILD STEEL

Gregory M. Brinker
Michigan State University
SERS Student, Spring 1995

ABSTRACT

A thermogravimetric study was performed to evaluate the interaction of water vapor with carbon steel at moderately elevated temperatures. It has been found that two separate corrosion mechanisms exist for the oxidation of low carbon steel. Dry oxidation occurs at low relative humidities, while aqueous electrochemical corrosion occurs at high relative humidities. Aqueous electrochemical corrosion enhances the oxidation rate relative to dry oxidation. This increased oxidation rate is evident by comparing the oxide layers formed on carbon steel during "dry" oxidation and aqueous electrochemical corrosion. Oxide layer thicknesses were calculated for two separate tests, one performed at 65% relative humidity and the other performed at 85% relative humidity. Both tests were run for approximately seventy hours. "Dry" oxidation formed a 0.15 micron thick oxide layer on the carbon steel, while aqueous electrochemical corrosion formed a 3.5 micron thick oxide layer on carbon steel. It was assumed that oxide layers formed uniformly over the test specimen's surface. The relative humidity(s) and temperature(s) that oxidation changes from one mechanism to the other is of interest. The relative humidity above which aqueous electrochemical corrosion begins is defined as the "critical relative humidity". This study investigated "critical relative humidity" vs. temperature in a previously uninvestigated temperature range (50°C-75°C). This work is part of Lawrence Livermore National Laboratory's Metal Barrier and Testing Task in support of the

Department of Energy's Yucca Mountain Site Characterization Project (YMP).

INTRODUCTION AND BACKGROUND

High-level nuclear waste (HLW) will be comprised of spent light water reactor fuel assemblies and Military high level waste encapsulated in glass. The waste will be placed in sealed metallic containers that will be put in a repository which is to be located above the water table. (See Figure 1)

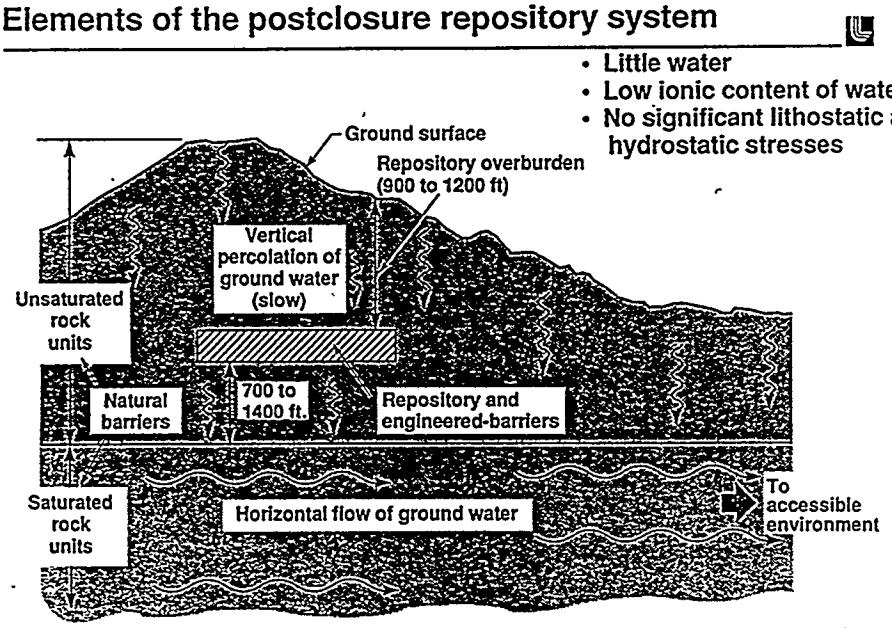

Figure 1
Proposed Nuclear Waste Repository at Yucca Mountain, Nevada

The environment surrounding the sealed metallic containers, also known as waste packages (WP), will be at atmospheric pressure and oxidizing. The metallic containers must limit the dispersement of the HLW to the surrounding environment for 300 to 1000 years.

Although the potential repository is above the water table, water is present in the porous "tuff" rock of Yucca Mountain. Heat

generated from the radioactive decay of the HLW will raise the temperature of the waste package and the surrounding rock. This will vaporize water in the vicinity of the waste package and humidify the local environment.

Depending on the "thermal loading" of the repository, numerous temperature and relative humidity scenarios are possible.[1] In particular, repository temperatures in the vicinity of the waste packages (WP) could reach 250°C under certain "thermal loading" scenarios.

Possible corrosive environments near the WP include:

- *Initial low humidity (<10% RH) and high temperature (>100°C) conditions. No condensed water will contact the waste container. This is the region where "dry" oxidation occurs.*
- *At longer times, high humidity (>70% RH) and lower temperatures (<100°C) conditions arise as the repository cools. Thin water films may form on the surfaces of the waste containers. This is the range where aggressive electrochemical corrosion will occur.*

One waste package design envisions a double-layer container comprised of a carbon steel outer layer and a nickel or titanium based alloy inner layer (Figure 2). The carbon steel is expected to slowly and uniformly oxidize at temperatures above 100°C and at low relative humidities for temperatures below 100°C. As the environment shifts to lower temperatures and higher humidities, the

[1] Thermal loading is dependent on heat generated per waste package and spacing between waste packages.

carbon steel will begin to electrochemically corrode and eventually degrade, then the inner Ni or Ti based alloy layer will function as the containment barrier. The Ni or Ti layer is intended to provide needed corrosion resistance for the aggressive aqueous corrosion. The behavior of the carbon steel during the transition from the initial oxidation environment to the final aqueous electrochemical corrosion environment is the focus of the present study. Of particular interest in the low temperature region *is the relative humidity at which the transition occurs, and its dependence on temperature. The relative humidity at which the transition occurs is known as the "critical relative humidity".*

High-Level Radioactive Waste Container

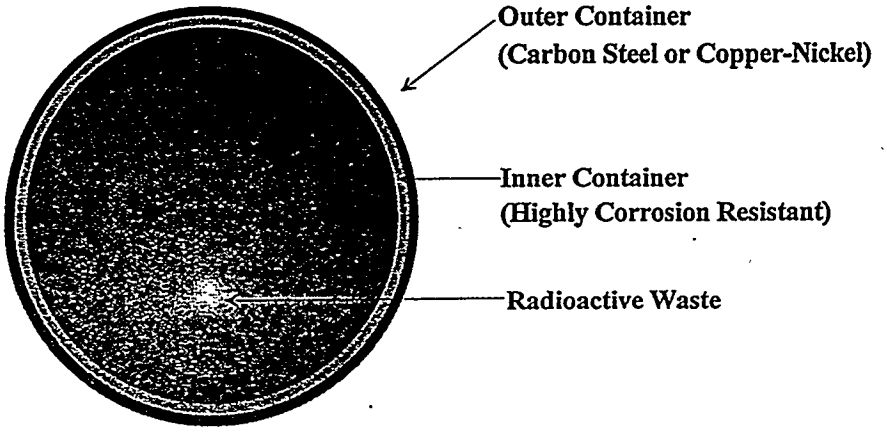

Figure 2
Proposed Waste Package Design

CORROSION MECHANISMS

Dry oxidation by gaseous oxygen, like aqueous corrosion, is an electrochemical process. Oxide layer formation may be divided into

three sequential stages: 1) adsorption of oxygen, 2) formation of oxide nuclei and 3) growth of a continuous oxide film. Oxide formation nucleates at surface sites where multilayer adsorption is favored, such as surface vacancies, ledges, or other imperfections (Uhlig,1971).

A solid reaction-product film forms on the metal surface (See Figure 3). For "dry" oxidation, this oxide layer serves as an ionic conductor, an electronic conductor and an electrode at which oxygen is reduced (Fontana and Greene, 1978). Thus, the oxide layer serves as the cathode while the metal serves as the anode during the electrochemical reaction.

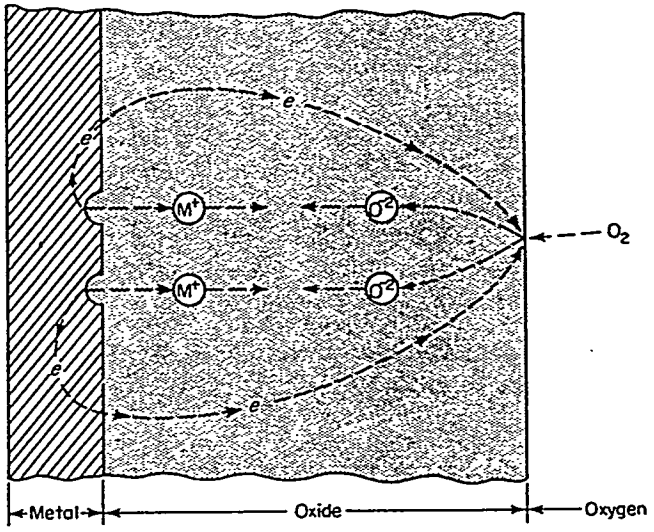

Figure 3

Metal-Oxide and Oxide-Environment Interfaces

Iron's oxide layer rate of growth for "dry" oxidation is controlled by the reaction rate (concentration of oxygen) remaining

constant at the metal-oxide layer interface. The reaction rate remains constant at the metal-oxide interface when there is an insufficient amount of oxide to completely cover the metal surface or when cracks and pores are present in the oxide layer. Thus, the oxide layer does not act as a diffusion barrier to the two reactants or is nonprotective (Fontana and Greene, 1978). For iron, the rate of growth in terms of oxide thickness (y) plotted vs. time (t) is a linear function (See Figure 4).

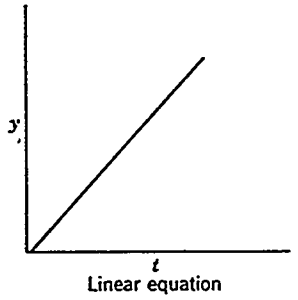

Figure 4
Oxide Thickness vs. Time for "Dry" Oxidation

Aqueous electrochemical corrosion is the process by which a metal will be oxidized in the presence of bulk H_2O or a thin film of water on the metal's surface. Iron oxidation in the presence of moisture arises from the formation of localized anodic and cathodic areas (Figure 5). (Whitten, Gailey, Davis, 1992) Anodic areas exist where iron is oxidized to iron(II) cations. The electrons produced flow through the iron to areas exposed to oxygen gas. These areas act as cathodes where oxygen is reduced and combines with water to form hydroxide ions. Concurrently, the iron(II) cations migrate from the anodic areas through the moisture or thin water film on the

specimen surface to the cathodic regions. It is here that iron oxide will form.

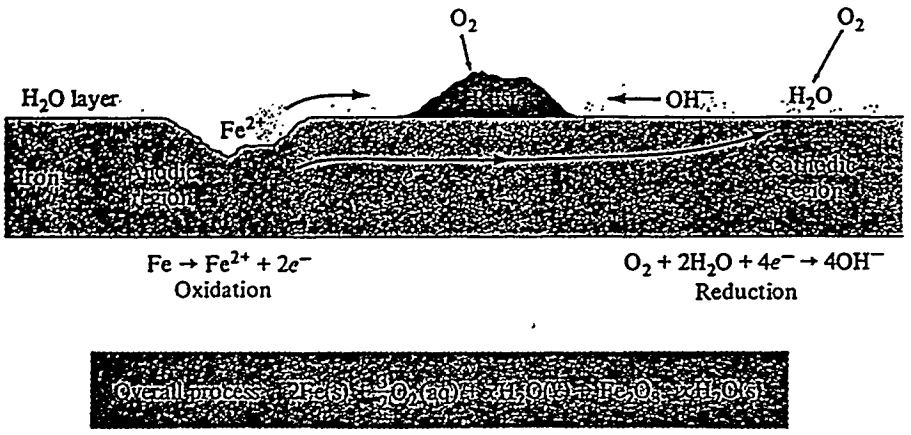

The corrosion of iron. Pitting appears at the anodic region, where iron metal is oxidized to Fe^{2+}. Rust appears at the cathodic region.

Figure 5
Aqueous Electrochemical Corrosion of Iron

Aqueous electrochemical corrosion's rate is initially controlled by the reaction rate (concentration of oxygen) remaining constant at the metal-oxide layer interface and finally controlled by the diffusion of metal and oxygen ions through the oxide layer after the oxide layer becomes protective. The rate of growth of the oxide layer is controlled by diffusion of metal cations and electrons through the oxide which is continuously increasing in thickness (Fontana and Greene, 1978). Oxide thickness (y) plotted vs. time (t) is a parabolic equation (Figure 6).

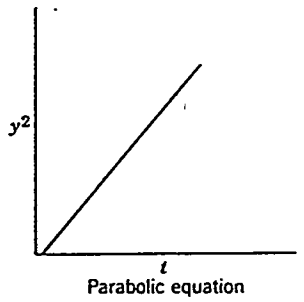

Figure 6
Oxide Thickness vs. Time for Electrochemical Corrosion

EXPERIMENTAL PROCEDURES

Tests were performed by use of the thermogravimetric analyzer (TGA) (Figure 8). The TGA, by use of a micro balance, measures the change in weight of a test specimen as it corrodes under controlled temperature and relative humidity conditions.

The test procedure is as follows. A specimen is hung on the test specimen side of the balance. A noble metal platinum specimen, which is the same weight as the test specimen, is hung on the tare side of the balance. The specimens are then enclosed in double paned glass vessels. Glass vessels allow the test specimen to be visually examined during testing. These vessels allow heated silicone to be circulate through them. This allows the local temperature of the test and tare specimen to be controlled. Water vapor, generated by circulating dry air through a water saturator, is then introduced into both the test and tare specimens environments. The relative

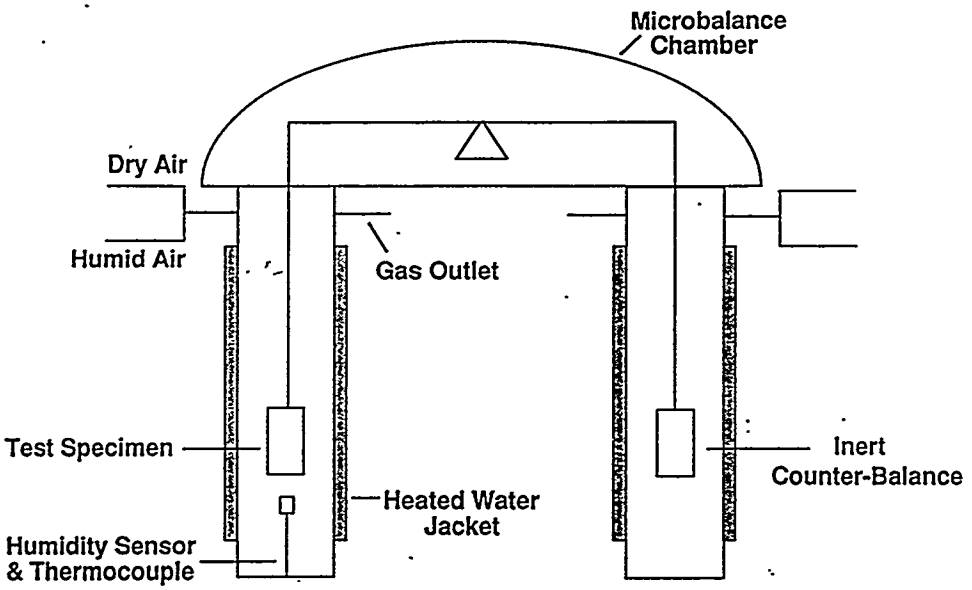

Figure 7
Schematic of the Thermogravimetric Analyzer

humidity is controlled by the ratio of the water saturator temperature to the glass vessel temperature. Temperature and relative humidity are monitored by the use of a sensor placed in the test specimen glass vessel. All testing is performed at normal atmospheric pressure.

EXPERIMENTAL RESULTS

Weight gain as a function of time was obtained for low carbon steel (ASTM 1020) exposed to a range of relative humidities (65% - 95%) and temperatures (50°C - 70°C). Steel test specimens were machined to a size of one inch by two inch by sixty five hundredths of an inch.

A typical plot of Weight Gain vs. Time generated at 65°C is shown in Figure 9. Weight Gain is represented by the y-axis while Time is represented by the x-axis. Weight gain is a strong function of relative humidity. In particular, accelerated weight gain, which is characterized by the majority of the weight gain occurs during initial exposure, occurs in environments of 85% and 90% relative humidities. Slower and smaller weight gains occur for relative humidities of 1%, 65%, and 75% .

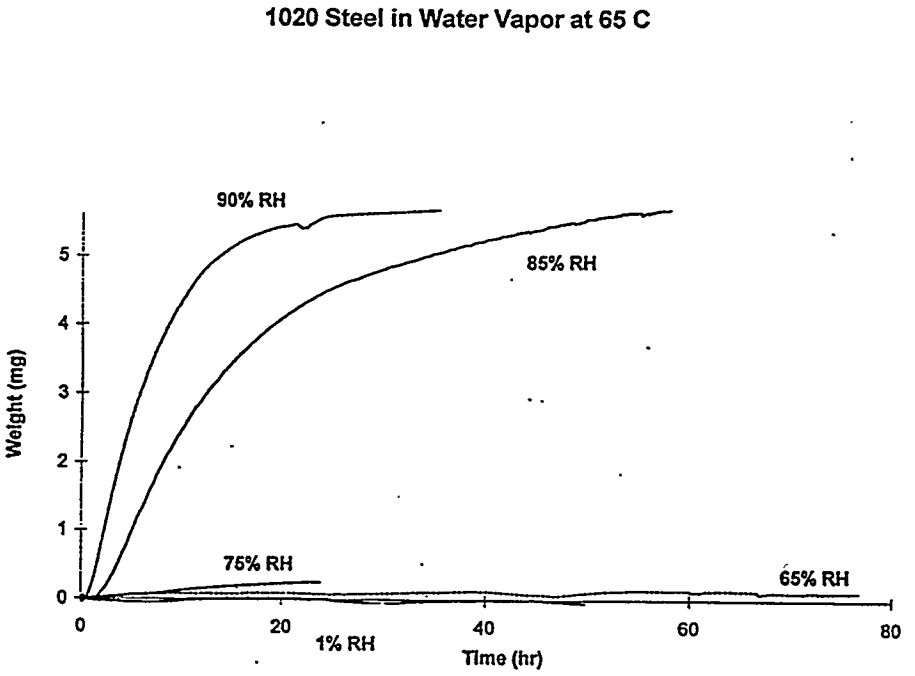

Figure 8
Weight Gain vs. Time at 65°C

Visual inspection of two specimens, both of which were tested at 65°C but at different relative humidities 65% and 90%, showed different surface features. The specimen tested at 65% relative humidity possessed a surface oxide layer which had just begun to

form on its transverse edges. These are the test specimen sides that measure sixty five hundredths of an inch. The specimen tested at 90% relative humidity was characterized by its entire surface having been oxidized.

The oxide layer that forms on the surface of iron may be comprised of several layers (Figure 7). This is because the concentration of oxygen decreases as the metal- oxide layer interface is approached. Metals that exhibit variable oxidation states, such as iron, react with a limited amount of oxygen to give lower oxidation

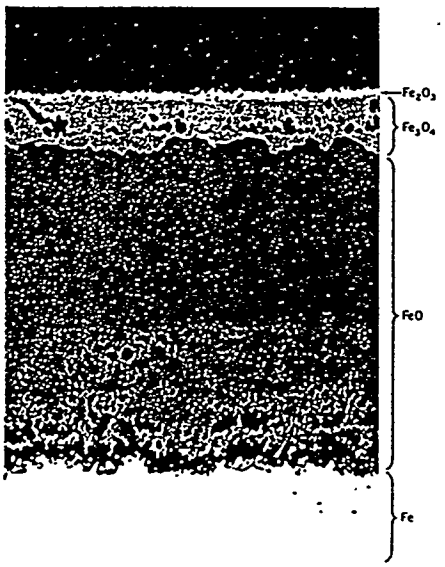

Fig. 11-3. Oxide layers formed on iron exposed to air at high temperatures. (Courtesy of C. T. Fujii.)

Figure 9
Distinctive Layers of Iron Oxide

state oxides and react with an excess of oxygen to give higher oxidation state oxides (Whitten,Gailey,Davis, 1992).

The effect of variable relative humidity on test specimen weight gain as a function of time is shown in Figure 10. During the

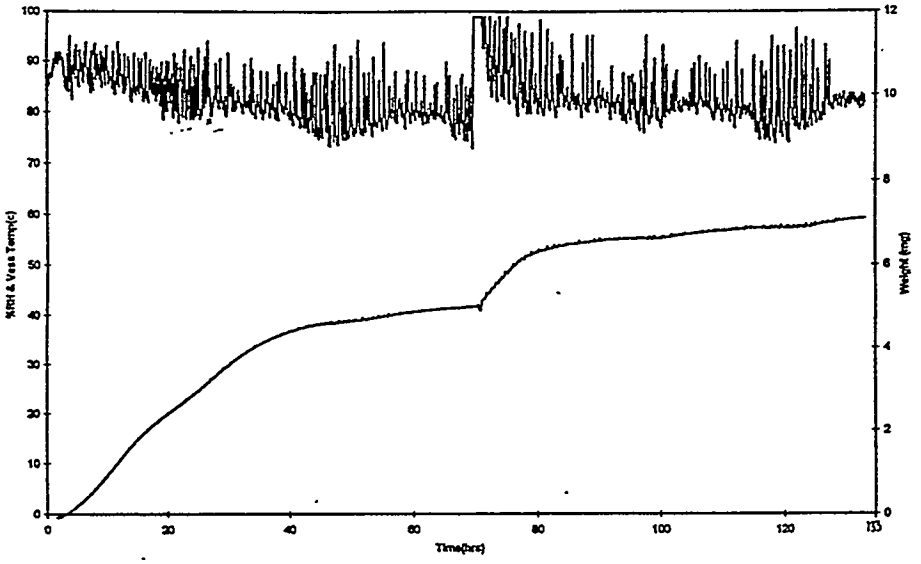

Figure 10
Relative Humidity & Weight Gain vs. Temperature

first seventy hours of the test, the RH was decreased from 90% to 70%. As the relative humidity decreased, so did the rate at which the specimen gained weight. At approximately 70 hours into the test, the relative humidity was raised back to 90% and the specimen again gained weight at an accelerated rate.

DISCUSSION

Both "dry" oxidation and aqueous electrochemical corrosion processes occurred during the corrosion of 1020 steel at 65°C. Figure 9 shows that at relative humidities less than 75% "dry" oxidation phenomena occurs, while for relative humidities greater than 85% aqueous electrochemical corrosion phenomena is predominant.

Therefore, the "critical relative humidity" for 1020 steel at 65°C is located somewhere in the range of 75%-85% relative humidity.

During the "dry" oxidation of carbon steel the rate at which oxide formation occurs is slow. Thus, the oxide layer will not completely cover the alloy surface during extended periods of time. Thus, the concentration of oxygen will remain constant at the metal-oxide interface. This phenomena occurs because no thin water film forms on the alloy surface.

During aqueous electrochemical corrosion of carbon steel the rate at which oxide formation occurs is rapid. Initially, the oxide will not completely cover the alloy surface, allowing the concentration of oxygen to remain constant at the metal-oxide interface. Thus, the linear relationship between oxide thickness and time will occur. However, oxide formation occurs at a much higher rate than during "dry" oxidation, such that the oxide will eventually form a protective layer. Thus, the rate of oxide formation slows over time. This accelerated oxide formation is do to the formation of a thin film of water on the alloy surface.

CONCLUSION

The theoretical weight gain curves previously discussed for "dry" oxidation and electrochemical corrosion (See Figure 4 and 6) were formulated for temperatures at or near ambient temperature. There seems to be close agreement between these theoretical weight gain curves and the weight gain curves formulated in this experiment (See Figures 4, 6 and 9). It may be possible to fit known curves, i.e.: linear and parabolic, to the weight gain curves generated

at elevated temperatures. Thus, corrosion kinetics at elevated temperatures and relative humidities, which are expected to exist within the proposed waste repository, will be available for performance assessment, materials selection, and safety analysis.

BIBLIOGRAPHY

Fontana, G. Mars, Greene D. Norbert, *Corrosion Engineering*, McGraw - Hill Book Co., New York, 1978. (Pages 348,350,356)

Uhlig, H. Herbert, *Corrosion and Corrosion Control*, John Wiley and Sons Inc., New York, 1971. (Pages 165,184)

Whitten, W. Kenneth, Gailey, D. Kenneth, Davis, E. Raymond, *General Chemistry 4th Edition*, Saunders College Publishing, New York,1992. (Pages 240,807)

PURIFICATION OF MAMMALIAN DNA REPAIR PROTEIN XRCC1*

Ingrid Chen

University of California, Berkeley

Lawrence Livermore National Laboratory
Livermore, California 94550

May 9, 1995

Prepared in partial fulfillment of the requirements of the Science and Engineering Research Semester under the direction of Dr. Michael P. Thelen, Research Mentor, in the Biology and Biotechnology Research Program.

*This research was supported in part by an appointment to the U.S. Department of Energy Science and Engineering Research Semester (hereinafter called SERS) program administered by LLNL under Contract W-7405-Eng-48 with Lawrence Livermore National Laboratory.

PURIFICATION OF MAMMALIAN DNA REPAIR PROTEIN XRCC1

Ingrid Chen
University of California, Berkeley

Biology and Biotechnology Research Program
Lawrence Livermore National Laboratory, University of California

Abstract. *XRCC1* (X-ray Repair Cross Complementing) is a human gene involved in the base excision repair pathway. Previously, an *XRCC1* cDNA minigene was constructed and cloned for the purpose of overproducing XRCC1 protein in both prokaryotic and eukaryotic cells, and also to facilitate rapid purification of XRCC1 from these systems. In this study, we overexpressed XRCC1 in E. *coli* and purified the protein by immobilized metal affinity chromatography. Using the purified protein sample to test four different XRCC1 monoclonal antibodies (MAb's 33, 62, 66, and 16), we found that MAb 33 had the highest titer. The results from a test comparing the purified antibodies with the hybridoma medium suggest possible weakening of the purified antibodies during the purification step, causing a decrease in its binding activity. To increase the level of overexpression and simplify purification of XRCC1, we are inserting the original minigene construct into a new expression vector. We also plan to produce defined fragments of XRCC1 containing conserved regions for use in structural studies.

PURIFICATION OF MAMMALIAN DNA REPAIR PROTEIN XRCC1

Ingrid Chen
University of California, Berkeley

Biology and Biotechnology Research Program
Lawrence Livermore National Laboratory, University of California

Abstract. *XRCC1* (**X**-ray **R**epair **C**ross **C**omplementing) is a human gene involved in the base excision repair pathway [1,5]. Previously, an *XRCC1* cDNA minigene was constructed and cloned for the purpose of overproducing XRCC1 protein in both prokaryotic and eukaryotic cells, and also to facilitate rapid purification of XRCC1 from these systems [2]. In this study, we overexpressed XRCC1 in E. *coli* and purified the protein by immobilized metal affinity chromatography. Using the purified protein sample to test four different XRCC1 monoclonal antibodies (MAb's 33, 62, 66, and 16), we found that MAb 33 had the highest titer. The results from a test comparing the purified antibodies with the hybridoma medium suggest possible weakening of the purified antibodies during the purification step, causing a decrease in its binding activity. To increase the level of overexpression and simplify purification of XRCC1, we are inserting the original minigene construct into a new expression vector. We also plan to produce defined fragments of XRCC1 containing conserved regions for use in structural studies.

Introduction

Malfunctioning DNA repair systems lead to cancer, mutations, and cell death. The human *x*-ray repair gene found to fully correct the DNA repair defect in Chinese hamster ovary (CHO) cell mutant EM9 is known as *XRCC1* [1]. The corresponding protein (XRCC1) encoded by this gene affects the activity of DNA ligase III, an enzyme involved in rejoining single-strand breaks in the backbone of DNA [2]. The protein is 69.5 kDa in mass and spans 633 amino acids. In order to study the characteristics of XRCC1, and address its specific involvement in mammalian DNA base excision repair, it is first necessary to obtain and purify the targeted protein in a quantity optimal for biochemical studies. For this reason, a prokaryotic expression construct, containing an XRCC1 cDNA minigene inserted into vector pET-16b (designated pET-16-bXH), was constructed such that a decahistidine tag would be included at the end of full length XRCC1. Once the protein is overexpressed, this histidine-tag proves effective in isolating XRCC1 away from any cellular contaminants, such as DNA, RNA, nucleotides and other host proteins [1].

In this project, we induced overexpression of his-tagged XRCC1 in E. *coli* and purified the protein with immobilized metal affinity chromatography. Proteins in individual chromatographic fractions were analyzed and compared to the initial crude samples using gel electrophoresis and protein determination. To overcome the low level of overexpression of XRCC1, we are presently re-inserting the XRCC1 cDNA minigene (along with its histidine tag) into vector pET-26b. The main difference between the two vectors is that pET-26b carries a bacterial leader (pel B) that has increased E. *coli* overexpression of two other DNA repair proteins, ERCC2 and ERCC4. This pel B leader could also simplify purification if it facilitates translocation of XRCC1 into the periplasmic space (between the cell wall and plasma membrane).

Materials and Methods

Overexpression

His-tagged XRCC1 was overexpressed in E. *coli* strain BL21(DE3) containing plasmid pET-16bXH. 20ml starter cultures (with Luria-Bertani medium, or LB, and 0.1mg/ml ampicillin) were innoculated with these cells, grown until turbid, and divided into two 500ml cultures. Cells were grown to an OD_{600} of ~0.6 and induced with 1mM IPTG for two hours. (All cells grown at 37°C). Bacteria were pelleted and frozen at 4°C. 1ml samples were taken at each step for an induction check by sodium dodecyl sulfate (SDS)-polyacrylamide gel electrophoresis (PAGE) on 10% or 15% SDS gels.

BL21(DE3) cell extract preparation

After induction, cells were resuspended and lysed by sonication in 20 mls of sonication buffer (50mM Tris[hydroxymethyl]-aminomethane hydrochloride (or Tris-HCl),pH 8.0; 10% glycerol, 0.5M NaCl, 0.1mM (ethylenedioxy)diethylene-dinitrilotetraacetic acid (EDTA), 10mM mercaptoethanol, 1mM phenylmethane-sulphonyl fluoride (PMSF)). Protease inhibitors, RNAse A and protamine were added post-sonication. Extracts were set on ice for 30 minutes and cell debris were removed by centrifugation at 15,000 rpm for 15 minutes.

Purification by immobilized metal affinity chromatography

The Pharmacia FPLC System was used to perform immobilized metal affinity chromatography, or IMAC [3], on the protein sample extracted from induced BL21(DE3) pET-16bXH. A Ni^{2+} nitrilotriacetic acid (Ni-NTA) column was used to bind histidine tagged XRCC1 to the beads, away from the other bacterial contaminants. Then, loosely bound protein were washed with wash buffer A (50mM Tris-HCl, pH 7.0; 10% glycerol, 0.1M NaCl, 0.1mM EDTA, 10mM mercaptoethanol). Bound XRCC1 was eluted with a gradient of imidazole solution (wash buffer A with 250mM

imidazole), beginning with [0] to 250mM imidazole. Fractions were collected and analyzed by SDS-PAGE on 10% gels.

XRCC1 monoclonal antibodies

Immunoassay tests were performed on four XRCC1 monoclonal antibodies (MAb) 33, 66, 62, and 16. Each well of a 96 well microtiter plates was coated with 50ng of IMAC purified XRCC1. The plates were dried overnight. The primary antibodies (MAb 33, 16, 62, 66) were diluted 1:10 in assay buffer (0.1M Tris-HCl, pH 7.75; 0.15M NaCl) and 100µl of each were loaded into four separate wells. Then, a serial dilution of either 1:2 or 1:4 was carried out consequtively over subsequent wells. The plate was incubated for 1 hour at 37°C, and washed 5 times in assay buffer. Peroxidase conjugated goat anti-mouse IgG (Sigma) was diluted 1:500 in assay buffer and loaded 50µl/ well. The plate was incubated again for another hour and then washed 5 times. Finally, the plate was developed with 100µl/well of substrate (30ml citrate buffer, 0.6ml 2,2'-azino-BIS(3-Ethylbenzthiazoline-6-sulfonic acid) stock, and .01ml hydrogen peroxide) and read at 405nm (see Figure 3).

Preparation for restriction digests

BL21(DE3) cells harboring plasmid pET-16bXH were grown up (from fresh colonies) in 5ml LB and ampicillin for 2 hours at 37°C. The plasmid was extracted from BL21(DE3) cells and resuspended into 30µl TE buffer (10mM Tris, 1mM EDTA), pH 8.0. E. *coli* (MAX Efficiency DH5α™ Competent Cells, GIBCOBRL Life Technologies) were transformed to ampicillin resistance by heat shock and plated out for overnight incubation at 37°C. Two 500ml cultures innoculated with a swipe of DH5α colonies with pET-16bXH and grown up overnight. Columns (Qiagen Plasmid Midi Prep) were used to purify the plasmid from the cells. The plasmid was resuspended in 100µl TE buffer, pH8.0. A phenol:chloroform treatment (4) was performed to clean up the DNA and the plasmid resuspended in 50µl TE buffer, pH8.0.

Expression vectors and restriction enzymes

The restriction enzymes being used to cut full length XRCC1 out of the original plasmid and insert into pET-26b are Nco1, Xho1, and Nde1 (New England Biolabs). HinDIII and Sma1 will be used to cut XRCC1 into specific fragments containing regions of interest. All restriction digests were performed in the conditions specified by New England Biolabs manual. Each restriction digest was analyzed on a 1% agarose gel.

Results and Discussion

Overexpression and purification of XRCC1 from pET-16bXH

Qualitative analysis by gel electrophoresis shows that overproduction of XRCC1 is low in BL21(DE3). The gel run of the protein extract from cells before and after induction with isopropyl thio-ß-D-galactoside (IPTG) is seen in figure 1. The description of each lane is as follows: lane 1- marker; lane 2- uninduced; lane 3- induced. The overproduced XRCC1 can be seen as the thin band in lane 3, just below the second marker (see blue arrow). One reason for the low expression level of this protein could be excessive rare codon usage (6). If there are multiple rare codons present in the XRCC1 cDNA sequence, it is possible that the quantity of tRNAs present in the host cell are low enough to limit the rate of translation. Another reason could be that XRCC1 is being degraded following translation by amino terminal degradation, the "N-end rule" (6).

Figure 2 shows the protein mixtures coming off the nickel column during elution with imidazole. The first, second, and third lanes describe respectively, the protein markers, the sample initially poured onto the column, and the unbound protein flowing through. Subsequent lanes show the elution of bound XRCC1 protein with 250mM imidazole. The peak fractions of purified XRCC1 were pooled together and the protein concentration was quantified by Bradford analysis. The final concentration of XRCC1 was 0.83 µg/µl. (We reconfirmed the purification of XRCC1 by performing a western blot using monoclonal antibodies 33, 16, 62, and 66). The gel analysis suggests that using IMAC with nickel metal and imidazole is effective in purifying his-tagged XRCC1.

ELISA tests of monoclonal antibodies

Figure 3 is a computer reading for an ELISA (enzyme linked immunosorbent assay) plate testing the titer of all four antibodies with the IMAC purified XRCC1. A strong signal around OD_{405} of 0.8 was detected for MAb 33 out to the 1: 2560 dilution. MAb 66 could bind XRCC1 at a dilution of 1: 80. MAb's 16 and 62 seemed weak, unable to bind XRCC1 after the initial dilution. Therefore, the titers of MAb's 33 and 66 were higher than MAb's 16 and 62. We have not yet determined the affinity of each antibody.

There did not seem to be any difference in the binding activity between the purified antibody and the hybridoma medium. This result was surprising because the purified antibodies, having a high concentration of pure antibody, should have produced a stronger signal. The MAbs were isolated using a Protein G column, and eluted with 10mM HCl, pH 2.0. The pH was later increased using Tris-base. The fact that the results from the crude hybridoma medium, containing other proteins along with the

antibody, were similar to the purified antibody suggests that the pH swings during purification has left the antibody weak and unstable.

Subcloning the XRCC1 cDNA minigene

Plasmid pET-16bXH was extracted from a liter culture of DH5α cells. The ratio of 260/280 for a 1:100 dilution was 2.0, indicating pure DNA. The DNA concentration was 0.4 mg/ml. To check if the correct plasmid had been isolated, 1µl of DNA was cut with 1µl BamHI for 1 hour in a 37°C water bath. The digested plasmid was analyzed on a 1% agarose gel. Lane 1 and 2 show the uncut plasmid versus the plasmid cut with BamHI, respectively. Lane 3 contains the 100bp DNA markers while lane 4 is the 1kb markers. The multiple bands seen in lane 2 indicates a partial digest has occurred.

The plasmid was also cut separately with 1µl NcoI and 1µl NdeI (again, for 1 hour at 37°C). We ran a 1% agarose gel to check the digest and found that neither enzymes cut the plasmid. A phenol:chloroform treatment was conducted to clean up the DNA and the same test was applied again. Unfortunately, the results turned out the same. One possibility is that the NcoI and NdeI site was destroyed when the minigene was cloned. At this point, further research is needed to cut the XRCC1 minigene out of pET-16b.

Acknowledgements

Much thanks is given to Dr. Michael P. Thelen, my supervisor, who not only provided the means for my participation in the SERS program, but also challenged me to experience the different areas in research. I would also like to thank Mona Hwang and Chris Parris for being such great supports and mentors; and Elena Pushnova for her guidance in subcloning. Finally, I'd like to express my appreciation to the SERS program, LLNL, and DOE for the privelege to have worked among the best and the brightest.

---

1. Caldecott, K. W., J. D. Tucker, and L. H. Thompson, "Construction of human *XRCC1* minigenes that fully correct the CHO DNA repair mutant EM9," Nucleic Acids Research (20), 4574-4579 (1992).
2. Caldecott, K. W., C.K. McKeown, J. D. Tucker, S. Ljungquist, and L.H. Thompson, "An Interaction between the Mammalian DNA Repair Protein XRCC1 and DNA Ligase III," Molecular and Cellular Biology (14), 68-76 (1994).
3. Cameron, G.W.W., and N. C. Bruce, "Introduction to Chromatographic Methods for Protein Purification, " Methods in Molecular and Cellular Biology (4) 184-188 (1993).

4. Sambook, J., E. F. Fritsch, and T. Maniatis, "Extraction and Purification of Plasmid DNA," Molecular Cloning (2nd edition) 1.25-1.27 (1989).
5. Thompson, L. H., "Somatic Cell Genetics Approach to Dissecting Mammalian DNA Repair," Environmental and Molecular Mutagenesis (14), 264-281 (1989).
6. Novagen Technical Services Staff, "Commonly Asked Questions About Expressing Proteins in Bacteria," Innovations (Vol. 1 No. 1) 10-11 (1994).

Figure 1. Overexpression of XRCC1. The first lane of this 15 % SDS gel contains the high molecular weight protein standards. The crude protein sample from the bacteria before induction is seen in lane 2. Lane 3 is the crude protein sample after induction with IPTG. Notice the small band (blue arrow) of XRCC1 is absent in the uninduced sample. (Although XRCC1 is 69.5 kDa in weight, it runs closer to the 80 kDa marker in a gel).

Figure 2. Purification of XRCC1 by IMAC. In this experiment, XRCC1 protein was enriched by using immobilized metal affinity chromatography. This particular gel shows the crude starting sample, the flow through (unbound protein), and peak fractions of XRCC1 being eluted off the column by imidazole. Lanes 1, 2, and 3 are the protein standards, starting sample, and flow through, respectively. Lanes 4 through 9 show the elution of XRCC1.

Figure 3. ELISA plate of XRCC1 monoclonal antibodies 33, 16, 62, 66. All four antibodies were tested on this 96-well microtiter plate (previously coated with 50 ng of XRCC1). Each antibody was diluted in assay buffer 1:10 and loaded in column 3. Successive columns were diluted 1:2. Columns 1 and 2 are the blank and second antibody only. The first, third, fifth, and seventh rows contain the purified antibody (the specific antibody labelled on figure), while the second, fourth, sixth, and eighth rows contain the hybridoma medium.

Figure 4. Restiction digest check of plasmid pET-16bXH cut with BamH1. The plasmid containing the XRCC1 cDNA minigene was isolated from DH5α cells and cut with BamH1. Lane 1 shows 1μl of the uncut plasmid. Lane 2 is the partially digested plasmid. Lanes 3 and 4 are the 100 bp DNA marker and the 1kb DNA marker.

Figure 1. Overexpression of XRCC1

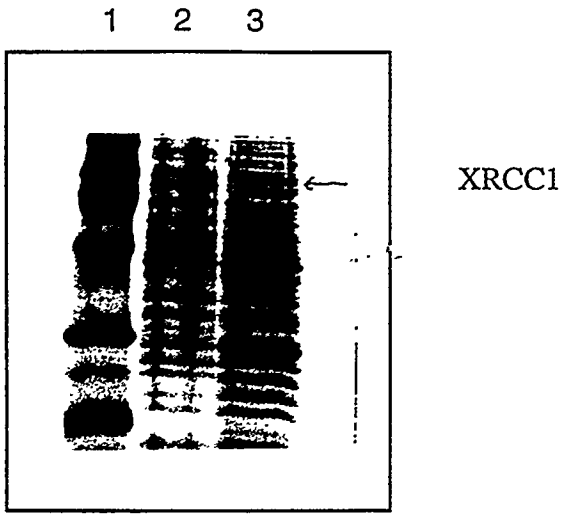

Figure 2. Purification of XRCC1 by IMAC

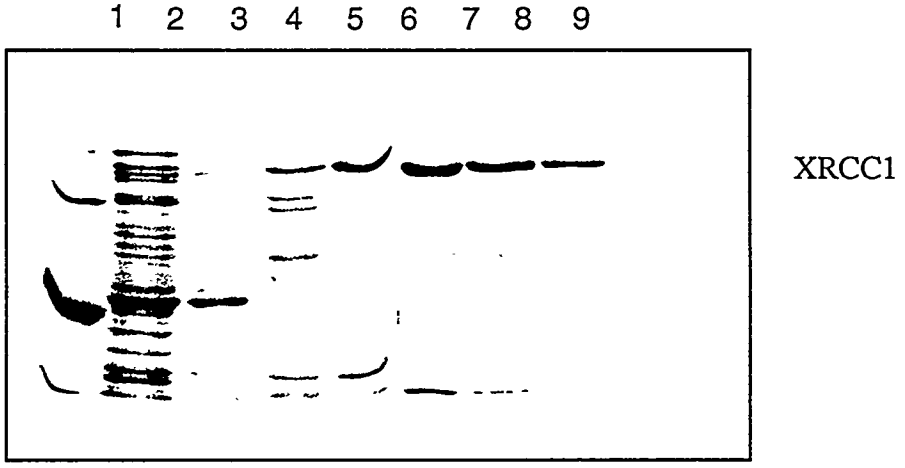

Figure 3. ELISA plate of XRCC1 MAb's 33, 16, 62, 66

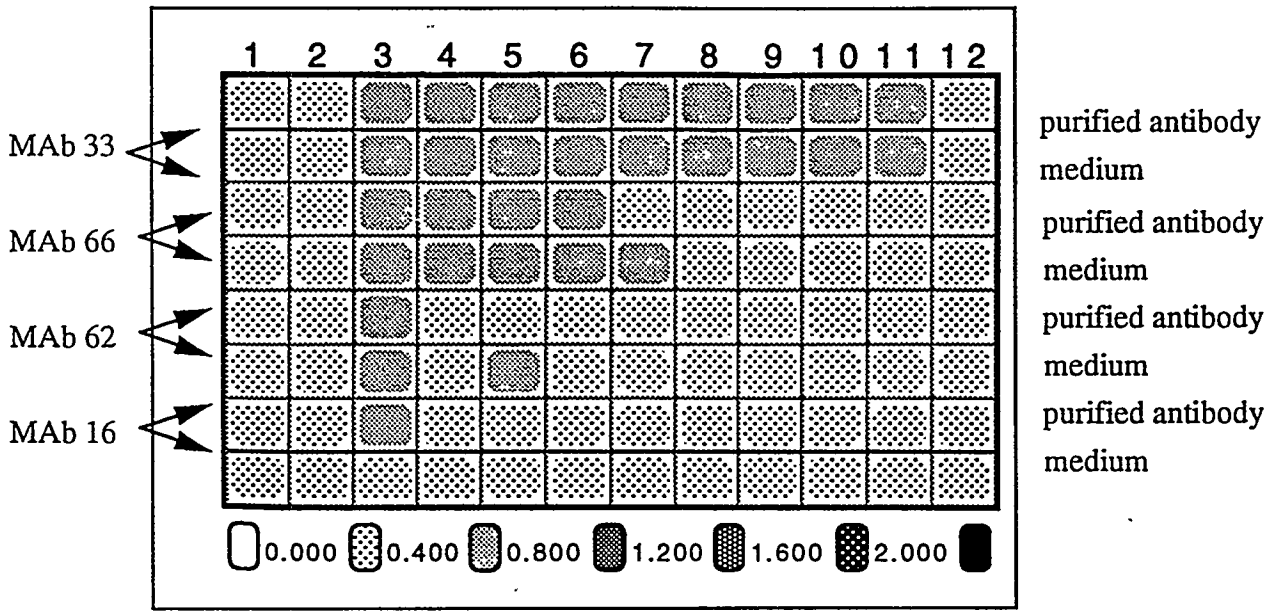

Figure 4. Restriction digest check of plasmid pET-16bXH cut with BamH1

New Technologies for the Detection of Chromosomal Aberrations Using the Fluorescence *In Situ* Hybridization Technique

A.J. Chmura

State University of New York
College of Environmental Science and Forestry

Lawrence Livermore National Laboratory
Livermore, California 94550

Prepared in partial fulfillment of the requirements of the Department of Energy (DOE), Science and Engineering Research Semester (SERS) under the direction of Francesca S. Hill, Kenneth T. Bogen and Joe N. Lucas in the Lawrence Livermore National Laboratory.

* This research was supported in part by an appointment to the U. S. Department of Energy, Science and Engineering Semester (hereinafter called SERS) program administered by the LLNL under Contract W-7405-Eng-48 with Lawrence Livermore National Laboratory.

Abstract

Up until recently, cytogenetic study of chemical and radiation induced chromosome damage has based many of its results on the detection of aberrations using banding techniques. This technique is tedious and takes a highly trained technician for analysis. In the 1980's LLNL developed fluorescence *in situ* hybridization which greatly speeds analysis and increases its sensitivity. We are currently developing new technological advances which will further increase the speed, clarity and functionality of the FISH technique, these include multi-labeled probes and amplification techniques.

Introduction

The goal of the Health and Ecological Assessment Division, Biological Dosimetry and Risk Assessment Group is to understand the way chemicals and radiation effect human beings and to qualify and quantify the risks associated with their use and misuse. The stochastic effects of these substances are widespread however they are based on the chemical's/radiation's effect in breaking chromosomes. When chromosomes break internal repair mechanisms attempt to reattach the pieces. This repair mechanism is not perfect and mistakes do occur. Mistakes in repair can lead to misalignment or deletion of chromosomal material. A summary of this genetic damage is in Figure#1. Some damage occurs naturally but is greatly accelerated by certain chemicals and radiation. The effects of radiation seem to be random, radioactive particles randomly bombard the nucleus breaking chromosomes in there path (1). Chemicals seem to infiltrate the nucleus by different methods and may localize their effects to certain specific areas.

In the 1970's Giemsa staining was developed to band chromosomes. Upon viewing a well trained cytogenetictechnologist can recognize abnormal banding patterns and break locations. However in complex translocation exchanges the chromosomes may be hard to identify. However a greater hindrance to the

technique is the requisite training and cost thereof and difficulty of analysis and the speed with which analysis can be done. As part of this work in biological dosimetry we are constantly trying to develop new methods to more accurately and efficiently measure and characterize aberrations. Our group is using the fluorescence *in situ* hybridization technique (FISH) which was developed here at LLNL in the 1980's by Gray, Pinkel, Straume and Lucas (2,3). This method fluorescently colors certain specific areas of genetic material, either certain chromosomes or certain parts of chromosomes. These tags, or probes, are visualized for analysis using a fluorescent microscope against a fluorescent counterstain, either 4,6-diamino-2-phenylindole (DAPI) or propidium iodide (PI). Viewing of these chromosomes can show the aberrations caused by the hazard because translocations can be seen as a obvious change in color, and dicentrics can be seen with a cocktail of whole chromosome paints (WCP) and centromere specific probe (4). Our object in this program is to optimize the FISH technique, in the following synopsis I will describe techniques that we have developed to optimize our use of multi-labeled probes and amplification techniques.

Methodology

With the advent of flow cytometry our ability to separate chromosomes in large quantities has increased substantially. In the past template DNA for whole chromosome probes were made by conventional cloning techniques. This method is very tedious and work intensive. The polymerase chain reaction (PCR) allows us to take a small amount of DNA and replicate it exponentially. We are using both of these to our advantage in making new WCPs quickly (5). Our new method uses DOP-PCR or degenerative oligonucleotide primed polymerase chain reaction to replicate our target DNA. DOP-PCR uses a primer 22 nucleotides long that is

degenerative throughout the human genome, it allows us to prime theoretically the whole chromosome for replication into small 300-3000 base pair lengths. The pure chromosomes are isolated by flow cytometry. The products of the PCR can then be labeled using random priming or nick translation without any further purification.

The number of fluorochromes is extensive however the colors with which they fluoresce is not. More colors would provide a clearer picture for analysis. To this end we have tried mixing colors as one would do painting a picture. Using two different labeled nucleotides, we have produced probes which can independently be labeled with a color which will 'mix' because of their proximity to each other on the chromosome to appear as a new color. In our proof of principle experiment we nick translated using a mixture of digoxeginin and biotin dUTPs and then stained with rhodamine anti-digoxeginin and avidin-FITC. The mixture of the green FITC with the red rhodamine gave a yellow signal.

Experimental

Chromosomes 19 and X were isolated from established cell lines and flow sorted. These were amplified using the DOP-PCR Master (Boehringer-Mannheim, Indianapolis, Indiana) using the long program as outlined in the procedure from the manufacturer.

PCR long Program

1. 5 min 95 °C
2. 5 cycles
   1 min 94°C
   1.5 min 30°C
   3min 30 - 72 °C (3.5°C/15 sec)
   3 min 72°C
3. 35 cycles
   1 min 94°C
   1 min 62°C
   2 min 72°C
   (+14sec at each cycle)
4. 7 min 72°C

5. Keep at 7°C until further use

The entire process takes approximately 6.5 hours

The amplification was done on a Perkin Elmer 9600 thermocycler. A 1 ul alliquot of product from the first amplification was amplified using the same procedure as the first. The product was then labeled with biotin using the Bioprime DNA labeling system (Gibco, Gathersburg, MD), which employs random priming. The procedure uses 1 ul of product from the 2° PCR reaction which is denatured with water, to which is added dNTPs, Primers, Klenow enzyme and water to 50 ul followed by incubation for 4 hours at 37°C. A 1 ul sample of the labelled product was mixed with 1 ul of Cot-1 DNA (to prevent nonspecific binding) 1 ul of water and 7 ul of a buffer/denatureing mix containing formamide. The probe mix was denatured for 5 minutes at 70 °C. The slides were made from human peripheral blood. T lymphocytes were cultured from whole blood in medium containing 20% fetal calf serum and stimulated with phytohaemagglutinin (PHA, 0.15mg/ml) and arrested with colcemid and following harvest fixed to glass slides with 3:1 methanol acetic acid. The human lymphocyte slides were denatured in 70 % formamide /2xSSC for 2 minutes at 70 °C followed by dehydration in 70, 85 , 95% ethanol. The probe was added to the slide and covered and sealed with a cover slip and rubber cement. The slide was incubated at 37°C overnight followed by washes in 50%formamide/2xSSC, 2xSSC and PN buffer. The slides were stained with one coat of avidin-FITC and one coat of anti-avidin-FITC. They were viewed with DAPI and PI as counterstains.

The multi-labeled probe was produced by nick translation using DNased chromosome 4, dNTPs in buffer and 0.5ul of 1mM dUTP-digoxigenin 0.5 ul of 1mM dUTP-biotin and water. DNA polymerase 1 was added and the mixture was allowed to incubate for 2 hours at 15°C. The probes were hybridized and washed as previously outlined and stained with one coat of anti-digoxeginin-rhodamine and one coat of avidin-FITC and one coat of anti-avidin-FITC. They were viewed with DAPI and PI as counterstains.

Results

The probes produced by DOP-PCR and random primed labeling are in Figures #2 and #3. Figure #2 shows Chromosome 19 on a normal metaphase spread, it shows uniform coverage of the paint. Figure #3 shows the X chromosome on a

normal male metaphase spread, it shows good coverage however the uniformity is not as even as the previous.

Figure #4 shows the multi-labeled chromosome 4 probe with only the FITC staining. As is obvious, the paint is spotty because it has only half the number of labeled nucleotides as is usually used(one half is digoxeginin dUTP). Figure #5 shows the same spread except the stain is rhodamine. Once again the coverage is spotty. Figure #6 shows the metaphase with both rhodamine and FITC stains, and the color is yellow not the green or red which it is made from.

Conclusion and Further Research

Advancement in the uses of FISH will give us greater insight into the effects we and our environment have upon our genetic makeup. FISH is obviously the fastest and most sensitive method for measuring chromosomal damage, and making it more powerful can only help our cause. We hope to take our proof of principle work and actually use it in our studies. Producing other colors by mixing other fluorochromes seems promising as well as mixing directly labeled nucleotides to get new colors. And using DOP-PCR to amplify all the chromosomes for labeling should just be on the horizon.

Special Thanks

I would like to thank Francesca Hill, Joe Lucas, Ken Bogen, Lynn Wilder, Hung He, Shane Brady, Cheri Nielsen, Joanna Albala and Tore Straume for there help. This research was supported in part by an appointment to the U. S. Department of Energy, Science and Engineering Semester program administered by the LLNL under Contract W-7405-Eng-48 with Lawrence Livermore National Laboratory.

References

1 Lucas J. N., Awa A, Gray J, Kodama Y, Littlefield G, Nakano M, Ohtaki K, Pinkel D, Poggensee M, Straume T, Weier U. Rapid translocation frequency analysis in human decades after exposure to ionizing radiation. Int J. Radait. Biol. (in Press, 1991)

2 Pinkel D, Gray JW, Trask B, van den Engh G, Fuscoe J, van Dekken H. Cytogenetic Analysis by in situ hybridization with fluorescently labeled nucleic acid probes. Symposia on Quantitative Biology, 1986;**51**: 151-157

3 Lucas J.N., Tenjin T, Straume T, Pinkel D, Moore D, Litt M, Gray J. Rapid humanchromosome aberration analysis using fluorescence in situ hybridization. Int J. Radiat. Biol. 1989;**56**:35-44.

4 Straume T, Lucas J.N. A Comparison of the yield of translocations and dicentrics measured using fluorescent *in situ* hybridization. Int J. Radiat. Biol. 1993;**64** :185-187

5 Carter , Nigel P. Cytogenetic Analysis by Chromosome Painting. Cytommetry. 1994;**18**: 2-10

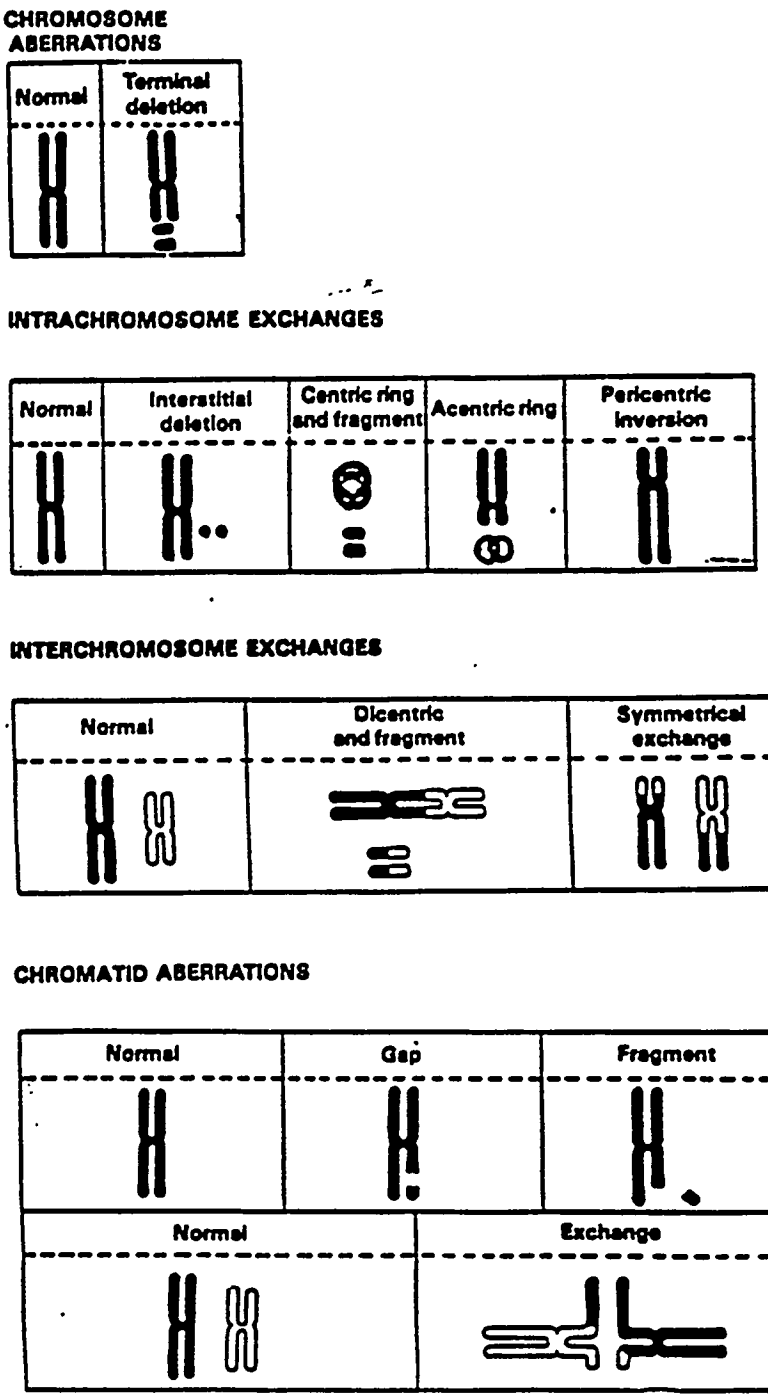

Figure #1 A summary of the principle types of rearrangements found in Chromosomes. Taken from Introduction to Radiobiology, Tubiana *et.al*, Taylor and Francis 1990 pg 71

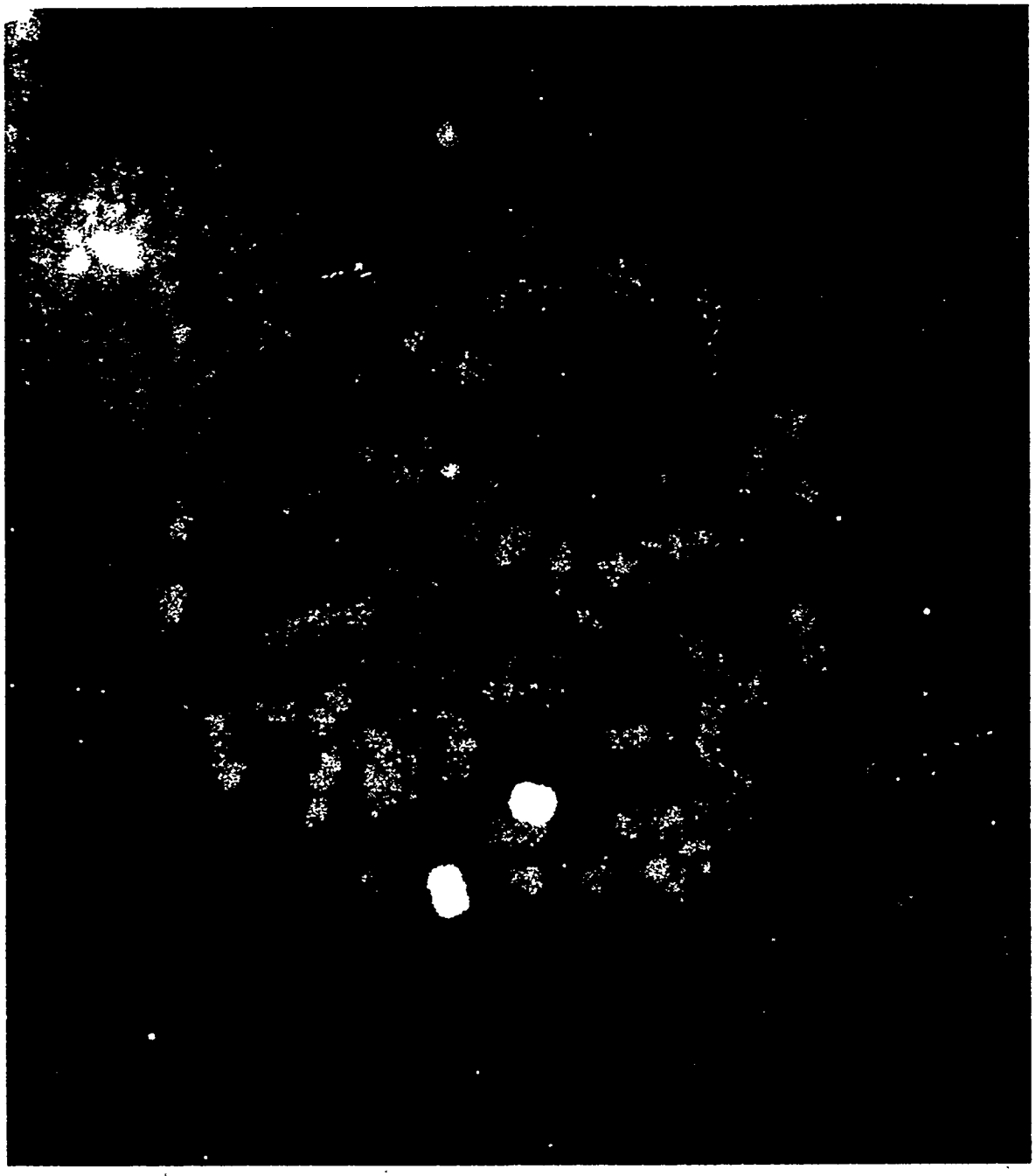

Figure #2:
Metaphase spread hybridized with DOP-PCR chromosome 19 and counterstained with PI.

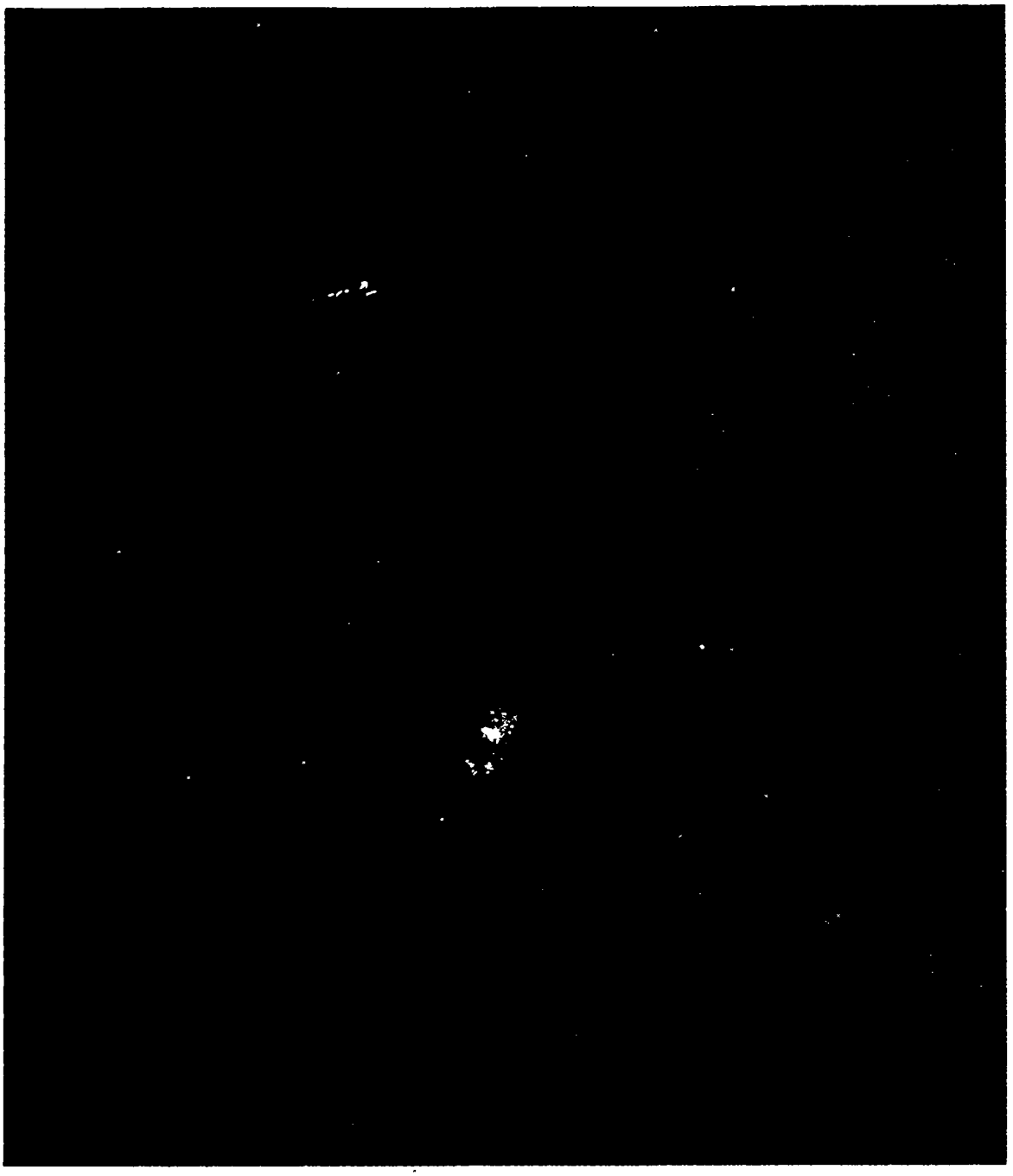

Figure #3:

Metaphase spread hybridized with DOP-PCR chromosome X and counterstained with PI.

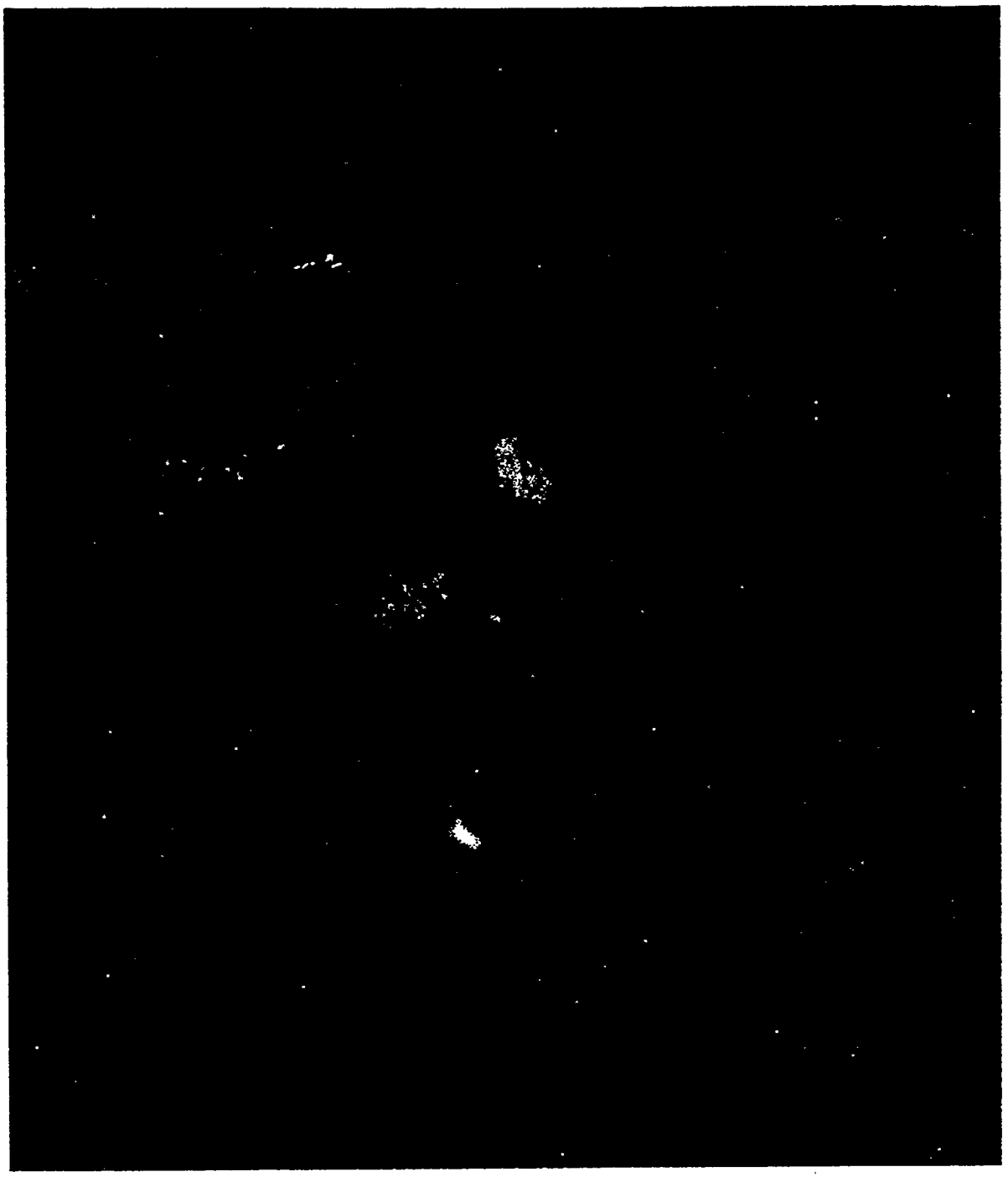

Figure #4: Normal metaphase spread of a biotin/digoxigenin whole chromosome probe for chromosome 4 with one coat of avidin-FITC.

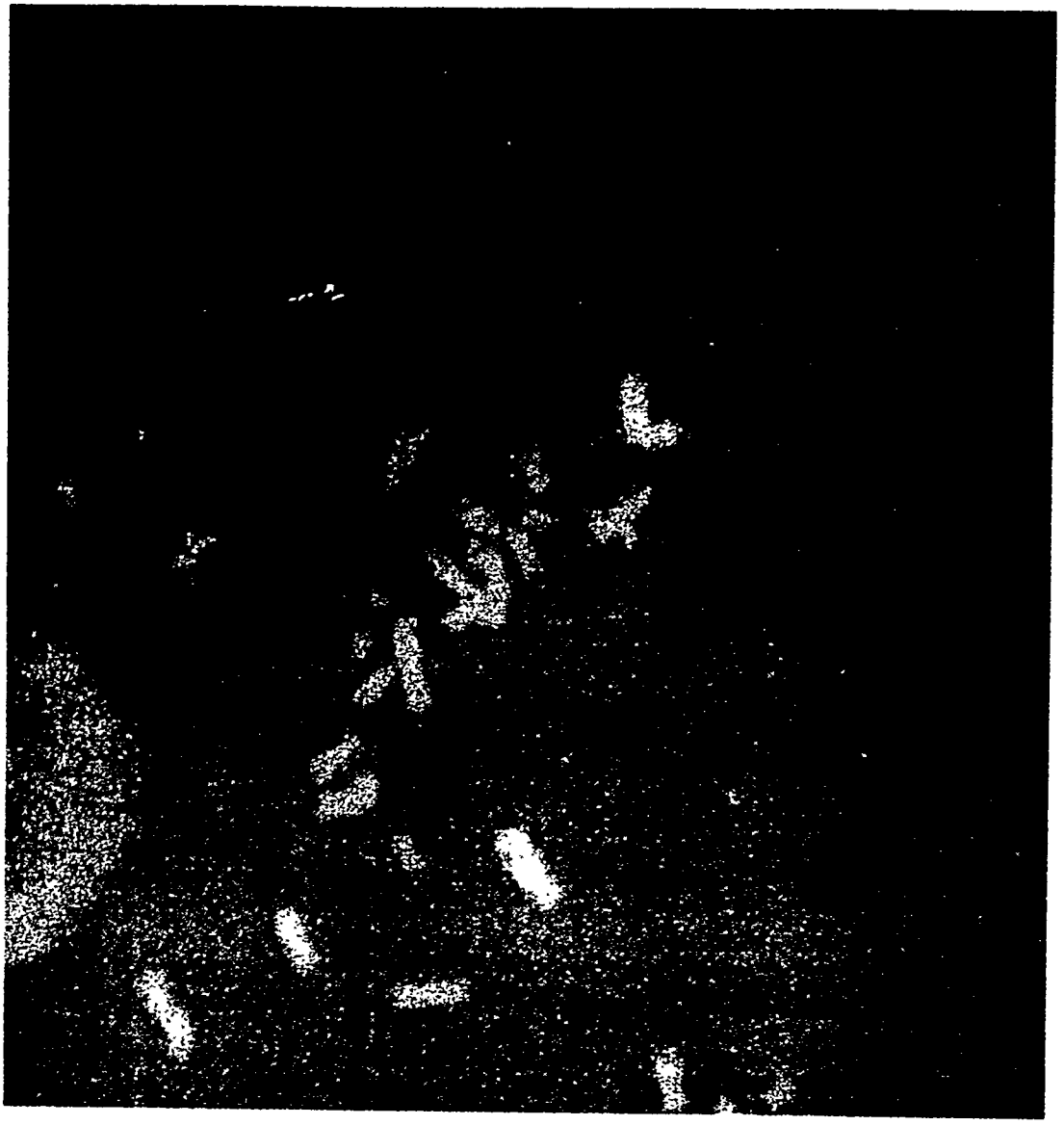

Figure #5: Normal metaphase spread of a biotin/digoxigenin whole chromosome probe for chromosome 4 with one coat of anti-digoxeginin-rhodamine.

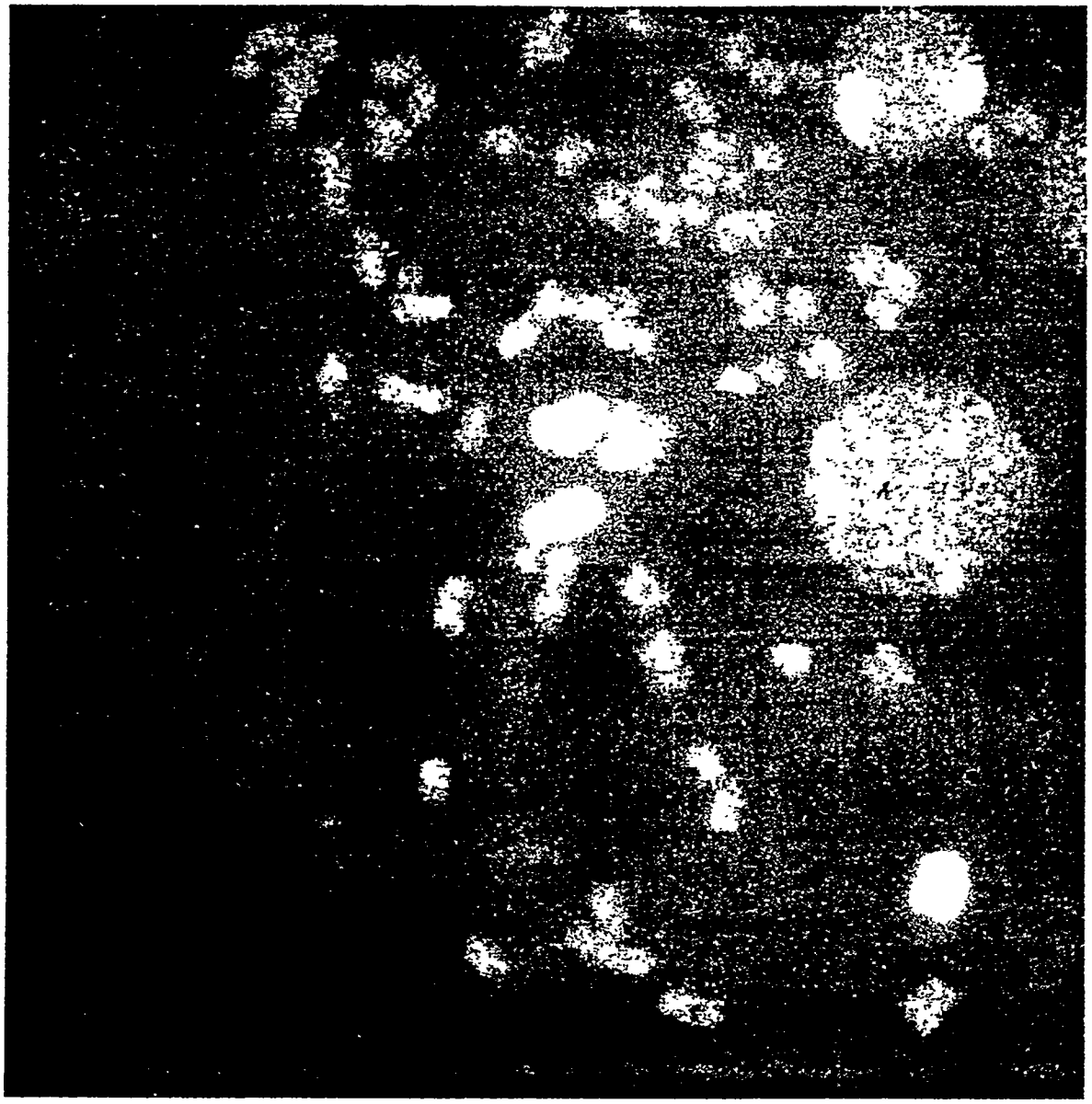

Figure #6: Normal metaphase spread of a biotin/digoxigenin whole chromosome probe for chromosome 4 with one coat of avidin-FITC and one coat of anti-digoxeginin-rhodamine.

UCRL-ID-

Production of Hydrogen from Municipal Solid Waste

Sherrell L. Coleman
Tuskegee University

May 10, 1995

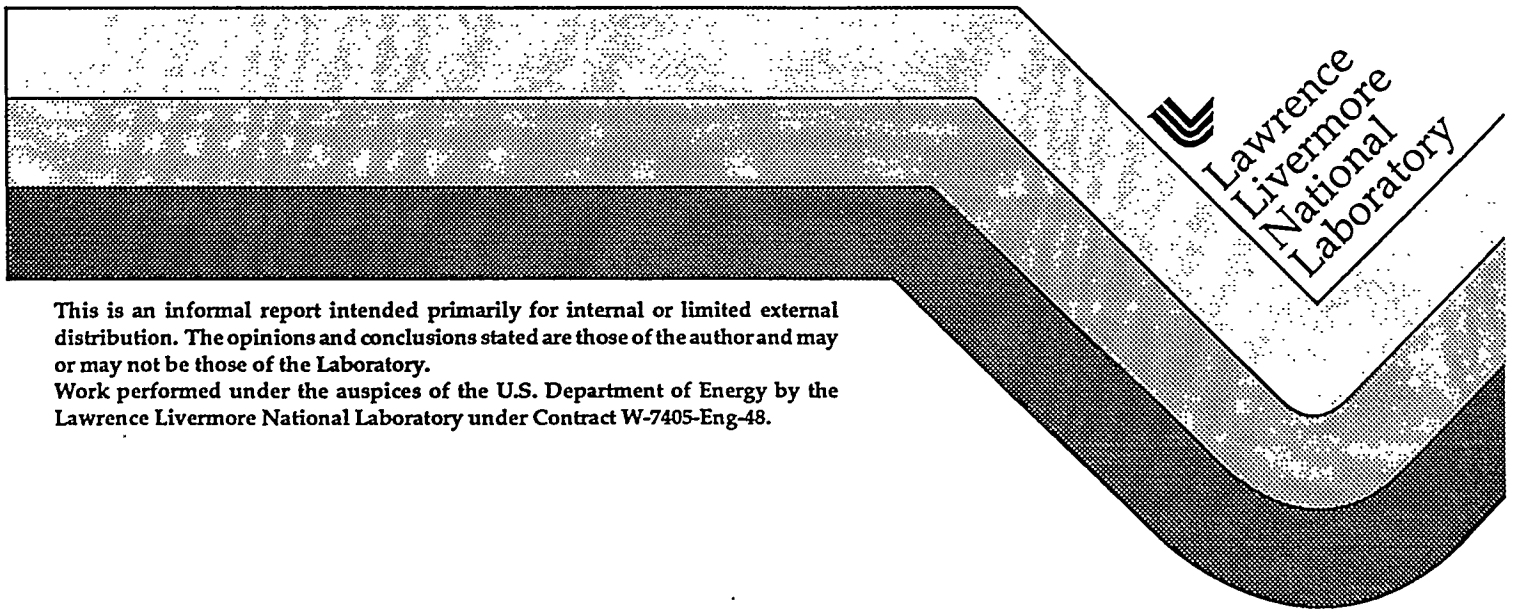

ABSTRACT

Lawrence Livermore National Laboratory, along with Texaco are developing a physical and chemical treatment method for the preparation and conversion of municipal solid waste(MSW) to hydrogen by gasification. Paper is one of the primary components of MSW. Preliminary work has shown that different paper grades produce different results, with low-quality paper forming better slurries than high-quality papers. This study deals with a systematic study of low-quality paper dunnage. The treatment process currently being explored is a hydrothermal treatment process that utilizes high pressure water to cause chemical breakdown of the organic material. Batch reactors have been used to determine product yields as a function of hydrothermal treatment conditions. Various ratios of water-to-paper ranging from 1 to 10 were used to determine solid product, gas product, and soluble product yields of MSW. The process variables examined included temperature, time, and water to paper ratio. Temperature had the strongest effect on product yields; the higher the temperature the lower the solid product residue. A temperature of 275^{o}C and a time of 30 minutes yielded 55% of solid residue, and at 2 hours a residue of 52%, mediating little influence of increased reaction time beyond 30 minutes. Water to paper ratios ranging from 1 to 10 showed constant product yields .

INTRODUCTION

The hydrothermal pre-processing scheme for Municipal Solid Waste (MSW) produces a slurry product that has a high fuel content and can be pumped in a Texaco gasifier. Hydrothermal treatment of (MSW) is a process for producing a gasificable slurry from raw MSW by using high pressures of steam. A potential energy source, MSW is composite of organic materials like

paper, wood, and food waste. The organic materials are composed primarily of carbon, hydrogen, and oxygen. Hydrogen can be produced from the MSW-based slurry by using high temperature gasification and processing of syngas. Also, use of MSW reduces the volume of material being deposited into landfills. The entire process provides renewable energy while improving our environment.

LABORATORY SCALE EXPERIMENT

Objective

The objective of the bench-scale laboratory work has been to establish operating conditions for a hydrothermal pre-processing scheme for municipal solid waste(MSW) that produces a good slurry product for conversion in a Texaco gasifier. A "good" slurry is one that can be pumped and atomized in the gasifier, and that has a high fuel content leading to a high yield of hydrogen.

Experimental Approach

140ml autoclave reactors were used for the bench-scaled work. Fig.1, shows a schematic of the experimental approach. In the figure the content of the autoclave reactor is shown before and after processing. The procedure was to load the reactors with the solid and aqueous-phase charge, heat the reactor externally in an electrically heated oven, cool down the reactor and unload for chemical analysis on the product. The internal reactor temperature and pressure were recorded during the heating, reaction and cool-down phase. After the cool-down the weight of the reactors and the charges were recorded.

Fig.1: Experimental Apparatus

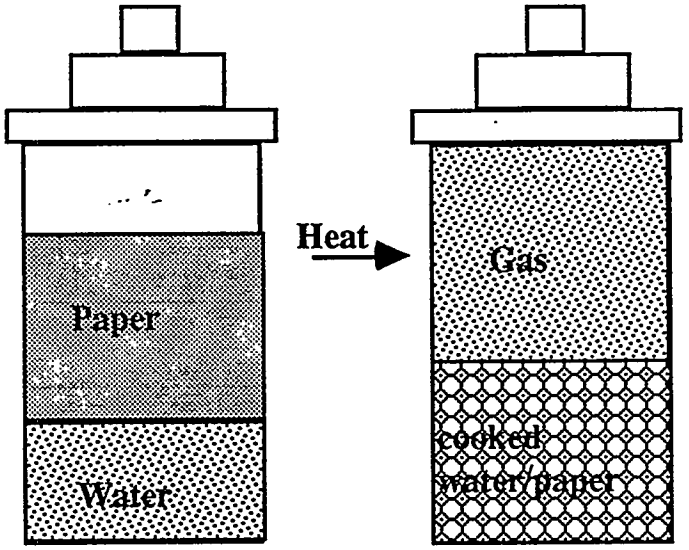

Reactor before the cook. **Reactor after the cook.**

The time that it took for the reactor to reach temperature was about 2 hours. Reaction times of 30 minutes or 2 hours were then counted from the time the internal temperature reached a temperature within 10°C of the desired temperature.

Various procedures were used to evaluate gas product, soluble product, and solid product yields. The gas yield was determined by allowing the product gas to fill an evacuated 1-liter volume at room temperature and recording the final pressure. Gas composition was determined by mass spectrometry. The water-soluble organic yield was determined by organic carbon analysis of a water sample along with the assumption that the composite soluble material had the same stoichiometry as the starting material (paper dunnage). The solid yield was determined by filtering the solids and drying the dried solid material in a vacuum oven to a constant weight.

Slurries were prepared from either the wet solid material (containing water and solubles) or from the dried solid material by adding back the separated water, and shearing the resulting mixture in a food processor (Quisinart). Several minutes in the food processor were adequate to liquefy

the material. It is believed that longer shearing time would not significantly change the mixture viscosity but formal measurements were not done to substantiate this observation. Viscosity measurements of these slurries will be carried out as part of the continuation of this project.

Yield Results

A number of tests were done with different water to paper ratios. These are summarized in Table 1. The results in Table 1 show: mean value, sum, solid product, gas product, and soluble product yields. This particular experiment was run at a temperature of 275°C, pressure of 2000 psi, and a time of 2 hours. The same paper dunnage was used through out the experiments reported in this paper. Table 1 shows that even at the same temperature and the same pressure the higher the water to paper ratio the more solid product yield.

Table 1.

Water/paper	Solid Prod. %	Gas Prod. %	Soluble Prod. %	Sum %
1:1	53	15.9	N/A	N/A
2:1	47.2	11.4	N/A	N/A
3:1	65.5	11.5	17.3	94
4:1	52.0	15.3	19.4	87
10:1	41.7	(30.6)	24.3	97
Mean value:	**51.9**	**13.5**	**21.9**	**87.3**

The yield results are summarized in Table 2 for a paper dunnage. This table shows the yield results of our most recent experiments.
The paper dunnage is composite of tailings from paper mills. With higher water to paper ratios the concentration of the gas product yield dropped proportionally resulting in a constant soluble yield for water to paper ratio in the range of 1 to 10. Most experiments in Table 2 were conducted at a water to paper ratio of 2 except for the last row which is the average of results obtained with ratios 1, 2, 3, 4, and 10. To interpret this further, the water to paper ratio of 1 appears sufficient to "wet" the solid reactant and that any extra water merely acts as a diluent.

Experiments were conducted with temperatures ranging from 260°C to 310°C and reaction times of 30 minutes and 2 hours. We found that a temperature of 275°C and a reaction time of 30 minutes produce a solid residue yield of 55%. The amount of residue dropped to 52% when the cooking time was increased to 2 hours. Therefore, an increase in cooking time from 30 minutes to 2 hours appears to have only a marginal effect on the yield structure.

Table 2. Product yields (wt% feed)

Feed material	Cooking Conditions	Solid Residue Stoich. (m.a.f.)	Solid Residue (incl. ash)	Soluble Product	Gas Product (mostly CO_2)	Water by balance
Paper dunnage, $CH_{1.66}O_{0.72}$						
	260°C, 30 min.	$CH_{1.00}O_{0.26}$	61	16	12	11
	275°C, 30 min.	$CH_{0.97}O_{0.23}$	55	17	12	16
	310°C, 30 min.	$CH_{0.94}O_{0.17}$	48	17	17	18
	320°C, 30 min.	$CH_{0.83}O_{0.13}$	50	16	16	18
	275°C, 2 hours*	$CH_{1.10}O_{0.32}$	52	22	14	12
	310°C, 2 hours	$CH_{0.93}O_{0.16}$	45	17	17	21

*** Average for water/feed ratios of 1, 2, 3, 4, and 10**

The solid fraction is around 50% at the higher severity increasing to 60% for the lowest temperature of 260°C. The paper dunnage at a temperature of 275°C produces acceptable conversion. The gas yield responds to increasing temperature with a slight increase: It is 12% at 260°C and 16% at 320°C. The gas is approximately 90% CO_2, 5% CO with a balance of minor components such as H_2, CH_4, and higher hydrocarbons.

Conclusion

From the results to date, we concluded that temperatures on the order of 300°C and pressures up to 2500 psi result in significant breakdown of paper dunnage and the production of a slurry suitable for gasification. Water/paper

ratios ranging from 1 to 10 were found to have no significant effect on the process. A reaction time of 30 minutes appeared adequate to produce the required slurry. Slurries produced for material held at reaction temperature for 2 hours appeared to give similar results to there using only a 30 minute reaction time.

Acknowledgments

I want to thank Henrik Wallman for his guidance in helping and teaching those things that were new to me. Also, Chuck Thorsness for being my mentor. I'm very glad that I had the opportunity to work with the both of you. Being here has truly been a stepping stone in my life. Thanks!

References

Wallman, P. Henrik "Laboratory Studies of a Hydrothermal Pretreatment Process for MSW" Department of Chemistry and Material Science, LLNL,1995

Integrating EDI into LLNL's Procurement System*

Nicholas H. Collins III

1Louisiana State University

Lawrence Livermore National Laboratory
Livermore, California 94550

May 10 1995

Prepared in partial fulfillment of the requirements of the Science and Engineering Research Semester under the direction of Kevin White, Research Mentor, in the Lawrence Livermore National Laboratory.

*This research was supported in part by an appointment to the U.S. Department of Energy Science and Engineering Research Semester program administered by LLNL under Contract W-7405-Eng-48 with Lawrence Livermore National Laboratory.

Integrating EDI into LLNL's Procurement System

Nicholas H. Collins III
Louisiana State University
Information Management Division

ABSTRACT

The Information Management Division (IMD) at LLNL is developing a new purchasing system for the Procurement Department. The first major development of this new system is called, "Total On-line Purchasing System" (TOPS). TOPS will help speed up the requisitioning process by having requisitions electronically entered by requesters and electronically sent to buyers to be put on purchase orders. The new purchasing system will use Electronic Commerce/Electronic Data Interchange (EC/EDI) to help increase transaction flows for shipping notices, RFQ's, Quotes, Purchase Orders, Invoices, and other procurement related transactions. This paper first describes what EDI is and then discusses the different options involved in integrating EDI into LLNL's Procurement System.

Definition of EDI

Electronic Data Interchange (EDI) is the electronic exchange of routine business transactions between two trading partners in a computer processable format using an agreed upon standard. These business transactions range from health care claims to purchase orders. A computer processable format means that the information can only be deciphered by a computer application, rather than a person. Before exchanging EDI transactions, trading partners must agree on a standard in which to send the information.

A standard is needed in order for a transmission from one computer application to be accepted by a different computer application. There are many EDI standards, but the two most popular are: EDIFACT and ANSI ASC X.12. EDIFACT is supported by the United Nations for international trade. ASC X12 was developed by the American National Standards Institute (ANSI) and is used mainly in the United States.

There are typically four requirements for EDI. These are: integrity, authenticity, non-repudiation of originator, and non-originator of recipient. First, the message must have integrity. In other words, it must confirm to a standard. Second, it must have authenticity, which means that the message must be real and genuine. The message must also ensure the non-repudiation of the originator and the non-repudiation of the recipient. This means that the message can prove who it came from and who it is being sent to, so that the sender nor the receiver cannot deny ever possessing the message.

Benefits of using EDI

The two most important benefits of using EDI are that it saves time and money. The EDI process is paperless. When a buyer keys in his or her information into their computer application, this is the

very same information that will populate the receiver's database. The data does not have to be rekeyed, therefore, saving time for processing and costs for labor. Since the information is sent electronically, there no longer is the need to use the postal system. This saves the time for the transaction to go through the postal system and the costs for postage, labor, and paper materials.

Using EDI also reduces the possibilities of producing errors. The data is only entered in one time, by the requester, as opposed to being rekeyed numerous times while being processed. Thus, chances of errors occurring are greatly reduced. This would also prevent time delays due to possible errors and prevent dissatisfaction between trading partners.

EDI allows a competitive advantage between suppliers. Many large businesses are integrating EDI into their businesses. When these businesses look for trading partners, they will seek trading partners that are also EDI capable. In addition, EDI exposes buyers to many more suppliers, including small businesses, which increases competition. How EDI allows interaction between these trading partners is described later.

Using the X12 Standard

There are three major parts to the X12 transmission. Figure 1 illustrates the relationship between the different X12 parts. The ST/SE envelope is the Transaction Set envelope. This contains an actual transaction such as an invoice or a shipping notice. The Transaction Set is divided into many parts called segments that describe the transaction. The GS/GE envelope is called the Functional Group envelope. This contains information such as date and time, standard code, version number, and the number of Transaction Sets contained. The GS/GE envelope groups together related Transaction Sets. The ISA/IEA envelope is the Interchange Control envelope. This contains information such as the segment terminator, element

separator, sender and receiver codes, and number of Functional Groups contained.

Each transaction used in X12 is assigned a transaction identifier number. This ID number is used in the Transaction Set Header to let the translator know how to translate the data. For example, an 850 is a Purchase Order, an 810 is an Invoice, and an 843 is a Quotation.

Some transactions are used to check that other transactions are received. A 997 is a Functional Acknowledgment (FA). This is sent automatically by the receiver's system to let the sender know that a transmission was received and translated without problems. However, some transactions have their own acknowledgments. One such is the Purchase Order (850), which has the Purchase Order Acknowledgment (855).

In Figure 2, the buyer begins the exchange by sending an 840 (RFQ). Many suppliers receive the RFQ and send an 843 (Quote) back to the buyer. A 997 (FA) is used after each of these transmissions. The buyer then sends an 850 (PO) to the desired supplier, and the supplier responds with an 855 (PO Ack). After this, an 856 (ASN) and an 810 (Invoice) are sent to the buyer. There are many other transactions that are possible in this type of exchange, such as: PO Change (860) and Order Status Inquiry (869).

How EDI Works

The translator is very important when using EDI. For outbound transactions, an EDI translator converts flat files into EDI standard documents, such as X12. For inbound transactions, the translator converts the EDI document into a flat file to be used by a computer application. A mapping tool creates mappings to be used by the translator to make the file conversions.

First, the translator converts the flat file, produced by an application, to an EDI document. A protocol electronically delivers the EDI document to a trading partner. The protocol used usually depends on the type of connection between the two trading partners.

The different types of communication connections are described later. When the receiver's translator receives the document, it converts the document into a flat file once again to be used in an application. If there is an error during the translation, the 997 will report these errors to the sender.

EDI Communication Connections

There are basically three types of EDI connections. These connections are direct, Value-Added Network (VAN), or Value-Added Network Hub. Any of these connection types may be used to connect to trading partners. However, some connections are better than others for different EDI users. This is described below.

Direct Connection

A direct connection is a dedicated line established between only two trading partners without using a third party. Figure 3 shows an EDI direct connection. This connection is very secure and private. The only cost is the length of time that the communication takes. Both partners must have the same transmission speeds. A direct connection is good for businesses that have only few EDI trading partner, but as the business adds more trading partners, direct connections become more difficult to maintain. For instance, the trading partners must agree upon times when they will transmit EDI messages to each other.

VAN Connection

These are third party networks that provide services to EDI trading partners. Figure 4 is an example of a VAN connection. The services include: protocol conversions, standard conversions, version conversions, archiving, and mailboxing. For businesses with many EDI partners, these services are very useful.

When a seller sends an 840 (RFQ), it is received by the VAN and forwarded to the mailboxes of the suppliers that are registered in selling that item. After the 840 has been retrieved by the suppliers, they then send their 843's to the buyer's mailbox on the VAN.

The usual costs of connecting to a VAN include: a monthly charge and a charge per transaction, per segment, or per 1000 characters. These charges apply to outbound and inbound transmissions. A VAN also specifies peak and off-peak hours to send transmissions. It is less expensive to send EDI documents at off-peak hours. Some VAN's may also charge enrollment charges, storage charges, and interconnect charges. An interconnection is a connection from one VAN to another.

Translation, mapping, and communication software is also needed to perform EDI with a VAN. This software ranges from $4,000 to $10,000 for a PC and from $16,000 to $30,000 for a UNIX machine. The difference in prices for each platform are due to training and software capabilities such as GUI, audit trails for tracking documents. PC's are typically used for businesses that have a low volume of transactions each day, but a UNIX machine is preferred for businesses with a high volume of transactions every day.

VAN Hub Connection

Instead of connecting to a VAN, a large business may choose to connect to a VAN Hub. A VAN Hub is a network with connections to more than one VAN. This is useful if a business has trading partners on different VAN's. Using a VAN Hub also increases the number of potential trading partners that one may have. One such VAN Hub is GATEC (Government Acquisition Through Electronic Commerce), which is the VAN Hub developed at LLNL.

GATEC VAN Hub

Currently, GATEC is connected to eight VAN's. These VAN's do not charge GATEC for their use. Instead, a VAN benefits by charging their users, the suppliers on their VAN, for receiving any transactions from their trading partners. By connecting to GATEC, a VAN increases the number of trading partners that can exchange EDI transactions with their users. Therefore, this increases the potential amount of transactions to a VAN's users. Figure 5 shows the GATEC VAN Hub.

GATEC uses the ASC X.12 standard. Currently, GATEC uses only six transaction sets from X.12 version 3010 and two transaction sets from X.12 version 3020. The mappings for these transaction sets are created by GATEC and distributed to the buyer sites connected to GATEC and to the registered vendors on the connected VAN's. Versions 3010 and 3020 are relatively old versions of X.12. In order for GATEC users to be able to use a newer version of X.12, GATEC would have to update all of their mappings. This could take as long as two or three months. Also, the VAN's must be notified in advance of a version change.

GATEC uses the Simple Mail Transfer Protocol (SMTP). This is an Internet protocol. When the EDI translator translates a flat file into an EDI ASC X.12 document, the X.12 document is put inside of a SMTP envelope and electronically mailed to GATEC. GATEC then reads the SMTP envelope address, and forwards it to the VAN of their trading partner.

LLNL Procurement and GATEC

Considering all EDI connection types, the GATEC VAN Hub is the best solution for the LLNL Procurement System. Since LLNL has many trading partners, a direct connection to all of these trading partners is not sensible. A VAN connection to these trading partners

would be expensive to maintain considering the number of transactions that LLNL may be sending and receiving. A VAN connection would also require LLNL Procurement to purchase EDI software.

The integration of EDI into the LLNL Procurement System is just beginning. The Procurement System will not use GATEC as other buyer sites use it. Instead of electronically mailing an ASC X.12 document, Procurement will mail only the flat file created by the computer application. When GATEC receives the flat file, GATEC will translate it into an X.12 document and electronically mail it to the vendor or the VAN of the vendor. However, the flat file must be a specific format in order for GATEC to translate it successfully. Boise Cascade is the vendor that LLNL will be testing EDI transactions with. It is expected that LLNL will be sending EDI documents through GATEC to Boise sometime this July.

References

Kevin White, Lawrence Livermore National Laboratory/Information Management Division

Ted Cole, Lawrence Livermore National Laboratory/GATEC

John Rhodes, Lawrence Livermore National Laboratory/GATEC

Schematic of an EDI Transmission

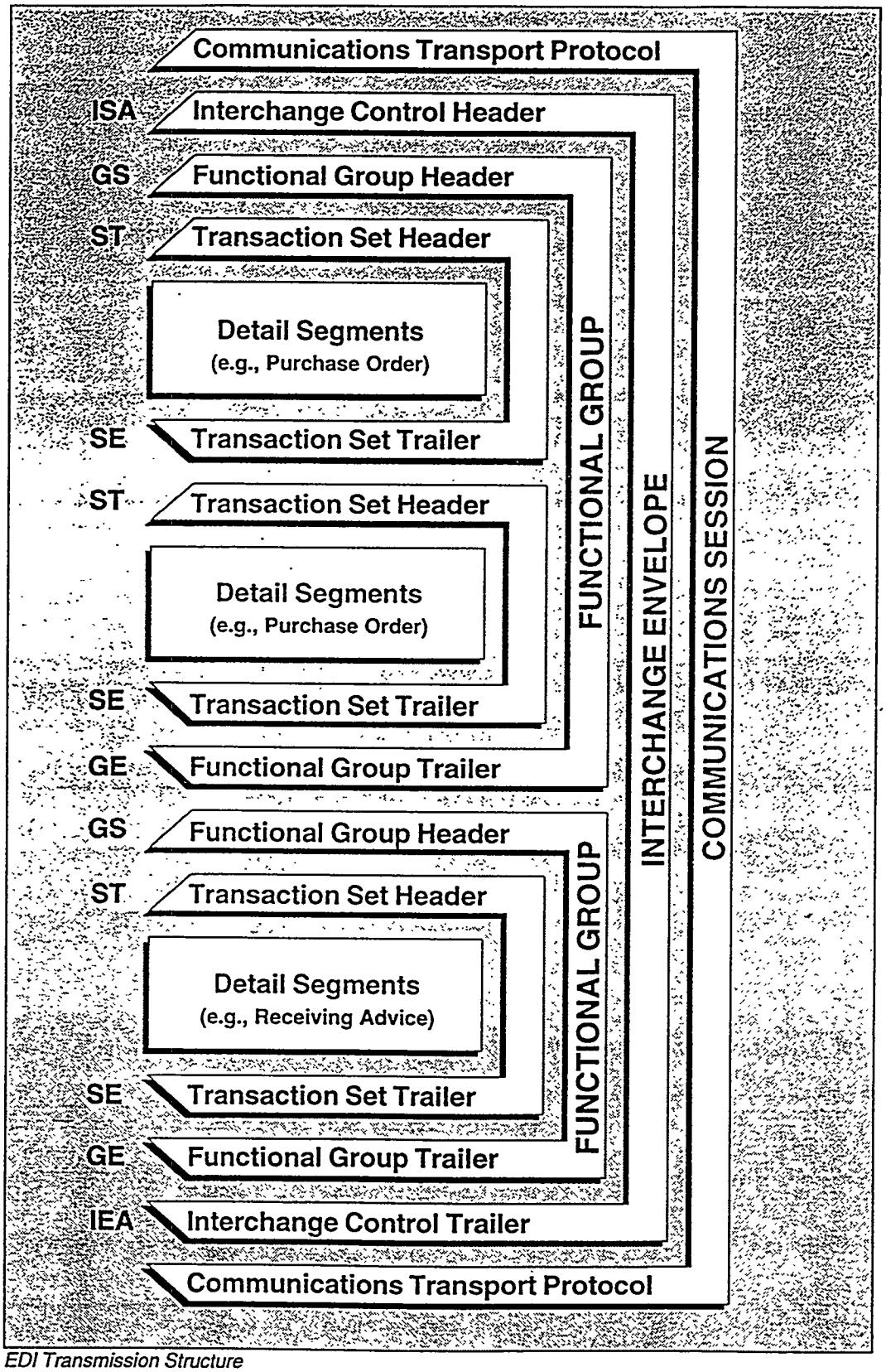

EDI Transmission Structure

Fig. 1

Using EDI with X12:

Buyer	Seller	Transaction Name
840 →		[Request for Quotation]
←	843	[Quote]
850 →		[Purchase Order]
←	855	[PO Acknowledgement]
860 →		[PO Change]
←	865	[PO Change Acknowledgement]
←	856	[Advance Shipment Notice]
←	810	[Invoice]
869 →		[Order Status Inquiry]
←	870	[Order Status]
820 →		[Payment Order] with banks
820 →		[Remittance Advice]

Fig. 2

Direct Connection

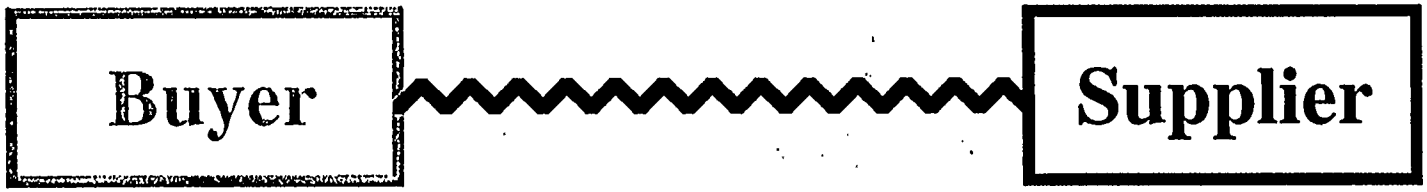

Fig. 3

VAN Connection

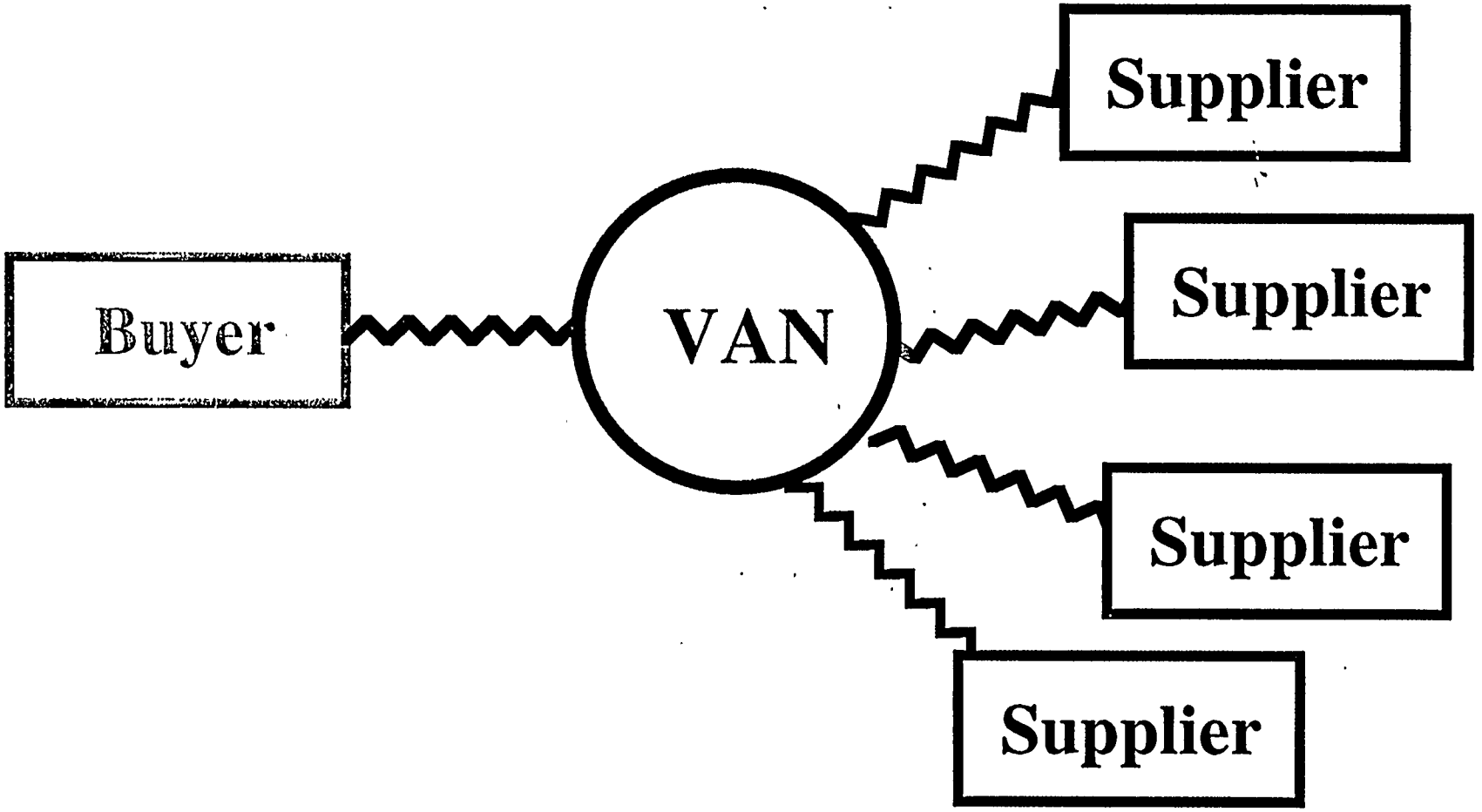

Fig. 4

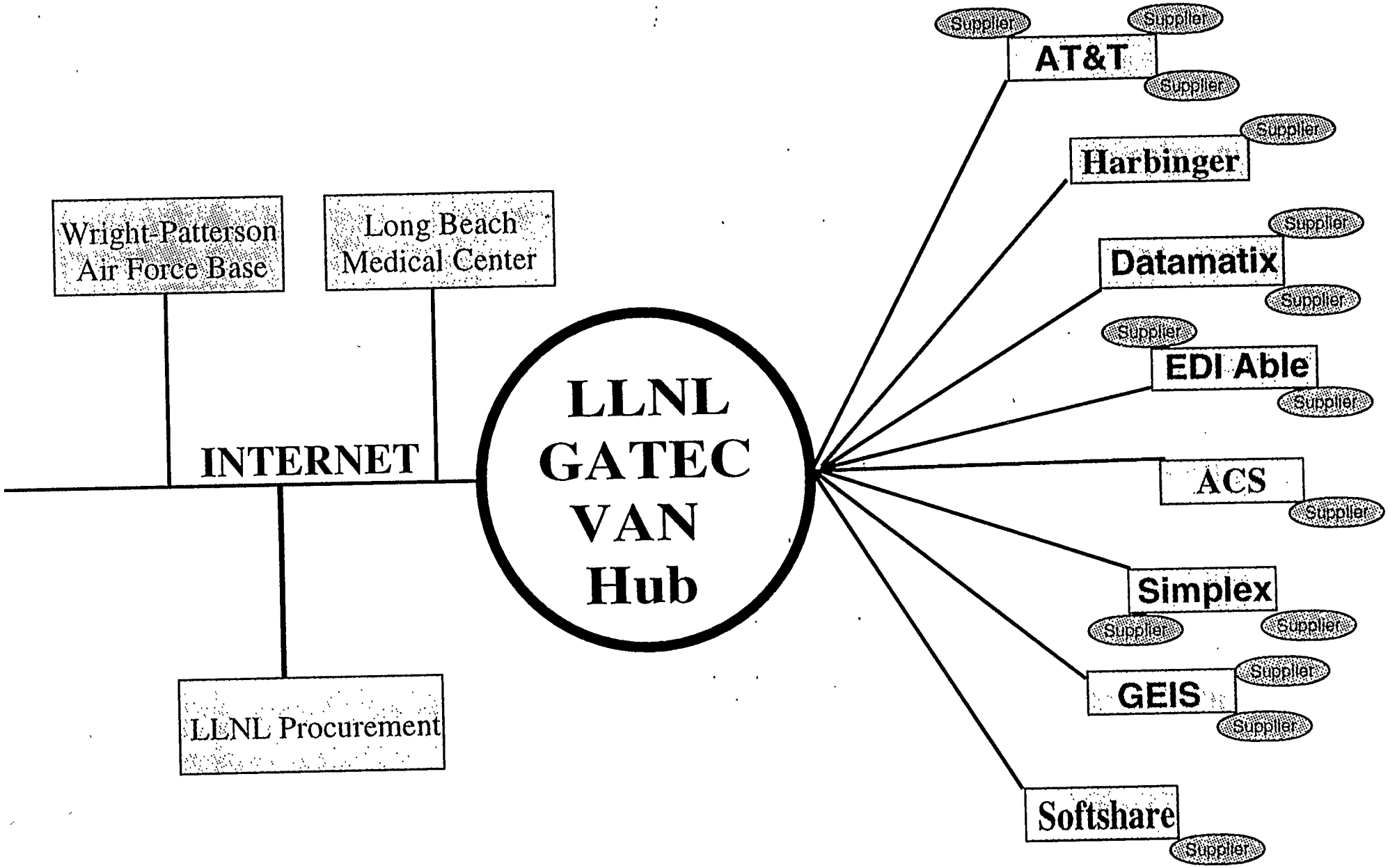
Wright-Patterson Air Force Base
Long Beach Medical Center
INTERNET
LLNL Procurement
LLNL GATEC VAN Hub
AT&T
Harbinger
Datamatix
EDI Able
ACS
Simplex
GEIS
Softshare
Supplier

Fig. 5

Micropower Impulse Radar Imaging and Its Applications

Michael S. Hall
New Jersey Institute of Technology

Science and Engineering Research Semester
May 10, 1995

Abstract

The Lawrence Livermore National Laboratory (LLNL) has developed new radar and imaging technologies for use in the analysis of civil structures (bridge decks and building foundations) and the detection of buried mines. These new systems use a patented ultra-wide band (impulse) radar technology known as *Micropower Impulse Radar* (MIR) imaging. MIR can be easily assembled into arrays that form ground penetrating radar (GPR). The radar has the ability to provide high-resolution 2-D and 3-D imaging of changes in the embedded material electrical properties. It transmits electromagnetic waves which penetrate most dielectric material such as soil, wood and concrete. The MIR module is lightweight, self-contained and constructed at low cost from commerically available compnents ranging from $10 - $15. Tests have shown that the MIR system has the ability to detect both metallic and plastic mines buried at depths of 5 to 10 cm in moist soil, and up to 30 cm in dry soil.

TABLE OF CONTENTS

I. INTRODUCTION

Pulse radar systems have been in operation for more than forty years. LLNL has developed a new pulse radar called the *Micropower Impulse Radar(MIR)*. The significance of this technology lies in it's cost-effectiveness. Stephen Wampler of the LLNL Newsline writes, "The Micropower Impulse Radar does for $10 to $15 in off-the-shelf components, the same tasks that formerly required equipment that today costs $40,000." This reduced cost factor will widen the scope of the radar's applications. For example, car manufacturers have made plans to incorporate the radar chip into automobile safety systems.

Our focus has been to use the MIR as ground penetrating radar (GPR) a form of pulsed radar. Coupled with LLNL's own 2-D and 3-D computer algorithms, these new technologies prove themselves powerful tools for mine detection and civil structure analysis. This analysis involves locating embedded structural components such as reinforcement bars, conduits, beams, columns, cables and enclosures within various materials (concrete, asphalt, wood, etc.) . In practice, structures such as bridges and phone polls could be tested for cracks ,voids, stress fractures or overall damage to their strength and integrity.

This paper explains the basic concept behind the MIR's technology; discusses its advantages over existing GPR systems. Testing procedures and results are also included.

II. THEORY

2.1 FUNDAMENTALS

The concept behind MIR is measuring radar target range. The radar transmits a known electromagnetic signal into a region of interest. It then records the echoed signals caused by reflections or scatterings of incident signals on interfaces. Interfaces are boundaries that have different dielectric constants and/or conductivities. The echoes are sent through an analog to digital converter where signal processing software calculates the position of that boundary. Next, scaled 2-D and 3-D images are produced of the region scanned. The resolution of multiple scatters is a major problem radar systems have to overcome. The solution is in the signal's pulse width. Narrower transmitted pulses keep scattered signals from overlapping to the degree that echoes are indistinguishable. The MIR generates pulse widths of approximately 100 picoseconds.

2.1-1 Time-delay

The MIR operates as a monostatic radar. A monostatic radar couples its transmitter and receiver into one unit. The most important factor for radar's of this type is the use of time-delay. The range is defined as,

$$R = v\,dt / 2 \qquad (1)$$

where v is the velocity of the incident signal in a particular medium (note: an electromagnetic wave travels at $c = 3*10^8$ m/s in air). The dt represents the time delay. Dividing by two accounts for the round-trip travel of the incident and reflected

signal. Non-homogeneous material will yield erroneous results if not taken into consideration before-hand.

Each echo recorded by the receiver is a rescaled and time-shifted version of the transmitted signal. A reference point on the pulse can be used to calculate the time-delay. The point can be located on either the leading or trailing pulse's egde. A peak at the time delay will be produced by correlating the echoed and transmitted signals.

The signal a the receiver can be represented mathematically as a linear combination of the scaled transmitted pulses, p(t). With t corresponding to the time-delay of the echo,

$$r(t) = \text{integral } \{c(t)p(T-t)dt\} \qquad (2)$$

where, c(t) is a coeffecient representing losses due to attenuation or scattering during propagation. Correlation of the echoed signal with the transmitted pulse results in,

$$r_c = \text{integral } \{c(t)R_p(T-t)dt\} \qquad (3)$$

Rp is the autocorrelation function of the transmitted pulse. It has a maximum at t=o (Mast, p.7).

2.1-2 Synthetic Aperture

For monostaic radars, a synthetic aperture is formed to gain spatial information using the time-delay profile. The synthetic aperture can be defined as an artificial window, formed by repositioning the radar along parallel lines and scanning a defined area. The objective is to acquire enough data to provide accurate spatial information about the location of embedded objects. This creates an array. Each dot

in figure 2.1 represents a repositioned line. At a given position the radar transmits a pulse and records echoes for a certain length of time. A space-time plot can be generated of the echoes recorded across the region.

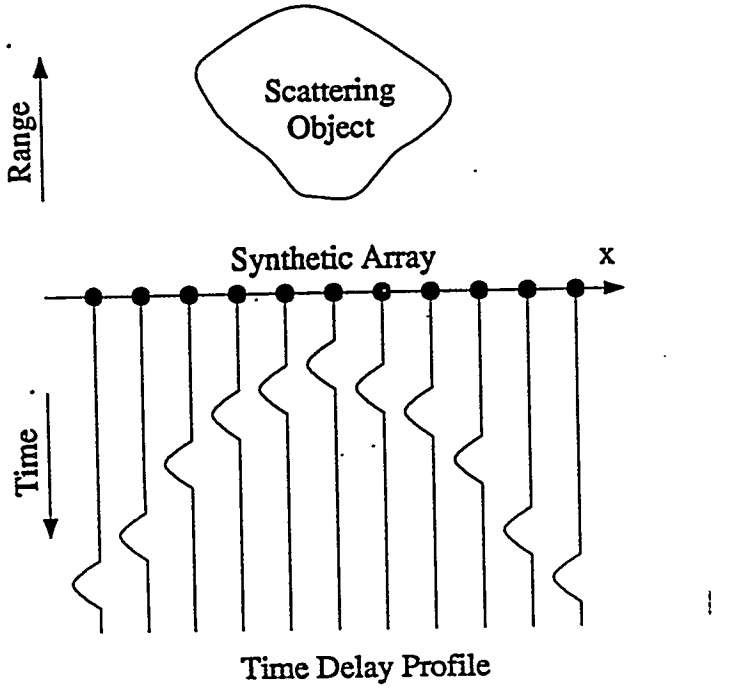

Figure 2.1 Geometry for the synthetic aperture for time delay profile

Two problems affecting Synthetic Aperture Radar (SAR) are range ambiguity and beam width. Reflected signals must not be re-recorded at subsequent positions. If they are how can we resolve echoes with their corresponding transmitted pulses. The rate at which the radar transmits pulses, known as the pulse repetition rate(PRF) must be low enough so that the amplitudes of echoes from previous positions are considered negligible. Figure 2.2 shows that there is a maximum range beyond

which range ambiguity occurs. The PRF for the MIR is set at 1Mhz. The antenna beam width not only determines the region in which the energy of the pulse is distributed but it also defines the directions in which echoes will be received. Furthermore, a wider antenna beam width provides better cross-range resolution. This will be discussed later in the report.

$$R_{max} = vT / 2 \qquad (4)$$

(Hovanessian, p.57).

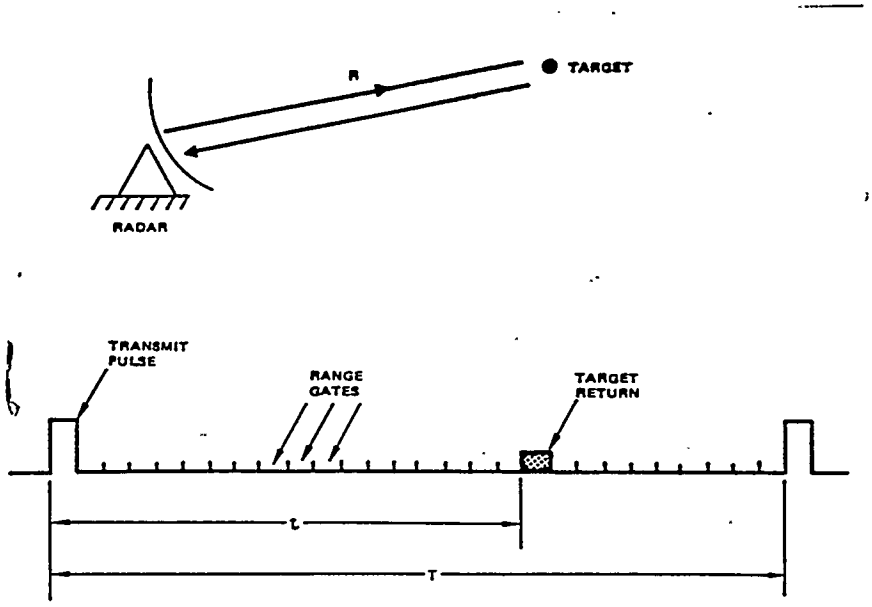

Figure 2.2: Pulse radar range measurement

2.2 Modeling

The time-delay profile recorded across the synthetic aperture will contain the data necessary to reconstruct an image of the embedded objects. We are now interested in using this time domain record to obtain a spatial estimate of scattering

objects by use of wave propagation principles. The following outlines two methods used to reconstruct images.

2.2-1 Inverse Source

The inverse source model is a technique used to form image reconstruction algorithms. The radar transmits an incident wavefield throughout the medium. This wavefield induces charges and currents on the object's surface. These charges and currents oscillate; acting as secondary sources which produce scattering objects. The scattered field is a re-radiated version of the incident wavefield. The wavelength content of the incident wavefield is defined by the relation,

$$\lambda = v / f \qquad (5)$$

where v is the propagation velocity and f is the temporal frequency of the pulse.

As the radar moves along the aperture , a portion of the scattered field is recorded at each receiver position. For monostatic radars, we scale the time-delay to remove the incident wavefield by dividing by two. Using the Fourier Transform's scaling property, scaling in time by one-half corresponds to scaling in frequency by two. Therefore, we can model the effective wavelengths of the secondary sources as,

$$\lambda = v / 2f \qquad (6)$$

As shown in figure 2.3, the radar transmits a modulated square pulse whose spectrum is defined by the sinc function. Most of the energy content of the pulse lies within the main lobe. The bandwidth is defined as $\Delta f = f_{max} - f_{min}$. The resulting secondary sources produce a wavefield made of wavelenths lying primarily in the band of

$$\lambda = v / 2f_{min} - v / 2f_{max} \qquad (7)$$

As shown in figure 2.4, we can expand the model into three dimensions. The synthetic aperture forms two dimension in space and the scattering objects form the third dimension.

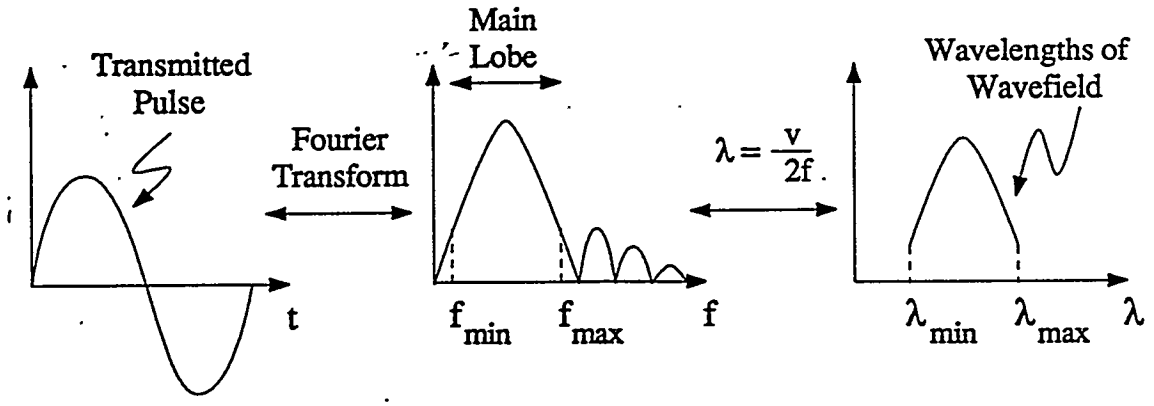

Figure 2.3: Wavelength content of secondary wavefield

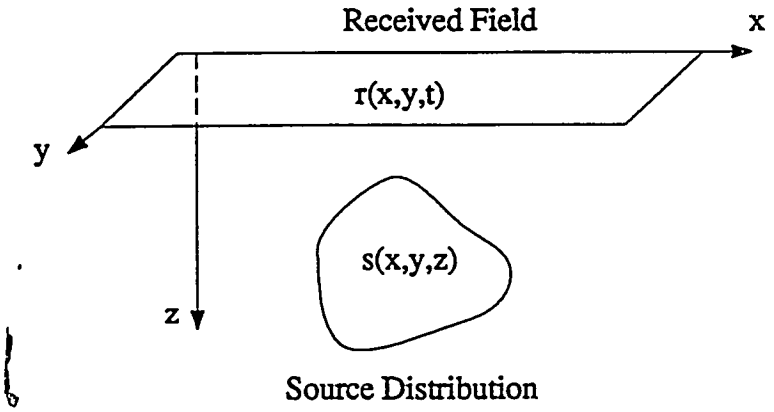

Figure 2.4: Geometry for inverse source model

In computer simulations of this model, we create a three-dimensional array containing some object(s). Each element in the array is assigned a value based upon preset parameters. Next a simulated pulse scans the first layer of the array, checking each element. If something is found a subroutine calculates the time-delay

of the pulse. Based upon the value returned from that element, a pixel of some intensity is placed in to the spatial-temporal array (raw data image). This is repeated over the entire structure. After the array is formed, each pixel is focused to make an image (refer to figure 3.5) (Mast, pp 9-14).

3.2-2 Backward Propagation

The Backward Propagation method is used to reconstruct the source distribution by inverting the forward propagation method(inverse model). The time domain profile is known. Based upon the amplitude and position at each point on the signal where would that translate in the spatial-temporal array. From here the concept of focusing the image remains the same as that mentioned in the previous section.

III. Data Acquisition Methods

For our purposes, the MIR was used as ground penetrating radar(GPR). The following discusses the specifications for the MIR's components and operating parameters. Additionally, testing procedures will be outlined.

3.1 MIR SYSTEM

The MIR system, is highly portable. It consists of three main components : alap-top computert, an analog to digital converter, and teh MIR module. The module itself weighs approximately 0.23 kg (0.5 lb.). Considering that the computer is the heaviest component, the MIR system can weigh as little as 5 pounds.

3.1-1 Specifications

MIR has many operating parameters. A synopsis of these parameters is provided on table 3.1. MIR operates on an ultra-wide bandwidth of 0.8 to 4.0 Ghz. The radar used

The radar used during these test operated at 3.2 Ghz. The rate at which pulses are transmitted, the pulse repetition frequency(PRF), is 1MHZ. The temporal pulse width was set to 100 picoseconds. The beam width of the antenna was 120°; it distributed power along the magnitude of 10^{-6} watts(<100 mW peak).

TABLE 3.1

Input Power	6 to 12 volts, < 1 mA, ~10 hrs on 9V battery
Range (maximum)	up to 10 m in air; 0.2 to 0.5 m in soils (depends on soil conductivity and standoff range)
Transmitter:	
Type	ultra-wide-bandwidth, impulse waveform
Pulse Repetition Frequency	1 MHz
Pulse Width (radiated)	~100 psec
Bandwidth	3.2 GHz (from ~0.8 to 4.0 GHz)
Radiated Power (ERP)	< 100 mW, peak; < 10 W, average
Antenna:	cavity-backed, resistively-loaded monopole
Beamwidth (-3 dB)	120°
Receiver:	
Front end:	
Type	equivalent-time sampler
Bandwidth	> 4.0 GHz
Noise Figure	25 dB
Antenna:	cavity-backed, resistively-loaded monopole
Beamwidth (-3 dB)	120°

3.1-2 Creating Synthetic Apertures

As mentioned earlier in this report, a synthetic aperture is formed by scanning the MIR module over the surface a region of interest. An example of the system being tested is shown in figure 4.1. Here a concrete slab is being analyzed to determine any elements enclosed within it. To obtain two-dimensional we for several one-dimensional scans by incrementing at a fixed Δy until the entire region has been scanned.

3.2 SAMPLING REQUIREMENTS

The echoed signal received through the synthetic aperture contains all of the information needed to reconstruct an image. However, their are constraints placed

on the radar while taking data. The received wavefield is a two-dimensional space-time signal that requires sampling on those dimensions for digital processing.

3.2-1 Temporal Sampling

From the Nyquist sampling theorem,

$$f_s - f_h <= f_h \qquad (8)$$

the temporal sampling of the received field depends on the highest frequency content of the transmitted pulse. The maximum spacing in time samples is

$$\Delta t_{max} = 1 / 2 f_{max} \qquad (9)$$

This may be varied if the energy of the signal is spread over a frequency band of $\Delta f = f_{max} - f_{min}$.

3.2-2 Spatial Sampling

The spatial sampling of the received field is defined by the spacing of the antenna positions when forming the aperture. The spatial sampling depends on the highest frequency component of the received field. This is determined by the highest cutoff of the forward propagation. Because the wavefield is composed of multiple wavelengths, the minimum wavelength determines the highest cutoff. The maximum spacing of the antenna positions is

$$\Delta x_{max} = \Delta y = v * \Delta t_{max} / 2 = \lambda_{min} / 2 \qquad (10)$$

Therefore, both temporal and spatial sampling is dependent upon the highest temporal frequency from the transmitted pulse.

Though spatial sampling is independent of the tow velocity, v_t. There is a maximum speed beyond which the radar is unable to record echoes successfully,

$$v_t = f_s * \Delta x.$$

IV. Imaging Resolution

Though MIR technology has many advantages over existing systems, there are still nonidealities which are inherent to any radar system. Finite apertures, attenuation, medium variation and reconstruction technique are all factors which can affect resolution. However, this report will only address the effects of finite apertures in resolving images. Ideally, an antenna is infinitely small in length having a beam width of 180°. But in practice antennas do have some finite length and subsequently their beam widths are less than 180°.

4.1 RANGE RESOLUTION

The range resolution is dependent upon the temporal width of the transmitted pulse. This dependence is based on the ability to distinguish between two echoes (refer to figure 2.2). The distance two objects can be separated in range which will not produce echoes that overlap is defined as

$$\textit{Pulse Width} = v\,T / 2 \qquad (11)$$

This relation gives an estimate of the range resolution for the MIR system. The relationship between pulse bandwidth and temporal width is

$$T = 1 / \Delta f \qquad (12)$$

4.2 CROSS-RANGE

Cross-Range resolution limit for a finite aperture will be less than for an infinite aperture. Cross-Range resolving capabilities for a single antenna at a fixed zo depends on the width of he main lobe , W, and the beam pattern. The relations for Cross-Range resolution are given on figure 4.1. Note that the maximum range for an

infinite aperture is one-half the minimum effective wavelength. The dot on in figure represent receiver positions. The scatters from an objects will not be seen at all of the positions along the aperture.

Image Resolution Limits

Cross-Range

$L_e < L_s$

$$\Delta CR \approx \max\left(\frac{\lambda_{min}}{2} , \frac{\lambda_{min}}{2 \tan(\theta_b/2)} \right)$$

$L_e > L_s$

$$\Delta CR \approx \max\left(\frac{\lambda_{min}}{2} , \frac{\lambda_{min}\, z_o}{2L_s} \right)$$

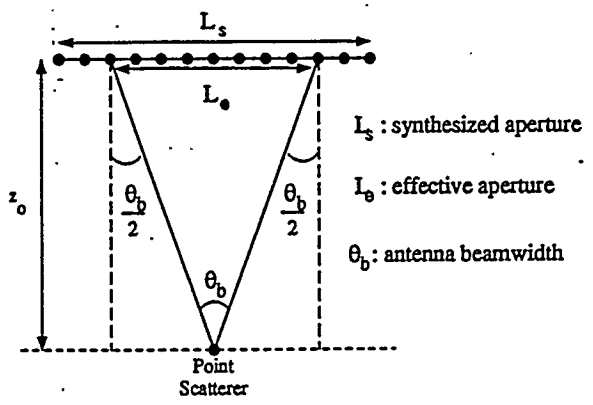

Example:

$\theta_b = 90$ degrees
$f_{max} = 3$ GHz
$v = 3e8$ m/s
$\Delta CR \approx 5$ cm

Range

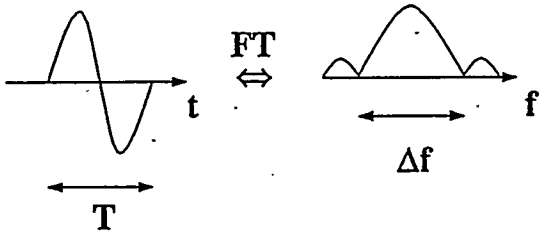

$$\Delta R \approx \frac{vT}{2} \approx \frac{v}{2\,\Delta f}$$

Example:

$v = 3e8$ m/s
$\Delta f = 3$ GHz
$\Delta R \approx 5$ cm

V. Applications

MIR technology will one day have a wide variety of applications ranging from automobile safety systems to healthcare. During my assignment at Lawrence Livermore we were concerned with the radar's use in the analysis of civil structures and the detection of buried mines.

6.1 CIVIL STRUCTURES

When we refer to civil structures we mean things such as bridges, decks and building foundations. MIR has the capability of providing accurate spatial images of embedded objects in mediums such as concrete or asphalt. The California area is highly prone to earthquakes. Recently major damage has been done to bridges and highway systems. Until now the only way to test analyze bridges was to a hole into the structure. MIR will make it possible to evaluate these types of structures in a nondestructive manner. Through using this technology coupled with imaging software an experience observer could determine any cracks, void, decay or damage which may otherwise undermine the integrity of the structure. Figure 5.1 and 5.2, respectively, show the elements of a concrete slab before the pour and the image that was later reconstructed. The data was collectected using a single MIR module to form a 2-D synthetic aperture in the manner described earlier. The radar imaging technology used for the evaluation of bridge decks can be directly applied other underground imaging uses such as mine detection

5.2 Mine Detection

The MIR system has also undergone an array of testing in mine detection. Preliminary results show that the imaging system has the ability to detect both plastic and metallic mines surrogates buried in 5 to 10 cm of moist soil. In dry soil, where the electrical properties of this medium differ, the radar system can detect buried objects at depths of 30 cm or better. Figures 5.3 and 5.4 show the results of tests conducted at the Nevada Test Site(NTS). In this test, two plastic mines, the M-19 and VS-2.2, were buried at various depths. From the imaging of these mines, we can see that they have definite features which will make them distinguishable from rocks or other ground clutter in an actual search.

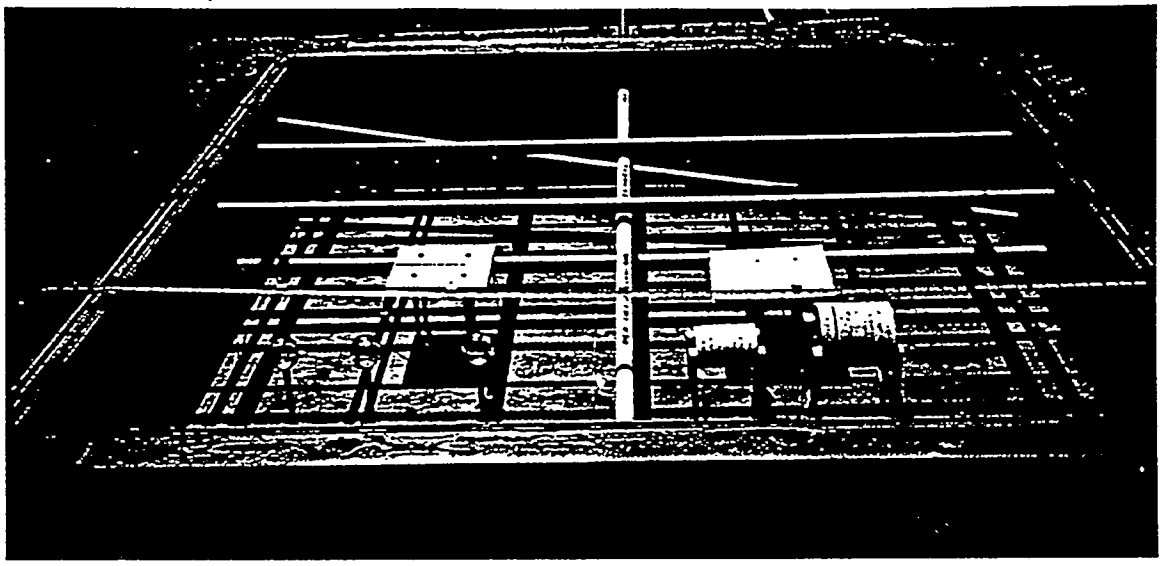

Figure 5.1: Before concrete pour

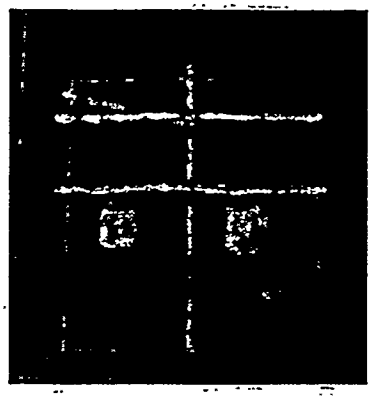

Figure 5.2: Imaging of embedded elements

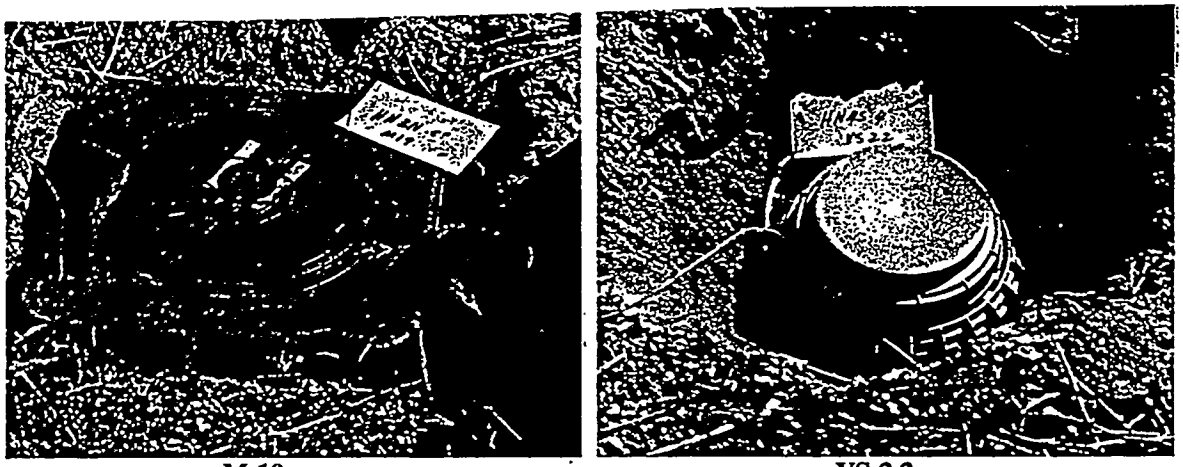

M-19 VS-2.2

Figure 5.3: M-19 and VS 2.2 plastic mines

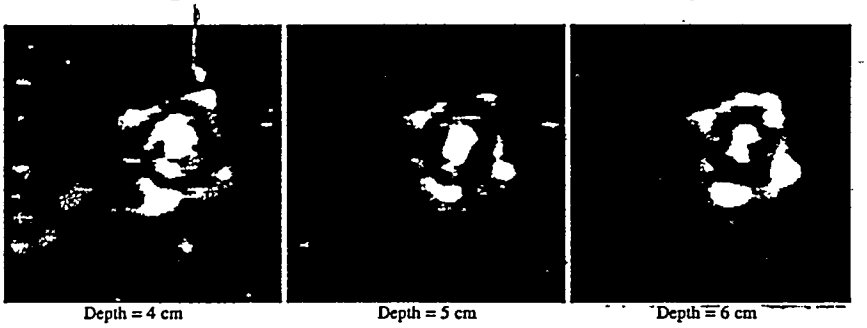

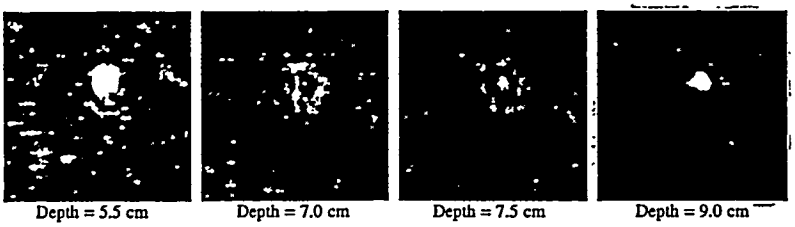

Figure 5.4: Reconstructed Images of mines, M-19 and VS-2.2, respectively

VII. Conclusion

The MIR imaging system is a revolutionary new technology developed at LLNL. It is cost-effective; consisting of off-the-shelf components ranging in price from $10-$15. The system is highly portable. It can easily be assembled into arrays that form synthetic apertures which provide 2-D and 3-D imaging capabilities. The radar system employs the use of the inverse source or backward propagation algorithms to provide high-resolution imaging. And though it has many advantages over existing systems in use today, there remain limits to its imaging resolution. However, MIR technology will soon have extensive use as an effective means to nondestructively analyze civil structures and accurately detect buried mines.

REFERNCES

[1] J. E. Mast, *"Microwave Pusle-Echo Radar Imaging For the Nondestructive Evalution Of Civil Structures"*. Univ of Illnois, Urbana: 1993.

[2] S. A. Hovanessian, *Introduction To Sensor Systems.* Norwood, MA: Artech House,INC., 1988.

[3] H. W. Cole, *Understaning Radar.* Cambridge, MA: Blackwell Scientific Publications, Inc., 2nd ed., 1992.

[4] D.K. Cheng, Field and Wave Electromagnetics. New York:Addison-Wesly Publishing Company Inc, 2nd ed., 1992.

[5] R.E. Ziemer, W.H. Tranter, D. R. Fanin, Signal and Systems: Continuous Discrete. New York: Macmillan Publishing Company, 3rd ed., 1993.

Assessment of Automobile Accessories

Marvin Jackson

Fort Valley State College

Energy Program
Lawrence Livermore National Laboratory
Livermore, California 94551

May 1995

Prepared in partial fulfillment of the requirements of the Science and Engineering Research Semester under the direction of J. Raymond Smith and Salvador Aceves, Research Mentors, in the Lawrence Livermore National Laboratory.

Assessment of Automobile Accessories

Marvin Jackson

Fort Valley State College

Lawrence Livermore National Laboratory

Livermore, CA 94551

ABSTRACT

This paper discusses the results of a four month study on automobile accessories. Automobile accessories, electrical and mechanical, have a small but significant impact on conventional vehicles. Accessories loads range from about 1 watt to 5000 watts of power. On an average, conventional vehicles today use from 1000 to 2000 watts of power on any given drive cycle. Careful assessment of major power consuming accessories will contribute to the development of electric and hybrid vehicles with consumer accepted range and mileage. The results of this study focuses on the importance of accessories and their impact on the fuel economy.

INTRODUCTION

Interests in improving the fuel economy began in 1971 with the Energy Policy and Conservation Act. This act required automotive manufacturers selling cars in the United States to increase the corporate average fuel economy (CAFE) of their new car fleet to 27.5 miles per gallon (mpg) in model year (MY) 1985 and thereafter, unless the requirement was relaxed by the Secretary of Transportation. Between 1975 and 1991 the fuel economy of the average new car improved by roughly 76 percent, from 15.8 to 27.8 mpg.[1] Attributing factors to the improvement of the fuel economy was due to the major changes to the engine and the design of the car. For more information on those changes consult the National Research Council.[1]

Goal 3 of the Partnership for a New Generation of Vehicles (PNGV) is to develop a vehicle to achieve up to 3 times the fuel efficiency (80 miles per gallon or BTU equivalent) of today's comparable vehicle (i.e., the 1994 Chrysler Concorde, Ford Taurus, and Chevrolet Lumina). PNGV is a collaboration of the federal government and domestic automotive corporations aimed at strengthening U.S. competitiveness by developing technologies for a new generation of vehicles.[2] In order to address Goal 3, research and development is needed in technology areas leading to vehicle and propulsion systems. Including advances in more efficient electrical systems would

be one of the technologies needed, although it would contribute less to the overall goal.

The California Air Resources Board (CARB) has mandated that at least two percent of the vehicles sold in the Los Angeles basin in the state of California produce zero emissions by 1998.[3] This mandate being a response to Environmental Protection Agency (EPA) standards, has increased the interest in electric vehicles. Electric vehicles (EV) being solely run by a battery system, face the problem of achieving range. An average EV battery provides around 80 miles between recharges which is considerably lower than the average gasoline tank that lasts for a few hundred miles before needing to be refueled. The problems surrounding EVs and the battery seem inseparable. Reducing the power demands on automobile accessories will have a significant impact in the improvement of range goals of electric vehicles.

A detailed listing of available accessories and the actual accessory loads of a typical mid-size sedan is provided in this article. The focus of this paper is to show the importance of accessory in comparison to other energy requirements of a conventional vehicle. This is achieved with the use of two vehicle simulation codes: An Electric and Gasoline Fuel Efficiency Software Package (EAGLES) and a Hybrid Vehicle Evaluation Code (HVEC). Graphs and charts will illustrate the impact that accessories have on the fuel

economy of conventional, electric and hybrid vehicles. Careful assessment of major power consuming accessories will help in the attainment of range and mileage goals of electric and hybrid vehicles.

AUTOMOBILE ACCESSORIES

A textbook definition of an accessory is that it is an object or device not essential in itself but adding to the beauty, convenience, or effectiveness of something else. The available accessories, as shown in List 1, on conventional vehicles enhances the driving environment. Consumer concerns today are not orientated in the high fuel economy or the engine efficiency of automobiles but in the available luxury and comfort provided by accessories. At minimum, consumers value interior room, acceleration performance, specific luxury features such as power steering, automatic transmission and air conditioning, and safety features such as collision resistance, anti-lock brakes and impact protection devices. The availability to purchase cheap gasoline at today's price gives the consumers no real concern about the range of their vehicle.

Referring again to List 1, accessories are categorized in the manner in which they would appear in typical catalog

brochures. Chart 2 provides data on the accessory loads of a typical mid-size sedan. As shown in the chart, heating and cooling, the electric defroster, and the engine cooling fan are the major power consumers. When used at maximum the heating and cooling system can range from 3.5 to 4.5 kilowatts.

The air conditioning load is one of the challenges faced by PNGV in the development of a "New Generation Vehicle". One potential solution for this problem is to reduce the climate control load with the invention of electrochromic windows. Another is to reduce the climate control energy requirement with a reliable, high efficiency, electric air conditioning system.

The current energy requirement for air conditioning might reduce the already modest range of an electric vehicle by some 10%.[4] One method employed by General Motors (GM) in their development of their electric vehicle, the Gm Impact3, was to use an AC induction motor and inverter to drive the compressor. This system is able to provide 3000 watts cooling for 1000 watts of electrical input, and in the a/c mode, uses only 1000 to 1500 watts of power.[5]

In performance testing of the Vehma G Van electric vehicle, use of the air conditioner in SAE J227a C cycle reduced the range of the vehicle by 25.1% when the average ambient

temperature was 34° C.[6]

The integration of electronic control systems will help in the reduction of overall vehicle efficiency. However because of the increase of control systems in a vehicle and the integration of control functions into the control systems, the energy consumption in each control system itself is becoming a critical issue. These systems now use less than 500 watts of power and are increasing with the addition of new systems.[7]

TEST RESULTS

As mentioned in the introduction there are two vehicle simulation tests which were employed in the research study. These two codes were used to make the calculations of the effects accessories have on conventional, electric and hybrid vehicles.

An Electric and Gasoline Fuel Efficiency Software Package (EAGLES)[8] was created at Argonne National Laboratory. This vehicle simulation codes allows the user to choose between simulation runs of either electric or gasoline vehicles on fourteen available drive cycles. Prior to the initiation of the simulation run, certain parameters can be changed

interactively, among those was auxiliary power demand.

A Hybrid Vehicle Evaluation Code (HVEC)[9] was created at Lawrence Livermore National Laboratory (LLNL). This vehicle simulation code allows the user the choice to choose between simulation runs of either electric or hybrid. This program consists of data files which the user can change the parameters of several variables.

In both simulation codes there were three drive cycles used to test the impact of accessories on the fuel economy. The Federal Urban Driving Cycle (FUDS), a highway driving cycle, and a 55 mph driving cycle.

Tests was conducted on representatives of three categories. A 1993 Ford Taurus was used for testing of energy consumption, accessory load importance and impact of accessories on mileage of a conventional vehicle. HVEC was used to show the impact of mileage on the LLNL Hydrogen Hybrid Concept Vehicle.[10] The GM Impact3 was used as a representative of electric vehicles to test the impact accessories have on range.

Graph 1 show the how the energy penalty of accessories increases as speed decreases. The energy values are a function of the driving cycle and not the vehicle. Thus these values can be applied to any vehicle as the energy needed to operate

accessories. In the urban driving cycle, which is slower, there is more time for energy to bee spent and thus the energy penalty increases. In the highway driving cycle, the vehicle's engine operates near it's maximum efficiency point. Therefore, there are less energy losses and there is less of an energy penalty on the vehicle.

Graph 2 shows the importance of accessories in comparison to other energy requirements. As can been in the graph, when accessories are compared to the energy needed for air drag, rolling resistance and braking the energy spent is substantially greater in the urban driving cycle.

Graph 3 show how there is small effect that accessories have on the mileage of conventional vehicles. There is more energy losses due to engine friction. In the highway cycle, there is minimum impact on the mileage of the vehicle because the energy being produce is consume instantly. In the urban driving cycle, there are energy losses due to idle time where energy is produced but are not being used. Therefore accessories would have a small effect on mileage in this cycle.

The next two graphs, Graph 4 and Graph 5, show the effects of accessories as applied to hybrid and electric vehicles. In hybrid vehicles, the engine operates at it's maximum efficiency point. Thus the impact of accessories on hybrid vehicles' mileage is more visible. In electric vehicles,

there is a limited amount of power available to operate the entire vehicle. Thus in this case an increase of accessory loads would hinder the vehicle from attaining range goals.

CONCLUSION

Automobile accessories loads, small in comparison to the overall vehicle, are important. The energy needed to operate these devices will cause barriers in the attainment of range and mileage goals of electric and hybrid vehicles. In efforts to meet the goals of PNGV and the comply with CARB mandate, a study on the reduction of accessory loads will prove to be beneficial when it comes to improving the fuel economy. However, with the implementation of new advanced technology, any reduction made to accessories may be replaced with more power consuming amenities such as collision warning systems and on board computers. Faced with many opposing problems such as limited power, outstanding improvements in the fuel economy cannot be solved solely by reducing accessory loads. But reduction in the power consumption of these devices will help engineers come closer to their goals.

ACKNOWLEDGMENTS

The author would like to thank the following individuals for their support and input in the comprising of this paper: J. Raymond Smith, Salvador Aceves, Don McMahon, Sandy Hadley, Alan Pasternick, and Glenn Rambach.

REFERENCES

1 Automotive Fuel Economy: How Far Should We Go? National Research Council, National Academy Press, Washington, D.C. 1992.

2 Inventions Needed for Partnership for a New Generation of Vehicles, March 1995.

3 Popular Science "We Drive The World's Best Electric Car", January 1994.

4 Dieckmann, John and Mallory, David, "Climate Control for Electric Vehicles", prepared by Arthur D. Little, Inc SAE 910250.

5 Popular Mechanics "New Age of the Electric Car", February 1994.

6 Whitehead, G. D. and Keller, A.S., "Performance Testing of the Vehma G Van Electric Vehicle", Electrotek Concepts, Inc. Chattanooga, TN, SAE 910242.

7 Mizutani, Shuji and Nakano, Yoshiaki, "Energy Management of Electronic Control Systems, Nippondenso Co.,Ltd, SAE 94C042.

8 Marr, W.W. "An Electric and Gasoline Vehicle Fuel Efficiency Software Package", Argonne National Laboratory, January 1995.

9 Aceves, Salvador and Smith, J. Ray, "A Hybrid Vehicle Evaluation Code and Its Applications to Vehicle Design", December 1994.

10 Smith, J. Ray and Aceves, Salvador, " Hybrid Vehicle System Studies And Optimized Hydrogen Engine Design", April 1995.

List 1

Automobile Accessories

(Electrical and Mechanical)

"At minimum consumers value interior room, acceleration performance, specific luxury features and saftey options."

SAFETY FEATURES

Air Bags
Anti-lock Brake System (ABS)
Door Locks
Seatbelts
Theft-deterrent key locking system

MECHANICAL

Anti-lock Brake System (ABS)
Battery Run Down Protection System
Compressor
Fuel Pump
Steering
Traction Control
Transmission

EXTERIOR

Flashers
Headlamps
Keyless Entry
Mirrors
Moonroof
Parking Lamps
Taillamps
Windshield wipers
Wiper system

ACCESSORIES

Security System
Telephones

AUDIO SYSTEMS

Antenna
Deluxe ETR (Electronically- Tuned Radio)
Cassette Deck
Compact Disk Deck
CD Changers

INTERIOR

Air conditioning
Cigarette lighter
Clock
Cruise control
Defogger
Door locks
Gauges - speedometer, tachometer, coolant temp. and fuel level; odometer,tripmeter, voltmeter
Illuminated entry/exit system
Lights - ashtray, glove box, engine compartment, front and instrument panel courtesy, and trunk compartment
Release - remote hood, trunk and fuel filler door
Seats
Warning lights - air bag, seatbelts, low-fuel level, door ajar, battery, check engine, oil pressure, brake and taillamp bulb failure
Windows

NEW TECHNOLOGY

Travel Pilot Navigation Systems
Electronic Control Systems, additional
Collision Warning Systems

Chart 2

Accessory Loads

Air Conditioning System	
Blower Motor (Hi Level)	240 W
Fan	80 W
Clutch	50 W
Amp.	20 W
Others	28 W
Engine Control System	
Fuel Pump Motor	80 W
O2 Sensor Heater	16 W
Solenoid	10 W
Electronic Control Unit	8 W
Injector	3 W
Fan (High)	440 W
Heater	410 W
Electric Defroster	312 W
Headlights (High)	260 W
Wipers (High)	100 W
Flashers	100 W
Lighter	90 W
Turn Signal	50 W
Interior Lights	30 W
Radio (Full Volume)	20 W
Power Steering/Power Braking	4450 W
Engine Cooling Fan	284 W
Anti-Lock Braking	43 W
Air Bags	7 W
Compact Disc	21 W
Transmission	43 W
Total Base Engine	170 W

Energy penalty of accessories increases as speed decreases

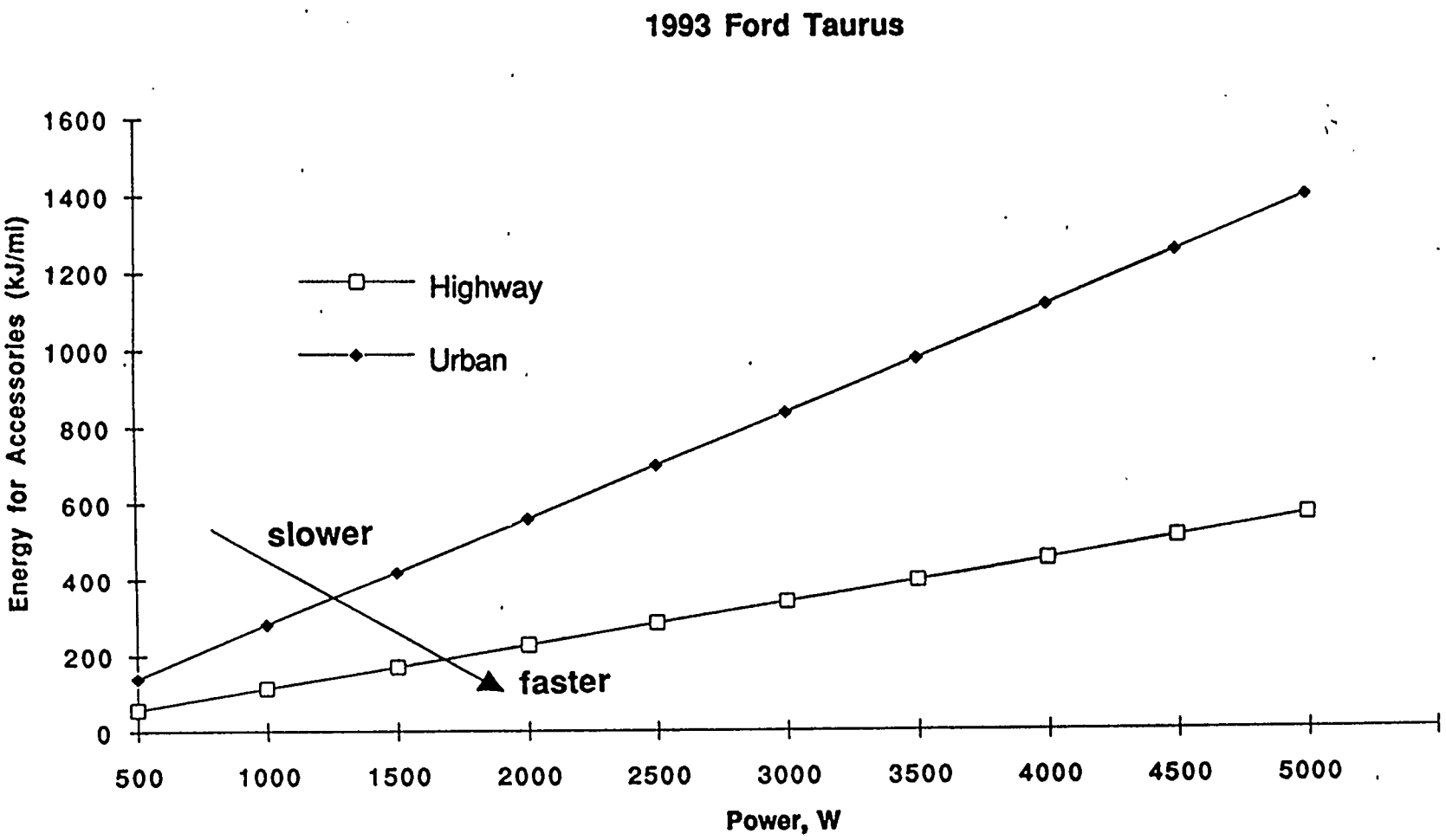

GRAPH 1

Vehicle load comparison

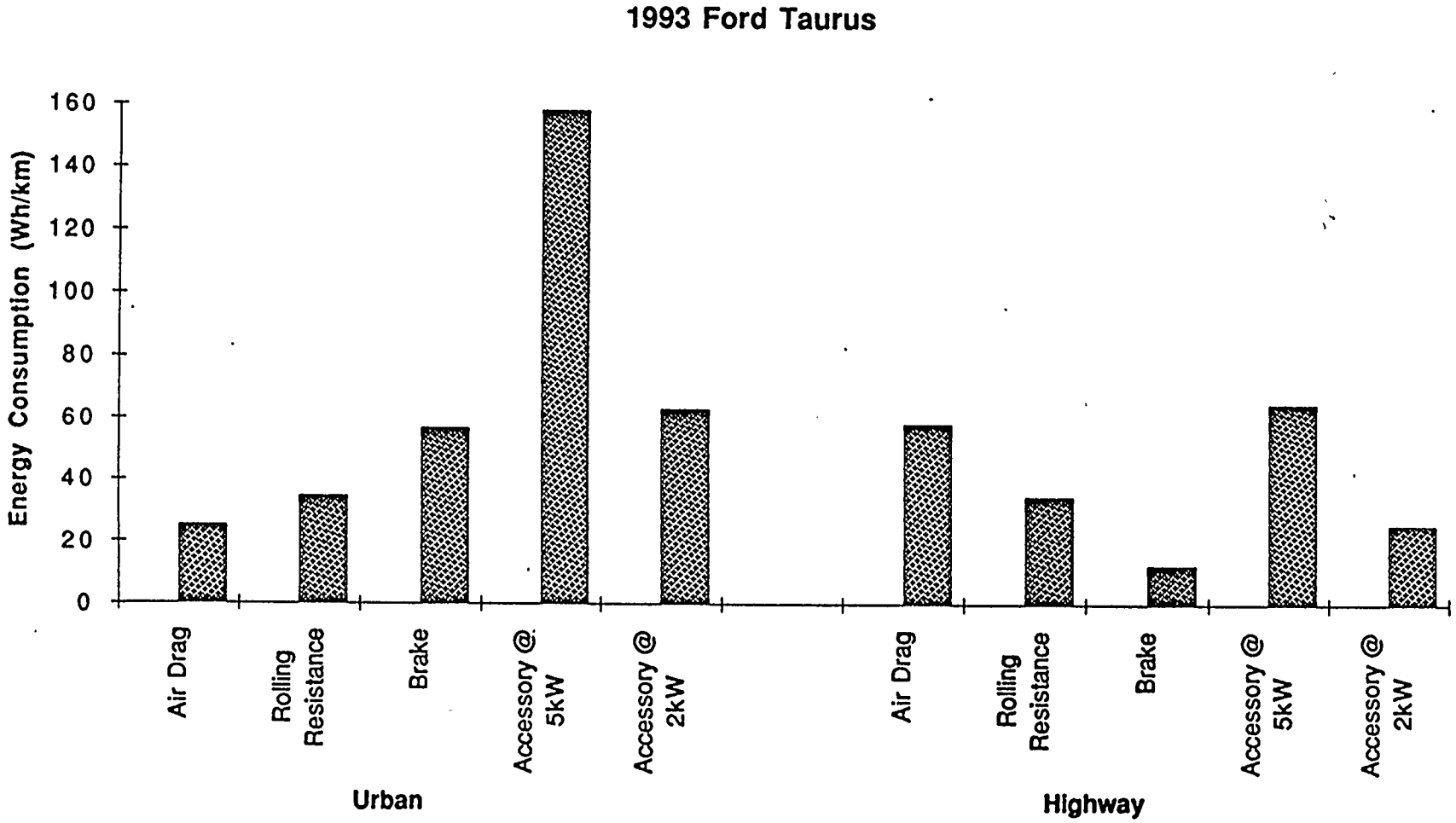

GRAPH 2

For conventional vehicles, accessory loads have small but significant effects on mileage

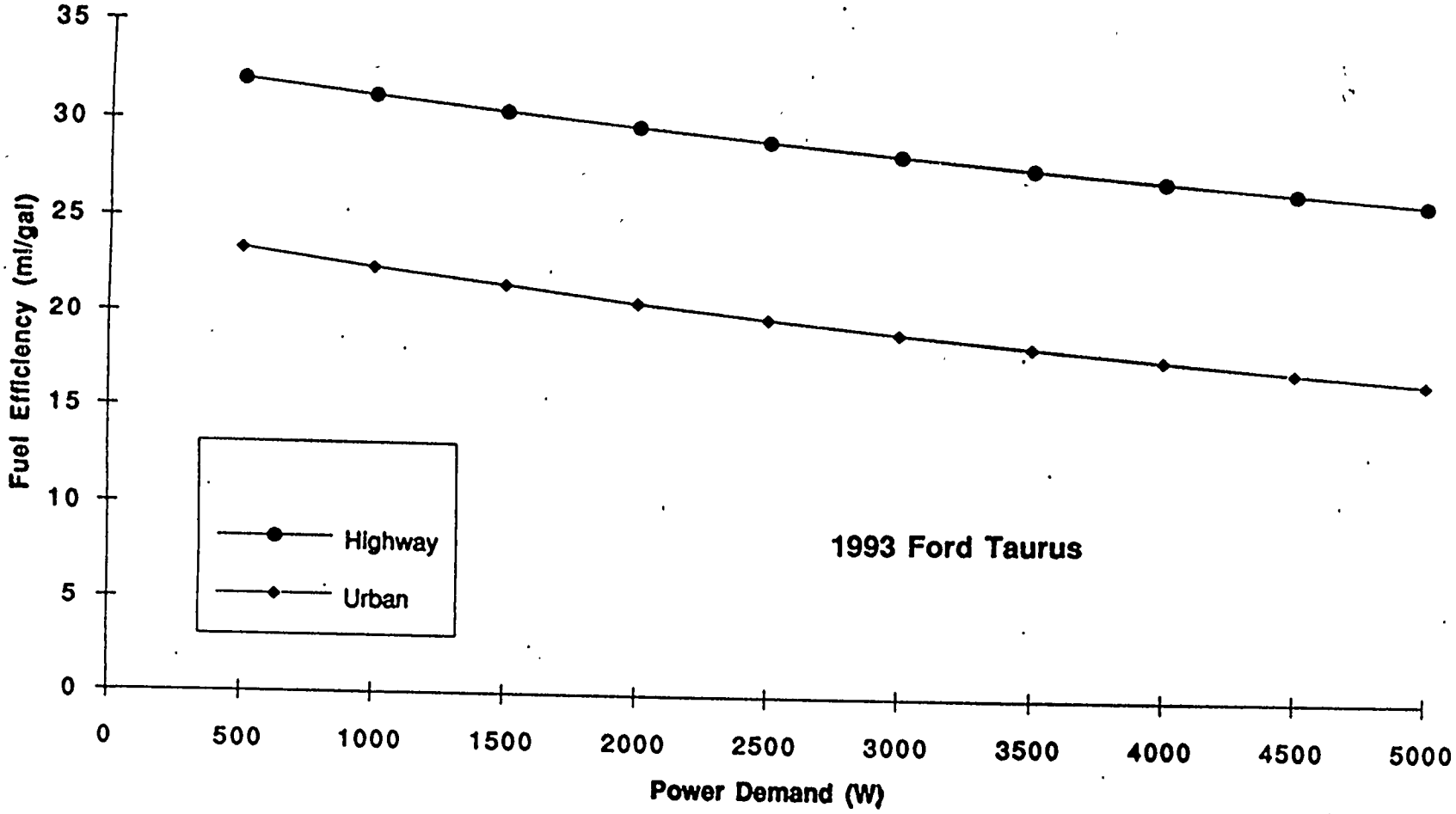

GRAPH 3

Accessories impact the mileage goals of hybrid vehicles

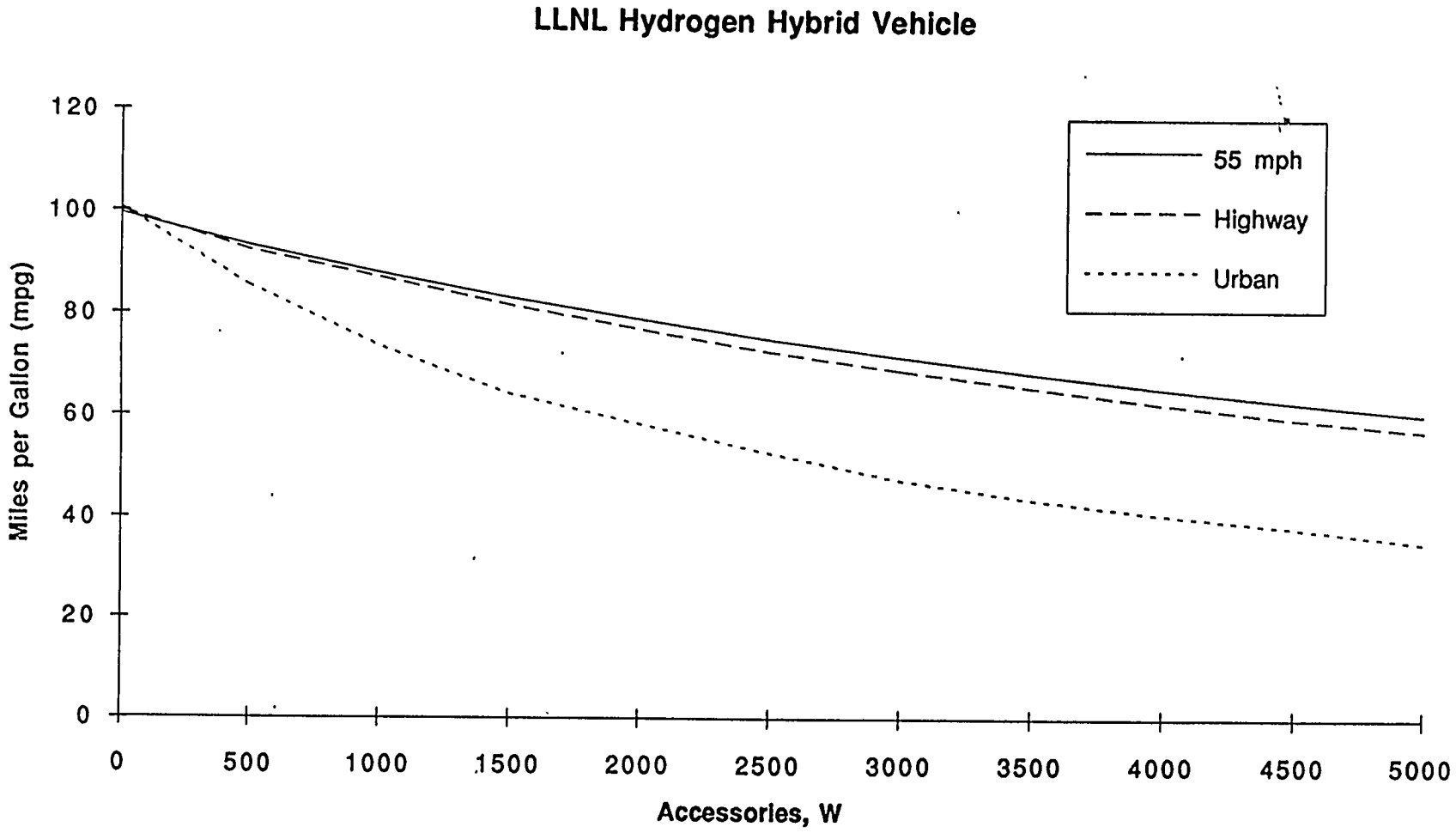

GRAPH 4

Accessory loads have a major effect on range for electric vehicles

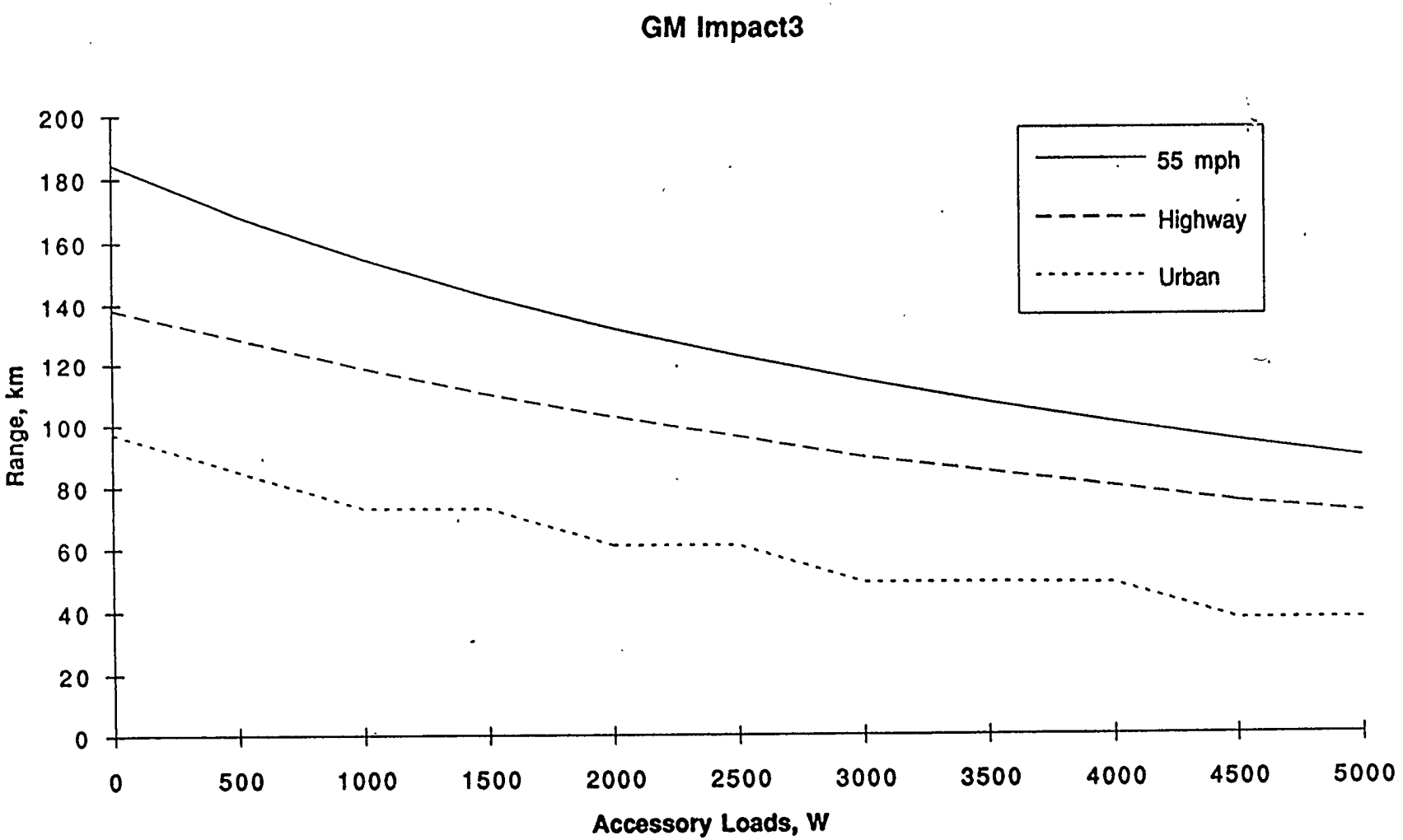

GRAPH 5

Designing an Effective Gateway for Documentation Search through a WWW Server

Vinh Nguyen Q.

George Mason University

Lawrence Livermore National Laboratory

Livermore,California 94550

05/01/95

Prepare in partial fulfillment of the requirements of the Science and Engineering Research Semester under the direction of Girill, T.R., Research Mentor, in the Lawrence Livermore National Laboratory.

*This research was supported in part by an appointment to the U.S. Department of Energy Science and Engineering Research Semester (hereinafter called SERS) program administered by LLNL under Contract W-7405-Eng-48 with Lawrence Livermore National Laboratory.

INTRODUCTION

LOOKUP, a National Engineering Reseach Supercomputer Center (NERSC) utility, searches several document databases to find the exact as well as approximate matches for the user's searchterm. It presents a prioritized list of terms and sources. The close matches are displayed first, then an alphabetical list of those with same matching degree are next. Pick any number in the list, and LOOKUP will execute the Unix commands to retrieve and display the corresponding passage. However, LOOKUP is only available for those who run it directly on the NERSC machines [1].

There have been several attempts to make distributed information available to the public, but I think a gateway is the most effective way to provide a wider access for LOOKUP and still preserve the special features crucial for effective practical use. The gateway is a bridge between any World Wide Web (W W W) client program (such as Netscape, Mosaic) and LOOKUP. It accepts information requests and returns the appropriate documents to the users.

BACKGROUND

From the users' perspective, W W W is a collection of documents, or pages that contain text, images and hypertext links to the other pages. By simply pointing and clicking, the user has an instant access to the collection of information distributed across the globe. Among the features that W W W offers, the most important ones that have been applied in my project are:

1. HTTP: (Hyper Text Transfer Protocol) is used to locate a document on a Web server.

2. URL: (Uniform Resource Locator) is a standard method to identify any document or resource on the Internet. A typical URL is "http://www.nersc.gov/doc/intro.html", which means using HTTP to retrieve the document "intro.html" from the server named "www.nersc.gov".

3. HTML: (Hyper Text Markup Language) is how the documents are formatted on the Web. Traditionally like any word-processor, HTML uses a proprietary method of presenting document's attributes such as font, pitch, weight, layout, etc.

4. CGI: (Common Gateway Interface) is an interface for running the external programs or gateways under an server. A gateway can be a script or a program written in C/C++, Perl, C shell, Bourne shell or TCI. It accepts the user's input and outputs HTML a URL or some data to the user via W W W.

5. An HTML Form is the computer equivalent of a paper form such as application form. A button or a link often labeled "submit" is found at the end of the form. When the user pushes this button, two things are sent to the server: the data the user types in the form and an ACTION, which tells the server the name of the program that knows how to process that form's data. The server simply invokes that program, passes the form's data to it, and arranges for the output of that program to be sent back to the browser [2].

IMPLEMENTATION

"/cgi-bin/vinh/pquery" is my gateway to interface LOOKUP. It gets the user's input and translates the result from LOOKUP to an HTML document. "pquery" is written in C. Though residing on the NERSC's machine, it must be compiled on another platform that has the same operating system with the server, such as the SUN workstation. Under "/www.nersc.gov/cgi-bin" directory, it is a worldwide executable program.

There are three main functions in my gateway: one is to get the user's input through the HTML form, another is to encode the output from "lookup" to HTML, and the other is to track the dialog history information to allow returning to previous searches for each user.

The first function in my gateway is to get user's input via an HTML Form. See appendix A for the HTML form and the HTML document that displays the form. The HTML form provides a way to collect data from the user and submit to the gateway program. FORM tag <FORM METHOD="GET/POST" ACTION="URL">...</FORM> specifies a fill-out form within an HTML document. There are two methods which can be used to access the form. These methods are GET and POST. Depending on which method is used, the encoded result of the form is different. The GET method causes the fill-out form contents to be appended to the URL that is specified by the ACTION attribute in the FORM tag. For POST method, the contents of form are encoded as with the GET method, but the contents are sent in a data blocks. The ACTION attribute is the URL to which the data block is posted. However, the POST method is strongly recommended and used in my gateway for the flexiblity of encoding data. With "METHOD=POST" in the form tag, the CGI program will receive the encoded form input on stdin. Moreover, in every form, each input item has a NAME and VALUE tag. When the user places data in these items in the form, that information is encoded into the form data. Form data is a stream of NAME/VALUE pairs separated by the & character. Each NAME/VALUE pair is URL encoded; for example, spaces are changed into plusses [3]. Therefore, the gateway program must convert plusses to spaces, and separate the name of input item and its value. Appendix B shows the C codes that process form data.

After the user's input has been handed to LOOKUP and the gateway has received a list of found passages back, the second function is called. It encodes the output from LOOKUP to an HTML document. The HTML document returned in a response to a search request either indicates that no document is found to satisfy the request or contains a list and associated URLs that can be used to retrieve document or man page.

Instead of letting the user pick a number and running the UNIX commands to display the document or page associated with the number in the list, I generate the URLs which point directly to all the documents or pages in the list. The hypertext links are formed in two different ways. If the source is a NERSC document, I search several directories to find its location. The URL for a document simply uses HTTP to retrieve it. For example, a hyperlink to the document "ezacess" is <A HREF=http://www.nersc.gov/doc/ndata/intro.ezacess.html"> View document</A>. Otherwise, if the source is a Unix man page, I also look for the man page's location. However , the URL is created by appending the man page's path to the man page conversion on the fly "bbc_man2html.pl". "bbc_man2html.pl" is a perl script to construct the execute line to retrieve the man page. A hyperlink anchoring the "brk" man page is <A HREF=http://www.nersc.gov/cgi-in/bbc_man2html.pl?/usr/share/man/cat2/brk.2> View man page</A>. Clicking on either "View document" or "View man page" will open the document or man page. See appendix C for the C codes to translate the LOOKUP output to HTML and to generate the URLs. Appendix D is one example of lookup output and appendix E is the HTML document with URLs of the output in appendix D. To obtain a maximum benefit from this documentation search interface, some updates to the auxiliary utility "lookup" are needed. NERSC is addressing this.

The third main function of the gateway is to track the user's searching history information. The W W W client-server interaction is stateless by nature [4]. The Web server does not know whether the form has been properly completed or what information is in it. However, maintaining state can be done, but the CGI program itself must keep track between the transactions [5]. The approach in "pquery" is to implement a blackboard - an independent source that is modified by one program and used by another one. For each user, I open his/her file area. The list of hits encoded in HTMLreturned in the response to a search request is temporarily saved in this file

area. Return to this file is enabled by a unique hypertext link for each searchterm - <A HREF=URL>searchterm</A> where URL is the location of the file in the file area. The hypertext link is appendded to a file also in the user's file area. When the user wants to reuse the previous searches, he or she has to get back to the HTML form. Checking on the box "Display previous searches" in the form will open the HTML document in his/her file area that contains the URL of his or her previous searches. See appendix F for the blackboard processing. However, backtracking may be costly when there are multiusers. Much space is needed for the storage and must be handled with care in the gateway.

During a certain time, a "cleanup.csh" shell script will clean up the user's file area.

CONCLUSION

Using a gateway program allows every one with a WWW client to reach special documentation search software (LOOKUP) that would otherwise be available only to those on NERSC machines. But instead of getting several stages of input from the users and continuing dialog with the search software, I generate an HTML document with the hyperlinks to the sources . Moreover, possible reuse of earlier results is implemented for each user. This does not happen automatically, because the WWW server is stateless.

Only careful design of the HTML input form and of the gateway program that manages the user interaction with the server software can overcome this statelessness and provide effective service to the users.

APPENDIX A

The HTML document that displayed the form in figure 1

```
<HTML>
<TITLE>Get query string</TITLE>
<H1><IMG SRC="http://www.nersc.gov/gifs/nersc_logo2.gif">
```

```
<B>Documentation Search Interface</B></H1>
<FORM METHOD="POST"
ACTION="http://www.nersc.gov/cgi-bin/vinh/pquery">
<BR><BR>
Enter search term: <INPUT NAME="QUERY_STRING" SIZE="60">
<BR><BR><BR>
Search fuzziness:
<SELECT NAME="FUZZY">
<option>default(14)
<option>1-5
<option>6-10
<option>11-15
<option>16-20
<option>21-25
<option>26-30
</SELECT>
<BR><BR>
<INPUT TYPE="CHECKBOX" NAME="PREVIOUS_SEARCH" VALUE="yes">
Display previous search
<BR><BR>
<INPUT TYPE="SUBMIT" VALUE="lookup">
<INPUT TYPE="RESET" VALUE="clear">
<A HREF="/NERSC/Projects/doc-gate/help.html">HELP</A>
</FORM>
</HTML>
```

Figure 1 is the HTML Form displayed by Netscape .

The <FORM> tagging pair is used to enclose the contents of the form and to identify the URL of the CGI program that will process the form output. <FORM ACTION=(URL)> .., </FORM> where URL is the path name of an HTML file. URL is included in plain ASCII non-marked-up text. In the Figure 1, URL /cgi-bin/vinh/pquery will receive the contents of the fill-out form as a standard input (by POST method). The input to the gateway program might be submitted and look like one of the examples below:

QUERY_STRING=preallocate&FUZZY=default(14)

QUERY_STRING=&FUZZY=default(14)&PREVIOUS+SEARCH=yes

The & separates the parameter pairs and = separates each parameter's name from its value, + is a substitute for a blank.

Inside the <FORM> tagging pair, other forms-related HTML tags and constructs can be used. In the figure 1, I use text entry field, checkbox, scrollable list, and push buttons. The INPUT field is defined for a text input by default. Checkbox stands for a simple Boolean attribute. Each selected checkbox generates a name/value pair in the submitted data. The submit key will send the current fill-out form into the remote gateway "pquery" while the reset causes the input elements in the form to be resetted to their default values. SELECT tag can be used with other HTML tags. The SELECT element allows the user to choose one of the set of alternative described by textual labels.

APPENDIX B

FORM DATA ENCODING

```
for (x=0; cl && (!feof(stdin)); x++)
{
        m=x;
        entries[x].val = fmakeword (stdin, '&', &cl);
        plus2space (entries[x].val);
        unescape_url (entries[x].val);
        entries[x].name = makeword (entries[x].val, "=");
}[6]
```

APPENDIX C

1. Create URLs for documents

```
...
strcat (url, "<A HREF=");
```

```
strcat (url, path);
for (i=0; url[i]!='\n'; i++);
url[i]= '#';
strcat (url, keyword);
strcat (url, "</A>");
```

2. Create URLs for man pages

```
...
strcat (url, <A HREF=http:/cgi-bin/bbc_man2html.pl?");
strcat (url, path);
strcat (url, "</A>")
```

3. Add HTML tags

```
fputs ("<DL>\n", f);
while ((c = getc (in) ) != EOF)
{
        if ( c >= 49 && c <= 57)
        {
                fputs ("<DT><B>", f);
                count ++;
                putc (c, f);
                while ((c = getc (in)) != '(' )
                        putc (c, f);
                fputs ("</B>", f);
                if (c == '(' )
                {
                        fputs ("<DD><I>", f);
                        putc (c, f);
                        while ((c = getc(in)) != ')' )
```

```
                putc (c, f);
            putc (c, f);
            fputs ("</I><BR>", f);
        }
    }
    else if (c == '(' )
    {
        fputs ("<DD><I>", f);
        putc (c, f);
        while ((c = getc(in)) != ' )' )
            putc (c, f);
        putc (c, f);
        fputs (</I><BR>", f);
    }
    else if (c == '<')
    {
        putc (c, f);
        while ((c = getc(in) ) != ' >' )
            putc (c, f);
        putc (c, f);
        while ((c = getc(in)) != '>')
            putc (c, f);
        putc (c, f);
    }
    else
        putc (c, f);
}
fputs ("</DL>\n", f);
```

APPENDIX D

One output returned from LOOKUP is:

(Items 1->9 of 200)

1 preallocate-storage (38 lines)
(synonym of ialloc in document ezjobcontrol)
(matchscore=679) (matchpath=preallocate..)

2 preallocate-storage
(synonym of ialloc for man page ialloc)
(matchscore=679) (matchpath=preallocate ..)

3 preallocate-storage (109 lines)
(synonym of ialloc in document unicoscalls)
(matchscore=679) (matchpath=preallicate ..)

4 preallocation (171 lines)
(in document ezjobcontrol)
(matchscore=599) (matchpath=preallicate ..)

5 deallocate-heap-block
(synonym of hpdeallc in document hpdeallc)
(matchscore=519) (matchpath=..eallicate..)

...

Press enter; or type a number (to select or start list at that point), REST, or ? (q to quit) (Press enter to continue with fuzzy match list for preallicate; or type a new string to match ...)

fuzzy match preallicate (select):

For each found item in the list, there are three important things. They are the keyword, the meaning of the source and the source's name. The keyword is usually right after the number in the first line of each item. However, when it is found as a synonym of another word, the synonym is the real keyword. The source can be a NERSC document or a Unix man page. Term "document" or "man page" is in the second line of the item defines the meaning of the source. Right after it is the source's name.

APPENDIX E

The HTML encoded version of the example above is:

```
<HTML>
<H3><B><img src="http://www.nersc.gov/gifs/training.gif>
Search term = PREALLICATE</B></H3><HR>
200 documents/man pages found
<BR><HR>
<DL>
```

<DT><B>1 preallocate-storage</B>
<DD><I>(synonym of ialloc in document ezjobcontrol)</I>
(A HREF=/doc/ndata/intro.ezjobs.html#ialloc>View document</A>
<DT><B>2 preallocate-storage</B>
<DD><I>(synonym of ialloc for man page ialloc)</I>
(A HREF=/cgi-bin/bbc_man2html.pl?/usr/share/man/cat2/ialloc.2>View man page </A>
<DT><B>3 preallocate-storage</B>
<DD><I>(synonym of ialloc in document unicoscalls)<I>
(A HREF=/doc/rdata/code.unicoscalls.html#ialloc>View document</A>
<DT><B>4 preallocation</B>
<DD><I>(in document ezjobcontrol)</I>
<A HREF=/doc/ndata/intro.ezjobs.html#preallocation>View document</A>
<DT><B>5 deallocate-heap-block</B>
<DD><I>(synonym of hpdeallc for man page hpdeallc)</I>
<A HREF=/cgi-bin/bbc_man2html.pl?/usr/share/man/cat3/hpdeallc.3f> View man page</A>

...
</HTML>

HTML encoding program will format the hit list. Several HTML tags are used in this program for the viewing access and the better look from WWW. For example, <DL>...</DL> will wrap the list; <DT><B>...</B> marks the keyword in bold; <DD><I>...</I> marks the source in italic.

Figure 2 is the output displayed by Netscape

APPENDIX F

1. Create URLs for each searchterm and the HTML document associated with the searchterm and then append to afile:

```
strcat (buffer, "<A HREF=http://www.nersc.gov/NERSC/Projects/doc-gate/");
strcat (buffer, filename);
strcat (buffer, ">");
```

```
strcat (buffer, searchterm);
strcat (buffer, "</A>");
fputs (buffer, afile);
```

where filename is the HTML document containing URLs.

2. Open the afile to retrieve the previous searches:

```
puts ("<HTML>");
puts ("<TITLE> Previous Searches</TITLE>");
puts ("<H1><IMG SRC=http://www.es.net/hypertext/pics/docs.gif>");
puts ("Previous Searches</H1><BR>");
while (fgets (line, 80, afile) != NULL)
    fputs (line, stdout);
puts ("</HTML>");
```

BIBLIOGRAPHY

[1] Girill, Terry, "Lookup: Solving the Search Problem." Livermore, CA: 1995

[2] See http://hoohoo.ncsa.uiuc.edu/cgi/intro.html

[3] See http://www.ncsa.uiuc.edu/SDG/Software/Mosaic/Docs/fill-out-forms/overview.html

[4] Weibel, Stuart, Eric Miller, Jean Godby, Ralph Le Van. "An Architecture for Scholarly Publishing on the World Wide Web." Dublin, OH: 1994.

[5] Liu, Criket, et. al. Mangaging Internet Information Services. Sebastopol, CA: 1994

[6] See ftp://ftp.ncsa.uiuc.edu/Web/httpd/Unix/ncsa_httpd/cgi/cgi-src

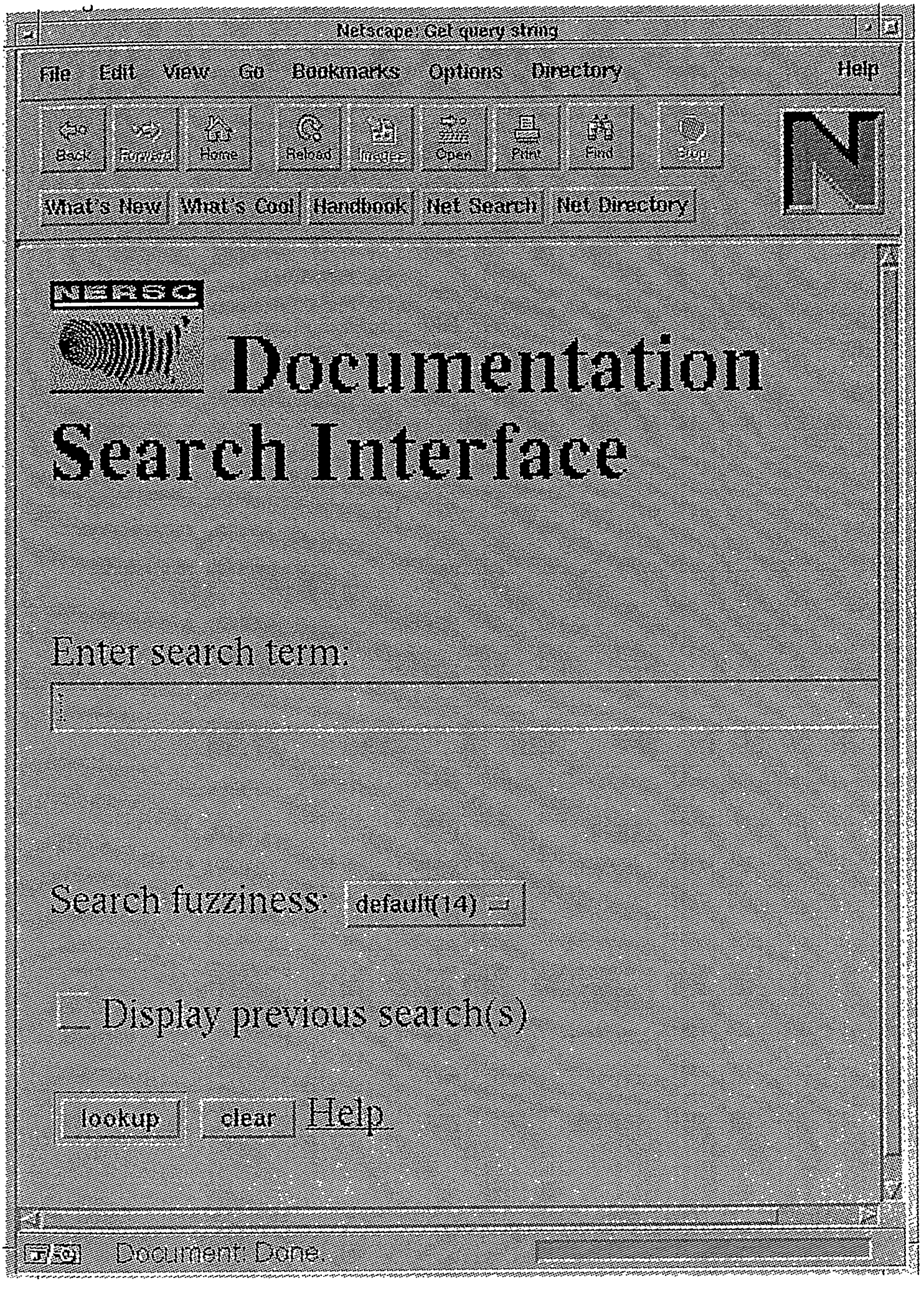
Netscape: Get query string
File Edit View Go Bookmarks Options Directory Help
Back Forward Home Reload Images Open Print Find Stop
What's New! What's Cool! Handbook Net Search Net Directory
NERSC
Documentation
Search Interface
Enter search term:
Search fuzziness: default(14)
Display previous search(s)
lookup clear Help
Document: Done.

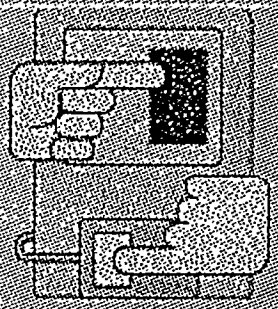

Searchterm = PREALLICATE

200 documents/man pages found

1 preallocate-storage
(synonym of ialloc in document ezjobcontrol)
View document

2 preallocate-storage
(synonym of ialloc for man page ialloc)
View man page

3 preallocate-storage
(synonym of ialloc in document unicoscalls)
View document

4 preallocation
(in document ezjobcontrol)
View document

5 deallocate_bcan_blank

Constructing Computational Models for Thumb Carpometacarpal Joint Implants

Cheri Nielsen

Dept. of Biomedical Engineering
The Johns Hopkins University

The Institute for Scientific Computing Research
Lawrence Livermore National Laboratory
Livermore, California 94550

May 1995

Prepared in partial fulfillment of the requirements of the Science and Engineering Research Semester under the direction of Karin Hollerbach, Scott Perfect, and Ken Underhill, in the Lawrence Livermore National Laboratory.

* This research was supported in part by an appointment to the U.S. Department of Energy Science and Engineering Research Semester (hereinafter called SERS) program administered by LLNL under Contract W-7405-Eng.-48 with Lawrence Livermore National Laboratory.

Abstract
Computer modeling of prosthetic implants presents orthopedic biomechanic researchers and physicians a means by which to understand possible *in vivo* failure modes, without resorting to lengthy and costly clinical trials. Realistic 3D models of three different carpometacarpal (CMC) joint implants were constructed. Preliminary results of prosthetic joint loading, without surrounding human tissue, are based on dynamic, non-linear finite element analysis.

Introduction
The thumb CMC joint afflicted with severe osteoarthritis is frequently replaced with a prosthetic joint. To provide pain relief in such patients it is important to eliminate incongruous articulating surfaces where high and non-normal forces are generated. The ratios of joint forces to the applied force have been calculated by Giurintano et al. (1994) to be about 18 times the applied load in a power pinch. The thumb power in pinch and grip measured by Crosby et al. (1994) is 27 lb. The normal CMC joint, then, routinely sees forces in excess of 500 lbs. A replacement joint must be able to handle these forces repetitively without dislocating, wearing out, or cutting out of the bones.

Three common failure modes exist in implant devices: material failure, failure at the implant/bone interface, and failure to reproduce normal joint kinematics. We specifically examined material failure in this study. Ultra-high molecular weight polyethylene (simply called "polyethylene" hereafter) is frequently used for the articulating surfaces of joint implants and is subject to high degrees of contact stress in normal joint articulation and loading. A common example of material failure in these polyethylene components is sub-surface cracking in the presence of high stresses (Wright et al. 1986, DeHeer 1992), such as those found in normal thumb activity. Examination of polyethylene total joint prosthetic components in pre-implant tests and in tests following revision or removal surgery has shown that polyethylene wear is a serious problem in joint replacements (Wright et al. 1986).

Our objective has been to test several thumb CMC joint implant designs by determining contact stresses under a well-defined set of boundary conditions: The implants were modeled alone, and uniaxial loading was applied to the articulating components of each.

Methods
The 3D joint implant models presented here were based upon 3D surface definitions of three commonly used implant designs. The surfaces were read into TrueGrid software (XYZ Scientific Applications, Inc., Livermore, CA), and a volumetric mesh was created for each component of each implant design. Constructing the volumetric meshes proved to be a difficult and time-consuming procedure. Factors that weighed heavily in determining the relative ease of constructing the models included the asymmetric nature of the implants, the orientation of the surfaces with respect to the coordinate axes, and the curvature of the contours.

Design A

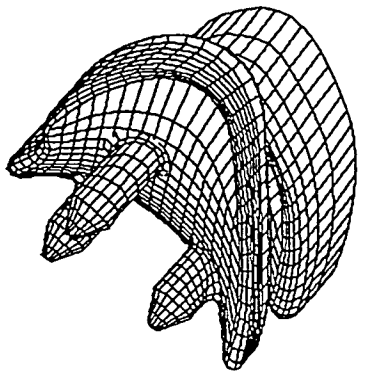

Figure 1

Design goals for implant design A (Fig.1) include long-term pain relief and restoration of thumb function, including strength and dexterity, following injury or disease. The implant consists of two components. The metacarpal component

is composed of a polyethylene articulating surface reinforced with a titanium saddle to prevent deformation, thus minimizing fatigue. The titanium stem is inserted into the metacarpal canal. The cobalt-chrome trapezial component is saddle shaped to increase metaphyseal bone surface contact area with the prosthesis, decreasing the forces per unit area of bone. Small pegs on the implant provide initial stability, but long term stability of the implant is largely dependent on wide metaphyseal bone contact. The articulating surfaces are the surfaces of revolution for the non-orthogonal CMC joint axes.

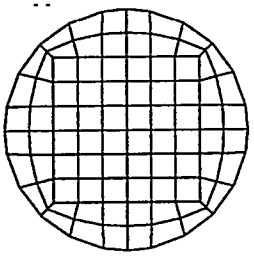

Figure 2

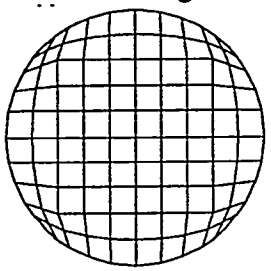

Figure 3

In constructing the volumetric mesh for design A, the trapezial component was broken up into seven sections: the three cylindrical pins, the conical sections at their tips, and the main saddle-shaped volume. Each of the blocks was initially constructed at the origin and collapsed into two dimensions. After all rotations were performed, the blocks were moved to their proper positions in space. Each pin was modeled from a rectangular block to which the "butterfly" technique was applied (Fig.2). This involves removing the four corner elements of the block at each cross-section; the two resulting edges at each corner are then moved to the center of the remaining space. A block mesh in Cartesian coordinates can thus be used to model a cylindrical object without introducing element angles that approach 180° (Fig.3). Each plane of the collapsed block was spread into three dimensions along the pin axis to match the position of a specific contour curve. The exterior points were then constrained to lie along these curves. The exterior faces were projected to the surfaces, and relaxation algorithms were applied as necessary. This method was modified by scaling the individual cross-sections and applied to the conical tip sections. The non-orthogonal axes of the implant design create asymmetric saddle surfaces; these necessitate a more complicated approach in building a computationally usable volumetric mesh. Loose cross-sections were obtained by defining contour curves along the surface at varying intervals. The initial block was of unit thickness and rectangular. Elements were removed from the edges until the block was similar in shape to the articulating surface. The jagged edges were smoothed with an application of the butterfly concept. Three-dimensional surface fragments were interpolated to fill the gaps in the trapezial surface left at the bases of the pins. The major faces of the block were projected to the articulating surface and the new trapezial surface, and additional nodes were included between these surfaces to provide for better clarity of the rounded connecting edge. These dummy indices were clustered towards the center of the volume before the faces were projected to the edge, due to the curvature of the surface. Equipotential relaxation was applied to the entire mesh after the final projections had been made. Tied interfaces defined at the base of each pin attached the three pins to the main saddle-shaped section. The nodes at the base of each tip section were merged with the corresponding nodes at the top of each pin. The metacarpal component was modeled as a single piece, using similar procedures to those used for the saddle-shaped section of the trapezial component.

Design B

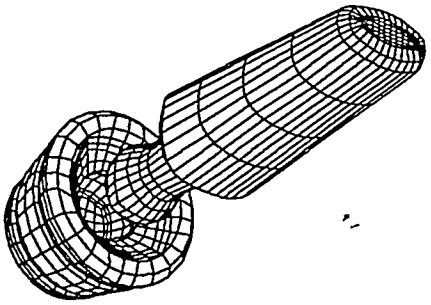

Figure 4

Design B (Fig. 4) is a ball and socket joint, a semi-constrained implant: the socket is on the trapezial side, and is lined with a polyethylene component; the titanium or cobalt-chrome ball makes up the articular surface of the metacarpal side. Design rationale includes the desire to make a geometrically simple joint connecting the two bones in such a manner that dislocation is resisted under axial loading and moderately resisted under anterior-posterior and medial-lateral loading. The implant, while used to replace a two degree of freedom biomechanical joint, is a three degree of freedom mechanism.

The volumetric mesh for Design B consists of two parts, one for each physical component of the implant. Again, both parts were constructed from blocks that were initially collapsed into two dimensions and centered about the origin. Only after all necessary rotations had been performed were they moved to the base of their respective axes. Parallel contour curves were defined along both the exterior and interior surfaces of the trapezial component, and the axis was determined and defined. Interior elements corresponding to the socket cavity were removed from the block. The butterfly technique was applied to the exterior corners, and points along the interior edges were moved to eliminate sharp corners. The faces were spread along the axis through the volume of the socket. All exposed edges of each face were constrained to lie along specific contours, and then the faces were projected to their corresponding interior and exterior surfaces. Equipotential relaxation was applied to the flat base of the socket. The metacarpal component was modeled from a rectangular block. The segments which were to make up the main stem retained their rectangular cross-section, while element deletions left the others square. Defined curves provided contours at each cross-section, and each plane of the block was scaled to fit within its corresponding contour. The planes were spread along the stem axis, and the four corner elements of the lowermost segment were deleted to improve the projection to the spherical surface. At each corner, the resulting three points were moved together in a three-dimensional variation of the butterfly technique. All exterior points were constrained to lie along contour curves. The exterior faces were projected to the surfaces of the ball and stem, and intermediate nodes were then added to increase the clarity of the model's structure.

Design C

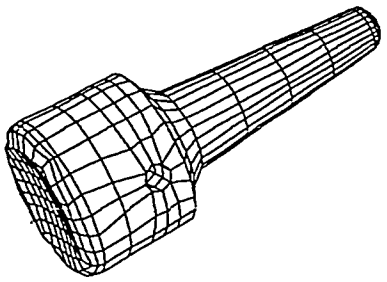

Figure 5

Design C (Fig. 5) is a one-piece silicone replacement designed to be implanted into the metacarpal bone with excision of the trapezium. This style of implant has been shown to be associated with destructive changes in the surrounding bone and related synovitis in a large fraction of clinical cases tested (Hofamann, 1987) and is usually recommended only in the elderly and only in hands of which little high-load activity is required.

Implant design C presents few modeling problems; the one-piece design is completely symmetrical and the axis of the hole is perpendicular to the main axis. The volumetric mesh was generated with an approach similar to that used for the stem of design B. The two axes were determined and a collapsed block with a square cross section was created at the base of the major axis. Contour curves were defined at intervals matching the desired placement of the faces, and each face was scaled so that the area was slightly smaller than that of its corresponding curve. The butterfly technique was applied to all faces before spreading them through the volume of the part. The initial design of the cross-section provided that the two central divisions would line up with either side of the hole in one direction. The faces were moved along the axes so that two adjacent faces would line the hole in the other direction. All elements that contained a part of the minor axis were deleted, and the resultant interior edges were constrained to lie along the cylindrical hole. The exterior faces were projected to the surfaces, intermediate nodes were added, and equipotential relaxation was applied to the base.

The NIKE 3D code was used to perform finite element analyses of all three models. NIKE 3D is a nonlinear, implicit, three-dimensional finite element code developed at the Lawrence Livermore National Laboratory for studying dynamic, finite deformations. Spatial discretization is achieved in this model using 8-node solid (hexahedral) elements. Metal pieces were modeled as rigid bodies; the preliminary material model used for the polyethylene pieces was isotropic elastic. Varying elastic moduli were tested for this model.

The results described here are based on two analyses with a well defined set of boundary conditions. In the first simulation, we fixed the trapezial component in all six degrees of freedom, and uniaxially loaded the metacarpal component to produce contact between the two parts. The resulting contact forces on the articular surface of the metacarpal and trapezial components were calculated, and some measure of congruency between the two components was established. Prior to loading, the parts were perfectly aligned with one another, so that the uniaxial normal loading force did not act to bring the components into proper alignment. This simulation describes the events that would occur inside a uniaxially loaded joint, assuming it had been implanted perfectly. In reality, joints are implanted with some degree of mis-alignment. In the second simulation, we began with the metacarpal implant mis-aligned slightly with respect to the trapezial implant. The uniaxial loading, however, was the same. Again, contact stresses and degree of congruency were established.

Results and Discussion

Three different implant designs were meshed and analyzed. Stage one of the analysis represented a proof of concept demonstration that the finite element code could be applied successfully to analyze large deformation dynamics involving articulating components. Successful application of the codes was demonstrated in all three cases.

Stage two involved uniaxial loading of the joints and calculations of congruency measures of the articulating implant components and the resulting contact stresses. Concentrated regions of high stress are thought to represent danger zones for joint failure due to the polyethylene surface failure mode. As expected, low measures of congruency tended to increase maximum contact stress.

The ability to model large deformation behavior of prosthetic joint implants is significant, because it sets the stage for realistic modeling analysis of the prostheses when implanted into the human joint. The work completed thus far has involved modeling of uniaxial loading of the joint implants alone. In addition, we have modeled contact

behavior simulating imperfect surgical implantation, with initial conditions set to model implant components offset from their ideal position and orientation with respect to one another. We are currently working to combine the implant models with our existing models of the normal joint biomechanics, without an implant. The resulting implant plus bone model will be used to describe the *in vivo* behavior of the implant. With such a model, we will then perform analyses of all three failure modes, polyethylene surface failure, failure to reproduce normal joint kinematics (e.g., by producing a joint with a different number of degrees of freedom or by producing incorrect offsets for the joint axes of rotation), and failure at the bone-implant interface. This work, in the larger context of being able to model the prosthetic implant-human tissue system and the interactions of the various materials, provides a significantly improved method for evaluation of prosthetic joint implant designs. The methods and codes used can be applied to any other joint for which surface descriptions of the implants and human tissues can be obtained.

References

[1] Crosby et al. (1994) Hand strength: normative values. J. Hand Surgery, **19(4)**:665-670.

[2] DeHeer (1992) Stresses in polyethylene tibial components for total knee arthroplasty. M.S., M.E. Dept., Purdue University.

[3] Giurintano et al. (1994) A virtual five-link model of the thumb (in press).

[4] Wright, TM, and Bartel, DL (1986) The problem of surface damage in polyethylene total knee components. Clinical Orthopedics and Related Research. **205**:67-74.

[5] Hofamann et al. (1987) Arthroplasty of the basal joint of the thumb using a silicone prosthesis: Long term follow-up. J. Bone Joint Surgery **69-A(7)**:993-997.

Software Interface and Data Acquisition Package for the LakeShore Cryotronics Vibrating Sample Magnetometer

Benjamin H. O'Dell, Guilford College Physics Department,
5800 W. Friendly Ave Greensboro, NC 27410
A. Chaiken and R. P. Michel
Material Science and Technology Division, Lawrence Livermore National Laboratory,
P. O. Box 808, Livermore, CA 94551

ABSTRACT

A software package was developed to replace the software provided by LakeShore for their model 7300 vibrating sample magnetometer (VSM). Several problems with the original software's functionality motivated the development of a new software package. The new software utilizes many features that were unsupported in the LakeShore software, including a more functional step mode, point averaging mode, vector moment measurements, and calibration for field offset. The developed software interfaces the VSM through a menu driven graphical user interface, and bypasses the VSM's on board processor leaving control of the VSM up to the software. The source code for this software is readily available to any one. By having the source, the experimentalist has full control of data acquisition and can add routines specific to their experiment. The source code can be obtained by e-mailing odell8@llnl.gov.

INTRODUCTION

The software that was developed interfaces the LakeShore vibrating sample magnetometer (VSM) via a GPIB (IEEE-488) interface[1]. The software was developed using the ASYST software package.[2] The ASYST software is a complete programming package, including a debugger, compiler, interpreter, and editor. The computer that was used was a 80486 IBM compatible. The user interface for the software is fully menu driven. Figure 1 is a schematic of the experimental setup for the VSM.

Many samples have very different magnetic properties. By these properties magnetic materials are classified in groups. The group of magnetic materials that show hysteresis in their magnetization loops are classified as ferromagnetic. Ferromagnetic samples consist of many small magnetic regions called domains. Each domain has its own intrinsic magnetic properties. The moment is a measurement that tells how the domains in a sample are aligned. If all of the domains in a sample are anti-parallel then they cancel out and a very small sample moment is measured. If the domains are aligned parallel to each other then a large moment is measured from the sample. Samples are classified ferromagnetic when the domains within the sample prefer to align parallel with respect to each other. When ferromagnetic samples are introduced to an applied field the domains in the sample align with the applied field and a saturated or maximum moment for that sample can be measured along the direction of the applied field. As the applied field is decreased the domains of the sample experience some shifting within the sample away from the direction of the applied field. This shift causes a small decrease in the directional moment. Once the applied field reaches zero, the domains are still aligned and a remanent moment can be measured for the sample. This remanent moment causes the sample to be magnetized. When the applied field becomes negative there is a particular field value where the domains reverse to align in the direction of the negative field. The field value where the sample has zero moment is called the coercive field (*Hc*). There is a coercive field for both the positive to negative, and negative to positive moment reversals, this causes the hysteresis in the sample's magnetization loop. The magnetization of a sample is defined as the moment of the sample divided by the samples volume. The remanent moment can then be related to the remanent magnetization simply by dividing it by the volume of the sample. Figure 2 shows a hysteresis loop of the magnetization (M) of the sample versus the field strength (H). There are several characteristic values that can be determined from a sample's hysteresis loop. One such characteristic is the saturation magnetization *Ms*, the samples maximum magnetization. Other characteristics include the samples coercive field *Hc*, the external field required for the sample to have zero moment, and the samples remanent magnetization *Mr*, the magnetization of the sample at zero applied field strength.

MODES OF OPERATION

The software supports three modes of operation. These include sweep, point averaging, and vector modes. Sweep mode is the only mode that utilizes the VSM's

existing operation for field and data acquisition control. Point averaging and vector modes give the software total control of the field and data acquisition.

In sweep mode the applied field strength is ramped from a maximum field value to a minimum field, and then back to the maximum field. The VSM takes moment and field measurements periodically depending on the number of user specified data points per loop. In sweep mode all of the experimental details are left to the VSM and the data points are transferred from the VSM to the computer as they are collected. Sweep mode collects moment readings as the field is changing and causes false hysteresis. The point averaging and vector modes of operation that this software adds eliminate this problem.

In point averaging mode, the software controls all of the experimental procedure. The software steps the field based on the field step size which is determined from the number of points and the length (in Oe) of the hysteresis loop. When the field is stepped, it is allowed to settle within a user specified tolerance. Once the field is settle the software accumulates the specified number of points to average.

The vector mode of operation is very similar to point averaging mode. In vector mode the software communicates with a LOCK-IN amplifier, in addition to the VSM, to measure the moment of the sample in the y plane. The software steps the field, allows it to settle and averages the specified number of points in the x and y moment directions.

SPECIAL FEATURES

This software has many special features that enhance its operation. Of the most important of these is field offset correction. The field offset is due to the positioning of the Hall sensor on the LakeShore VSM. The Hall sensor is positioned closer to one of the magnet coils than the other, causing it to be several centimeters from the position of the sample. This causes the measured moment's corresponding field reading to be incorrect. Figure 3 shows a hysteresis loop from the original LakeShore software. This software did not correct for field offset and it is clear to see the loop is not centered. The offset is easily determined by placing an external gaussmeter in the samples position and measuring static fields on the VSM and the external gaussmeter. This data will vary linearly, and a line can be fit to the data for each of the VSM's gaussmeter ranges. The software has a configuration file that contains the slopes and intercepts from the linear correlations of each VSM gaussmeter range. Figure 4 shows a hysteresis loop taken with our software for the same sample as the loop in Figure 3.

Due to the field offset the coercivity and retentivity calculations that are calculated by the old VSM software are incorrect. This new software recalculates the retentivity and

coercivity based on the corrected field data from the VSM. Another calculation this software provides to the user is a comparison of the saturated magnetization of the sample, and an input comparison magnetization. The last calculation that the software provides is the conversion of the sample's moment at the given field values from emu to the magnetization in $\frac{emu}{cm^3}$. Having the samples plotted magnetization versus field enables us to compare different samples much easier. Since pure moment readings vary with the samples volume it is difficult to compare the moments of different size samples.

The output from the software includes a plot of moment versus field, and if in vector mode, y and x moments versus field. Figure 4 is the output from our software. Above the graphing area is a status bar that contains a great deal of information about the sample. These fields include the time, date, time constant, emu sensitivity, data file name, sample name, orientation, coercivity, retentivity, magnetization, and a comparison between the sample's saturated magnetization and an input magnetization. The sample name holds a description of the sample, while the orientation holds another description of the sample, this group uses the orientation as the angle specified on the VSM drive head. The coercivity is reported in Oe, the retentivity is expressed as the fraction of the retentive magnetization and the saturated magnetization.

CONCLUSIONS

This software has greatly benefited this group. The addition of point averaging mode has led to more accurate data collection. Point averaging mode has also enabled data collection from samples that have very small magnetic moments, and that are influenced by ambient magnetic noise. The y axis moment readings added by the vector mode of operation are also a great aid, because they show the method of moment reversal during hysteresis loops.

The ASYST source for this software is available and gives the experimentalist complete control of data acquisition. Point averaging and vector modes of operation are completely controlled by the software rather than the VSM's internal electronics. The source can be modified to support two additional GPIB devices increasing the amount of data collected for samples. The source is available by e-mailing odell8@llnl.gov.

We would like to thank the US Department of Energy's Science and Engineering Research Semester Program for financial support of this project.

REFERENCES

1. Available from LakeShore Cryotronics, Inc., 64 East Walnut Street, Westerville, OH 43081-2399

2. Available from Keithley Metrabyte, 440 Myles Standish Blvd., Taunton, MA 02780

FIGURE CAPTIONS

Figure 1. A schematic of the VSM setup. This configuration consists of a Hewlet Packard Vectra 486/33N IBM compatible. The PC communicates with the VSM and LOCK-IN via a GPIB (IEEE-488) interface. The VSM controls the power supplies, sample drive head, and electromagnetic coils. The VSM reads the Hall sensor and the x direction emu sensors. The LOCK-IN amplifier reads the y direction emu sensors.

Figure 2. A hysteresis loop for a ferromagnetic sample. It is plotted in units of magnetization, $\frac{emu}{cm^3}$, versus field, H. Hysteresis occurs when a ferromagnetic sample is placed in an external magnetic field and the field is ramped from a maximum value, through zero to a minimum value, and then back through zero to the maximum value. The important characteristics derived from a hysteresis loop are shown. The saturated magnetization, *Ms*, for the sample is the maximum magnetization of the sample. The remanent magnetization for the sample, *Mr*, is the magnetization at zero applied field. The coercive field, *Hc*, is the applied field required for the sample to have zero magnetization.

Figure 3. The output from the LakeShore software. Notice that the loop is off centered from zero. This causes the retentivity and the coercivity to be incorrectly determined.

Figure 4. The output from our developed software. The solid line is the x direction magnetization versus field and the dotted line is the y direction magnetization versus field. Notice loop is correctly centered around zero field strength. This causes the retentivity and coercivity to be correctly determined. Status bar holds many features about the sample. These features include, the retentivity, coercivity, time, date, time constant, sensitivity, sample name, orientation, saturated magnetization, and a comparison between the sample's saturated magnetization and another sample.

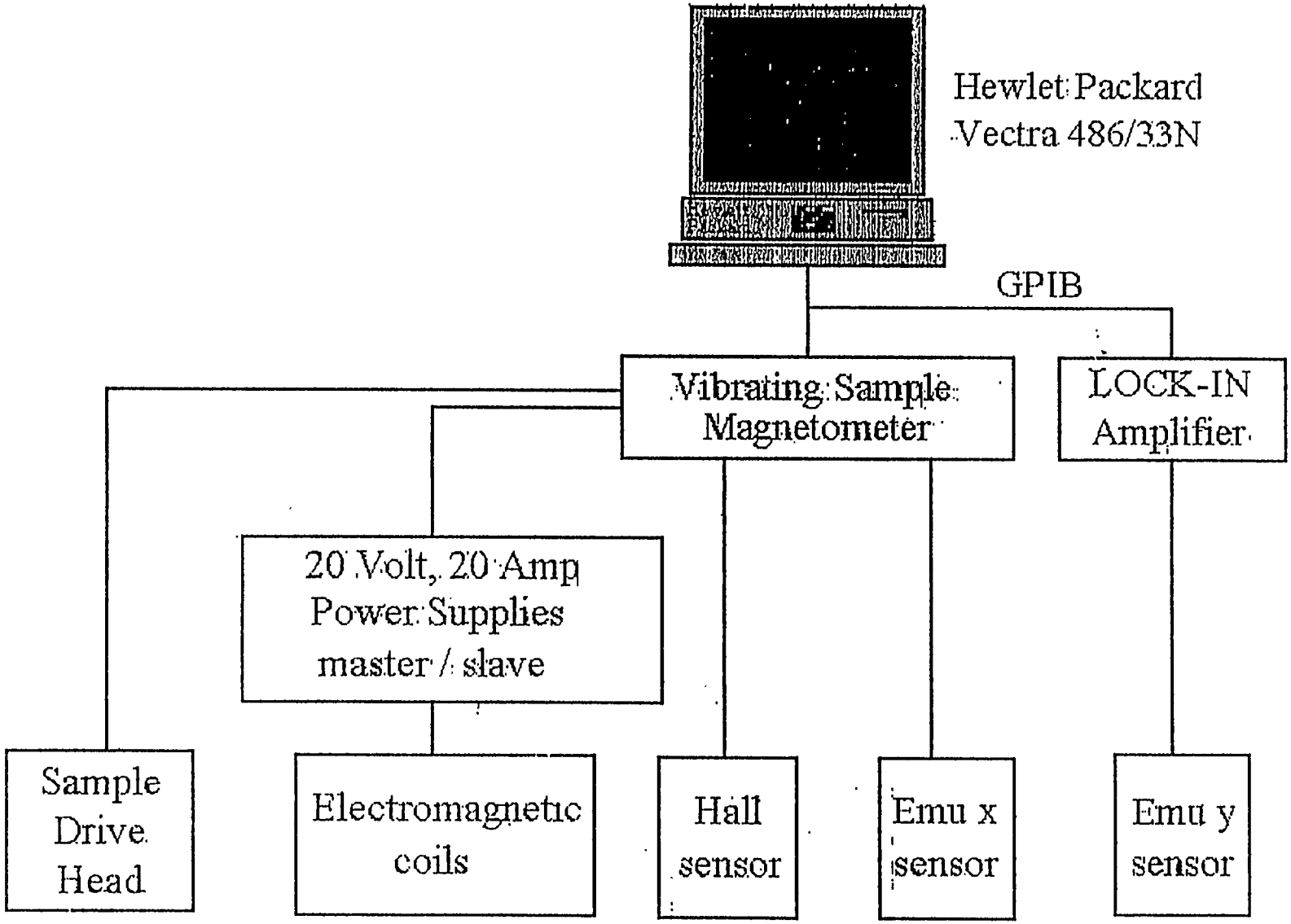
Hewlet Packard
Vectra 486/33N
GPIB
Vibrating Sample
Magnetometer
LOCK-IN
Amplifier
20 Volt, 20 Amp
Power Supplies
master / slave
Sample
Drive
Head
Electromagnetic
coils
Hall
sensor
Emu x
sensor
Emu y
sensor

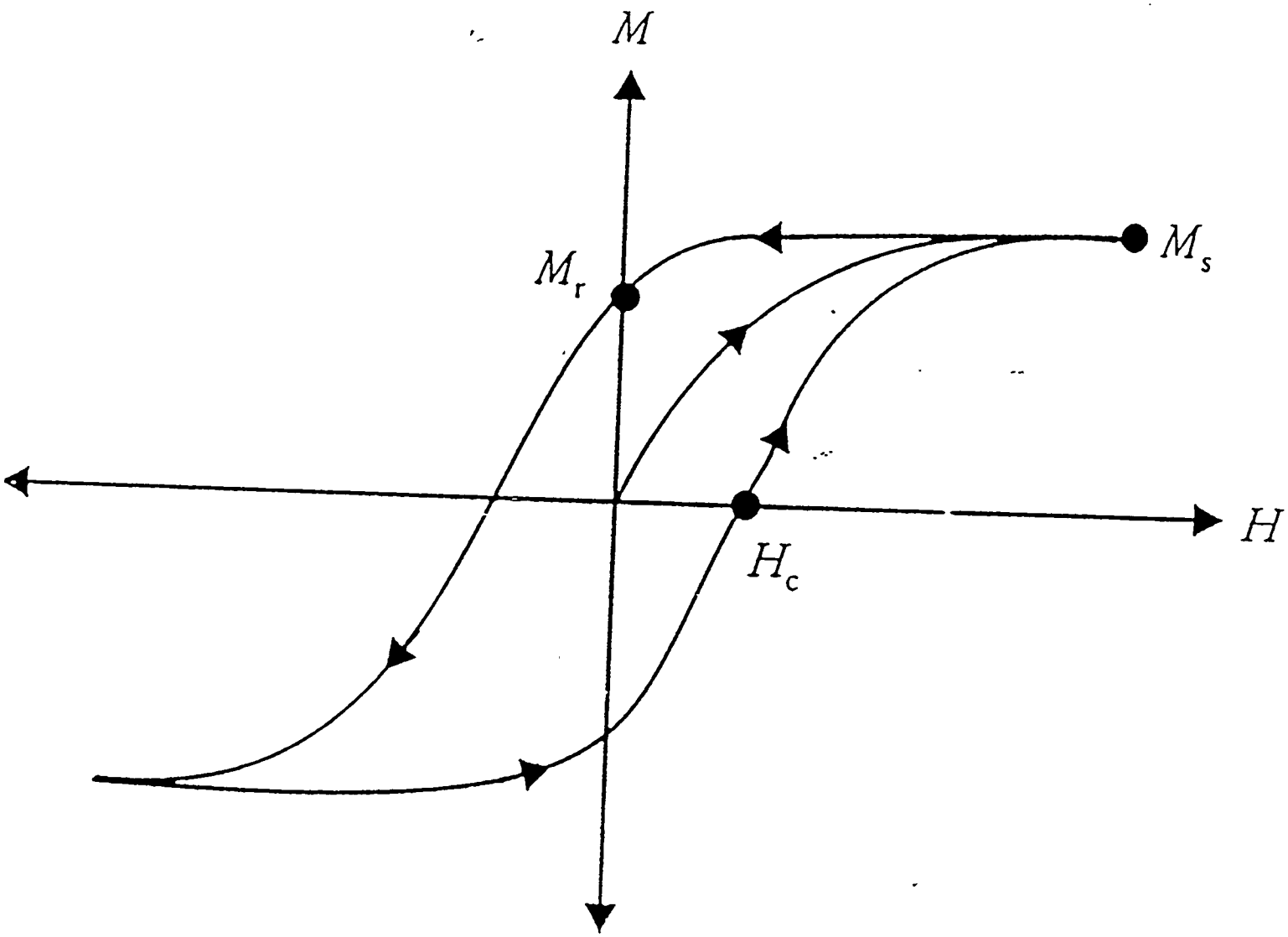
M
M_r
M_s
H
H_c

11/2/94 90° (Hard axis)

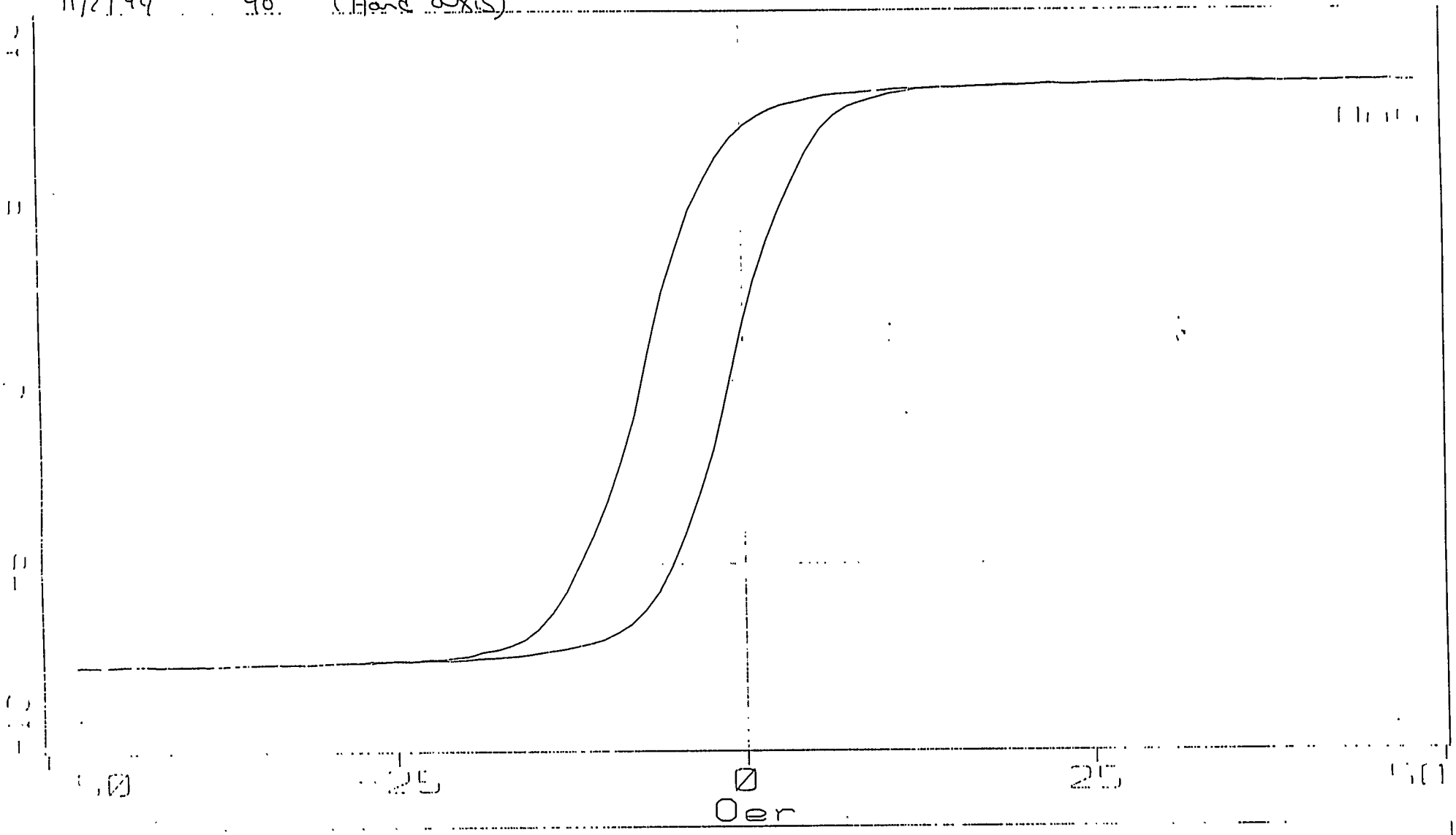

Date
1/01,/'11

Sensitivity
0.01 EMU

Mass
0.00817 EMU

Time of Day
18:10:41

Sweep Time
5 Min

Total Area
0.0986 ergs

Filename
4PyAlxCo.dal

Time Constant
1 sec

Coercivity
3.11 Oer

Sample ID
PyIK/Al20/CoIK/Cu2W4

Squareness Ratio
0.3235 EMU/Oer

Date: 05/03/95 Time of day: 09:20:24.72 Sensitivity: .010 emu
Time constant: .10 sec Coercivity: 2.26 Oe Retentivity: .47
Sample ID: Py1k/Al170/Co1k/Ge 200A 11/2/94
Orientation: 90 degs (Hard axis)
Filename: PyAlxCo.dat Area: .470 cm^2 Thickness: 2000 Angstroms
Magnetization: 787.404 emu/cm^3 Comparison: .460

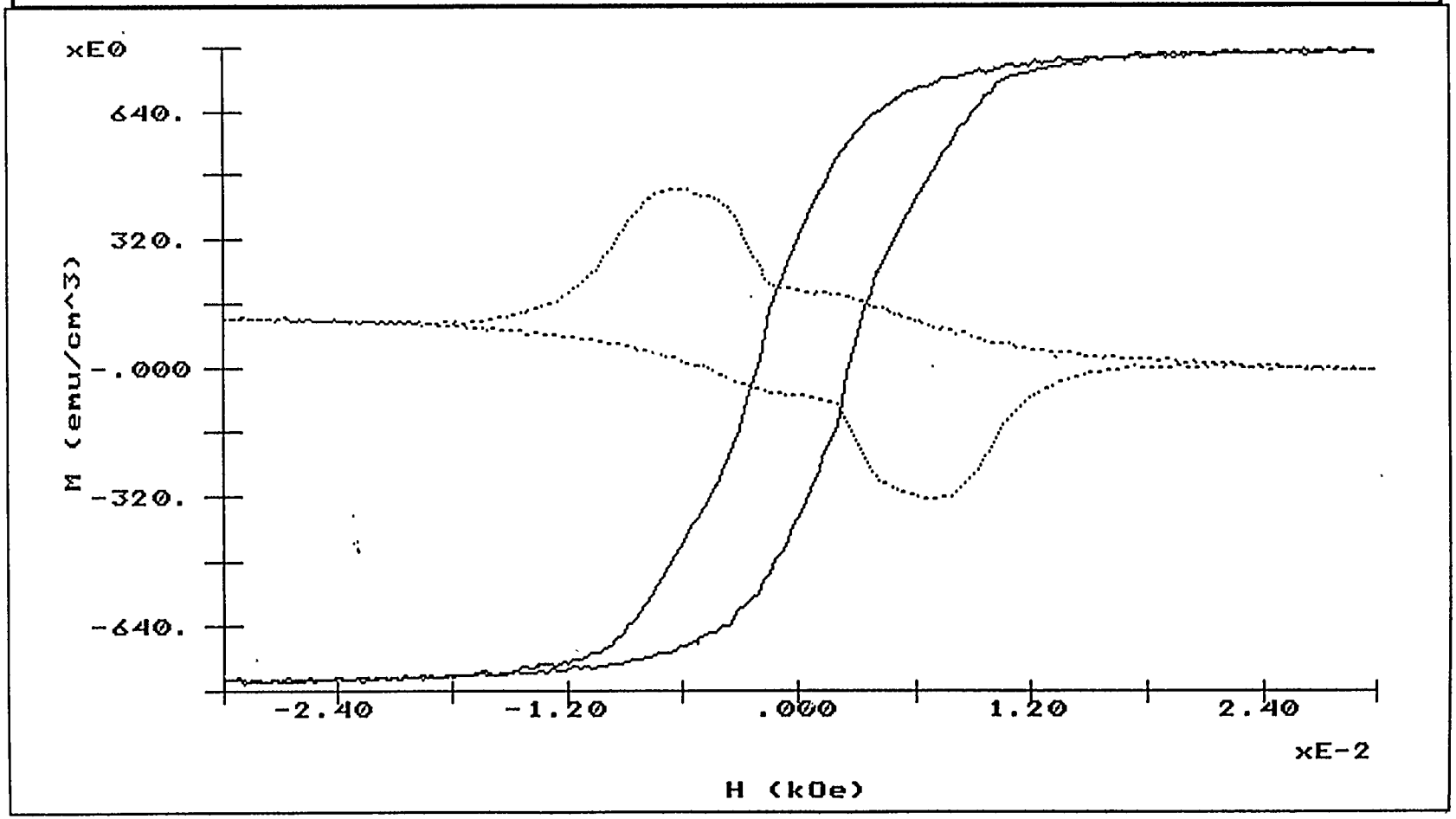

Shooting Stars: *Our Guide to the Early Solar System's Formation* *

Jennifer O'Reilly

Kean College of New Jersey

Lawrence Livermore National Laboratory
Livermore, California 94550

5/13/95

Prepared in partial fulfillment of the requirements of the Science and Engineering Research Semester under the direction of Ian Hutcheon, Research Mentor, in the Lawrence Livermore National Laboratory.

* This research was supported in part by an appointment to the U.S. Department of Energy Science and Engineering Research Semester (hereinafter called SERS) program administered by LLNL under Contract W-7405-Eng-48 with Lawrence Livermore National Laboratory.

Shooting Stars: Our Guide to the Early Solar System's Formation

Jennifer O'Reilly
Kean College of New Jersey
Isotope Sciences Division

Abstract: Plagioclase grains were studied from the Allende meteorite, sample 916, to determine a chronology of events that occurred within the first 10Ma years of the solar system's formation. Radiometric dating of the ^{26}Al-$^{26}Mg^*$ system was accomplished on the ion microprobe mass spectrometer. The excess $^{26}Mg^*$ in core plagioclase grains of calcium-aluminum-rich inclusions (CAI's) provided a time of original condensation for ^{26}Al of ~4.55Ma years ago, 100Ma years prior to the formation of the planets. This data has been found to correlate with other excess $^{26}Mg^*$ samples. Measurements of plagioclase in the CAI's periphery dated 1.52Ma years later, suggesting an interesting history of collision and melting.

Introduction

Before the formation of the solar nebula, nucleosynthesis occurred in a supernova and added new material, including ^{26}Al, to the proto-solar cloud. The supernova triggered a region of the cloud to condense and nucleosynthesis ended. The solar nebula formed from this region approx. 4.553 Ga years ago. This hot, gaseous cloud was comprised of dust and ice particles. The nebular's temperature slowly decreased over the next few million years and the first condensates began to form. Calcium-aluminum-rich inclusions formed from the first condensates ~4.55Ga years ago. Chondrules formed between one to five million years later. The solar nebula dissipated around 4.535Ga years ago and meteorite parent bodies (asteroids) were formed. The terrestrial planets formed by the accretion of asteroids, almost 90Ma years after the nebulas break-up.

Because the earth is not old enough to provide us with a chronological depiction of how and when the solar system formed, scientists have turned to meteorites for answers. Although meteorites have five distinct categories of classification, only one is significant to this study: chondrites. On February 6, 1969, two tons of carbonaceous chondrite, which is a subclass of chondrites, plunged into Pueblito de Allende in northern New Mexico, opening a new chapter in studies of the early solar system. Carbonaceous chondrites are particularly important because they contain pristine chondrules and calcium-aluminum-rich inclusions (CAI's) that are ten to twenty million years older than most whole meteorites. The CAI's are believed to represent the first solid objects that formed at high temperatures in the early solar nebula.

The focus of this study is to determine a chronology of events during the first few Ma of solar system history. Radiometric dating using ^{26}Al enables age determination of plagioclase in CAI's. The principle behind radiometric dating is that an unstable parent atom decays into a stable daughter atom. The time required

for half of a given quantity of parent atoms to decay into daughter atoms is called the element's half-life ($T_{1/2}$). Certain assumptions are made about radioactive decay that are necessary for precise age determination. The first is that the decay constant is accurate. It works on the premise that each atom of a particular nuclide decays independently from all of the others at a constant rate. The number of atoms that decay during a given time period is proportional to the number of atoms present.

Long-lived radio nuclide systems are useless in this study because there isn't sufficient time resolution. For example, ^{238}U-^{206}Pb has a $T_{1/2}$ of 4.8Ga. Our investigation focuses on a time period of a few million years, therefore, little ^{238}U would have decayed. Short-lived radio nuclide systems, like ^{26}Al-^{26}Mg, are ideal for dating purposes. ^{26}Al decays with a $T_{1/2}$ of 720,000 years into the stable daughter isotope $^{26}Mg^*$ (radiogenic Mg). The type of decay is electron capture, whereby an electron falls into the nucleus, a neutron is gained at the expense of a proton and the atomic number decreases by one unit ($^{26}Al_{13}$ to $^{26}Mg_{12}$). Two traits make this radio nuclide system ideal for radiometric dating. First, as previously stated, the short half-life provides precise time resolution. Second, the CAI's are aluminum-rich, so any excess radiogenic magnesium is easily traced. Too many half-lives have passed since the production of ^{26}Al, resulting in an undetectably small amount left in the solar system today. We can still calculate the age of the CAI, though, using the precise ^{26}Al $T_{1/2}$ and $^{26}Mg^*$ present. As the number of ^{26}Al atoms decrease, fewer parent atoms remain to decay. The result is a proportionate decrease in the rate of ^{26}Al decay and a corresponding growth rate of $^{26}Mg^*$ (Fig. 1).

Assuming the mineral sample won't gain or lose any parent or daughter atoms, we can determine the original amount of ^{26}Al. The sum of the remaining parent atoms plus the daughter atoms will always equal the amount of original parent atoms. The ratio of daughter atoms to parent atoms will exponentially increase as half-lives elapse.

Corundum (Al_2O_3), for example, is the ideal sample for ^{26}Al-^{26}Mg dating because it is an aluminum- rich, Mg-poor mineral. As the $T_{1/2}$ elapse, the large concentration of ^{26}Al decays into a correspondingly large amount of $^{26}Mg^*$. The ratio of radiogenic magnesium to normal magnesium can be very large (up to 30). Olivine (Mg_2SiO_4), on the other hand, is nearly void of any ^{26}Al, but has plenty of normal magnesium. This means that as half-lives elapse, no radiogenic Mg * will result from decaying. The ratio of $^{26}Mg^*/^{24}Mg$ will consistently remain at zero. Plagioclase ($CaAl_2SiO_8$) in CAI's usually contain ~.10% normal Mg and the ratio of radiogenic Mg* to normal Mg falls between 0.05 and 0.3 (Fig. 2).

Methods

CAI's have a complex mineralogy, which lengthens the analytical technique. The inclusions are riddled with magnesium-rich minerals like spinel, pyroxene, and melilite, as well as aluminum-rich grains like plagioclase. The grains overlap and mesh together, making it difficult to get a clear plagioclase reading without interference. In these Mg-rich minerals, the trace amounts of radiogenic $^{26}Mg^*$ resulting from ^{26}Al decay are indistinguishable from the normal ^{26}Mg. Because there is no known method for separating the two, minerals with low amounts of normal magnesium, such as plagioclase, are required.

Three analytical techniques were used in this study: (1) the optical microscope, (2) the electron microprobe, and (3) the secondary ion mass spectrometer. The first step in searching for radiogenic magnesium in a thin section of a CAI from the Allende meteorite, is to locate plagioclase. In a petrographic microscope, the specimen is viewed in polarized, transmitted light to view the array of colors and identify the minerals present. In reflected light, the specimen looks identical to the image in the ion probe. The plagioclase-filled area of the CAI is photographed in this light to

help recognize the same spot in the next two instruments. The second step is to transfer the sample into the electron microprobe. This verifies the plag-filled regions by displaying three different images: a back-scattered electron, a x-ray, and a secondary electron. The back-scattered image depicts the composition of the sample by showing contrast in the shades of black and white. Elements with a lighter atomic number appear darker in color, while the heavier ones look pale. A x-ray spectrum of the specimen identifies the elements and their concentrations. Magnesium-rich phases like spinel are distinguished from aluminum-rich ones like plagioclase. A secondary electron image portrays a topographic profile of the sample. The third process is to put the sample in the secondary ion mass spectrometer (ion probe). *In situ* age determination of single mineral grains in a complex CAI sample is possible because of its spatial resolution of ~10 microns. The ion probe works on the premise that solid material can be analyzed by separating charged particles according to their masses. The instrument consists of three main parts: (1) the source of primary ion sputtering; (2) a magnetic analyzer, and (3) an ion detector. Before we do isotope analysis of the CAI on the ion probe, we first run standards of known terrestrial minerals to ensure the machine's accuracy. Minerals with high magnesium, like spinel and pyroxene, are measured. They contain Mg with a 26Mg/24Mg ratio of ~0.139%, which is the same value as the sun. The $^{26}Mg/^{24}Mg$ ratio from the standards should lie along a line with the slope of zero because they contain no radiogenic $^{26}Mg^{*}$.

We single out a plagioclase grain and bombard it with a beam of charged particles, drilling a hole in it. The mass spectrometer collects the secondary ions sputtered off and separates them by their charge-to-mass ratio in the magnet. We vary the magnetic field setting from ^{26}Mg to ^{24}Mg , and measure the ratio 100 times, without changing the ion source or detector controls. Because isotopes have different charge-to-mass ratios, a mass spectrum displays a series of peaks and valleys that

correspond to different isotopes. Also, an image distribution of the elements enables us to isolate plagioclase grains with high $^{26}Mg/^{24}Mg$ ratios. The final step is to download the data into a computer program, which corrects for error. The program automatically plugs the incoming data into an equation which produces the delta $^{26}Mg^*$.

$$\text{Delta } ^{26}Mg^* = \left\{ \frac{\left(^{26}MG/^{24}MG\right)_X}{\left(^{26}MG/^{24}MG\right)_S} - 1 \right\} x1000$$

The equation relates the plagioclase ratio (x) to the standard ratio (s) to get a relative excess $^{26}Mg^*$ reading. The computer automatically converts the products into parts per thousand to accentuate even the smallest change in the ratios (Fig. 3). We plot the results on an isochron diagram, which shows the amount of $^{26}Mg^*$ versus the Al/Mg ratio. Then we compare different line slopes and calculate relative ages for the plagioclase grains.

Results

The plagioclase grains we measure were from opposite ends of the CAI. The first sample's location was in the core area, where clearly defined, elongated laths were located. There was very little overlapping of minerals, like spinel, that interfered with accurate signals and results. All but two of the samples were taken from this interior region. The exceptions were located near the edge of the CAI, where it borders with the matrix (Fig. 4). After downloading the data into the computer, we plotted the Al/Mg ratio versus the $^{26}Mg^*$. Surprisingly, all of the samples plotted along the same isochron with a slope of $3.8x10^{-5}$, except for two. These were the samples taken from the inclusion's periphery. We took more measurements of

plagioclase grains along the rim, yet they were on the opposite end of the CAI. The results were conclusive that these samples from the exterior of the CAI all plotted along a different line with a slope of $9x10^{-6}$. The standards were plotted along yet another line with a slope of zero, showing no excess $^{26}Mg^*$ (Figure 5). The different slopes indicate two different ages for plagioclase in the CAI. The slope of $3.8x10^{-5}$ contained the highest amount of $^{26}Mg^*$, so it is the oldest material. We compared that slope with the average past CAI results, which plot along a line with the slope of $5x10^{-5}$. From this difference our sample was calculated to be 0.3Ma years younger than most CAI's. Ratio's obtained from its exterior, with a slope of $9x10^{-6}$, were 1.52Ma years younger than the core material.

Discussion

The $^{26}Mg^*$ concentration was homogeneous from one end to the other, yet varied from the inside out. This heterogeneity suggests a complex history of the CAI. According to our results, the ^{26}Al was produced and condensed in our inclusion ~4.549Ga years ago; the time of origin for $^{26}/_{27}Al$ in the first CAI's was ~4.55Ga years ago. The younger material in the inclusion's exterior suggests that a collision melted its face, causing the plagioclase crystals to realign. The time clock for ^{26}Al was reset. The collisions took place 1.52Ma years later, which is evident from $^{26}Mg/^{24}Mg$ calculations in CAI's.

Age determination of plagioclase in CAI's is possible because of radiometric dating. This technique, coupled with technological advances in mass spectrometery, allowed us to determine a chronology of events during the first few Ma of solar system history. The study supports past theories of a supernova explosion that injected radioactive material, like ^{26}Al, to the proto-solar cloud before it condensed into the nebula. CAI's have been proven in this project, as well as others, to be of

the oldest material known. Studying these inclusions have given us important clues in deciphering how and when the solar system formed.

FIGURE 1

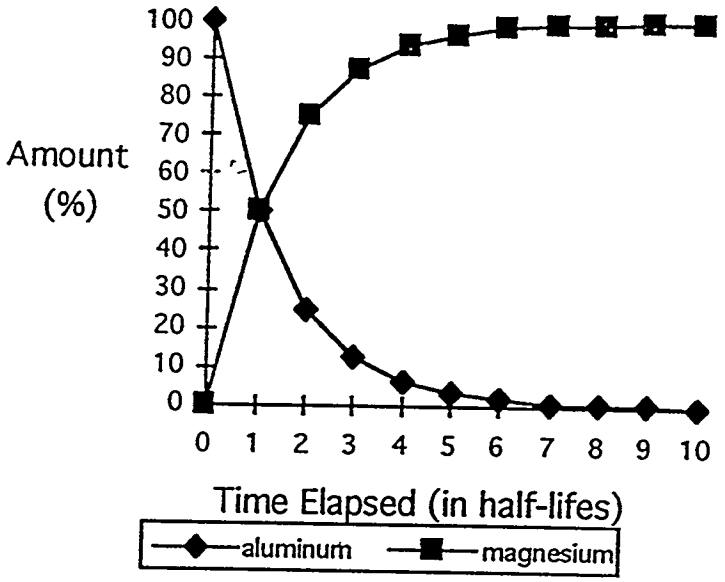
Amount
(%)
100
90
80
70
60
50
40
30
20
10
0
0 1 2 3 4 5 6 7 8 9 10
Time Elapsed (in half-lifes)
aluminum
magnesium

FIGURE 2

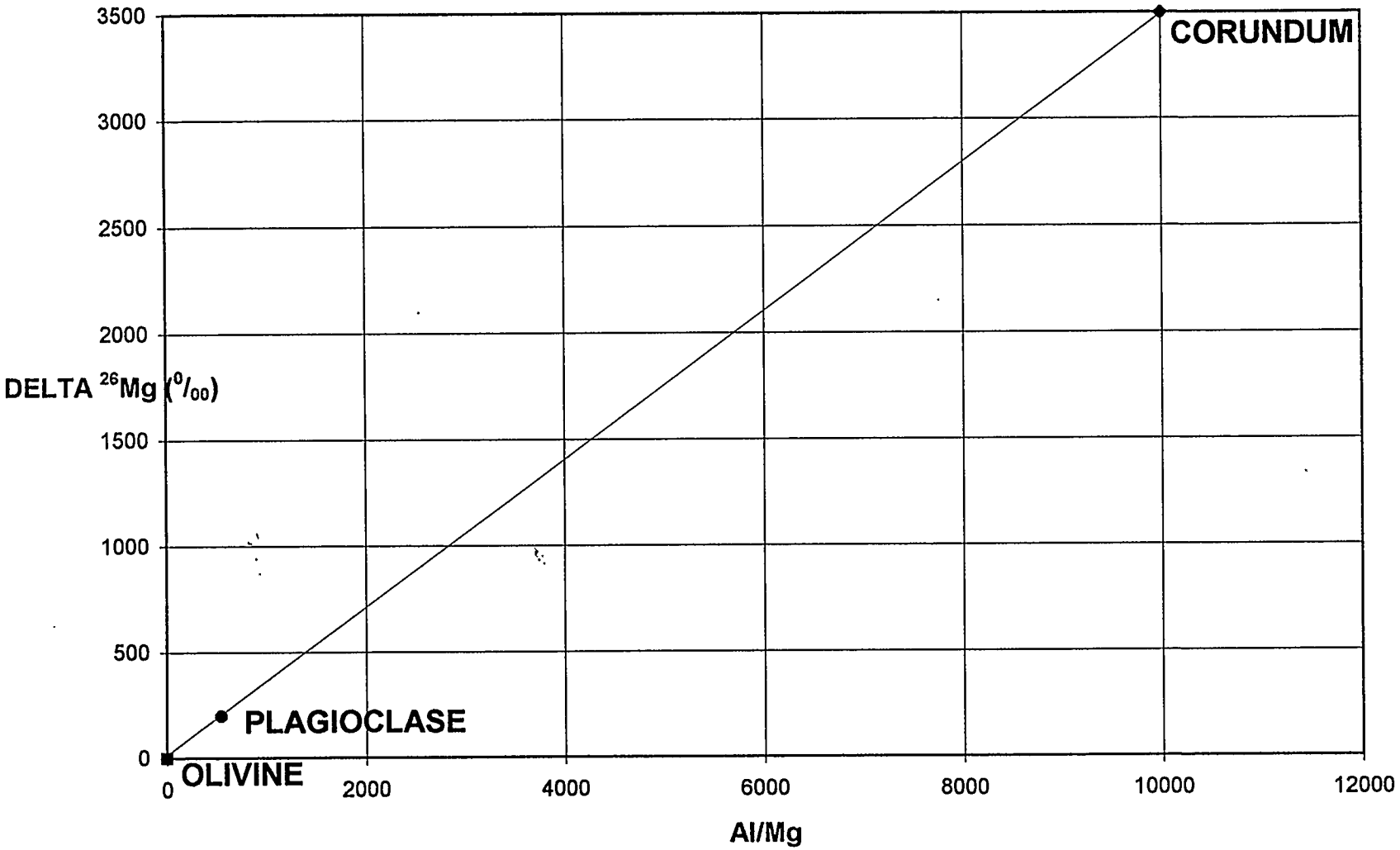
3500
3000
2500
2000
1500
1000
500
0
DELTA ^{26}Mg ($^{0}/_{00}$)
CORUNDUM
PLAGIOCLASE
OLIVINE
0
2000
4000
6000
8000
10000
12000
Al/Mg

FIGURE 3

	SAMPLE	42Ca/24Mg	27Al/24Mg	DELTA 26Mg*	STDEV
STANDARDS					
PYROXENE	1	0.023	3.7605	1.64	3.38
PYROXENE	2	0.026	4.251	3.66	2.92
PYROXENE	3	0.0644	10.5294	6.74	6.35
PLAG-TERRESTRIAL	4	0.642	104.967	1.21	6.53
PLAG-TERRESTRIAL	5	0.64	104.64	4.89	3.72
SPINEL	6	0.022	3.597	4.51	1.72
PLAGIOCLASE					
CAI-INTERIOR	1	1.835	300.0225	90.86	5.38
	2	2.635	430.8225	118.28	6.77
	3	2.88	470.88	143.8	6.9
	4	3.25	531.375	134.4	7.5
	5	4.76	708.26	177.7	6.3
	6	4.3	703.05	187.5	8.1
	7	1.134	185.409	63.6	11.41
	8	1.354	221.379	59.83	4.58
CAI-EXTERIOR	9	0.077	12.5895	6.89	22.99
	10	1.603	262.0905	12.37	6.7
	11	2.14	349.89	23.94	6.1
	12	1.335	218.2725	15.38	15.12
	13	2.083	340.5705	16.78	5.07
	14	2.298	375.723	33.67	7.53
	15	1.292	211.242	22.87	8.02

FIGURE 4

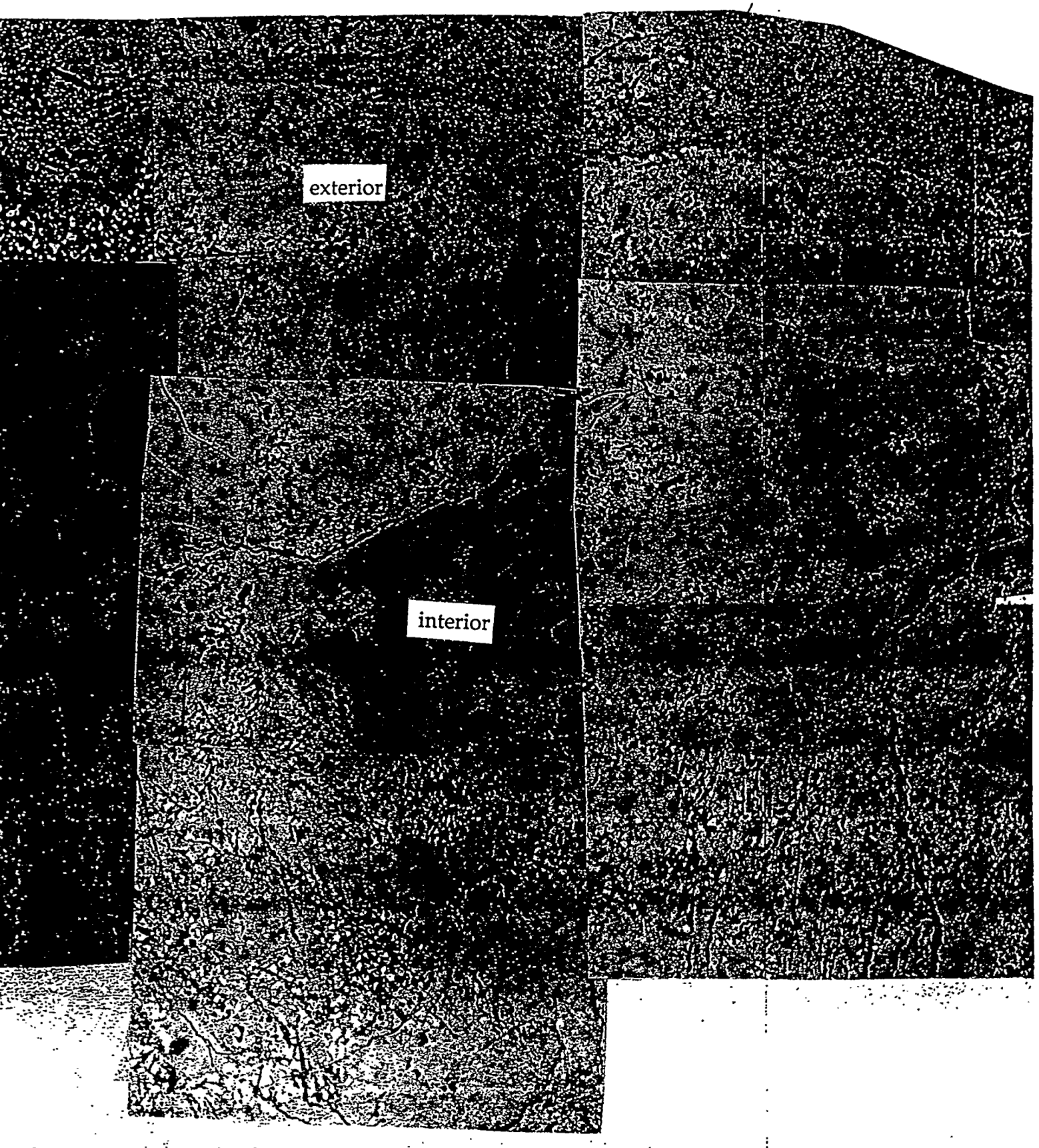

FIGURE 5

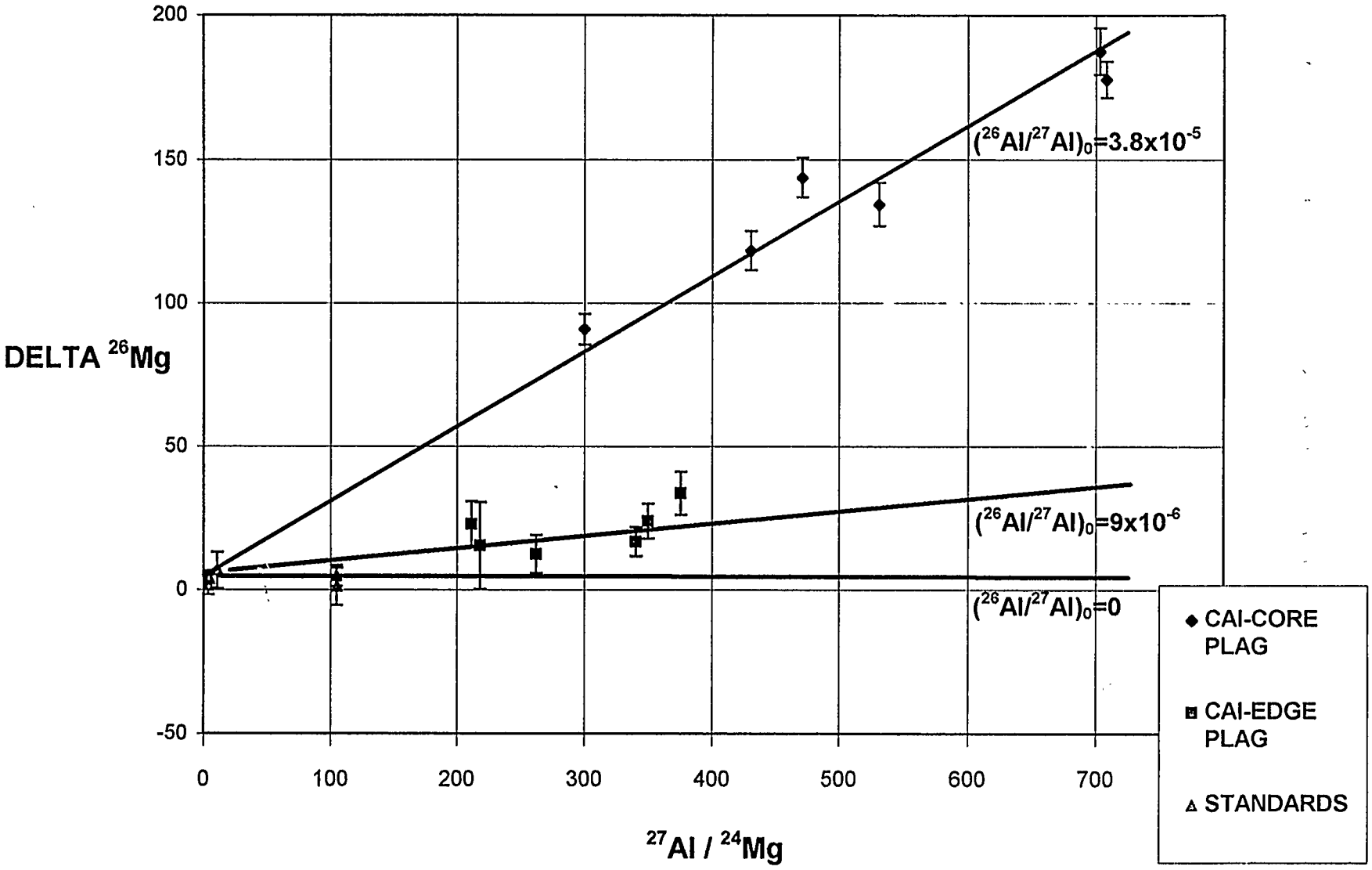

LLNL

Geogenic Generation of Cr(VI) in Groundwater Systems at LLNL

Chris Parsons, SERS Program, Environmental Restoration Division
Maureen Ridley, Mentor, Environmental Restoration Division

ABSTRACT

Oxidation of trivalent chromium to hexavalent chromium has been investigated as a function of total manganese in soils as well as various incubation conditions. Chromium and manganese contents were analyzed by atomic absorption (graphite furnace and flame emission respectively) following acid digestion (EPA METHOD 3050). Total hexavalent chromium generation capacity was determined by the addition of 0.001 M $CrCl_3$, incubation (sample left undisturbed in the hood), and analysis by s-diphenyl carbazide (Bartlett and James, 1979). Samples were then leached with 0.005 *M* $CaSO_4$ + 0.005 *M* $MgSO_4$ and pretreated in various environments (oven, freeze-drier, ultrafreezer), followed by incubation to test for geogenic generation of Cr (VI). All fresh field samples had the ability to oxidize Cr (III) to Cr (VI) when in presence of excess Cr (III). Cr (VI) concentrations were in the range 7.6 µg - 73.0 µg per 5.0 grams field fresh sample. Post-leaching samples also possessed the ability to generate Cr (VI) after incubation. Incubated samples demonstrated Cr (VI) generation potential in the range 0.062 µg - 0.538 µg per 80.0 grams field fresh sample. Fresh samples were then leached and re-incubated successively for up to eighteen days. Samples demonstrated the consistent ability to produce Cr (VI) in ranges up to 4.69 µg per kg sample.

INTRODUCTION

Among the various concerns of environmental chemistry, the sanctity of groundwater undoubtedly ranks with the most important. Considering that over 125 million Americans and over 1/3 of the U.S.' largest 100 cities depend on groundwater daily for their drinking supply (Cleary, Princeton Groundwater Course), contamination demands public attention due to the potential hazards it presents.

One particular contaminant of concern is hexavalent chromium, carcinogenic to humans in concentrations over 50 parts per billion (ppb) and toxic to fish over 11 ppb. Consequently, the interconversion of chromium between its two stable oxidation states, Cr (III) and Cr (VI), becomes of considerable intersest. A proposed mechanism for the oxidation of trivalent chromium involves electron transfer at the surface of various naturally occuring manganese oxides. Since many of these oxides are inherently present in soils around the water table, Cr (III) could be oxidized naturally at potentially harmful levels.

Various oxides of manganese are the only known oxidizing agents capable or transforming Cr (III) to Cr (VI) below pH 9.0. Visible nodules of the manganese oxide birnessite are present throughout the soil cores chosen for the incubation. While the ability of manganese oxides to convert Cr (III) to Cr (VI) has been well established by the work of Bartlett and James (1979) as well as Burau, Chung, and Zasoski (Present), the mechanistic and kinetic factors which contribute to the natural formation of Cr (VI) have not been documented. Part of the motivation for this work involves an investigation into the mechanistic aspects of the conversion of Cr (III) to Cr (VI). A possible contributing factor is the presence of microbes which are capable of *reducing* Cr (VI) to Cr (III), thereby acting to reduce the oxidative effects of the reaction. Soil samples underwent various treatments prior to incubation in order to elucidate the possible interactions between microbes, surface characteristics, and solution variables in the reaction.

Protocol

Soil Characterization

Samples were gathered from four different boreholes around the Lawrence Livermore National Laboratory (LLNL) site. A total of five cores were ascertained ranging in depth bewteen 67.5 feet and 105 feet. All samples were gathered and sealed within one week of drilling. Samples were then ground sufficient to pass through a 2 mm sieve. Preliminary soil charaterization consisted of consecutive acid digests followed by atomic absorption analysis for total manganese and chromium in soil. Total moisture content was determined by the gravimetric method.

Chromium Oxidation Quick Test

The capacity of each soil to generate Cr (IV) was determined through a modified version of the Chromium Oxidation Quick Test, developed by Bartlett and James in 1979. Five grams of fresh sample were placed in a 50 mL centrifuge tube along with 25 mL of a 0.001 *M* $CrCl_3$ solution. In order to determine the effect of pH on the extent of oxidation, two solutions of .001 $CrCl_3$ were used, pH 3.6 and pH 6.9. Each mixture was then shaken for approximately 15 minutes on a Lab-Line Vortex Super-Mixer and centrifuged for approximately ten minutes (until clear). Supernatant was then filtered through 22 µm filter and analyzed by s-diphenyl carbazide colorimetric method.

Non-Anthropogenic Cr (IV) Generation

Samples were divided into eighty gram units in preparation for the leaching procedure. Four units from each core and corresponding depth were leached with 0.05 $MgSO_4$ + 0.05 $CaSO_4$ in 50 mL aliquots and analyzed for Cr (IV). Atomic absorption analysis was utilized for the leaching eluents due to the large volume of samples; however, spot checking for Cr (IV) generation with the s-diphenyl carbazide method was successfully employed. After leaching each sample underwent either freeze-drying, ultrafreezing (-69°C), oven baking (60°C), or field moist. Each sample was then re-moisturized and incubated for nine days after which centifugation and analysis for Cr (IV) were performed.

Results

While the phenomenon of trivalent chomium oxidation to the hexavalent species has been observed and well established, the mechanistic factors which contribute to this process continue to be relatively nebulous. Soils undergoing three post-leaching, pre-incubation treatments were capable of producing Cr (VI) in the range of 0.062 µg-0.538 µg per 80 grams of soil per sample. The samples were incubated in a moist environment for nine days at 25°C. Upon consummation of incubation, the samples were centrifuged with additional nanopure water and the supernatant was analyzed for Cr (VI). Total Cr (VI) amounts were then reported in terms of µg Cr (VI) generated per 80 grams of air-dried sample.

Upon characterizization of the soils from the four different boreholes, a modified version of the Bartlett "Quick Test" was employed in order to determine the potential of each soil to generate Cr (VI). The test was performed at two pH values (3.6 and 6.9) in order to determine the effect of pH on the extent of the reaction. As expected, the lower pH produced significantly higher yields of Cr (VI) in every case, indicating the oxidative reaction is related inversely to pH. Cr (VI) concentrations were in the range of 5800-14600 µg Cr (VI)/kg dry sample for pH 3.6 and 1520-5720 µg Cr (VI)/kg dry sample for pH 6.9.

Leaching was performed in glass columns (~200mm long, ~25 mm in diameter with outlet tube ~50 mm in length and ~4 mm in diameter) fitted with teflon stopcocks. The soil was placed over glass beads and approximately two inches of loosely packed glass wool at the bottom of the column. Fifty mL aliquots of 0.005 *M* $MgSO_4$ + 0.005 CaSO4 were run through the column and analyzed for Cr (VI) by atomic absorption with spot-checking by s-diphenyl carbazide method for Cr (VI). For each original sample location the profile characteristics of each leaching was recorded. In all samples the majority of Cr (VI) was removed in the first two leachings. Successive leachings ensured near complete removal of available Cr (VI).

After leaching, the samples were divided and treated in order to isolate a specific variable of the reaction. One fourth of the samples were freeze dried, one fourth ultrafrozen, and one fourth oven baked. The balance of samples were placed in a hood, untreated. All samples were then remoistened to original moisture content and incubated for nine days at 25°C. Of the four treatments, four fifths of those samples which were oven baked produced the highest Cr (VI) concentrations. The samples which had been freeze-dried generally produced the lowest Cr (VI) concentrations. The control and ultrafrozen group generally produced Cr (VI) concentrations between that of the oven baked and freeze dried-samples.

While the number of samples available to establish a trend is statistically insufficient, the removal of water appears to have the most drastic impact on Cr (VI) production. Samples generating the highest levels of Cr (VI) were heated while inherent water was removed while those samples yeilding the lowest Cr (VI) concentrations were subjected to a low temperature water extraction. In both cases, as well as in the ultra-freezing case, any microbes present in the sample would likely have been killed, increasing the the oxidation rate. Such a trend does not appear in the data obtained by this work. Perhaps the most telling observation in that the control sample did not consistently produce lower concentrations of Cr (VI) even though it underwent no pretreatments. Regardless of the behavior of individual soils, the geogenic generation of Cr (VI) continues to be well observed at detectable levels.

Successive Incubation

Since the geogenic generation of Cr (VI) has been observed and well established in this work and in that of others, a profile of the Cr (VI) generation rate becomes of interest. Soil from the location labelled "C," B-1105-70', was chosen to conduct this test based upon its readily observable ability to oxidize Cr (III) and its copious supply in the laboratory. In precisely the same manner as in the previous leachings, four 80 g samples were weighed into leaching columns and leached with 50 mL aliquots of 0.005 *M* $CaSO_4$ + 0.005 *M* $MgSO_4$ until the leachate contained less than 1ppb Cr. As in previous analyses, atomic absorption was employed to obtain Cr concentrations.

After the leachings were complete, the wet soils were combined, sufficiently mixed to obtain homogeneity, and divided into ten equal partitions. Each unit was then individually sealed and freeze-dried to reduce reactions during the water extraction phase. Each sample was then remoistened to its original water content and placed in the hood at room temperature for incubation.

Each day up to four samples were withdrawn from the incubation environment and analyzed for Cr (VI). The first day, one sample was analyzed for Cr (VI). The second day, both the aforementioned sample and a fresh sample were extracted and analyzed. This process continued until four samples were being analyzed daily, when the group of analyzed samples would shift by one sample. Such a scheme allowed for a diverse distribution of data as a function of time, and one that revealed some significant trends.

Upon examining the data, it becomes immediately clear that measurable concentrations of Cr (VI) are extracted from the samples at all times throughout the test. Samples generally contained Cr (VI) concentrations between 1 ppb and 5 ppb when reported in terms of the dry weight of sample. Such consistent generation of Cr (VI) indicates at least one facet of the oxidation reaction at hand. Current theory involves electron transfer at the site of the manganese complex, birnessite in the case of the LLNL site. If the Cr (III) undergoing oxidation must be associated with the surface of the manganese complex in order to be oxidized, a repetitive incubation process should be accompanied by a fresh supply of Cr (III) coming into contact with the birnessite surface. Since the soil sample contains total Cr concentrations in the range of 35 ppm, the oxidation process is limited not by Cr content, but by available electron tranfer sites in the birnessite complex. The trend demonstrated by this test supports the idea that successive oxidation of available Cr will continue at a relatively steady rate until all Cr is depleted.

A concurrent theory proposes the possibility of Cr ions inherently present in the crystalline structure of birnessite. If the inherent ions are of the trivalent form, their oxidation would take place prior to their extraction from the crystal. However, Cr (VI) ions could also be present in the manganese complex. These ions would then be extracted from the crystall lattice in pore water extraction. If such a process is occuring in the soils at LLNL, it is likely an additional source of Cr and not the sole source of Cr (VI) production. The consistent generation of Cr (VI) supports a strong surface dependent reaction at the site of the manganese complex.

Particle Separation:

In addition to the original soil characterization which related various physical and chemical properties of the samples, a separation process based upon particle size was performed. The presence of Cr (VI) in pore water is thought to be associated with birnessite nodules disseminated throughout the sample. A possible source of Cr in soils is believed to be located inside the crystalline structure of the birnessite complex. Therefore, isolation of birnessite nodules and subsequent analysis for Cr content merits attention.

Soil from the same location as in the previous test, B-1105-70', was air-dried and prepared for dry-sieving. A network of sieves was selected to isolate particles ranging from 2 mm to 180 μm at the smallest diameter of the particle. Twenty five grams of sample was sieved for fifteen minutes in a sieve shaker. Such a relatively brief amount of sieving time allows for sufficient particle separation without synthetically breaking down existing particles into smaller units. At each level of separation (180 μm, 250 μm, 500 μm, fines) the particles collected underwent acid digestion and were analyzed for total Mn content. While it appeared that the strata labelled "fines," which passed through all the sieves, contained the highest content of visible birnessite nodules, acid digestion and atomic absorption analysis indicated a consistent level of Mn concentration. The mean Mn content of each layer was 3.65 mg/L in acid with a relative standard deviation of 4.4%, indicating an extremely close set of data.

The upshot of the above situation appears to be that while higher percentages of birnessite may be present in smaller particles, a significant portion of manganese remains undigested after acid reflux. Approximately fifteen barely visible specs were separated manually and acid digested. The digestion procedure left at least some of the specs still visible, indicating the necessity of a more powerful acid to *completely* hydrolyze the specs. Atomic absorption analysis will indicate if significant concentrations of Mn and Cr are present in the acid digests of these specs. As previously mentioned, the presence of chromium in these digestates would contribute to the theory of inherent Cr ion association with the birnessite complex.

Soil Characteristics

Sample ID	Depth (ft)	Total Cr * (mg/kg soil)	Total Mn* (mg/kg soil)	Moisture % **
B1101	105	52.6	563.1	19.62
B1102	105	51.2	550.2	14.18
B1105	70	35.6	454.2	11.67
B1105	90	104.4	554.7	17.17
SIB-543-102	67.5	59.6	508.8	14.54

* Total analyte concentrations determined by acid digest and atomic absorption analysis

** Moisture % determined by gravimetric method

Data from "First Leaching -Position 2"

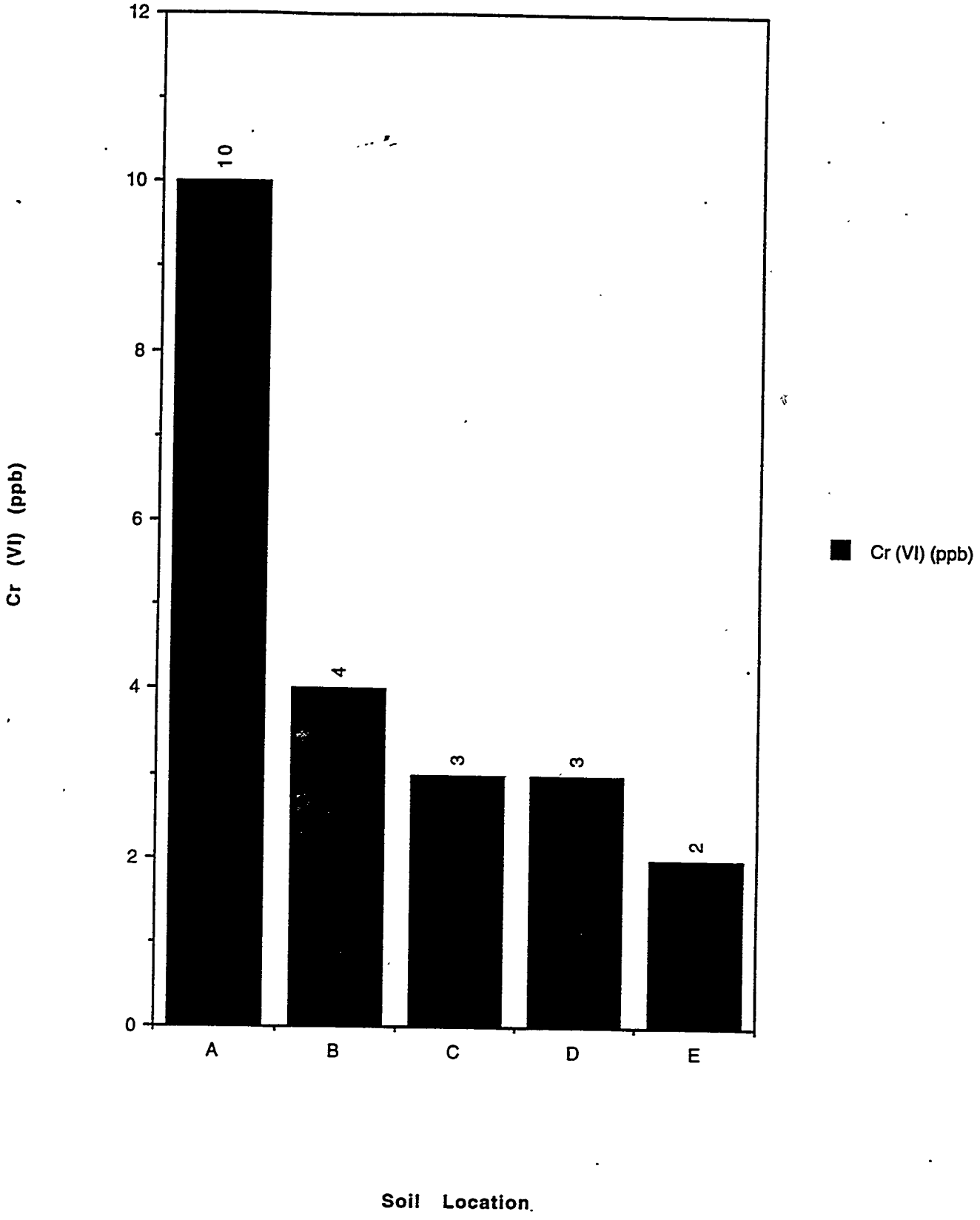

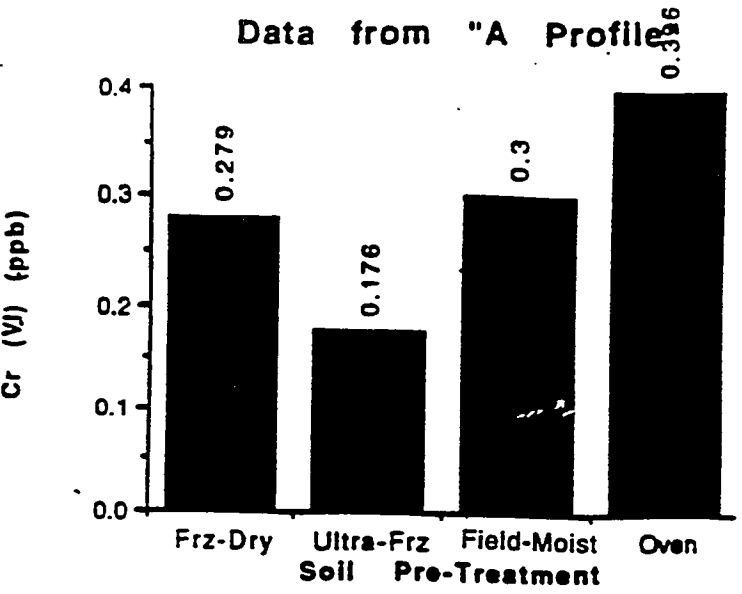
Data from "A Profile"
Cr (VI) (ppb)
0.4
0.3
0.2
0.1
0.0
0.279
0.176
0.3
0.386
Frz-Dry
Ultra-Frz
Field-Moist
Oven
Soil Pre-Treatment

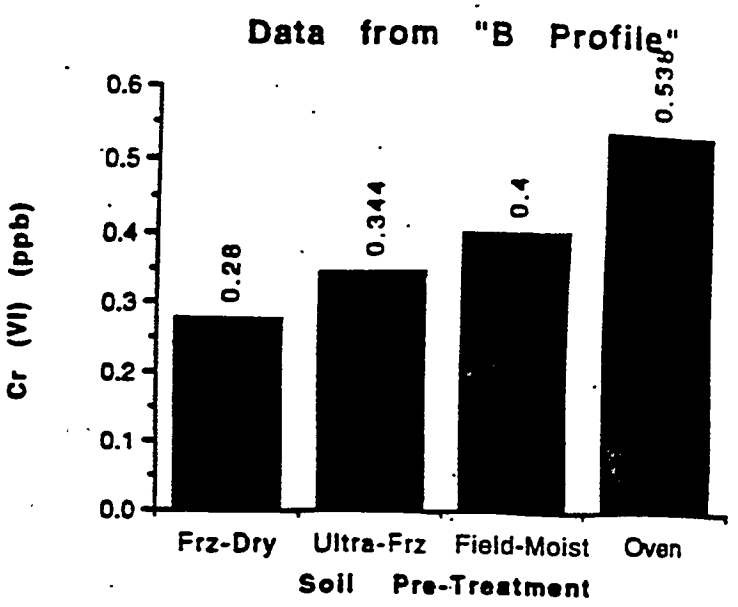
Data from "B Profile"
Cr (VI) (ppb)
0.6
0.5
0.4
0.3
0.2
0.1
0.0
0.28
0.344
0.4
0.538
Frz-Dry
Ultra-Frz
Field-Moist
Oven
Soil Pre-Treatment

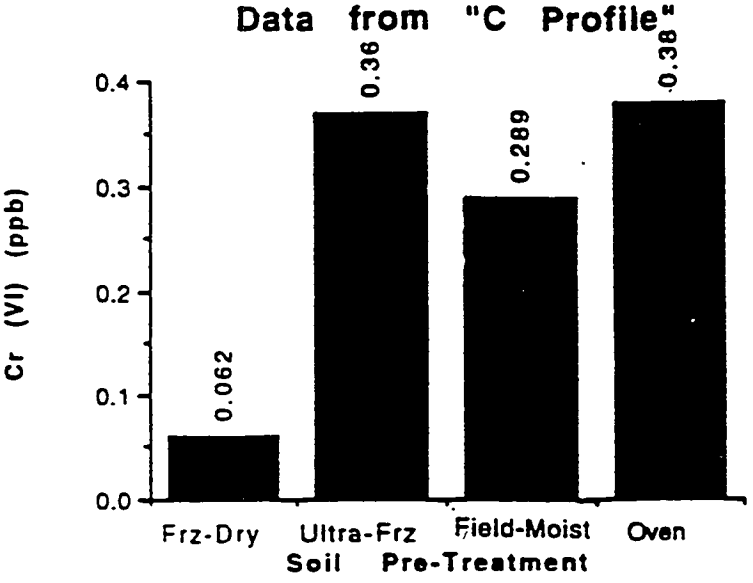
Data from "C Profile"
Cr (VI) (ppb)
0.4
0.3
0.2
0.1
0.0
0.062
0.36
0.289
0.38
Frz-Dry
Ultra-Frz
Field-Moist
Oven
Soil Pre-Treatment

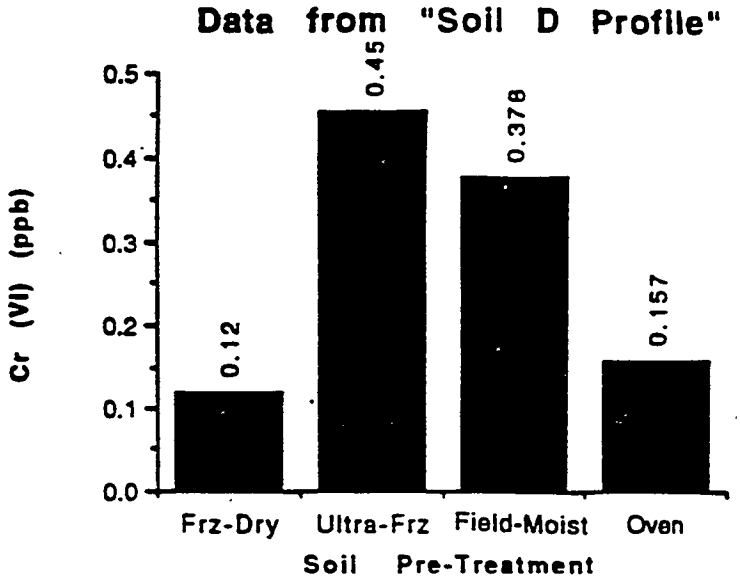
Data from "Soil D Profile"
Cr (VI) (ppb)
0.5
0.4
0.3
0.2
0.1
0.0
0.12
0.45
0.378
0.157
Frz-Dry
Ultra-Frz
Field-Moist
Oven
Soil Pre-Treatment

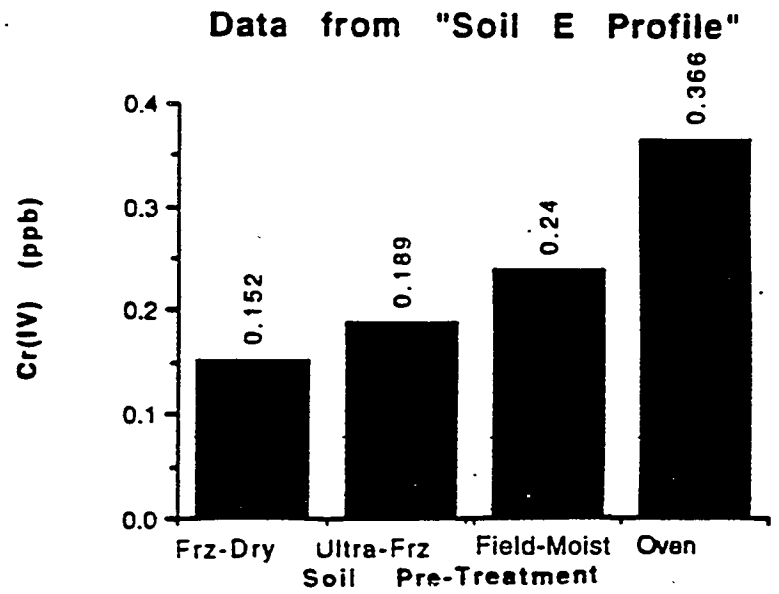
Data from "Soil E Profile"
Cr(IV) (ppb)
0.4
0.3
0.2
0.1
0.0
0.152
0.189
0.24
0.366
Frz-Dry
Ultra-Frz
Field-Moist
Oven
Soil Pre-Treatment

Sample C1	
Day #	Cr (VI)
1	1.56 ppb
2	2.34 ppb
3	ND
4	4.49 ppb

Sample C2	
Day #	Cr(VI)
2	3.90 ppb
3	1.56 ppb
6	2.18 ppb
7	4.69 ppb

Sample C3	
Day #	Cr(VI)
3	2.34 ppb
6	2.00 ppb
7	1.78 ppb
8	3.05 ppb

Sample C4	
Day #	Cr (VI)
6	1.75 ppb
7	1.16 ppb
8	1.78 ppb
9	4.69 ppb

Sample C5	
Day #	Cr (VI)
7	ND
8	ND
9	ND
13	2.93 ppb

Sample C6	
Day #	Cr (VI)
8	0.92 ppb
9	1.55 ppb
13	1.73 ppb
14	2.63 ppb

Sample C7	
Day #	Cr (VI)
9	ND
13	3.25 ppb
14	1.11 ppb
15	0.328 ppb

Sample C8	
Day #	Cr (VI)
13	1.61 ppb
14	ND
15	0.388 ppb
16	3.22 ppb

Sample C9	
Day #	Cr(VI)
14	1.62 ppb
15	0.713 ppb
16	1.05 ppb
17	1.16 ppb

Sample C10				
Day #	Cr (VI)			
15	0.725 ppb			
16	0.24 ppb			
17	0.83 ppb			
18	0.75 ppb			

DCSP Hardware Maintenance System

Melissa Pazmino
St. Andrews Presbyterian College
Lawrence Livermore National Laboratory
Department of Energy
Spring 1995 Science and Engineering Research Semester

Abstract

This paper discusses the necessary changes to be implemented on the hardware side of the DCSP database. DCSP is currently tracking hardware maintenance costs in six separate databases. The goal is to develop a system that combines all data and works off a single database. Some of the tasks that will be discussed in this paper include adding the capability for report generation, creating a help package and preparing a users guide, testing the executable file, and populating the new database with data taken from the old database. A brief description of the basic process used in developing the system will also be discussed. Conclusions about the future of the database and the delivery of the final product are then addressed, based on research and the desired use of the system.

Introduction

Presently, DCSP has six databases for tracking hardware maintenance costs, two for DEC, two for Sun, and two unused. The two for DEC are named DecDB and TelosDB and the two for sun are named SunDB and GrummanDB. The two unused contain old data that was used to create Dec, Sun, Telos and Grumman.

It is very inconvenient to manage this many databases that all serve similar purposes. Time is wasted in updating because many of the databases possess the same tables and date, and thus referential integrity for common information is lost across the different platforms. Any changes need to be made to each database separately. In addition, the current system is inefficient with respect to user processes because it lacks a Graphical User Interface package and menus, all which make maintenance of the database more orderly.

As a solution to these problems, development of a new database was begun in the summer of 1994. This new system will combine all data and work off a single database. It will also provide menus and tables for easier access of the database. The new DCSP database will be time efficient, practical, and simplistic to use.

The Executable File

Currently, the executable file for the database is accessible. The executable file contains dynamic menus that are retrieved from a menutree and then compiled into the main program. Each

menu item contains an abbreviated tag for a command, a description of the command, and a menu type. The main menu types are 'M', for menu activation, 'R', for report activation, 'D' for data entry activation, 'S' for sub process activation, and 'B' for a blank line, which is not shown in standard mode.

Activating a command with an 'M' type will generate a sub menu that is linked to the command. Activating a command of type 'M' will always take the user into another menu. From here, the user may be able to go to a different menu link, or activate another command type

Activating a command with an 'R' type will send a message to run a specific report. This command will either run a report writer script, sub process or program associated with this report. Reports can be run interactively or in batch mode. The user will have the choice of sending the output to the printer, screen or file. In some cases, the user may be required to enter initial arguments for the report to run properly.

A command with a 'D' type will generate a data entry screen. This is a screen that the user can enter necessary and/or default data to be used by the system. An example of this is the Report FY command that is displayed on the home menu of the executable file. This command will allow the user to set the reporting fiscal year. Many data entry screens in the system contain default values should the user not choose to activate the command.

A command with an 'S' type will activate an underlying sub process. These sub process are not executed in the system

environment. Instead, a separate shell is created, and the system environment is temporarily exited while the sub process is running. Upon completion of the sub process, the user is returned to the previous menu in the system environment.

The 'B' type specifies a blank line. This is not shown in user mode, and can be seen only by the system developers. Activating the Menutree function key on the system menus will put the user into development mode. This mode displays an identical menu to the previous, however the screen can now be used as a data entry screen for developers to modify and add to the system. The Menutree function key is only available to system developer users. Standard users do not have access to this function key.

Tasks

Although development of the system began months ago, many tasks still remain to be accomplished before the system can be put into production. Some of the tasks include adding the capability for report generation, creating a help package, testing the executable file, and populating the new database with data from the old database.

In order to add the capability for report generation, all report writer scripts, various programs, and sub processes must be compiled and made available in the system. In addition, all tables associated with the report must have been created.

The current report writer scripts available on the old system can be compiled into the system, but many will need

modifications. This is because the correlation between the tables on the old system to the tables on the new system is not identical. Thus many of the tables referenced by the scripts running on the old system are nonexistent in the new system. Since the tables in the new system will be containing data from four different databases, efforts are being made to combine some of this data in an orderly fashion. Thus, some scripts may need to be rewritten entirely.

When a report writer script is run, the first step executed is to load the report specifications. Specifications include: 1) a report header; this specifies textual information that the user may wish to know, and can also be used to specify report layout options, such as margins and spacing. 2) page headers and footers; the page header is printed at the top of each page, with the exception of the first page, and can include a title, date, page number, etc. Similarly, a page footer can be printed at the bottom of each page. 3) a break header; this will cause a break in the report anytime a new group of data is about to be processed. This is helpful in highlighting important information. 4) a detail section; the statements in this section are processed each time a new group of data is read. 4) a break footer; this is processed at the end of a group of data rows. Break footers show the subtotals of previous columns or rows just processed. 5) a report footer; this is textual information that can be printed at the end of the report.

After the specifications have been loaded, the next step is to perform the database query. This is why it is so important that

all tables associated with the report are accessible. If the report cannot retrieve data requested in the script, error messages will be returned. Finally, the report is formatted to be printed either to a file, a printer or the users screen.

Another major task to be completed is the creation of a help package. This package will offer on-line help in the form of definitions and examples. Users will be able to retrieve immediate help on commands, table structures, report definitions, and even view sample reports.

As an interesting example, a user may wish to run a specific report, but may be uncertain which command is associated with that report. Activating the help function key will display a menu that will allow the user to view a sample of the report, and get a description of the report to be run. Thus, the user can locate the specific report by referencing the descriptions.

The menu will also allow the user to screen what tables in the database are referenced. This could be important in helping the user determine whether the needed tables are available and up to date. If desired, a brief description of each field in the table is accessible.

Since there is currently no data in the DCSP database, one of the first steps in testing the executable file will be to populate the new database with data. Most of the data will be taken directly from the old database, and thus is it possible to write a shell script that will perform this task quickly and efficiently. A script may also be used to insert any new data into the database, depending on the amount to be appended.

As stated already, any report writer scripts, underlying sub process, and programs need to be compiled and available to the system. These functions should be pre tested before being incorporated into the system. This will allow for easier debugging, and also quicker and more orderly evaluation.

The menus and menutree accessed by the executable file will need to be tested and debugged. Any errors in links could generate confusing outputs, and faulty data. In development, most of the menu creation can be done with the cut and paste method, thus can be tested while still in development.

Finally, any output that is generated while using the system will need to be verified. This is to assure that the system is handling output requests properly and that the output data is consistent with the data in the database. This should be the final step in testing because it will be difficult at this point to find an error in the system. If all previous parts of the system have been tested, this lessens the possibility of the system generating faulty output.

Development

The first step in continuing with the development of the system that had begun last summer was to come up to speed with how the old system works. From gaining an understanding of how the system worked and what it was lacking, it was then possible to come up to speed on what work had been completed on the new system and why.

Gaining an understanding of the rough idea of the new system was the next step. It was important to understand how the system worked, where the tools for the system are located, and what the limitations of the system were. After coming up to speed with the system, it was then time to determine what the correlation between the four original databases and the new DCSP database would be. Do this, it was necessary to learn the basic commands and capabilities of Ingres Report Writer, since this is what most of the scripts in the old system are written in.

After coming up to speed with Report Writer, it was necessary to determine what reports in the old system were necessary in the new system. Deciding this would help determine which reports needed to be modified, and if any new reports needed to be created. Also, which reports needed to be done away with entirely.

Much of deciding on which reports needed to be modified depended on determining the mapping of the table structures in the old system to the table structures in the new system. Since all the data contained in the four databases is being combined into the one DCSP database, many of the table structures bear little to no resemblance to the old tables. The correlation between the tables must be determined before any scripts, programs or sub processes addressing these tables can be compiled into the system.

Testing the executable is the final stage of development. The timetable of this is unknown since it will more than likely require many changes and modifications. However, once testing is

complete, the system can finally be moved out of development and into production.

Conclusions

The DCSP database system will be more efficient than the current system in use. As already stated, it will run off a single database rather than four, and thus referential integrity will be easily enforced. In addition, backup and monitoring of the database will be less time consuming. Platform independence is continuously being strived for, as that is a requested attribute for the system from the future users of the database. Using the new system as a prototype for future systems is a possibility, which will make the system available to various users. Finally, there is still the possibility of implementing a Graphical User Interface package into the system, thus making the system even more user friendly. Thus, although much work remains to be done before the system is complete, the future of the DCSP database holds many possibilities.

The Numerical Simulation of a Driven Nonlinear Oscillator

Cindy Shew

Murray State University

May 12, 1995

mentors: Brian Bonner & Kirk Keller

Lawrence Livermore National Laboratory

Science and Engineering Research Semester
Spring 1995

sponsored by The Department of Energy

Abstract

The torsional oscillator in the Earth Sciences Division was developed at Lawrence Livermore National Laboratory and is the only one of its kind. It was developed to study the way rocks damp vibrations. Small rock samples are tested to determine the seismic properties of rocks, but unlike other traditional methods that propagate high frequency waves through small samples, this machine forces the sample to vibrate at low frequencies, which better models real-life properties of large rock masses. A numerical model that simulates the forced torsional oscillations of the machine is currently being developed.

The computer simulation implements the graphical language LabVIEW, and is looking at the nonlinear spring effects, the frictional forces, and the changes in amplitude and frequency of the forced vibration. Using LabVIEW allows for quick prototyping and greatly reduces the "time to Product" factor. LabVIEW's graphical environment allows scientists and engineers to use familiar terminology and icons (e.g. knobs, switches, graphs, etc.). Unlike other programming systems that use *text-based* languages, such as C and BASIC, LabVIEW uses a *graphical* programming language to create programs is block diagram form.

Introduction

Rocks damp vibrations in different ways. Some rocks, such as granite, damp vibrations very quickly, whereas other rocks, sandstone for example, damp vibrations much more slowly. Understanding more about how rocks react to seismic waves is very important and has many practical applications. For example, determining the safety of various building sites is often based upon how the particular rock at that site

damps vibrations. There are other factors involved, but knowing that a certain rock does not damp vibrations well would be a definite precursor to determining that a particular building site would not be safe during an earthquake.

To study how rocks damp vibrations in a laboratory setting is a great challenge. Large rock samples, such as those that would be of interest to future builders, vibrate at low frequencies for propagating waves. The smaller the rock sample, the higher the frequency of the propagating wave. This proportionality between frequency and the size of the sample causes difficulty when trying to determine how large rock samples would react during seismic activity. Unfortunately, most laboratories are not equipped to test large rock samples. They have to rely upon small rocks, but as explained earlier, these small rocks do not vibrate at the same frequency that the larger rock samples do. This forces scientists into approximating how the larger rock samples would react based upon the data assimilated about small rock samples. These approximations may not be as close as many scientists assume they are.

To study rock behavior in the laboratory, a small rock sample is placed into a machine that forces vibrations without using propagating waves. Even though it is a small rock sample and wants to naturally vibrate at a high frequency, since propagating waves are not used, the machine forces the rock to vibrate at a low frequency. This driven low frequency vibration in a small rock sample, is a much more accurate test of how large rock masses vibrate. Using this method, it is then easier to study how large rock masses damp vibrations in real world settings.

Background

The torsional oscillator was originally built to study the way that rocks damp vibrations. Most machines up to this time studied vibration damping with the use of propagating waves. The interest here lied in studying the seismic properties of rocks as

they moved from large rock masses to smaller rock samples. The machine works without propagating waves, so that low frequency waves can be forced through small rock samples. The machine is really a forced vibrator. It forces samples to move at a particular frequency at a force that is time dependent. The machine originally measured the damping and stiffness of small rock samples. Stiffness and damping are two inherent properties of rocks. The machine also needed to use other parameters. It was then modified to use the amplitude and frequency of the forced twist in tests

Another interesting aspect of the machine is that it becomes nonlinear when rocks with nonlinear properties are tested. Most scientists model rocks with nonlinear properties with linear analysis. Even though they know that certain rocks have nonlinear properties, they assume that linear and nonlinear testing gives similar results. This is mainly because using nonlinear analysis is very time-consuming, extremely difficult and complex, and calls for intensive mathematical skills that are not required for most geologists and geophysicists.

Since this machine becomes nonlinear naturally when testing nonlinear rocks, it is easier to test rocks with nonlinear analysis. The data that comes from the testing of rocks with nonlinear properties is used to determine instances in which linear approximations are different form nonlinear approximations. The data still needs some quantitative analysis to produce accurate results. We are looking for ways to classify the independent variables that cause the linear and nonlinear approximations to be different. For example, in some classes of sensitive sandstone, the stiffness of the rock changes when humidity is added to the test.

How the Oscillator Works

The basic concept of the oscillator is very understandable (see Figure 1). There is a computer system into which the initial experimental variables are inputted. These

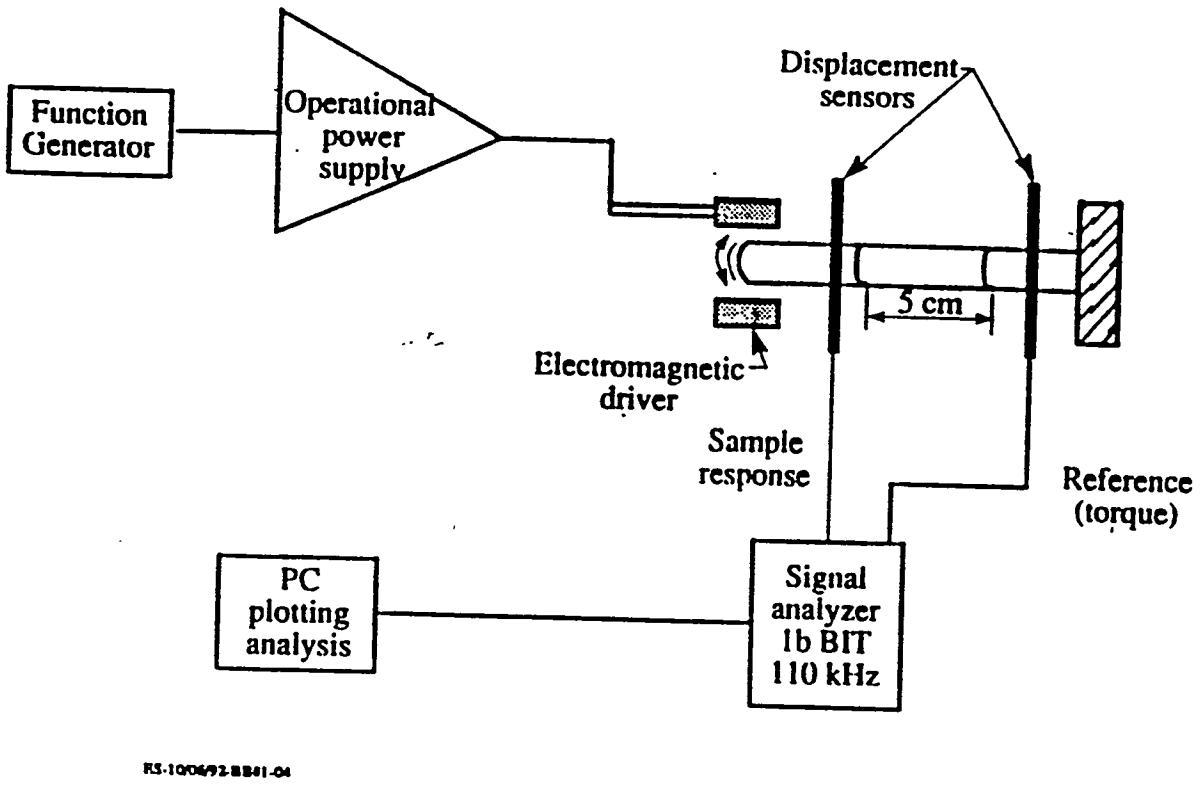

Figure 1 - Basic schematic of the torsional oscillator, showing the relationship between it, its power supply, and its inputs and outputs.

variables are transferred to the machine itself, which is run by an external power source. The machine begins to twist, causing the rock sample to vibrate with a periodic force. The response is then outputted, via the computer manipulating it, to a spreadsheet, where the data can later be studied.

To better understand how the torsional oscillator works, look at Figure 2. The forced twist occurs inside the electromagnetic driver. From the outside, the driver looks like a hollow casing, but this is just a cover to protect the magnets underneath. The magnets are put in a positive, negative, positive, etc. order, so that they are constantly repelling and attracting each other. This causes the collets to twist as the magnets turn towards and then away from each other.

The amount of the twist is then measured by the proximity detectors. As the machine twists, there are stationary magnets below the proximity detectors. The detectors never

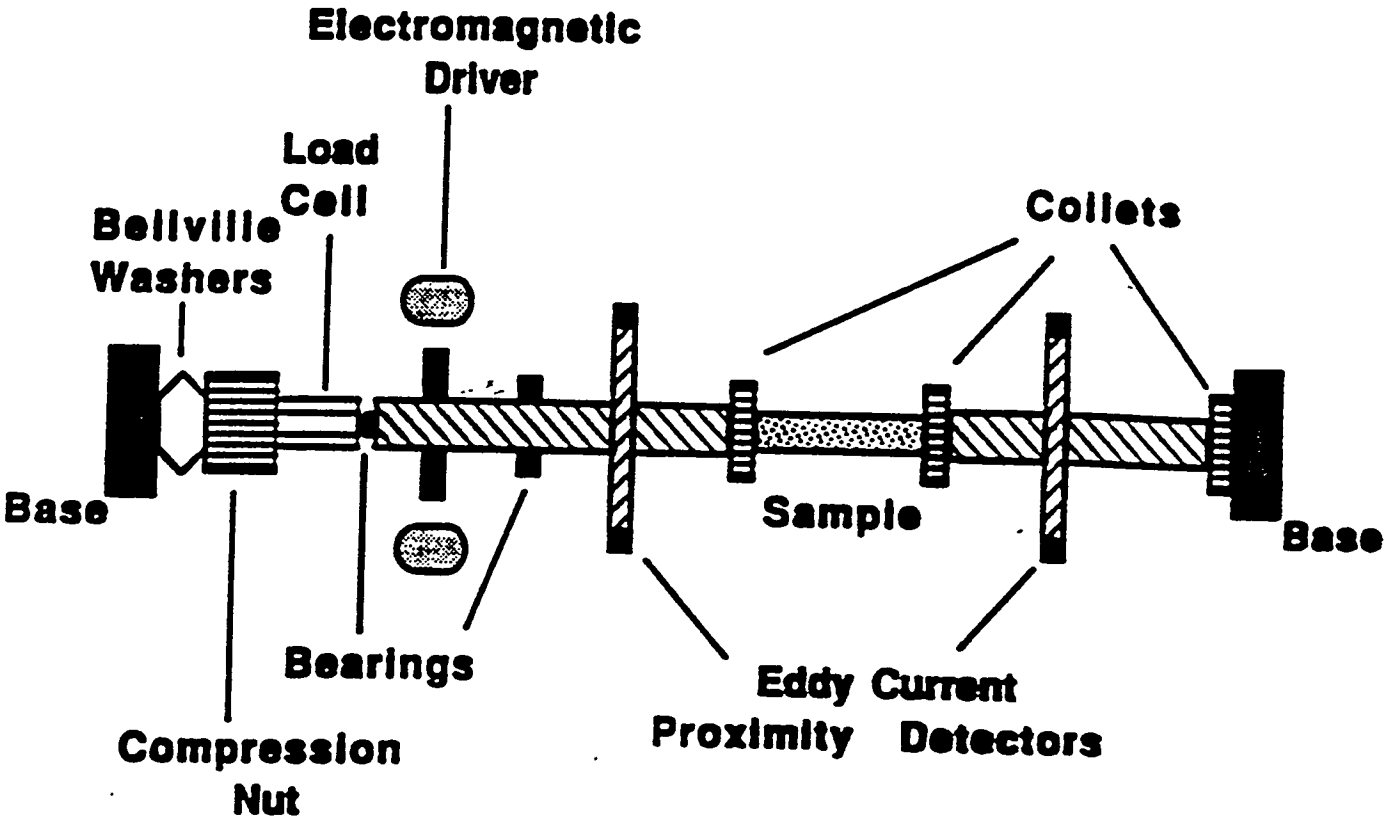

TORSIONAL OSCILLATOR

Figure 2. Detailed schematic of the oscillator

quite touch the stationary magnets, but they are used to measure the gap that occurs between the magnets and the detectors. These measurements are then used to determine the amount of the twist.

The rock sample is placed between the collets and is then forced to twist. The rock samples are first cut in the field. They are then brought to the lab and cut into approximately two inch samples with a diamond core barrel. Some of the softer samples, such as sandstone and clay are cut in different ways. The samples come from sites where structures will be, or have been, built. The machine tests what seismic sheer waves will do to the sample, to determine the safety of the site. Currently,

laboratory testing is being done on rock samples upon which the freeway that collapsed during the 1994 Northridge earthquake in Southern California was built.

About LabVIEW

LabView is a graphical based language. It allows scientists and engineers to use terminology and icons that are familiar to them. They can use knobs, switches, diagrams, sine waves, buttons, graphs, and other icons that makes LabVIEW resemble a drawing instead of a computer program. A LabVIEW program has two distinctive parts. There is the front panel (see Figure 3), which is where all of the initial information is inputted, and is also where the final data can be outputted.

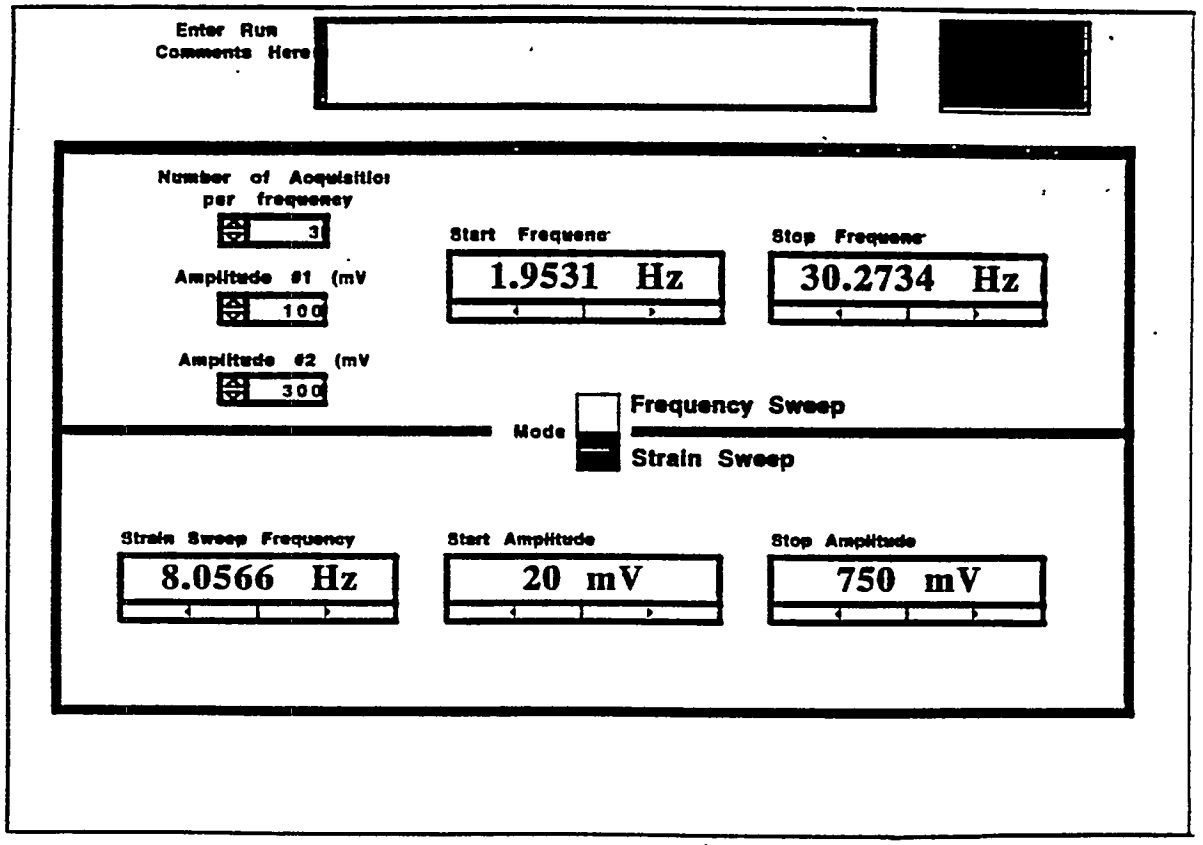

Figure 3.

This is the actual front panel of the computer program that runs the torsional oscillator. The oscillator can run either a frequency sweep or a strain sweep by clicking the switch in the middle to either position.

A frequency sweep is one amplitude over a range of frequencies. The frequencies usually run from 30 MHz to 100 MHz, and the amplitudes are usually either 100 or 300 mV.

A strain sweep is one frequency over a range of amplitudes. The frequency of choice is 8 Hz, and the range of amplitudes run from 10 mV to 1.25 V.

Then, there is the program itself which resembles a detailed flowchart. The program looks like a lot of squares and triangles, connected by lines, but this is really an intricate program. LabVIEW has just condensed certain functions into an icon form. Compare the text-based code in C, below, and what the same code looks like in LabVIEW.

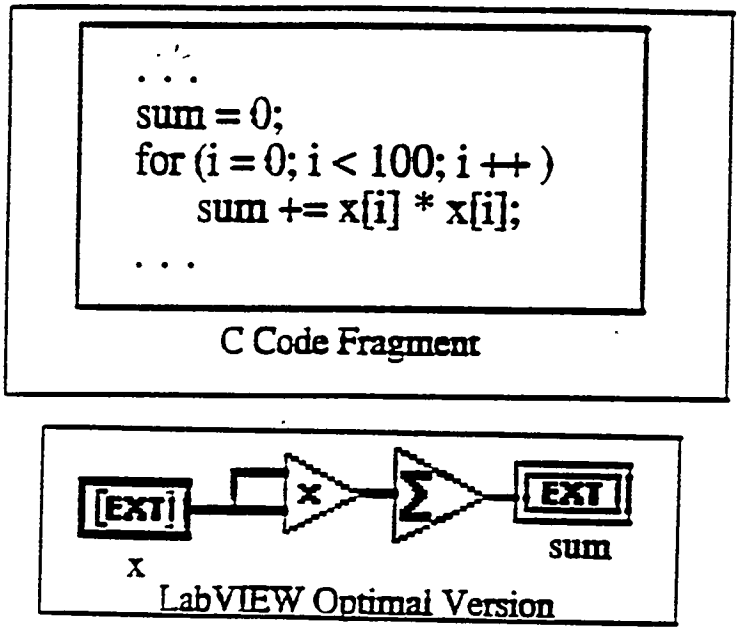

Figure 4

Research and Methods

The first step towards developing a computer simulation of the torsional oscillator began with understanding how the oscillator worked, and the purpose of the computer simulation. The oscillator is very slow when running its frequency and strain sweeps. With a computer model, data can be assimilated much more quickly and efficiently. The model would also lessen the number of man-hours, which in turn could be used towards analyzing the data.

The other challenge was in developing some basic skills in using LabView. To better understand LabVIEW, the first project was to develop a one-dimensional model that determined velocities and accelerations when given certain inputs. Upon successful completion of this basic model, the real work began.

The oscillator uses basic concepts of friction, velocity, spring forces, etc.. but the problem was to find some type of real-life system that was similar to our own. We began

by studying various nonlinear and linear systems that were governed by forced or self-excited oscillations. We perused several books and papers concerning chaos and nonlinear dynamics, and found various topics addressed in each. There is much research done with nonlinear phenomena, from undamped, unforced nonlinear oscillators, to forced nonlinear oscillators with periodic attractors, but none that were exactly right. We needed a damped, forced, nonlinear oscillator, so we finally settled upon Duffing's equation, which is a damped, periodically forced nonlinear oscillator with displacement x (Stewart and Thompson, p 2). The equation is as follows:

$$\ddot{x} + k\dot{x} + x = B\cos t \quad \textit{(eqn. 1)}$$

We modified this equation to better model our system and ended up with the following equation:

$$m\ddot{x} + f\dot{x} + kx = F\sin wt \quad \textit{(eqn. 2)}$$

Where mx is the inertial term, fx is the frictional term, kx is the spring force term and $F\sin wt$ is the forcing function. Making the assumption that we are moving very slowly to find the equilibrium, we can then rationalize dropping both the inertial term and the damping forces. This reduces equation 2 to:

$$k(x)\, x(t) = F\sin wt \quad \textit{(eqn. 3)}$$

To solve this equation, we also needed some more information to make the solution easier. This came in the form of knowing what we wanted the final graphical output to look like. From observing the behavior of the rocks when tested on the oscillator, the data was then graphed as stress vs. strain, and a hysteresis loop was produced.

Figure 5

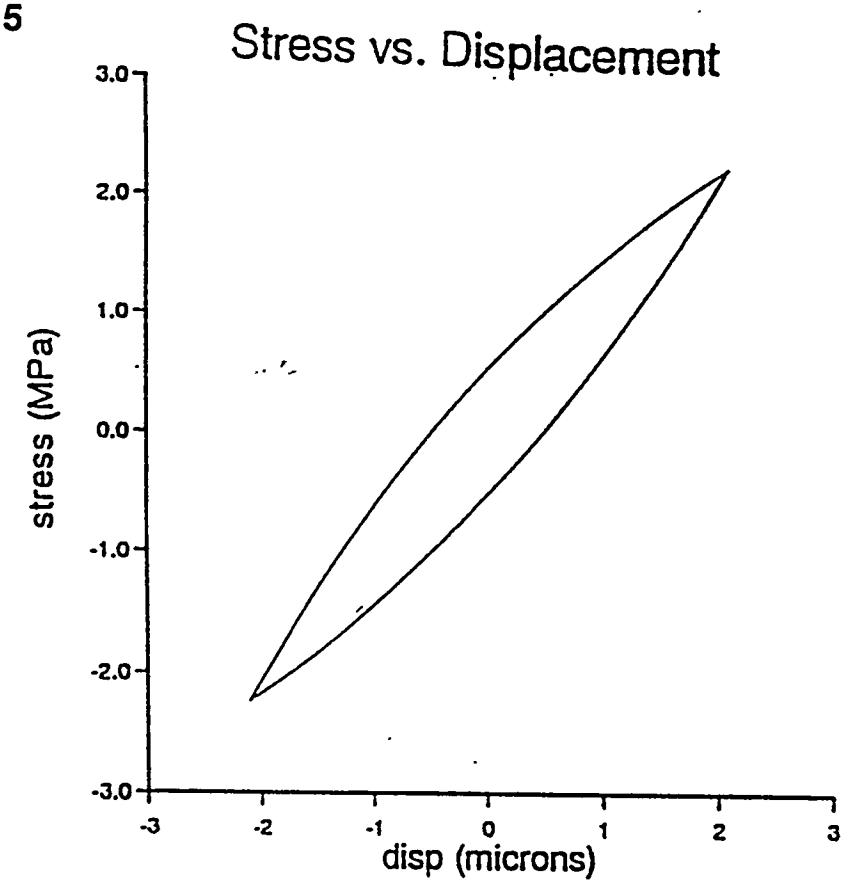

A point by point differentiation of the hysteresis loop then led to the following graph, which we refer to as the Stars & Bars.

Figure 6.

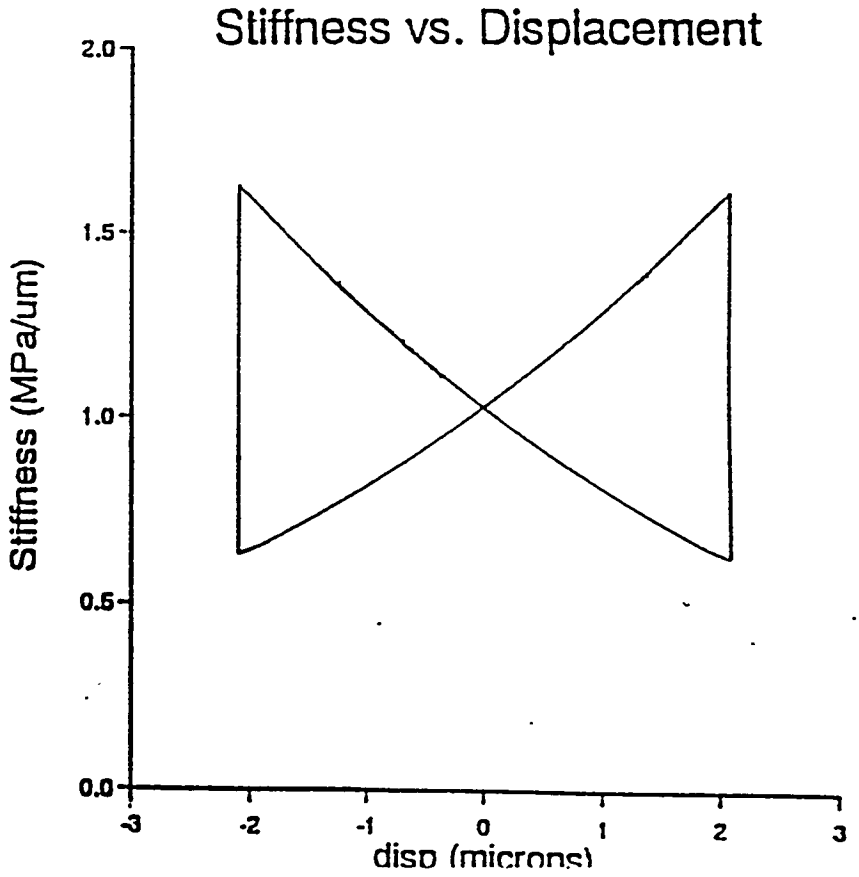

Modeling Approaches

To solve this equation in computer form, we began by working backwards from the Stars & Bars graph. Just looking at this graph in its simplest form, it is jtwo lines crossing, forming two symmetrical triangles. The lines are of the form y = mx + b and y = -mx + b.

We developed a simple program that created the Stars & Bars graph (or so we thought), but the final graph was not at all what we wanted. We then realized that we had incorrectly solved our basic geometry of lines. The problem was that the form of the lines were really y = mx +b2 and y = -mx +b1. We had mistakenly written our program as if the y-intercepts were the same for the Stars & Bars graph.

We then modified our original program, but this time we addressed the hysteresis loop as well. We began a step by step solution of equation 3, and were then able to write the solution in a new form. We first had to use the following conditions:

If the derivative of the forcing function (F$\sin wt$) is < 0, then the equation of the Stars & Bars must be y = -mx +b1, otherwise the equation is y = mx + b1.

$x_1(t) = F_1 / K_0$ another form of equation 3 where F = F$\sin wt$

Using mathematical induction, equation 3 can then be written as:

$x_n(t) = F_n / K_{n-1}$ where n = 0,1,2,3.....

With these conditions in mind, we developed a new model that used these conditions to solve equation 3. (See figure 7). The program produced output much closer to our hysteresis loop and Stars & Bars graph, but there were still some problems. Looking at the x graph in Figure 8, there is a noticeable "jump" in the sinusoidal hump.

Figure 7.

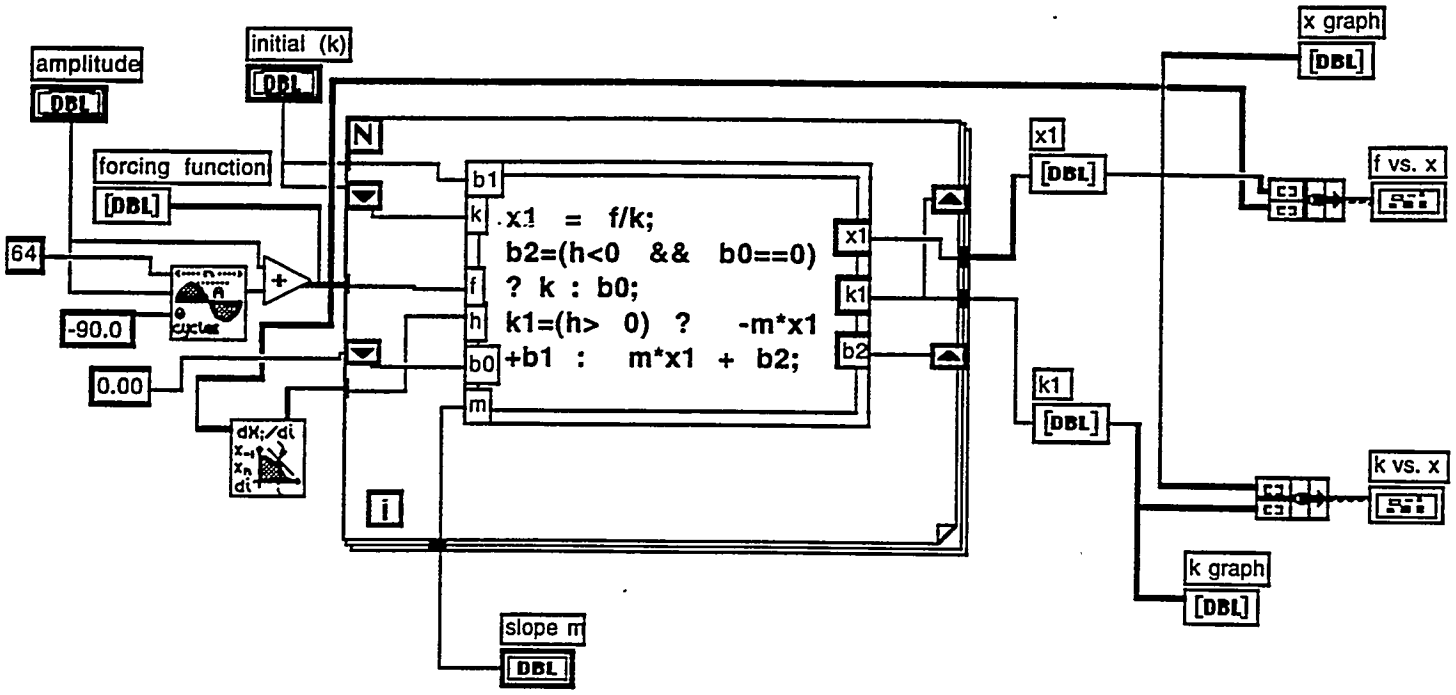

Figure 8.

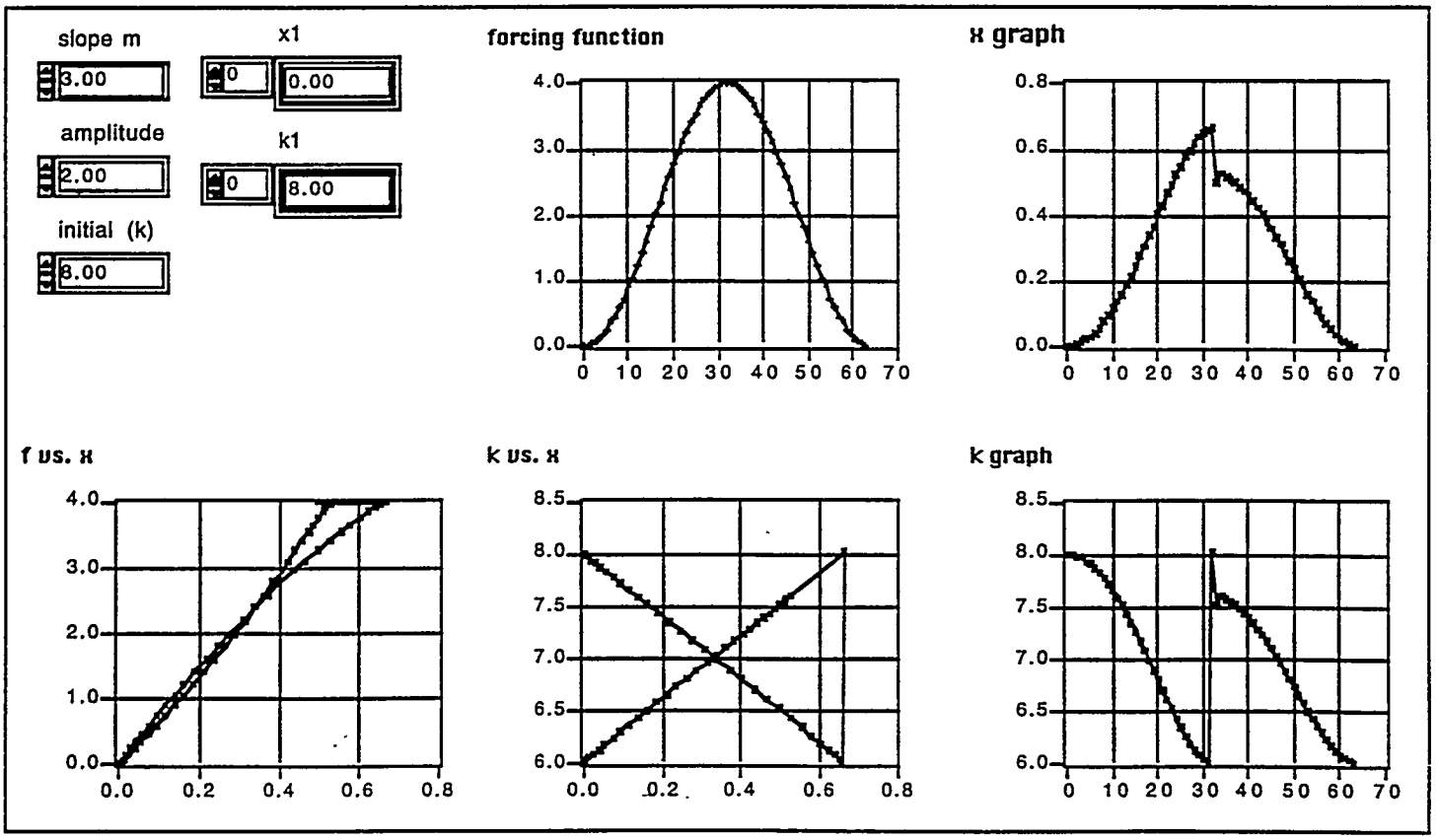

The "jump" in the x graph causes the distortion in the other graphs as well, most noticeably the crossover in the hysteresis loop. We realized that the distortion was occurring where the loop became discontinuous. We then addressed this problem in our model, and with several modifications, we came up with the following output. (Figure 9)

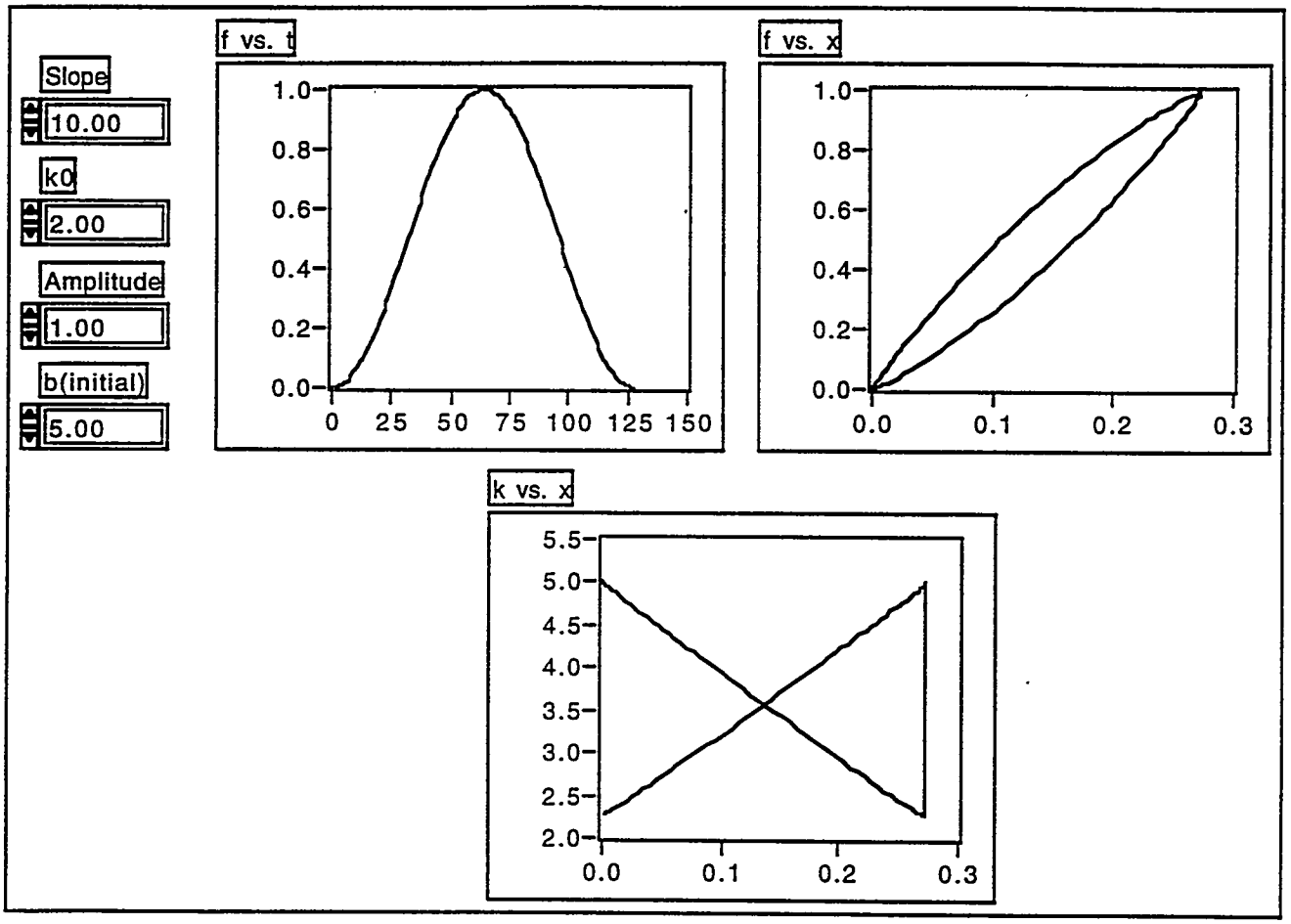

Figure 9.

This is exactly what we were wanting to come up with, and this shows us that the computer simulation is fairly accurate to the original oscillator. Further modifications will need to be done, but the model now has some validity.

Conclusion and Future Work

The torsional oscillator can be used to study small rock samples in ways that more closely simulate real-life seismic waves. These studies may eventually result in safer structures that withstand earthquakes better. They will promote a greater understanding of how seismic sheer waves effect rocks and minerals.

There is still much work to be done. The computer model needs to be modified and updated with new variables. The model also needs to be ran through a Fast Fourier Transform to validate its accuracy. The FFT will show a power spectrum that needs to be compared to the machine's output from the spectrum analyzer. There is also a large amount of data, from years of the machine's test runs. This data needs to be organized and statistically analyzed, to determine if there are any noticeable trends that have occurred. This could lead to greater insight into the stability of various ground sites.

After this work is completed, there will even be other uses for these studies. It will not be limited to just areas of geophysics. Engineers and architects will be able to use these studies in building safer bridges, roads, houses, etc. There may even be applications in biomedicine. For example, the study of rough, abrasive surfaces grinding against each other can be applied to testing the friction that occurs between joints. This could be used for improving artificial bone and joint replacements that are added to the human body.

References

Boitnott, G.N., *The Role of Rock Joints in Non-linear Attenuation in Moderate Strain Amplitude Regimes*, Defense Advanced Research Projects Agency, 1992

Hayashi, Chihiro and Ueda, Yoshisuke, *Computer Simulation of Nonlinear Ordinary Differential Equations and Non periodic Oscillations*, Electronics and Communications in Japan, Vol. 56-A, 1973

Ramirez, Robert W., *The FFT - Fundamentals and Concepts*, Prentice-Hall, INC., New Jersey 1985

Tabor, Michael, *Chaos and Integrability in Nonlinear Dynamics*, John Wiley & Sons, INC. 1989

Thompson, J.M.T. and Stewart, H.B., *Nonlinear Dynamics and Chaos*, John Wiley & Sons Ltd. 1986

Ueda, Yoshisuke, *Randomly Transitional Phenomena in the System Governed by Duffing's Equation*, Journal of Statistical Physics, Vol. 20, 1979

Yu, Lois, *Hysteresis Loops and Nonlinear Behavior in Rocks*, Faculty Mentor Program Research Paper at the University of California, San Diego, 1992

Necessary Services for a Client/Server Technical Architecture at Lawrence Livermore National Laboratory

Kevin Shuk

May 10, 1995
Science and Engineering Research Semester
"Data Warehouse Technical
Architecture Research"
Administrative Information Systems
Francine Alford, Mentor

Table Of Contents

Abstract

The current computing environment for the ASSIST data warehouse at Lawrence Livermore National Laboratory is that of a central server that is accessed by a terminal or terminal emulator. The initiative to move to a client/server environment is strong, backed by desktop machines becoming more and more powerful. The desktop machines can now take on parts of tasks once run entirely on the central server, making the whole environment computationally more efficient as a result.

Services are tasks that are repeated throughout the environment such that it makes sense to share them; tasks such as email, user authentication and file transfer are services. The new client/server environment needs to determine which services must be included in the environment for basic functionality. These services then unify the computing environment, not only for the forthcoming ASSIST+, but for Administrative Information Systems as a whole, joining various server platforms with heterogeneous desktop computing platforms.

Introduction

This paper describes a core technical architecture, based on Apple's Virtually Integrated Technical Architecture Lifecycle (VITAL), that outlines the services necessary for a client/server environment within Administrative Information Systems at Lawrence Livermore National Laboratory. This represents the ideal to be striven for; a utopian plan. By itself, useless, but when taken as a goal to move towards in light of the current operations, it becomes a crucial piece in the framework within which we build the new system. This is also not the complete technical architecture, but rather the minimum set of services needed to implement a "whole" client/server model throughout the enterprise.

The plan calls for five major environments, and each area has what are called services. This document deals strictly with services, which are processes that are common in that they are used time and again and/or they are used by different applications.

These five environments are:

Systems Infrastructure. These are the most common of all services, used in all the other four environments. Such services are email and file transfer.

Data Capture. This environment is comprised of the current operational systems already in production, and the usage associated with them.

Data Access. This is the data warehouse, the access to it, and the methods of getting information from the Data Capture environment to this environment.

Repository. This provides the storage for any objects and data that is common to the whole enterprise. Application building blocks, security access information and the like live here.

Desktop Integration. This is the one section missing from this document as it is incorporated with the Mission Critical Infrastructure Services section. This environment houses the desktop portion of any infrastructure service that has one.

This paper is purposely written in a very coarse manner, explaining the essentials of each service, then moving along. This is since the document is more referential in nature, identifying the necessary services. Finer details on each service should be obtained from the original documentation if desired.

Mission Critical Infrastructure Services

Security Services

Access Control Services

Access Control Services authenticate user or process identities and provide detailed information about the data for which a particular authenticated user or process is authorized. They protect against the following security threats:

- unauthorized disclosure
- unauthorized modification
- unauthorized destruction
- unauthorized use
- masquerade
- replay
- denial of service
- installation of malicious software (VITAL Systems Infrastructure Guide, 78)

Access Control Integrity

Some computer and network systems require more stringent access controls than others. All systems that provide a service to others require a high degree of both physical and logical security (VITAL Systems Infrastructure Guide, 79).

Authentication

VITAL applications must provide both user and host authentication. A single user identifier is used. The method of authentication must be independent of the user's location and platform. One goal of the Authentication service is to minimize the number of redundant accounts (e.g., a remote-access account, a platform-specific OS account, an application account to maintain secure documents on the desktop, a DBMS user name and authorization record, etc.).

Authentication should verify that the client service (and person, if the client is a desktop service) is genuine. Validation should be performed on a highly secure and trusted platform during the initial connection negotiation, unless the required data or services do not merit authentication

In addition to the issue of the server trusting the client, a client application must be able to protect itself from impostor servers running on the network.

Authentication mechanisms involve the use of a key or token, password, or some other unique characteristic such as retina, voice, or finger prints that identifies a valid entry.

Two common authentication processes use asymmetric or symmetric encryption algorithms in conjunction with entity credentials or tickets. For instance the encryption process scrambles (encrypts) data in it's readable form by passing the clear text thorough an algorithm with a piece of variable data called the key. The process can be reversed by passing the encrypted data through a decryption algorithm with the proper key (not necessarily the same as the one used to encrypt the data).

Authentication requires an interface between the entity seeking to be authenticated and the Authentication service. The Authentication service is the supporting framework that takes care of maintaining identities and authenticators, and facilitates authentication requests (VITAL Systems Infrastructure Guide, 80-81).

On the desktop

Authentication performs the tasks needed to ensure that the entity requesting authentication is what it claims to be. In the case of authenticating a user, it is a verification of the identity of the user — that is, the user is verified as being the person he or she claims to be. This is done by using something only the user has, such as an access badge, or digital signature and something only the user knows, such as a password (VITAL Desktop Integration Guide, 61).

Authorization

Authorization mechanisms involve the establishment of an entity's right to access a resource, such as a user's ability to read, write, execute, and delete specific files on a computer system. Authorization requires an interface between the entity requesting access and the Authorization service. The Authorization service receives the request for access and verifies that the requesting entity has the permission or capability required to access the resource. The Authorization service assumes that the requesting entity has been adequately authenticated and is the supporting framework that

maintains the associations between identities, permissions or capabilities, and resources.

Authorization is much more difficult than authentication. Once the user has been authenticated, the actions a user can do must be restricted in some manner. Elements that usually come under the venue of authorization include:

- access to particular services offered by the server
- access to tables in the database
- access to individual rows or fields in the database

Access to particular services is fairly easy, and can be resolved a number of ways, including access levels, flags, and access control levels. Access to tables is also fairly straightforward, and can be accomplished using database grants or restrictions. Access to individual rows or fields in the database can be accomplished, in some cases, with database views or rules. However, some depend upon complex business rules that cannot be resolved in such a manner (VITAL Systems Infrastructure Guide, 82).

On the desktop

The desktop authorization service performs the tasks needed to ensure that only authorized users can use the enterprise resources and access or update data. This service works in close conjunction with an authorization service in the Repository, which informs this service of the information, data, services, and servers that the user is able to access or update (VITAL Desktop Integration Guide, 61).

Service Directory

The Authentication and Authorization services allow an application to request and verify the identity of a user or process to receive information about the resources for which a specific user or process is authorized. This is done through a set of highly secured standard queries to the Repository security directory containing the Authentication and Authorization profiles accessible only by a trusted Infrastructure Security Service, and changeable only by specially authorized individuals through highly secured maintenance programs.

Authentication profiles contain the specific identification keys and secret password information about an individual that are used to determine if the person requesting the service is the same person

they claim to be. The authentication profiles are used by the Authentication service.

Authorization profiles contain data-access, ownership, user-update, and operational privileges. They contain the access and update rights list for any particular service or application as a whole. A rights list associated with a user profile is the concatenation of the user ID and the specific access and update rights to services and data allowable for that user. The rights list is contained as a highly secure profile accessible only by a trusted Security service (VITAL Systems Infrastructure Guide, 80).

Application Utility Services

Value-Added Message and Transfer Service

Value-Added Messaging Services provide a variety of email-like services and direct message/file delivery vehicles (VITAL Systems Infrastructure Guide, 96).

Store & Forward service

Store and Forward performs three functions. First, it manages the batch temporary storage or messages that are enveloped files submitted to it by another service (typically EDI). Secondly, initiated by some trigger (time, batch size, or other event), Store & Forward sends the entire batch of messages to another receiving cache on the network node designated by the send-to address. Finally, Store & Forward notifies the recipient service of message arrival in the cache so that the target service can retrieve the messages. The message source has control over the submission of the data and the recipient service has control over its delivery (VITAL Systems Infrastructure Guide, 96).

Electronic Data Interchange (EDI) service

The EDI service is considered an essential Application Utility Service for non-human-interfaced Data Capture transactions or for those transactions from external sources that have an industry-standard transaction format.

As with all VITAL services, EDI should be invocable by logical name anywhere in the world. The messages it accepts, the function it performs, and the return message should be uniform throughout the network regardless of how many replicated copies of the service exist or the platform on which the service executes (VITAL Systems Infrastructure Guide, 97).

File Transfer

File Transfer provides the services for transferring files between platforms. Without knowing any of the details of the server's operating system or platform, a desktop application should be able to request a file transfer from a server to the desktop, from the desktop to a server, or from a server to another server.

One service (application) should be able to populate or overwrite another file on one or more selected servers. Optionally, the file can be selected to update a generation of the file by the same name (VITAL fundamentals, 248).

On the desktop

Performs the tasks for transferring files to and from any of the VITAL environments. A desktop application should be able to request a file transfer from a server to the desktop, or from the desktop to a server, without knowing any details regarding the server's operating system (VITAL Fundamentals, 115).

Distributed Output Services

This category of service is used to provide printer management and report distribution to a variety of information consumers within the network. An application should be capable of delivering the output of a report to any location to which the user has sending privileges. Furthermore, an application should be capable of sending multiple copies of the same output to a variety of locations. Finally, information consumers should be able to subscribe to the output of any application whenever that output is generated. The services in this category manage all of the above.

Print Spool Management

Report Distribution Services

On the desktop

Print & Distributed Output performs the tasks to create device-, resolution-, and font-independent output on a wide variety of devices, from desktop ink-jet printers to full-size CAD plotters. When this service is implemented, IS developers do not need to worry about what devices are attached to the network, and users do not have to determine whether the right paper size, fonts, and page-description languages are available. Print & Distributed Output interacts directly with the Infrastructure's Print Spool Management service for direct output to a specified device, and

with Report Distribution when the output is scheduled, prioritized, and distributed to more than a single device. All three services cooperate with each other to provide complete network-enabled, hardware-transparent output management (VITAL Desktop Integration Guide, 62).

Electronic Mail (email)

Main Purpose

Email provides the services needed to send, receive, and respond to messages sent by an individual using the email desktop application or by another service on a server. An "action request" created on the desktop may be sent as messages to an administrator on a server.

Email in the VITAL context is considered to be a subset of overall Messaging Services. Email traditionally deals with the human recipient or *user agent*.

X.400 is the recommended messaging standard in the VITAL TAGs, minimally having an X.400 gateway that operates transparently from the perspective of the individual.

Minimal email services include the following features:

envelope display

Selected fields from the message envelope detail (headers) displayed on the desktop including origin, title, date, and other items of information.

message display

The ability to display the textual contents of any selected message and, optionally, to receive any multimedia documents or attachments.

recipient notification

The ability to notify a user, during a current operation at a desktop, that an email message has arrived.

index of received messages

A desktop display summarizing all received messages and a means of selecting messages from the index (VITAL Systems Infrastructure Guide, 100).

Address/Host abstraction

Ideally, the actual host machine that acts as the mail server will be abstracted from the user's publicized address. For example, user carol1 sends and receives email using the machine redhook.llnl.gov. However, the address that user publicizes is simply carol1@llnl.gov. This is also the address that appears in the reply-to portion of the header of outbound mail. Abstraction of this sort allows the user to change host machines, but retain the same email address resulting in not having to publicize a new address to anyone who would mail that person. A relatively small amount of systems administration is executed to make this possible, but the ability to make necessary mail delivery changes can be released to the user through related services (Shuk).

Email use by the Data Capture Environment

Data Capture uses this service to send acknowledgment and error messages to individuals who need to be informed that particular tasks have successfully or unsuccessfully been completed (VITAL Data Capture Guide, 126).

On the desktop

Performs the tasks needed to store, forward, send, receive, or respond to mail sent by another user or a service. The endpoint for distribution of mail is the user with provision for notification of receipt. This service presents the user with mail in the format of the user's choice. The content of the mail may include text, voice, and video. Complexities of mail from different mail vendors is handled transparently to the user. Notifications of status regarding batch processing or deferred processing on a server are sent to the desktop user by means of mail notification. An action request created on the desktop may be sent to an administrator on a server (VITAL Desktop Integration Guide, 62).

Create & Send Action Request

Create & Send Action Request is a specialized email-send service that provides a finite set of preformatted and pre-addresses action requests. New request types can be added to the profile as necessary.

Any VITAL service may invoke this service to create an action request using the data it has acquired about the situation. The initiating service must receive an explicit request from the

individual to create an action request on the user's behalf. The requesting service can then invoke Create & Send Action Request, sending it the pertinent data it gathered during the session. Create & Send Action Request then sends the action request as a standard email message to the mailbox of the person responsible for taking the particular action (VITAL Systems Infrastructure Guide, 100-102).

The following are functions of the Create & Send Action Request service:

Produce Action Request

Produce Action Request is the main control routine of the Create & Send Action Request service, which accepts action requests from Integration Services and the Produce System Document component of the Manage Access to Collections (Data Access) service. All return messages are handled by Process Response From Support Organization.

Create Request for Acquisition

An acquisition request may be generated when data is known to be readily available within another system, but has not yet been released to the data warehouse network. This order is transmitted to the custodian of the transaction-update system, who is the owner of the system-of-record for the required data. The data may be made available, when feasible, if all the following criteria are met:

- The data capture environment for this data has a Create & Send Snapshots service
- The data is deemed sharable
- The customer has sufficient security authorization

Create Request for Authorization

An authorization request is generated when the data is available, but the user is not currently authorized to see it. The request is sent to the appropriate business owner. The reply goes directly to the information consumer.

Create Request for Definition

A define request is used to request the definition of a new business rule, entity, attribute, or standard. This request is forwarded to the data administration group, which negotiates with the involved parties to accept or reject the new definition.

If accepted, the metadata and data in the data warehouse network are modified or augmented to reflect this definition. Changes to existing Data Capture environments, or at least the tasks performed by the Create & Send Snapshots service may be required.

Create Help Line Request

A help request may be submitted to solicit direct support from the data warehouse network system manager or a hot-line organization. Help is requested by means of the order process to provide a single point of contact for the consumer.

Process Response From Support Organization

Process Response From Support Organization receives responses to action requests from support organizations. It retrieves the request from the action request log along with the identifying information concerning which service invoked Create Action Request, the specific order request number, (if an order request triggered the action request), and the identity of the information consumer requesting the action.

In all cases, the responses are sent back to the service that originally requested the action request. It is the responsibility of the invoking service to take appropriate action based on the returned messages.

There are two situations that can be handled:

action acknowledgment

indicates that the requested action occurred and when it was completed.

action denial

a reject message containing one or more reject codes (VITAL Systems Infrastructure Guide, 100-102).

On the desktop

Create and Send Action Request performs the tasks needed to format and send mail messages called action requests to designated owners for administrative action. These actions include some decision or action by an administrative authority such as granting authorization rights to database resources. An approval by the authority would initiate the appropriate services with the required

data to perform the requested action. The Create and Send Action Request service can be invoked by any VITAL service with pertinent data gathered by the requesting service and after explicit confirmation by the requesting individual (VITAL Desktop Integration Guide, 64).

Time Synchronization service

The diversity of applications on clients and servers distributed over global zones create the need for a single time reference in order to schedule activities and determine program event sequencing and duration. A distributed time service regulates the system clocks in a computer network so that they closely match each other (VITAL Systems Infrastructure Guide, 103).

Job Scheduling service

A job scheduler ideally provides the functions of accepting jobs to be scheduled, initiating the jobs, and providing status on the jobs (VITAL Systems Infrastructure Guide, 103).

On the desktop

The desktop interface of the Job Scheduling service accepts predefined scripts or the name of an application to be invoked, the appropriate trigger that should start the application job dependencies, execution priorities, alert escalation identifiers, a user/administrator notification list, and job run-time constraints. Minimally, Job Scheduling should allow future dates and times to be specified as triggers and should allow one-time or recurring standing orders (VITAL Desktop Integration Guide, 251).

Initiate Event Processing service

Initiate Event Processing uses a job profile (or a portion of the application profile) created by the Job Scheduling service to identify events that occur in the operating system or in the network that cause other services to be invoked. Events that trigger services to be invoked can be passed to Initiate Event Processing from the Event Management or other services. Trigger-processing rules defined in the Repository are applied by the service to process the triggered events.

The Initiate Event Processing service contains no interface to the desktop (VITAL Systems Infrastructure Guide, 104-105).

Event Management service

The Event Management service provides a centralized facility for managing and reporting events that occur during the execution of jobs. It is primarily used by other services, such as the standard application service, Return Status Messages, and applications or scripts to obtain status information of initiated jobs and transactions.

The programs and scripts that make up a job may declare milestone events by using messages that are stored in the event management database. Each event consists of a type, time, name, optional message, and description. Events may be displayed in order of declaration, retrieved by an application for action, or mailed to a destination address. Programs may register to obtain events declared by others as they occur.

Events are associated with jobs that run on a scheduled basis. Job scheduling is performed by the Job Scheduling service and the status of completed jobs is maintained in the job scheduling database. The Event Management service maintains a separate database to track the status of executing jobs. Typically, a job consists of one or more programs the perform some related activity on application data. During execution of each run, the job programs may declare a begin event, certain milestone events, and a completion event to Event Management. At job completion, an alert or completion status may be mailed to a mail system address or directly to the service initiating the request (VITAL Systems Infrastructure Guide, 105).

On the desktop

Provides a desktop interface to the Event Management service in the Infrastructure environment to inquire on the status of jobs executing or completed. Events can be posted to the desktop environment by the Event Management service to initiate action by a desktop application or to inform users. Desktop applications can declare or retrieve events from the Event Management service using this interface. Jobs can be scheduled for execution using this interface from the desktop (VITAL Desktop Integration Guide, 64).

Terminal Emulation software

This represents the lowest level of desktop-integration software. Terminal emulation is used to allow machines with built-in human interface to defeat that interface in favor of a host-driven terminal dialog. This is usually done to allow desktop platforms to interface with legacy host systems (VITAL Systems Infrastructure Guide, 106).

On the desktop

The terminal emulation software package runs on the desktop device (VITAL Systems Infrastructure Guide, 106).

Front-ending software and scripts

Front-ending software is commercially available to intercept the terminal data streams from host-based applications and remap them onto a windowed desktop environment. The mapping is done by means of a script written in the scripting language of the front-ending tool. Some tools have intelligent event-triggered scripts that are dynamically executed when the event is observed. Event-triggered scripts are the preferred method of implementing VITAL front-ended applications.

A broad range of front-ending scripts should be cataloged and made sharable in the network. The source code management of these scripts is handled in a sharable script library within the Repository environment and documented in a sharable script directory. The scripts propagated throughout the enterprise for run-time sharing are managed as Application Utility Services, as identified earlier in this chapter (VITAL Systems Infrastructure Guide, 106).

On the desktop

Performs the tasks needed to let desktop computers run applications that connect to a host and provides a graphical user interface as the user interacts with the host system. The desktop front-ending application intercepts character streams from the host and interprets them for a graphical user interface display. In addition, the desktop front-ending application can collect information from the user and send it to the host as pseudo-key strokes. The approach may be used in transaction systems with a high degree of human interaction and with purchased packages that do not separate terminal dialogs from processing logic, or in existing systems that cannot be modified or maintained (VITAL Desktop Integration Guide, 64).

Mission Critical Data Capture Services

Provide Operational Access

Provide Operational Access provides system access routines that are isolated from other routines. This service is part of the client/server "server" process that accepts remote procedure call messages from the client process. In a relational DBMS environment, a portion of this functionality is provided by the SQL engine of the DBMS, and a set of rules implemented as stored procedures in the DBMS. In less-sophisticated environments, the functionality defined in Provide Operational Access may need to be completely hand-crafted (VITAL Fundamentals, 148).

Provide Operational Update

This service isolates record locking and record writing from other routines in the application. In a relational database environment, this is also essentially the DBMS SQL engine that accepts and performs record locking and contention management, integrity enforcement, as well as commitment and rollback control. In less-sophisticated environments, these functions may require hand-crafting or a variety of unintegrated utility tools. It is important that the specific syntax of update code be isolated from the internals of the application.

Note: Though Provide Operational Access and Provide Operational Update have been called out as separate services, in today's technology they are provided by the same DBMS product. However, there are several activities that take place between reading data and writing back the data as described by the services in the Data Capture environment (VITAL Fundamentals, 148).

Capture Data

Capture Data supports processing transactions received front he desktop or other Data Capture environments. In terminal emulation, front-ending, and host-driven client/server systems this service also deals with screen handling code and human interactions. This isolates the screen and human-interface characteristics from the mainline logic, allowing migration to desktop-driven client/server approaches over time. Validation or revalidation of transaction data received from client applications including collision detection and resolution is performed by this service. Algorithmic routines are isolated into function specific tasks that operate using externally stored formulas (VITAL Fundamentals, 148).

Deliver Transaction

This service manages the sequence of transaction delivery and acknowledgment of receipt from all destinations when a transaction must be sent to multiple files or to more than one other system. Furthermore, if there are different formats required by the individual systems receiving this transaction, then the reformatting is done by a component of this module. This service isolates the business application from the housekeeping activities of routing, sending sequence, acknowledgment rules, two-phase commit rules, and rollback or recovery logic. In other words, two-phase commit logic, integrity rules, and delivery sequences, and translations should be managed from this separate routine. Many relational DBMS products offer two-phase commit services and ISO TP standard rollback control. Often a standard EDI transaction-set translator module can be used to perform all the transaction translations needed in Deliver Transaction. If these capabilities are not present in the Systems Infrastructure environment, then they will have to be hand-crafted as general utilities (VITAL Fundamentals, 149).

Create Update Transactions

Create Update Transactions consists of periodic-processing tasks triggered by an event or on request such as month-end processing and nightly consolidations. The tasks are application-specific and involve creating transactions that update operational data or aggregate summary data in the operational databases (VITAL Fundamentals, 149).

Initiate Event Processing

This service operates as a job scheduler to trigger any of the above services (particularly Capture Data and Create Update Transactions) based on the completion of a particular business or system event, or based on a particular date and time. This is normally an operating system function found in a job scheduler. It incorporates job scheduling and Event Management Services as defined in the Infrastructure Services. If the chosen platform does not have these Infrastructure Services, then the function must be programmed. Therefore, a platform with such capabilities is recommended (VITAL Fundamentals, 149).

Mission Critical Data Access Services

Acquisition

Entails getting data out of the legacy systems and into the base tables of the Data Warehouse. Acquisition includes six sub-processes called Extract, Transport, Clean, Map, Transform, and Populate (Haisten, 2).

All of these processes but Clean fall under Data Access in the ASSIST+ paradigm as we are building a pull model versus a push model. The Extract, Map, Transport, Transform and Populate are all being driven from ASSIST+'s end (Alford).

Clean — Inspect and Correct Validity

Clean inspects data for integrity, quality, buried information, etc. After the inspection, Clean then may eliminate, flag, annotate, modify, or augment the data as necessary to improve information content (Haisten, 2).

This is performed on the business rules at the Operational end as data is posted to that system-of-record. The issue remaining here is to identify which services will aid in this (i.e., Validate and Post Data to Operational System) (Alford).

Extract — Create Snapshot

Extract creates a data snapshot from a source system based on identified information needs captured during data warehouse modeling sessions. This snapshot may be used alone or in conjunction with other snapshots. It is used to either refresh or to update a base table in the data warehouse (Haisten, 2)

The Extract process is the Create portion of the Create and Send Snapshot service as outlined by VITAL.

Map — Relate Source and Target

Map creates and maintains the correspondence between fields or columns in the operational sources and the target column in the Data Warehouse. Minimally, it is a physical correspondence between the two (Haisten, 2).

Still looking for counterpart in VITAL TAGs .

Transport — Send Snapshot

Transport is the other component of VITAL's Create and Send Snapshot service. Its purpose is to send the snapshot taken of the legacy system from the point of creation to where it will be loaded into the Data Warehouse (Haisten, 2).

Sharable data is released to the data warehouse network through the use of a data envelope (VITAL Fundamentals, 156).

A Systems Infrastructure file transfer service is used to route the data to the appropriate data warehouse (VITAL Fundamentals, 156).

The Transport service can be segmented into two more specific services:

Direct Transport

Direct Transport involves an explicit procedure or utility to handle the move.

Indirect Transport

Indirect Transport uses interoperability software to make the different locations "transparent," that is the data does not appear to be in separate places. (Haisten, 2)

Transform — Convert Values

Transform specifies and implements conversion logic to calculate, project, translate, aggregate, or otherwise compute a new value from source fields to be inserted into a data warehouse column (Haisten, 2).

Populate — Load Base Tables

Populate loads base tables from one or more snapshots. The base table may be refreshed, appended to, or updated (physically or logically) (Haisten, 2).

Publish and Subscribe

Publish and Subscribe Services maintain data collections derived from the warehouse base tables to support the information needs of direct access and subscription consumers. The sub-processes include Build Standard Collections, Build Consumer Collections, Manage Warehouse Inventory, and Manage Warehouse Archive.

Build Standard Collections

Standard Collections are sets of relational tables derived from data warehouse base tables to satisfy a broad spectrum of related needs. They are the "intermediate assemblies" of the data warehouse created to improve ease, efficiency, or timeliness of access. Standard Collections often join data from multiple base tables to provide a broader integrated perspective and/or are summarized from lower level detail (Haisten, 3).

Build Consumer Collections

Consumer Collections are sets of data configured specifically to satisfy a defined need. They are generally highly denormalized and are often (but not always) in non-relational forms including spreadsheet files, hypercubes, or EIS load files (Haisten, 3).

They are subsets of a Standard Collection or logical database view ordered by an information consumer and specified by a particular system (VITAL Glossary, 5).

Manage Warehouse Inventory

The Warehouse Inventory includes all datasets which are created by data warehouse processes and made available to warehouse consumers. This includes base table, standard collections and consumer collections. The Manage Warehouse Inventory process uses statistics derived by Operations processes to evaluate usage of all inventory items and to either recommend or carry out changes to the inventory. This may include eliminating under-utilized collections or defining new standard collections ("assemblies") based on observed patterns of use (Haisten, 3).

This service (3.3 in the VITAL TAGs) manages consumer orders, and its functions optimally take place in the background of the data warehouse network (VITAL Data Access guide, 143).

Components of Manage Warehouse are defined as follows by VITAL:

Analyze Quality and Usage

Analyze Quality and Usage is where the evaluation (based on operational statistics) mentioned above takes place. A report is submitted to the custodian of the transaction-update systems detailing recommendations (VITAL Data Access Guide, 146).

Michael Haisten looks a step further and hints at a "cybernetic self-optimizing warehouse environment" (VITAL Data Access Guide, 146) when stating that Manage Warehouse Inventory may either

make recommendations or actually carry out the changes to the inventory (Haisten, 3).

Process New Orders

In response to new orders, Process New Orders may modify a standard collection specification to incorporate newly requested attributes or domains that are in base tables but not part of a particular standard collection. As an option, another specification may be submitted for a particular order as a result of superseded specification that better suits the order needs (VITAL Data Access Guide, 146).

Optimize Collection Specifications

Key functions performed by Optimize Collection Specifications are:

Analyze the transform and propagate orders to maximize data warehouse network efficiently while achieving the customer's desired results.

Create a new specification and update the relevant orders to point to this new collection.

Mark the old collections "inactive" when several collection specifications include substantially similar data.

Archive a collection specification when a collection is no longer being used. The corresponding specification is made inactive. Receive Data and Build Collections (3.4) archives the collection later.

Create a new distribution plan from the forecasted demand and optimized specifications (VITAL Data Access Guide, 147).

Build Action Request Detail

Build Action Request Detail is used whenever it is determined that action is required from a service organization.

This component provides for the following functions:

Sends a request to the custodian of the transaction-update system and to the data warehouse management organization if the data is known to exist on another system or data base but is not marked as collectible.

Forwards *define* requests to the organization responsible for the new data definition and data standardization.

Sends an appropriate notification to the information consumer that action requests were sent, along with a specified time period to expect a response.

Logs that action request were sent for potential follow-up (VITAL Data Access Guide, 148).

Create Extract Specification

Create Extract Specification places a requirement on the Data Capture system-of-record to provide the necessary operational data in the proper format and in the proper frequency for updating the source data warehouses (VITAL Data Access Guide, 148).

Manage Warehouse Archive

The Warehouse Archive is off-line storage managed to maintain a consistent historical perspective for the data warehouse. All base tables, and standard collections which are computationally intensive to create, are archived at regular intervals along with their metadata. This is not to be confused with backup and recovery processes whose purpose is to restore the operating environment (Haisten, 3).

Operations

Operations Services consist of monitors and tools which support the smooth and consistent operation of the Data Warehouse Environment. Sub-processes include Usage Monitor, Performance Monitor, Event Manager, Warehouse Analyzer, Backup and Recovery, Version Control and Synchronization, and Meta Manager (Haisten, 4).

Usage Monitor — Resource Consumption and Billing

The Usage Monitor records the usage patterns of all inventory items and processes within the Data Warehouse Environment using DW control tables (Haisten, 4)

Performance Monitor

The Performance Monitor records the performance pattern (time and resources) of all processes executing within the Data Warehouse Environment (Haisten, 4).

Event Manager

The Event Manager allows the specification, invocation and tracking of events within the Data Warehouse Environment. Events are logical specifications of tasks which are expected to initiate at a specific time or depend upon one or more tasks. The Event Manager provides consumer, producer, and operator messaging, alerts, escalation control, and query access (Haisten, 4).

Warehouse Analyzer

The Warehouse Analyzer is an expert-system based operations tool which interprets the usage, performance, and event control data in order to identify processing bottlenecks and to suggest more optimal processing configurations (Haisten, 4).

Backup and Recovery

Backup and Recovery is intended to ensure a high degree of consistent availability but without the heavy artillery of transaction fail-safe techniques needed for mission critical data production applications (Haisten, 4).

Version Control and Synchronization

The Version Control and Synchronization (VCS) sub-process is invoked by all Data Warehouse processes to ensure that the correct (current) version of the software is being used. If not, VCS downloads the appropriate version or disallows the use of the invalid version (Haisten, 4).

Meta Manager

The Meta Manager is an application to manage the metadata tables (Alford).

It provides query and update access to all metadata maintained in the Data Warehouse Environment. This includes all information required for Core Warehouse Services and Information Consumption Services. In addition, any external metadata may be defined, imported and integrated (Haisten, 4).

Delivery Services

Delivery Services support the ability to send data collections from the data warehouse to another processing site, possibly in a more suitable modified form, at a particular time or on a periodic basis. Delivery Services allow consumers to specify what they want, what form they want it in, where they want it delivered, and the timing and periodicity of the delivery.

The Core Warehouse Services of Acquisition, Preparation, and Operations ensure that the raw materials for analysis and information integration are available. The Information Consumption Services help delivery on the promise of finding and using the right data, in the right form, at the right location, and at the right time.

The first stages of a data warehouse implementation generally have a "come and get it" orientation using manual time intensive access techniques. They offer basic Access Services without Navigation and Delivery support. Future stages of data warehouse evolution involve both a "we deliver" subscription orientation and an automated "come and get it" orientation using selection agents (Haisten, 8).

Subscription Processes

Place Order for Collection

Place Order allows a consumer to specify where, when, and in what form they would like a pre-specified data collection to be delivery. The order may be a one time order or a standing order for periodic delivery. Access Services are used to define the contents of the consumer collection to be delivered (Haisten, 8).

Place Order for Collection allows information consumers to place orders for delivery of data from the data warehouse network. It is essentially the order placement system for shared data (VITAL Data Access Guide, 130).

Available from Virtual Integration Technologies (Chowdary 2/7/95, 3).

Fulfill Order for Collection

The Fulfill Order process transforms and delivers collections at the given time (Haisten, 8).

Available from Virtual Integration Technologies (Chowdary 2/7/95, 3).

Manage Orders

The Manage Order process allows data warehouse staff to manage the processing sequence of orders and modify order details if necessary to optimize delivery (Haisten, 8).

Agent Processes

Define Agent

The Define Agent Process allows consumers to specify information requirements which will result in automatic delivery of data to the consumer specified location in a specified form when certain event, or trigger, conditions are met. The consumer defines an order via Place Order then attaches an agent to the order (Haisten, 8).

Monitor Agent

Monitor Agent lives on the server side to track agent activity, modify the priority of the agent's task, or kill the agent if necessary (Haisten, 8).

This along with Define Agent provide Client Driven Event Management (Alford).

Access Services

Access Assistant

The Access Assistant helps the consumer define an access request to retrieve data from the data warehouse. The consumer has the option of using the generic Collection Builder tool that will create and catalog a new consumer collection or one of the supported report, query, or DSS tools (Haisten, 6).

Collection Generator

The Collection Generator allows generic specification of data requirements to generate custom consumer collections from available base tables and collections. This utility generates new data tables more finely tuned to the consumer's needs thus reducing the sophistication required in the use of the chosen access tool. The specification and the results are cataloged for use by other consumers (Haisten, 7).

The ASSIST+ plan is to use metadata tables built to see if ETI Extract can use them to generate collections (Alford).

Meta/Control Bridge

The Meta/Control Bridge provides both an adaptable application programming interface and a general import/export mechanism to synchronize metadata between various third-party access tools and the data warehouse environment (Haisten, 7).

Mission Critical Repository Services

Navigation Services

Dynamic Selection service (DSS)

Dynamic Selection service selects an optimal instance of a logically named service or resource based on the available instances in the network. It also assures that a reliable connection can be made to some instances as long as any instance is available. DSS can be configured to provide very sophisticated selection algorithms to manage and smooth the queue length and workload on the various servers containing replicated instances of a service. DSS uses the sharable services directory and the sharable data directory to determine available services and to retrieve the service profiles (VITAL Repository Guide, 33).

Directory Registration service (DRS)

The Directory Registration service updates the network registration indicator in the sharable services directory. All services are required to use this service as an agent to update their availability whenever they are launched, change availability status, or close down. This service is critical to keeping an accurate accounting of available services instances in the network (VITAL Repository Guide, 34).

Administration Services

Version Control and Synchronization service (VCS)

Version Control and Synchronization provides the essential indicators of which versions of software and databases are current. This synchronization service must be done prior to any data or metadata synchronization itself, and must be completely propagated to all locations where the old and new versions reside in the network. Therefore, the Version Control and Synchronization service uses a traditional scheduled two- or three-phase commit process to ensure that all propagated copies of directories have the new version number before any one of the new version of the software, metadata, or data is propagated (VITAL Repository Guide, 61).

Metadata Synchronization service (MS)

Metadata Synchronization populates the repository with captured metadata for use by applications at runtime.

Currently available from Virtual Integration Technologies (uses captures from Silverrun) (Chowdary 2/7/95, 3).

Software Synchronization & Distribution service (SS)

Software Synchronization and Distribution service is essentially the same as the Metadata Synchronization service except that it applies to bulk replacement of software files. Unlike the Metadata Synchronization service, software synchronization can be performed by either the scheduled lazy replication or by strict lazy client methods. The main difference between this service and the Data Synchronization service is that both software and metadata should be replaced as bulk file overwrites rather than applying net-record replacements as is sometimes done by the Data Synchronization service (VITAL Repository Guide, 61).

Data Synchronization service (DS)

Data Synchronization service uses variations of the lazy replication synchronization technique first introduced by Dr. Barbara Liscov of the Massachusetts Institute of Technology. Data synchronization is the fundamental service used by the Data Access environment to manage the integrity of sharable data propagated to a variety of mid-tier warehouses, local-access databases, and direct access databases. However, every environment that must ensure data value integrity can use the Data Synchronization service. Because data files tend to be much larger than either metadata or software files, data synchronization is done by either applying net changes to the data or by bulk file overwrite. If greater than 10 percent of the file must be changed when it is synchronized, the bulk file overwrite is used, otherwise net changes are applied (VITAL Repository Guide, 62).

Metadata Updates and Changes (a category of services)

The Metadata Updates and Changes category includes all maintenance of metadata, including mappings between Repository environment components. This would include all CASE system development tools and Data Capture update programs that create, modify, and delete metadata (VITAL Repository Guide, 62).

Change Management service (CMS)

Change Management service enforces a rigorous change-control process during the deployment phase following the integration testing and "golden master" release of new system enhancements. CMS is the service that controls version updates to the production copy of the master data dictionary from the development copy of the master data dictionary (VITAL Repository Guide, 62).

Software License Management service (SLM)

Software License Management service allows for the central administrative process to keep control inventories of established software licenses. This service can be programmed to poll platforms occasionally to determine the serial numbers of serialized software to inventory the instances and to detect duplicates. The invocation of any synchronization or distribution service triggers this service to check and log the serial numbers that are propagated. These are registered in the version number directory along with the other instance-specific attributes of the resource (VITAL Repository Guide, 62).

Report Distribution Profile Management (a category of services) (RDPM)

Report Distribution Profile Management services are driven and maintained by a set of profile tables. Infrastructure management applications are required to load, update, and delete entries in the profile tables. This service maintains the distribution profiles so that the data synchronization service can manage the propagation of these reports as a standard collection (VITAL Repository Guide, 62).

Bibliography

Alford, Francine, ASSIST Group Leader. Administrative Information Systems. Lawrence Livermore National Laboratory.

Dishon, Danny, Chairperson Desktop Integration Workgroup. VITAL Desktop Integration Guide. Apple Computer, Inc. 1993.

Gans, Ray and Brenda Yamasaki, Chairpersons Data Capture Workgroup. VITAL Data Capture Guide. Apple Computer, Inc. 1993.

Haisten, Mike. VITAL Data Warehouse Process Model. VITAL Technologies, Inc. July 11, 1994.

Haisten, Mike (version 2.0) and Lani Spund (version 3.0), Chairpersons Data Access Workgroup. VITAL Data Access Guide. Apple Computer, Inc. 1993.

Hirsch, Ben, Chairperson Repository Workgroup. VITAL Repository Guide. Apple Computer, Inc. 1993.

Hughes Enterprise Architecture. **Technology Architecture.** Hughes Proprietary. March, 1993.

Skelton, Ron, Chairperson Systems Infrastructure Workgroup, VITAL Systems Infrastructure Guide. Apple Computer, Inc. 1993.

Spund, Lani, Chairperson Client/Server Task Force. VITAL Fundamentals. Apple Computer, Inc. 1993.

Photosynthetic acclimation to enriched CO_2 concentrations in *Pinus ponderosa.*

Matthew P. Torres [1], James L.J. Houpis [1], James C. Pushnik [2], Janna Beck [3], Thorpe Loeffler [1], [1] Health and Ecological Assessment Division, Lawrence Livermore Nat. Lab, Livermore, CA 94550; [2] Dept. Bio. Sci., Cal St. Chico, Chico, CA 95929, [3] University of Oslo, Norway

Abstract

By the middle of the 21st century earth's ambient CO_2 level is expected to double to 700 uL/L. Higher levels of CO_2 are expected to cause major changes in the morphological, physiological, and biochemical traits of the world's vegetation. Therefore, we designed an experiment to measure the long-term acclimation processes of *Pinus ponderosa.* As a prominent forest conifer, *Pinus ponderosa* is useful when assessing a large scale global carbon budget.

Eighteen genetically variable families were exposed to 3 different levels of CO_2 (350 ppm, 525 ppm, 700 ppm), for three years (April 1992 to April 1995). Acclimation responses were quantified by assays of photosynthetic rate, chlorophyll fluorescence, and photosynthetic pigments. We also supplemented the three assays with growth measurements (stem diameter, stem volume and stem height), in an attempt to correlate positive treatment responses to physiological and biochemical changes.

Photosynthesis increased with increasing CO_2, approximately 1.4 umol m^{-2} s^{-1}) ($p < .05$). At 700 ppm CO_2 photosynthesis for seedlings from Families 3087 and 3088 decreased by .008 umol/m^2/s and .361 umol/m^2/s respectively. Stomatal conductance decreased significantly by approximately .023 mol m^{-2} s^{-1} ($p < .05$), with increasing CO_2. Conductance values, however, did not vary with family. Internal CO_2 concentrations (Ci) increased relatively to the external CO_2 concentrations (Ca). Ci/Ca values were at 71.4% in ambient chambers and 74.9% in enriched chambers. Chlorophyll fluorescence values as expressed by Fv/Fm decreased by 10.4% with increasing CO_2. A 41.7% increase in Fo suggested that trees in high CO_2 lost PSII reaction centers. Photosynthetic pigmentation also decreased with increasing CO_2. Chlorophyll a dropped 21.0%, and carotenoid pigments dropped 18.5% in enriched CO_2.

Introduction And Background

In the past century, atmospheric CO_2 levels have increased drastically due to the consistent burning of fossil fuels. Once at 280 uL L^{-1} concentrations (prior to the industrial revolution), atmospheric CO_2 levels have risen above 350 ppm in 1995. We expect major shifts in the global carbon cycle from ground to atmosphere to continue. In recent years, scientists have devoted their energy to studying the short-term effects of enriched atmospheric CO_2 on crop plants. We chose to research the effects of long-term CO_2 enrichment on a prominent forest conifer: *Pinus ponderosa*. As large atmospheric carbon sinks, forest conifers are important factors in determining changes in the earth's carbon budget. Furthermore, a long term study enables us to predict the characteristics of future forest ecosystems.

In previous years, most studies have pooled species variation into one large assay of tree response to elevated CO_2. A review by (Wullschleger et al. 1994) revealed that plant responses ranged from -50% to +350% in the compiled studies of 70 tree species. This range of variation is too wide to be classified as one unit. The goal of the current project is to determine why large amounts of intraspecific variability occur; and, how variability can be genetically tagged for identification and use in forest management. In particular, we chose to study variable intraspecific acclimation quantified by photosynthetic rate, chlorophyll fluorescence, and light harvesting leaf pigmentation. In addition, we correlated these physiological and biochemical observations with the good or bad growth patterns of the different tree families.

Photosynthesis is the process by which chlorophyll rich organisms assimilate carbon. Generally, photosynthesis increases with increasing CO_2 (Pushnik et al. 1994). When CO_2 concentrations rise, photosynthesis increases due to a rise in internal CO_2 levels, which causes an increase in the ratio of CO_2 to O_2 and to Rubisco within the cell. Rubisco is an enzyme which catalyzes the bonding between the C in CO_2 and ribulose bi-phosphate. The increase creates a natural pressure for carboxylation (or carbon fixation), by Rubisco, and thus, carbohydrate assimilation. The ratio of internal CO_2 (C_i) to external CO_2 (C_a), otherwise known as the stomatal limitation, maintains the natural CO_2 pressure within the leaf at approximately 63% of the ambient CO_2 level (Pushnik et al. 1994). Although CO_2 induces stomatal closure, trees exposed to enriched CO_2 levels maintain higher photosynthetic rates because of a constant C_i/C_a ratio.

Though partially controlled by the stomates, photosynthesis also relies upon light use efficiency (quantified by chlorophyll fluorescence). "The inverse relationship between in vivo chlorophyll fluorescence and photosynthetic activity...can be applied to study the potential photosynthetic capacity of plants as well as to detect damage to the photosynthetic apparatus." (Lichtenthaler et al. 1990) Chlorophyll fluorescence is the light energy used to excite the electrons within chlorophyll pigments and promote their capture by a primary e^- acceptor Q_a. Fluorescence measurements enable quantification of photosystem II efficiency within the thylakoid membranes in chloroplasts. Photosystem

II is the light harvesting antennae (containing almost entirely chlorophyll a), which traps photons of light energy and converts them to chemical energy. The trapped light excites electrons within the chlorophyll. The excited electrons are captured by the primary acceptor Q_a, then released and allowed to return to their original energy level via an electron transport system. In the process, ATP is formed for plant energy. Researchers such as Schmidt et al. (1990), Greaves et al. (1992), and Lichtenthaler (1992), support the use of modern chlorophyll fluorescence measurement techniques as useful indicators of plant stress. Four fluorescence parameters are important to this study: Fo, Fv, Fm, and Fv/Fm.

Fo is the amount of chlorophyll fluorescence apparent after a leaf has been dark acclimated for about one hour. Fo may be considered the base line fluorescence level, or the period when the fewest number of Q_a acceptors are reduced by excited electrons. Fm is the maximum fluorescence apparent after all of the primary electron acceptors have received the excited electrons of PSII (during illumination). Fv is the variable fluorescence or the difference between base line and maximum. Fv/Fm is a quantifying ratio of the photochemical efficiency of PSII. An increase in the base line fluorescence indicates a decrease in the number of PSII reaction antennae, (Greaves 1992). With an increase in Fm, there is an increase in the number of PSII reaction centers. The closer the variable fluorescence comes to the maximum fluorescence, the greater the efficiency achieved. Greater efficiency = Fv/Fm = 1.00. Greater inefficiency = Fv/Fm = 0.00.

Leaf chlorophyll content couples chlorophyll fluorescence and PSII efficiency. Researchers use leaf pigmentation analysis alone to quantify levels of air pollution plant stress (Houpis et al. 1988). Light harvesting pigments reside within photosystem I and II. The three primary pigments within the chloroplasts of leaves are: Chlorophyll a, b, and Carotenoids. Chlorophyll a and b absorb red light at 662nm and 644nm respectively. Chlorophyll a is the predominant pigment within PSII, and thus, responsible for 90% of the variation of the four fluorescence parameters used in this study. Lichtenthaler et al. (1990) demonstrated a direct relationship between chlorophyll content and fluorescence at 690nm and 730nm. Carotenoids absorb blue light at a wavelength of 440nm. They are responsible for absorbing light from the opposite side of the spectrum for photosystem efficiency purposes.

Methods and Materials

Experimental Species and Growth Conditions

Ponderosa pine trees were subjected to three different levels of CO_2 (350 ppm, 525 ppm, and 700 ppm). We used nine families to measure their intraspecific response variability. Four of the families were half siblings (3087, 3088, 3399, 3354), obtained from parent species located in the Sierra Nevada mountains of California . The other five families were open pollinated species picked from five sources within California: Mendocino (OP5); Sierra (eastern) (OP6); San Bernandino (OP7); Santa Clara (OP8); and El Dorado County (OP9).

12.8 L pots were used to contain each tree. Eighteen cylindrical open-top chambers (3m x 3m) contained the trees for exposure to elevated CO_2. Six chambers were devoted to each level. In addition, three control plots without chambers were used to correct for open-top chamber effects. The trees were consistently well-watered and fertilized frequently. (Houpis et al. 1995)

Photosynthesis Measurements

Photosynthesis/gas-exchange was measured using an infra-red gas analyzer system (IRGA Li-6400) in conjunction with a light controlled cuvette. All measurements were taken at a constant light level of 1000 uE m^{-2} s^{-1} and at a constant temperature of 15 C.

Chlorophyll Fluorescence Measurements

Chlorophyll fluorescence measurements were measured using a Morgan CF - 1000 Chlorophyll Fluorescence Measurement System. Needles were dark acclimated in sample cuvettes for 45 minutes. Next, each sample was exposed to 1000 uE m^{-2} s^{-1} of light for 20 seconds. Ratios of variable fluorescence (Fv) to maximum fluorescence (Fm) were used to determine the photochemical efficiency of photosystem II.

Pigmentation Analysis

Chlorophyll a, b, and carotenoid pigments were based on a per unit leaf area system. Each fascicle collected was detached from the bundle sheath, then measured for surface area. Samples were placed in viles containing 5 ml dimethyl formamide for 21 days in the dark and at 4 C to remove all pigments from the leaf tissue. Following pigment extraction, a 100 ml aliquot was diluted to 2 ml and measured spectraphotometrically (Hewlett Packard HP8452A), at 440, 644, and 662 nm. Concentrations of each pigment were analyzed with the calculations according to Wellburn and Lichtenthaler (1983).

Results

Preliminary Growth Measurements

Growth response showed a wide variability in the response to CO_2 (Figure 1). All families' stem diameters increased with increasing CO_2. However, stem height growth responses were near null or negative for all families but 3399, which grew 33.73% above ambient levels. Families 3088 and OP7 responded negatively to enriched CO_2. For these families, stem height decreased in 700 ppm levels by -11.17% and -1.35% respectfully. Furthermore, stem volumes were 68% and 75% lower than the families with the highest stem volumes. Families 3087, 3399, and 3354 displayed positive stem volume growth at 88%, 79%, and 58% increase respectively. Families exhibiting the most positive growth responses to enriched CO_2 were considered more suitable for a future CO_2 rich atmosphere.

Table1:

High Positive Growth Response	Low to Negative Growth Response
3087	3088
3399	OP7
3354	

Photosynthesis and Conductance

Total CO_2 assimilation rates increased with increasing CO_2 (Figure 2). Levels ranged from 5.34 umol/m^2/s in ambient chambers to 6.72 umol/m^2/s in 2x ambient CO_2 chambers. Families 3354, and 3399 showed the greatest increases in photosynthesis at the 700 ppm level (Figure 3). Of the three families, percentages ranged from 46.6% to 78.8% greater than ambient photosynthetic rates. This correlates well with their growth response (Table 1), though, it can not explain the entire scheme of positive growth under high CO_2. For example, Families 3087 and 3088 displayed negative assimilation responses to high CO_2 at -4.2% and -6%, respectively. The decrease in CO_2 assimilation by Family 3088 at the 700 ppm level correlates positively with its growth response. Stomatal conductance rates decreased by .023 mol/m^2/s in the 700 ppm level (Figure 4a). Most families followed this trend except for OP9 and 3354 which increased .018 and .012 mol/m^2/s, respectively. Although conductance rates decreased in the 700 ppm level, total carbon assimilation was not hindered because of a constant stomatal limitation of ~ 73% (Figure 4b).

Chlorophyll Fluorescence

Values of Fv/Fm decreased by an average of 10.4% with increasing CO_2 (Figure 5). This follows the trend observed by (Houpis et al. 1994). Families OP5, OP6, and OP8 expressed the least amount of decrease in PSII efficiency (from -8.5% to -10.8%), correlating positively to increasing stem diameter. Families 3087, 3399, and 3354 (the positive growth responders), displayed decreases in PSII efficiency (from -14.3% to -17.1%), even though they had the greatest increases in stem diameter. Greaves et al. (1992) associated a reduction in PSII reaction centers with the dramatic increase in base level fluorescence (Fo), (Figure 6), and (Table 2). This may explain the large drop in PSII efficiency and chlorophyll a at the 700 ppm level.

Table 2: Degree of PSII reaction center loss characterized by an increase in Fo and a subsequent decrease in Fv. Higher values signify greater PSII reaction center loss. All values shown are from 700 ppm CO_2 levels.

Family	3087	3088	3399	3354	OP7
Fo	261.2	461.2	671.3	575.0	495.7

Light Harvesting Pigments

Chlorophyll a decreased in 700 ppm CO_2 levels by -27.0% (Figure 7a). Carotenoids decreased by -18.5% (Figure 7b). Both good and poor growing families displayed a decrease in chlorophyll a at 700 ppm CO_2 levels.

Discussion

Our study revealed the existence of very similar physiological trends among the various tree families. Generally, enriched CO_2 concentrations enhanced photosynthesis, decreased chlorophyll fluorescence, and decreased chlorophyll. There were, however, differences within the various families (Table 3).

Table 3: Average physiological rates and levels of both poor growing families and good growing families at 700 ppm CO_2.

	Photosynthesis ($\mu mol/m^2/s$)	Fluorescence (Fv/Fm)	Fluorescence (Fo)	Chlorophyll a (g/cm^2)
Poor Growers	5.66	0.62	478.4	1148.6
Good Growers	7.06	0.62	502.5	1100.5

Apparently, positive growth responders are assimilating more carbohydrate with less chlorophyll a and less PSII reaction centers per unit area. Houpis et al. (1988) observed the same trend and concluded that the trees may undergo adaptive physiological alterations to compensate for the increase in CO_2. Previous and ongoing studies have showed that the photosynthetic apparatus can adjust within hours to new CO_2 levels, then readjust to original levels in the same amount of time (W.J. ARP 1991). Thus, we might consider the photosynthetic apparatus a buffer system which can balance the affects of atmospheric gas stress within the plant. A possible explanation for the buffer response is that the trees require less light harvesting pigmentation and PSII reaction centers because of the abundance of internal CO_2. With high ambient CO_2 concentrations there are high internal CO_2 concentrations which give the photosynthetic apparatus ample time for assimilation via sunlight harvesting. The increased Ci values induce greater carbon assimilation (S.B. IDSO 1991), thereby compensating for the lack of PSII reaction centers and chlorophyll a levels. Hence, the photosynthetic process appears to be flexible through moderation of chlorophyll and PSII reaction centers. In addition to the general physiological trends observed in high CO_2 we also noticed a wide range of intraspecific variability.

At high CO_2 good growing families assimilated carbon more efficiently than poor growing families did in 700 ppm CO_2. This trend is especially noticeable in Families 3399 and 3354 which displayed the same physiological and growth responses. The same trends are not noticeable in Family 3087 which decreased in photosynthetic rate, and expressed the lowest values of Fv/Fm and chlorophyll a despite records of positive growth response in 700 ppm CO_2. Measurements taken on 3087 in previous years have not revealed the same results. Possibly, after 2.5 years of high CO_2 exposure, trees from Family 3087 are experiencing a degeneration of their photosynthetic apparatus.

The poor performance of Families 3088 and OP7 may be explained by the hypothesis that different families of trees function intraspecifically. Betsche (1994) suggests that photosynthetic inhibition may be induced by an accumulation of large starch granules in the chloroplast. The starch may disrupt CO_2 pathways into the needle or it may contort thylakoid membranes (housing the PSII reaction centers), within the chloroplast to the point of malfunction. This could explain the large decrease in the number of PSII reaction centers (characterized by the increase in Fo at 700 ppm). Pushnik et al. (1993) suggests that photosynthetic obstacles such as starch accumulation are a result of low levels of carbon allocation enzymes which are characterized differently for different families. He relates this hypothesis to source-sink relations in *Pinus ponderosa*. He mentions that a tree with low carbon storage space tends to have less carbon transport mechanisms, because of negative feedback inhibition. The carbon transport mechanisms, such as Sucrose Phosphate Synthase, might aid in depleting starch accumulation in the chloroplast, and enabling more efficient photosynthesis. Some plants may be able to produce many transport enzymes, and some may not. Hence, the intraspecific differences in carbon transport mechanisms may be the cause of physiological differences between the good and poor growing families at 700 ppm CO_2. In a progress report of the current

CO_2 exposure experiment, Houpis et al. (1994) also discovered noticeable variation among carbon allocation enzymes between *Pinus ponderosa* families. We plan to extend this research to encompass starch and carbon allocation enzyme assays during the summer of 1995. This research was funded in part by the United States Department of Energy, the California State University at Chico, and the Lawrence Livermore National Laboratory education department.

Literature Cited

ARP W.J., Department of Ecology and Ecotoxicology (1991) Effects of source-sink relations on photosynthetic acclimation to elevated CO_2. Plant, Cell and Environment **14**: 869 - 875

Betsche, T. (1994) Atmospheric CO_2 enrichment: kinetics of chlorophyll a fluorescence and photosynthetic CO_2 uptake in individual, attached cotton leaves. Environmental and Experimental Botany **34**: 75 - 86

Greaves, J.A., Blair, B.G., Russotti, R.M., Law, E.A., Cloud, N.P. Measurement of chlorophyll fluorescence kinetics in photosynthesis research with a new portable microprocessor and computer-operated instrument. In: Cf-1000 chlorophyll fluorescence measurement system instruction manual version 2.00, pp. 43 - 62, Morgan Scientific, Inc., Andover, MA

Houpis, J.L.J., Surano, K.A., Cowles, S., Shinn, J.H. (1988) Chlorophyll and carotenoid concentrations in two varieties of *Pinus Ponderosa* subjected to long-term elevated carbon dioxide. Tree Physiology **4**: 187 - 193

IDSO S.B., U.S. Water Conservation Laboratory (1991) A General relationship between CO_2-induced increases in net photosynthesis and concomitant reductions in stomatal conductance. Environmental and Experimental Botany, **31**: 4: 381 - 383

Lichtenthaler, H.K., Hak, R., Rinderle, U. (1990) The chlorophyll fluorescence ratio F690/F730 in leaves of different chlorophyll content. Photosynthesis Research **25**: 295 - 298

Lichtenthaler, H.K. (1992) The Kautsy effect: 60 years of chlorophyll fluorescence induction kinetics. Photosynthetica **27**: 45 - 54

Pushnik, J.C., Demaree, R.S., Houpis, J.L.J., Anderson, P.D. (1993) Sink-source characteristics of two distinctly different forest species and riparian species as affected by elevated carbon dioxide and soil moisture. Submitted to: Western Regional Center for Global Environmental Change, University of California at Davis 1477 Drew Avenue, Suite 104, 95616-8756

Pushnik, J.C., Demaree, R.S., Houpis, J.L.J., Flory, W.B., Bauer, S.M., Anderson, P.D. (1995) The effect of elevated carbon dioxide on a sierra-nevadan dominant species: *Pinus Ponderosa*. In: Submittal for proceedings 88th annual meeting and exhibition air & waste management. San Antonio, TX, June 18-23, 1995

Schmidt, W., Neubauer, C., Kolbowski, J., Schreiber, U., Urbach, W. (1990) Comparison of effects of air pollutants (SO_2, O_3, NO_2) on intact leaves by measurements of

chlorophyll fluorescence and P_{700} absorbance changes. Photosynthesis Research **25**: 241 - 248

Wullschleger, S.D., Zisk, L.H., Bunce, J.A. (1994) Respiratory response of higher plants to atmospheric enrichment Plant Physiology **90**: 221 - 229

Figure 1

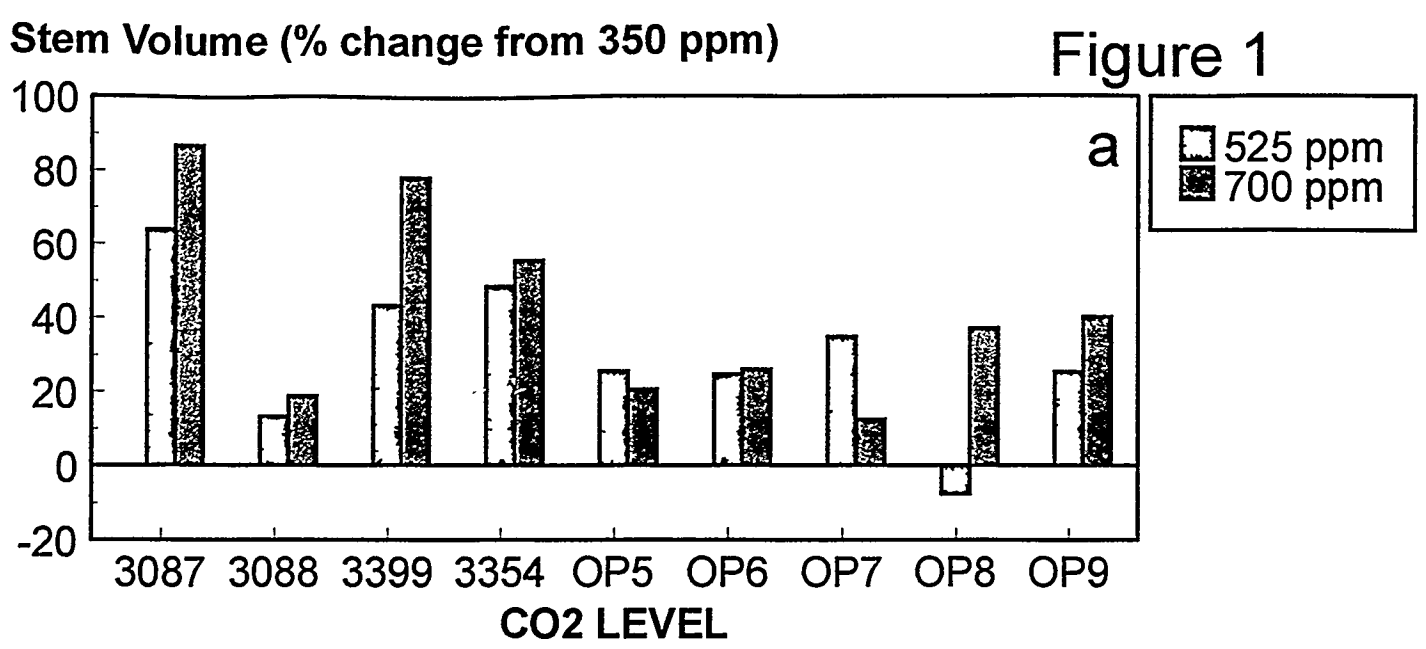
Stem Volume (% change from 350 ppm)
100
80
60
40
20
0
-20
a
525 ppm
700 ppm
3087 3088 3399 3354 OP5 OP6 OP7 OP8 OP9
CO2 LEVEL

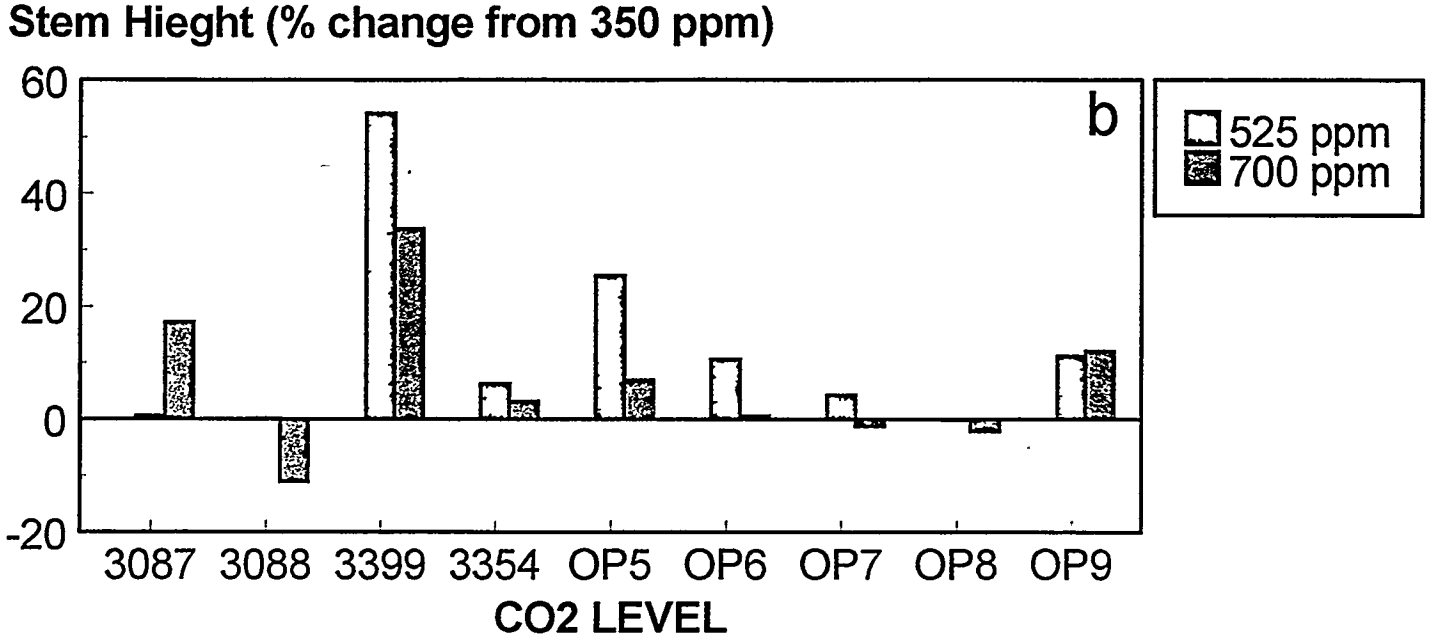
Stem Hieght (% change from 350 ppm)
60
40
20
0
-20
b
525 ppm
700 ppm
3087 3088 3399 3354 OP5 OP6 OP7 OP8 OP9
CO2 LEVEL

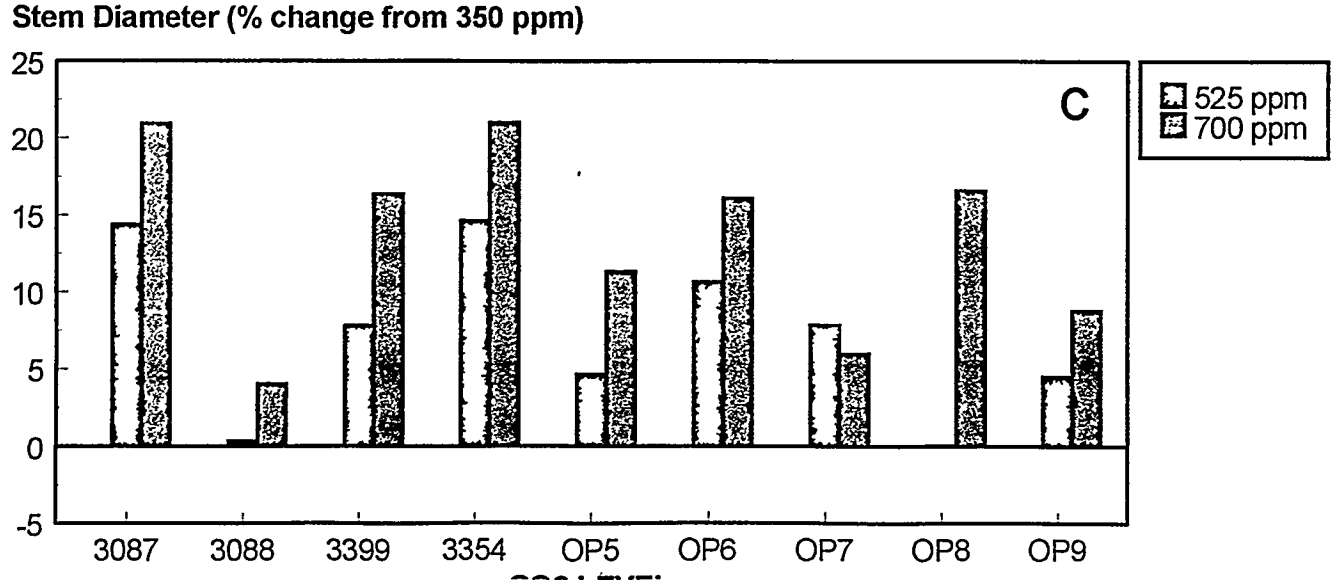
Stem Diameter (% change from 350 ppm)
25
20
15
10
5
0
-5
c
525 ppm
700 ppm
3087 3088 3399 3354 OP5 OP6 OP7 OP8 OP9

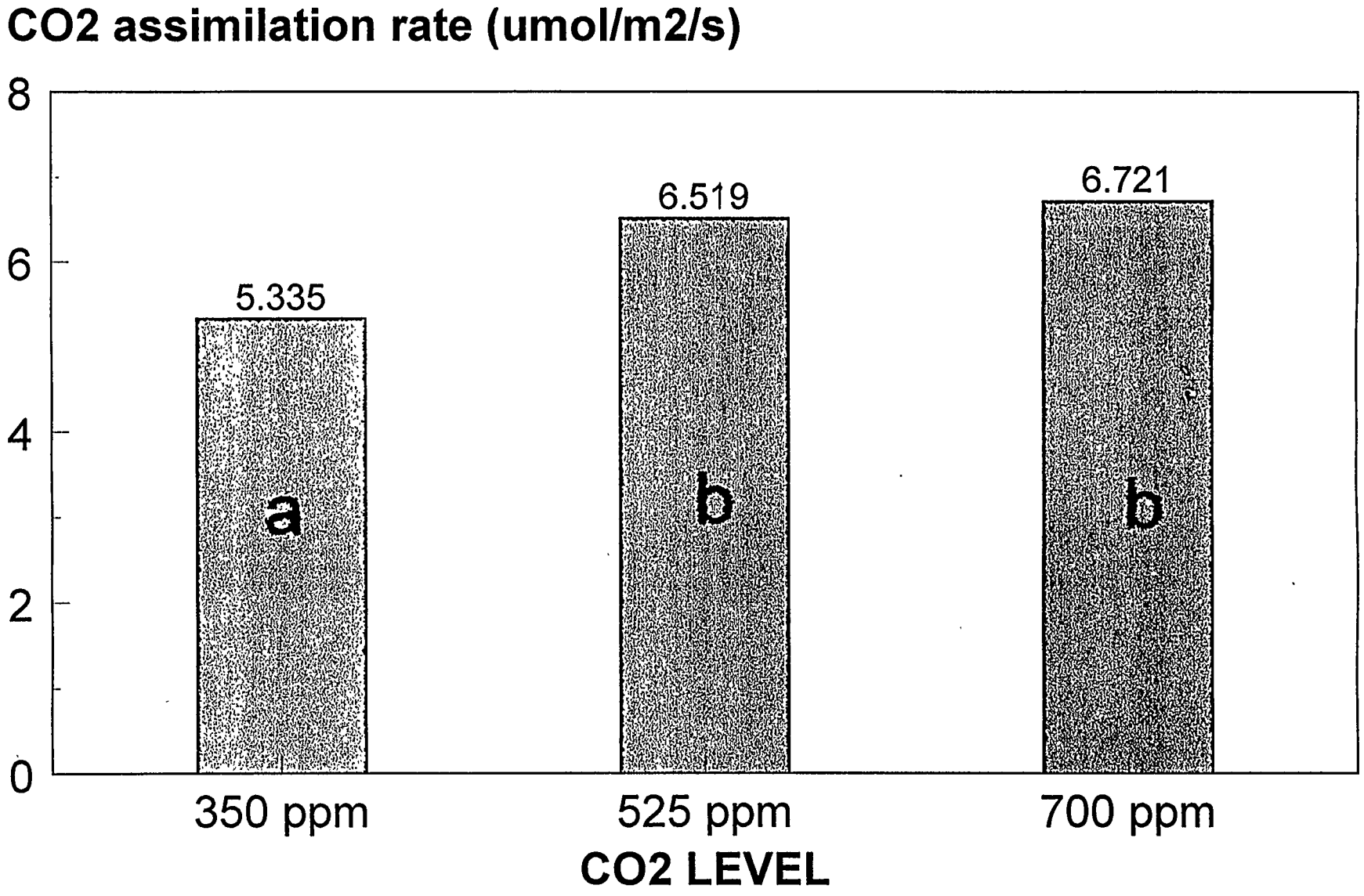

Figure 2: CO2 assimilation rates in umol/m2/s. Values with different letters are significantly different at $p<.05$.

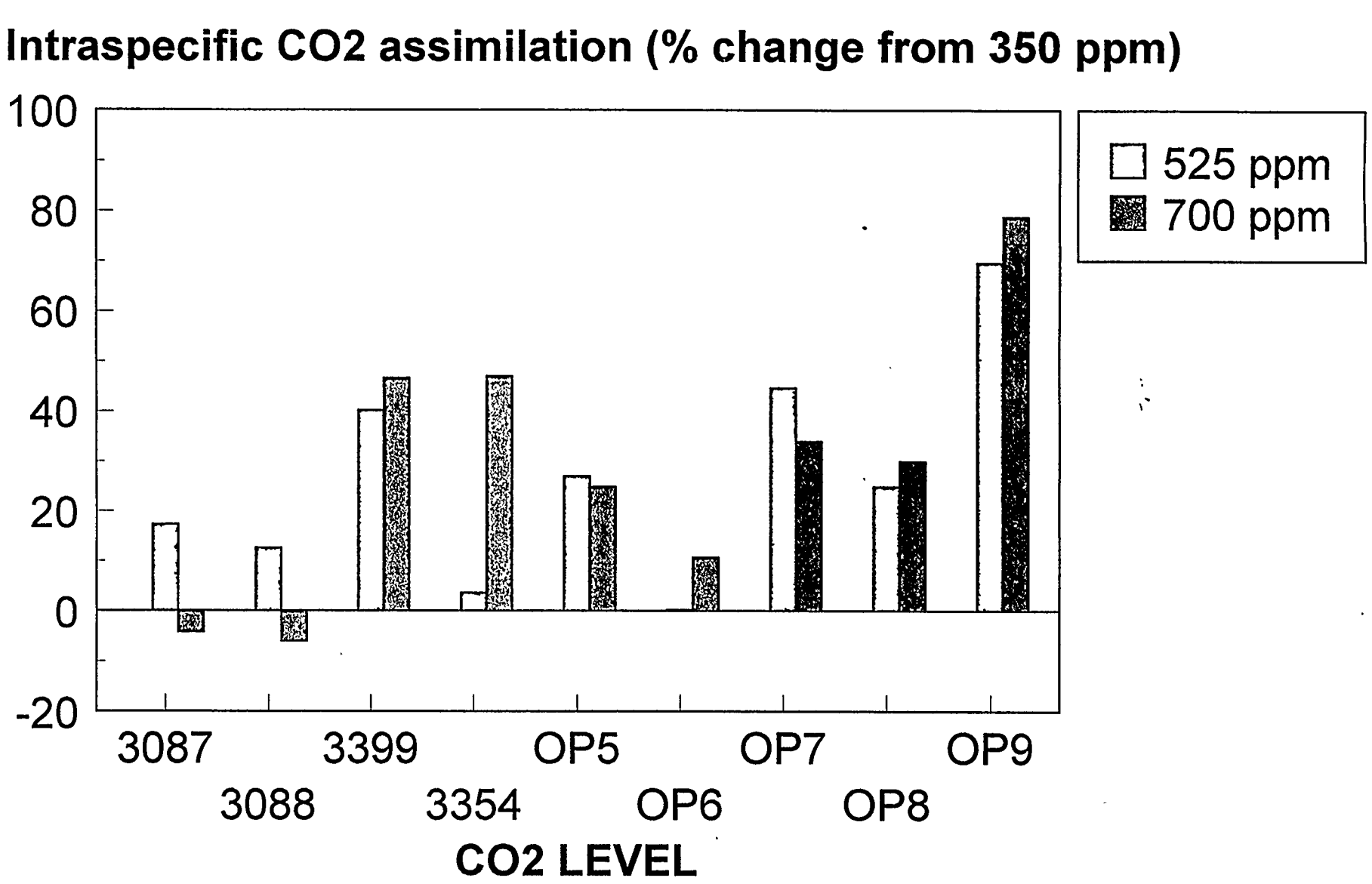

Figure 3: Intraspecific CO2 assimilation rates in % change from 350 ppm.

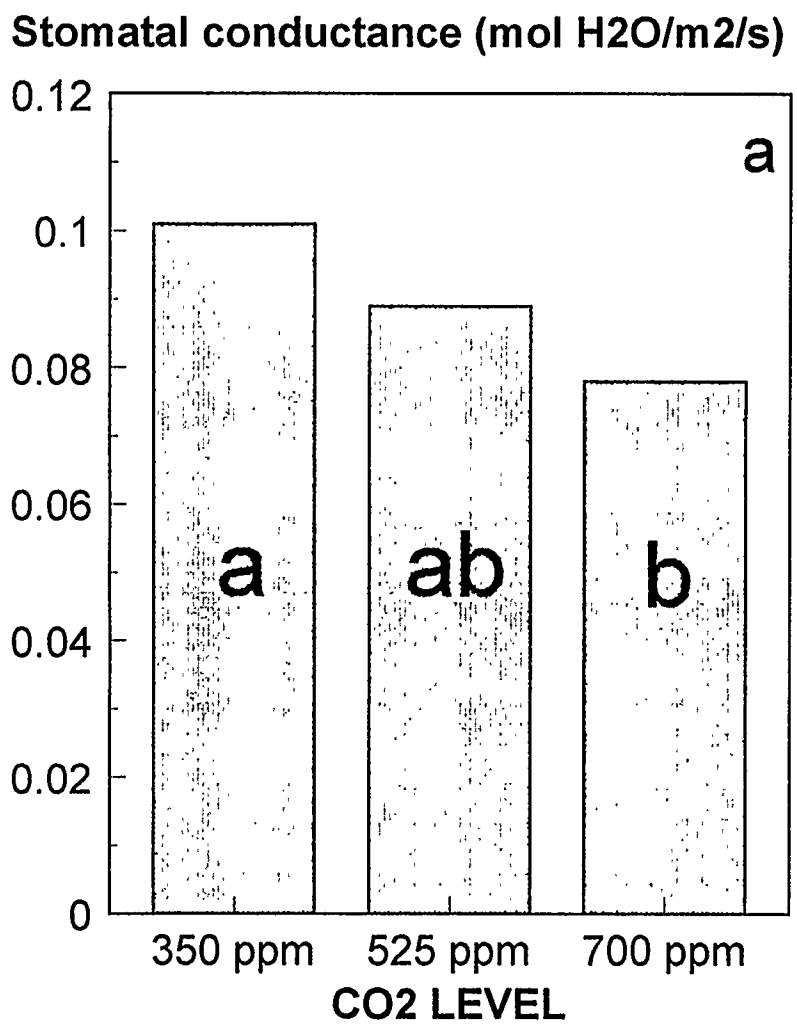

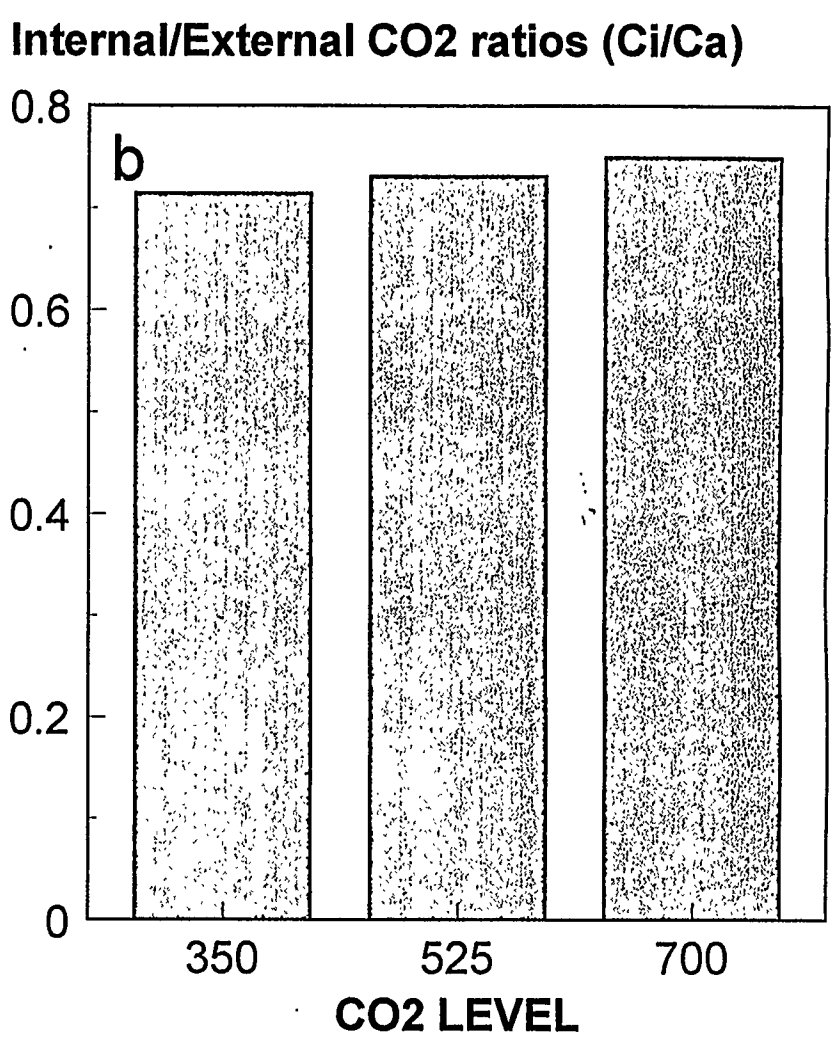

Figure 4: (a) Conductance, given in (mol H2O/m2/s). (b) Ci/Ca ratio in %. Values with different letters are statistically significant at $p < .05$.

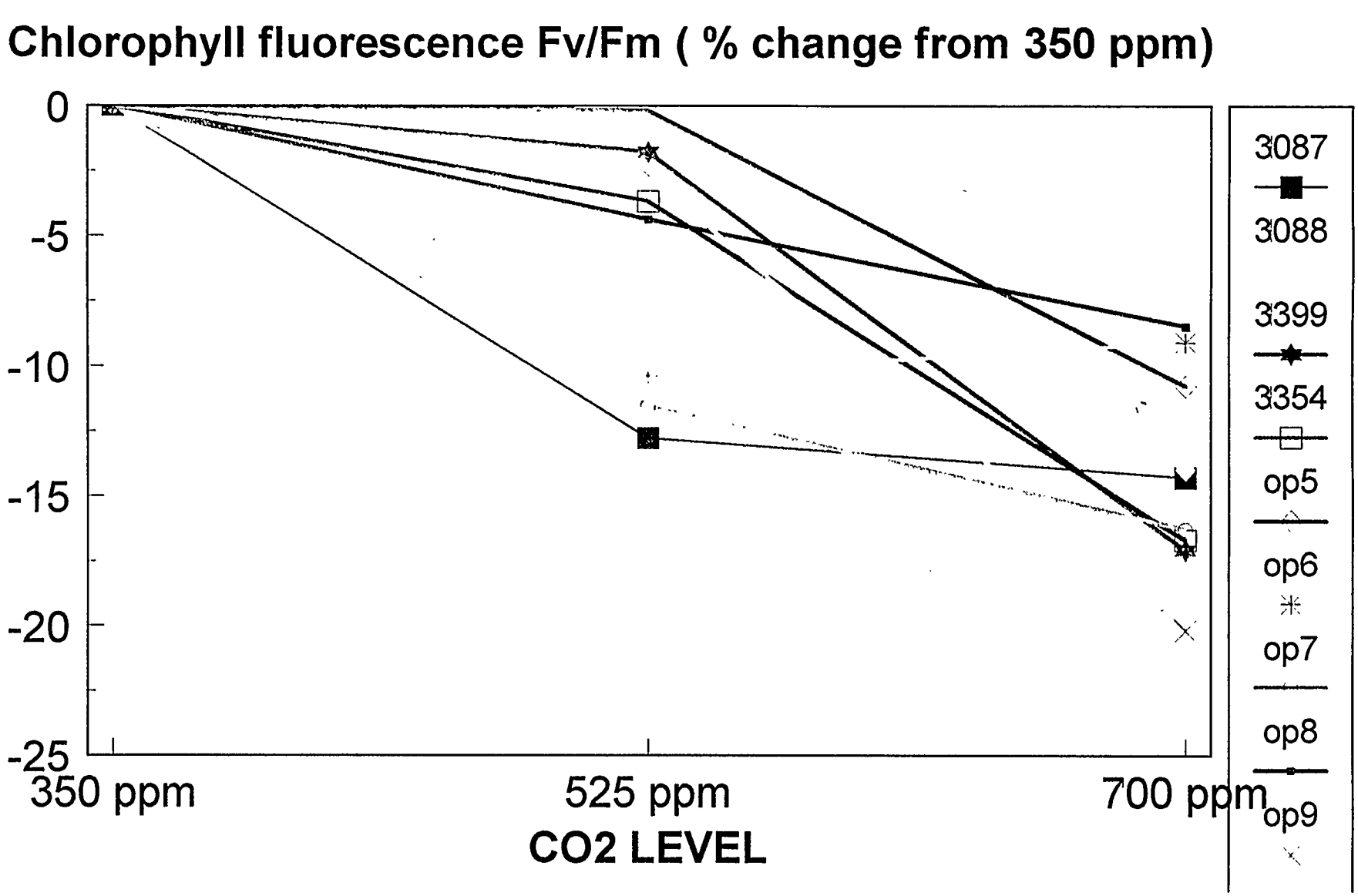

Figure 5: Photosystem II efficiency as quantified by Fv (variable fluorescence)/ Fm (maximum fluorescence).

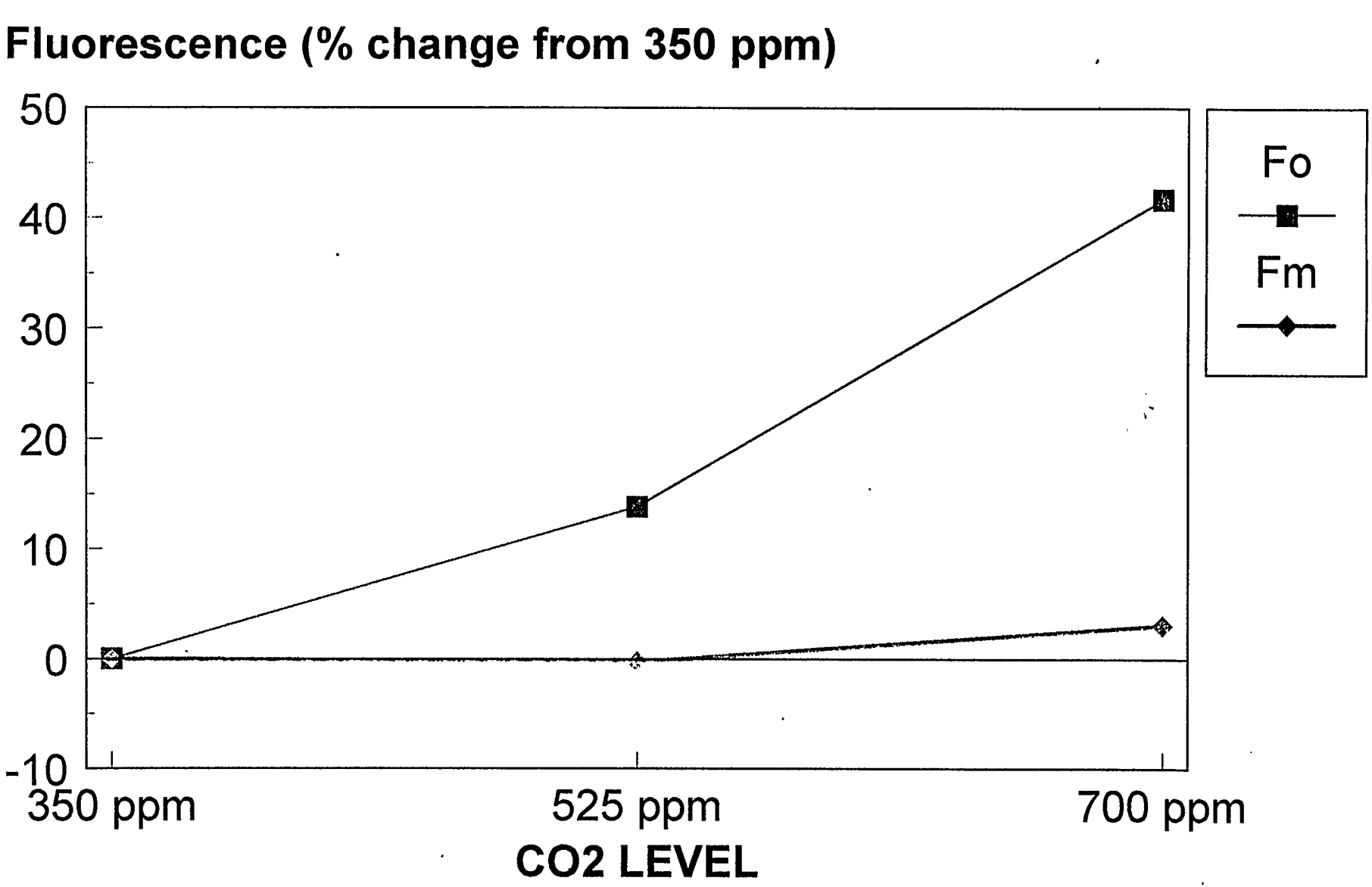

Figure 6: Line diagram depicting the relationship between base level fluorescence (Fo) and maximum fluorescence (Fm).

Figure 7

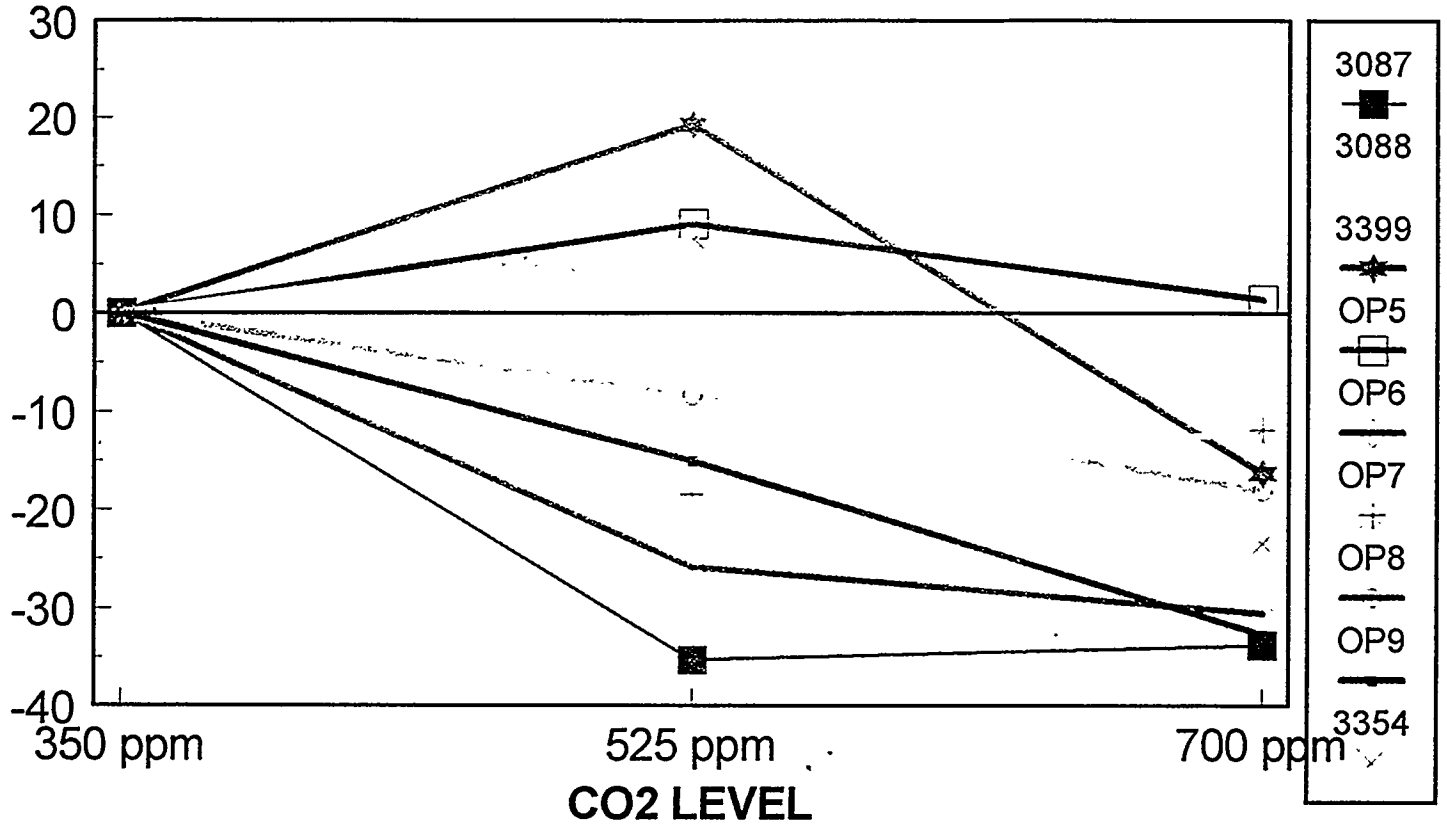
Chlorophyll a concentration (% change from 350 ppm)
30
20
10
0
-10
-20
-30
-40
350 ppm
525 ppm
700 ppm
CO2 LEVEL
3087
3088
3399
OP5
OP6
OP7
OP8
OP9
3354

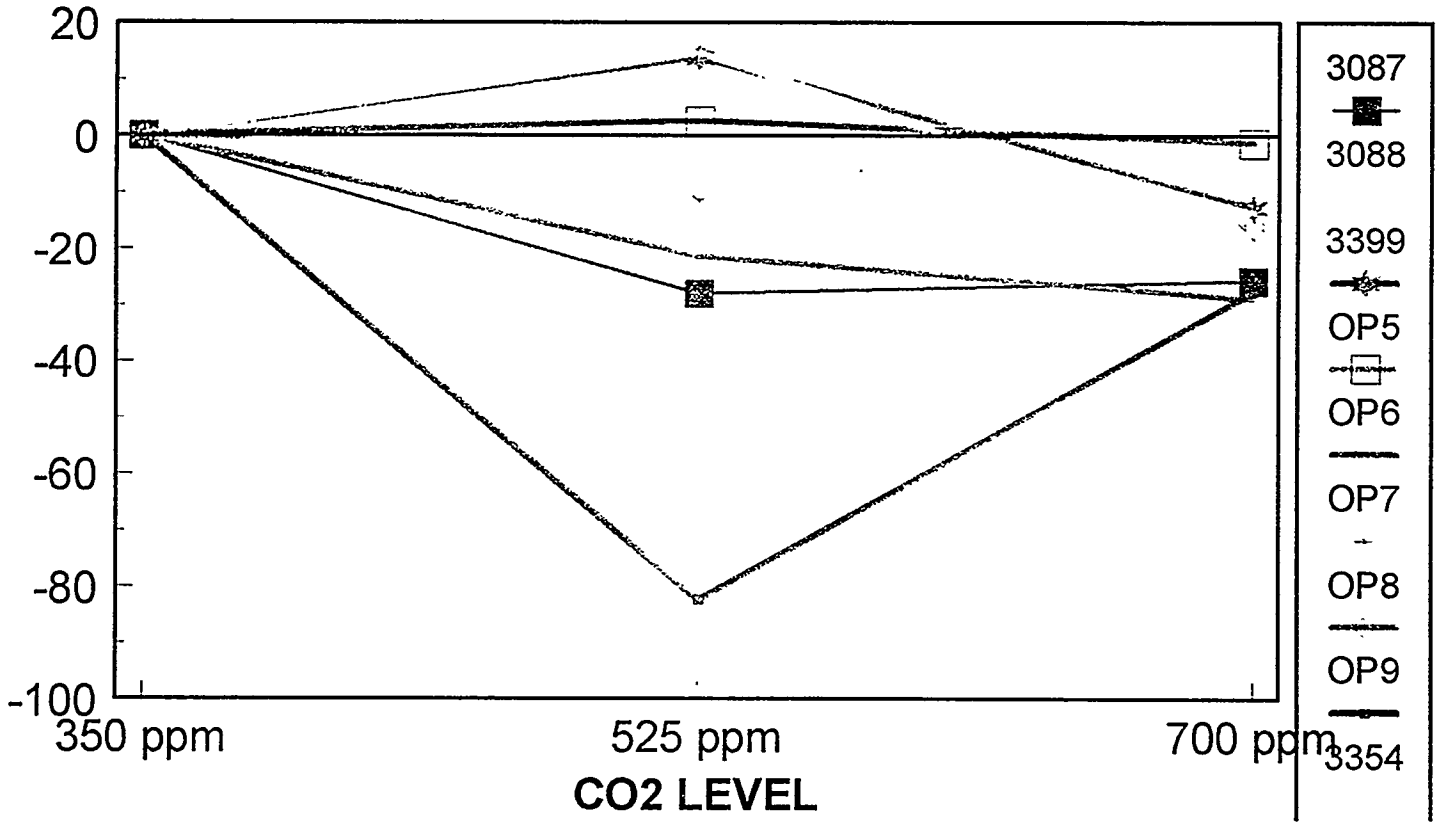
Carotenoid concentration (% change from 350 ppm)
20
0
-20
-40
-60
-80
-100
350 ppm
525 ppm
700 ppm
CO2 LEVEL
3087
3088
3399
OP5
OP6
OP7
OP8
OP9
3354

A Heterogéneous Chemistry Model for Sulfate Production in Cloud Droplet

Tao Ye

State University of New York at Stony Brook
Global Climate Research Division
Lawrence Livermore National Laboratory
Livermore, CA 94550

May 10, 1995

Prepared in partial fulfillment of the requirements of the Science and Engineering Research Semester program under the direction of research mentors Britton Chang and Joyce Penner in the Lawrence Livermore National Laboratory.

*This research was supported in part by an appointment to the US Department of Energy Science and Engineering Research Semester program administered by LLNL under Contract W-7405-Eng-48 with Lawrence Livermore National Laboratory.

A Heterogeneous Chemistry Model for Sulfate Production in Cloud Droplet

Tao Ye

State University of New York at Stony Brook
Global Climate Research Division

Abstract

A basic heterogenous chemistry model, including the main program CLOUD9.F and its supporting modules, has been developed as a tool for investigating the production of sulfate (S(VI)) in cloud droplets. The model simulates gas phase reactions, aqueous phase reactions and the mass transfer between the two phases. The mechanism is a composite of the gas phase reactions in Crutzen's model [Lelieveld and Crutzen,1991)] and the aqueous reactions in Pandis and Seinfeld's model [Pandis and Seinfeld, 1989]. It is designed to represent a small region of the atmosphere, so that it can be integrated into a more complete global model at a later stage. Sample simulations are presented and agree with published results.

Explanatory Notes

In this paper, the following type face conventions are used:

Italic -- variables in the program

bold -- subroutines in the program

underlined -- constants that are defined in the header files

Introduction

This document is a description of the code CLOUD9.F, its structure, its subroutines, its input and output files, its compilation execution.

CLOUD9.F is developed on SUN workstation under SUNOS. However it should be portable to other platforms easily since all variables are declared as double precisions in Fortran, as opposed to being specified as physical bytes.

Code History:

When we inherited this code from Sonia Kriedenweis, it was never compiled. This left us without a clue on the correctness of its two thousand lines of coding. Furthermore the structure of the program was opaque because it passed most of variables through common blocks rather than through argument lists. It had fortunately generous amounts of comments from which we could deduce the intent of each subroutine.

After some investigation, we found that this code was modeled after a smaller code built also by Sonia Kreidenweis. Since the smaller code AQCHEM.FOR contains only 11 chemical species and 11 reactions, we were able to sort out the physics in it. We were able to first compile and run the smaller code on the Cray C-90, then successfully port it to SUN workstation. This enables us to follow the code's programming logic. Given the physics and the logic, we went back to CLOUD9.F. This time we were able to debug it till it actually ran on the SUN.

We found that the the older code(CLOUD9.F) had subroutines which computed more than one physical process. The conglomeration of processes made the reading of the code and its debugging difficult. In the process of reengineering the code, we first made it more modular by breaking up the larger subroutines into smaller ones, which represent single physical transformations. Further, we rearranged the calling sequence of the subroutines to truly mimic the processing sequence of gases by cloud droplets. We also made the code more readable by changing the indices of variable arrays from numerical numbers to the names of the chemical species. For example, the species concentration ya[1], ya[2]... in the old code are changed to ya[O3], ya[O] for the obvious purpose. After a lot of typos were corrected, all the chemical rates were checked, now we have confident that the new CLOUD9.F truly represents the chemical mechanism that combines Crutzen [Lelieveld and Crutzen, 1991] and Seifeld [Pandis and Seifeld, 1989]'s models.

Physics and Chemistry Background

In the past, the complexity of heterogeneous chemistry system, as well as the lack of computing power have limited climate models to the study of only gas phase chemistry. However many

chemicals of great importance to the climate are produced mainly by aqueous phase reactions. For example, the sulfuric acid found in acid rain is produced not by gas phase reactions but is produced primarily in situ of the water droplets of clouds [Calvert et. al., 19853]. Furthermore clouds can significantly reduce the oxidation efficiency of the troposphere by depleting the oxidants from the gas phase [Lelieveld and Crutzen, 1991]. The computational limitations of yesteryear's computers can be overcome by present day super computers. The new computers will help us push back the frontier in atmospheric research by enabling us to incorporate the chemistry of aqueous reactions into our current models.

In order to develop a building block for a climate model, we start with a zero dimensional model which describes the reactions that can occur simultaneously in two phases of matter. The material states are characterized by physical parameters. The liquid state is characterized by the liquid water content, droplet size, and temperature. The gaseous state is characterized by the pressure. The liquid and gaseous states are assumed to be in thermal equilibrium. Gaseous species are inputted in ppbv and liquid species are inputted in Mole/liter.

The mechanism used in CLOUD9.F consists of 30 gaseous species, 31 aqueous species, 37 gas phase reactions [Lelieveld and Crutzen, 1991] and 73 aqueous phase reactions [Pandis and Seifeld, 1989]. The reactions are listed in the program.

Program Description

Files needed:

The package CLOUD9 consist of the following files:

- cloud9.f:

  Main program.

- dropcl.for:

  A header file that consists of description of common blocks and some major constants like number of species(ngas & naqgrp), number of equations(neqn), etc.

- assignment.for:

  A header file that defines an integer constant for each species' name . The names are used in the main program to index the species concentration(*ya*) and derivative(*yderiv*).

- aqinp:

  The input file that consists of all the initial concentration of species, the important parameters like liquid water content(*lw*), droplet radius(*rad*) and the information on how the simulation should be run(*iters, xstep*). A more detailed description of how to construct aqinp can be found in the 'How to construct the input file' section.

- dvode.o:

  The object file for dvode.f, the differential equation solver. Right now it is placed in my library directory. For the future use, the user needs to modify the makefile to specify his/her library directory that dvode.o is put in. As an alternative, dvode.f can also be one compiling object in

the makefile instead of being a part of the library. Called by main program.

- rtflsp.f:

  A numerical rootfinder to compute the pH value in subroutine **electro_neut**. Called by main program.

- makefile:

  To make compilation process easier.

Upon every simulation run, the program will generate three output files:

- aqout.inp:

  Mainly a confirmation output file for all the initial input data. It also contains the rate constants and their corresponding gas phase reactions. It specifies the format of the data in aqout.gas and aqout.aq.

- aqout.gas:

  A plain ASCII data output file containing all ***gas phase*** species concentration during the simulation. The concentrations are printed out at the end of each call to dvode, this makes up one row of the file. The file will be read in column major fashion by gtx. The first column is the time, the second is the pH value, after that are all the concentrations.

- aqout.aq:

  A plain ASCII data output file containing all ***aqueous phase*** species concentration during the simulation. It's in the same format as aqout.gas.

To compile and execute:

After modifying the library directory where dvode.o is located, type 'make' to compile the programs. The output executable will be 'cloud'. Type 'cloud' to run the program.

Main Program Structure

The main program CLOUD9.F consists of three major parts:

1. Read input[**rdinput, xmolcon, wrtoutput**]. **[rdinput]** Read in all initial concentrations of both gas phase and aqueous phase species. They are put in array *ya* with dimension *nspec*, which is a constant defined in dropcl.for. The unit of gas phase species initial concentration is ppb. **[xmolcon]** We therefore convert them to mol/L, the same as aqueous phase concentration unit. **[wrtoutput]** Then we write out the input for confirmation.

2. Set up coefficients for mass transfer **[accoeff, xkmcoef]. [accoeff]** The accommodation coefficient *eta[i]* is calculated first. It is then used in **[xkmcoef** for the calculation of *xkmt[i]*, which is the combined rate coefficient for gas phase plus interfacial mass transport. The mathematical description of the mass transfer is equation (2) and (3) in [Pandis and Seinfeld, 1989]. *xkmt[i]* will be used later on in subroutine **mass_tran** to set up mass balance differential equations.

3. **dvode** is called to evolve the species concentrations over a time period. **diffun** is called by dvode to give the derivative of each species at each step.

diffun first calls **electneut_ungroup** to ungroup the grouped aqueous species based on the electroneutrality in liquid. Then it calls **henry** to calculate the effective Henry's Law coefficient using the *xkmt* computed at the last phase of the program.

Now everything is ready, **diffun** then calls **aq_source, gas_source** and **mass_tran** subroutines to compute the production and reduction of every species from aqueous reaction(*da*), gas phase reaction (*dg*) and the mass transfer between them(*dy_mt*). Each of these subroutines will call the corresponding subroutine for reaction rate. For example, **aq_source** calls **aq_rate** to get the reaction rate, **aq_rate** calls **aq_rate_con** to get the rate constant.

The total derivative of gaseous species *yderiv* is the sum of *dg* and *dy_mt*. Similarly, the total derivative of aqueous phase species is the sum of *da* and *dy_mt*.

Flow Chart:

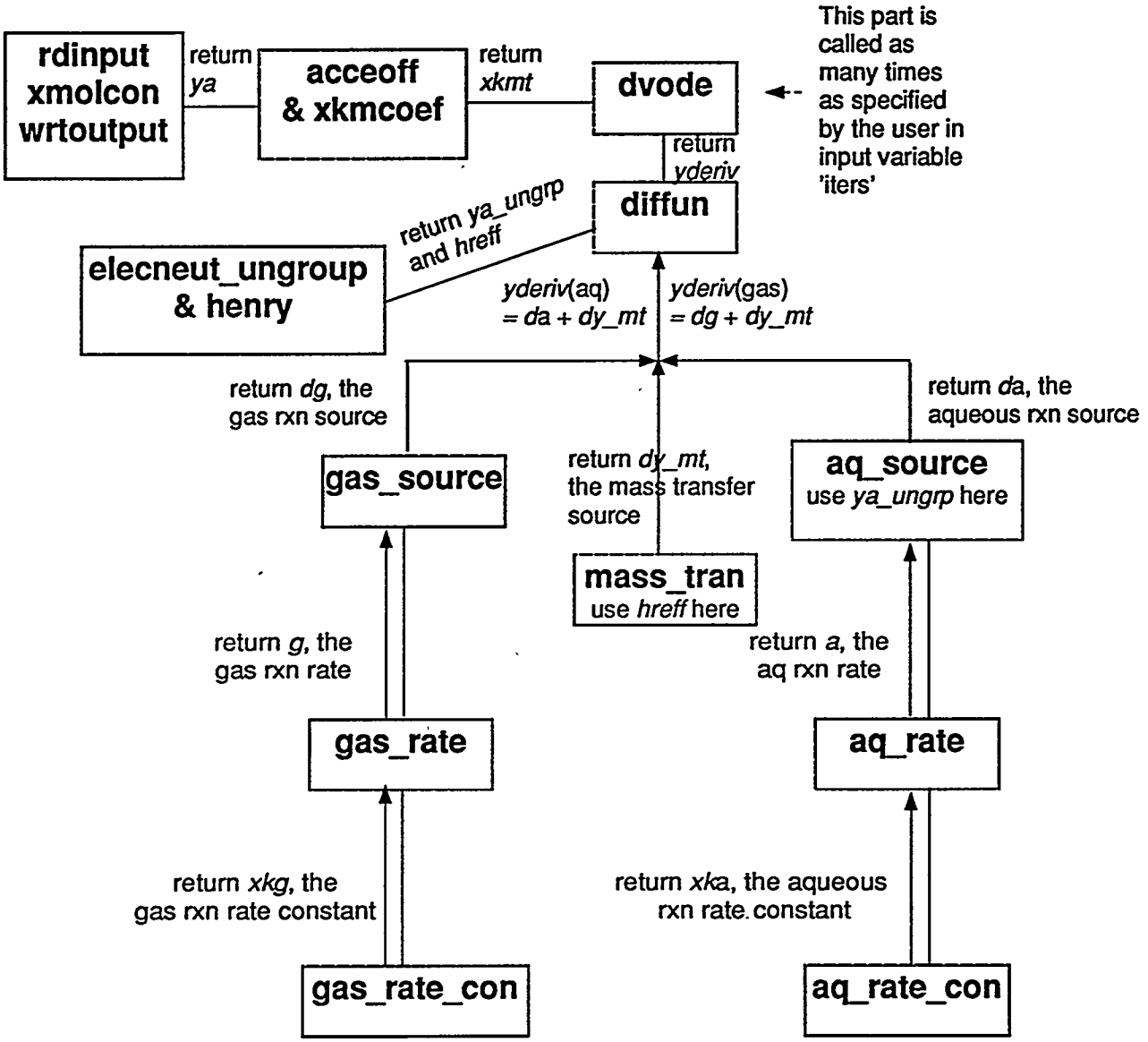

How to construct the input file:

Sample input file is attached in appendix 1. Comments concerning the specific simulation can be included by beginning a line with "c". Species are identified by numbers at the beginning of the file.

The data in input file consists of basically two parts:

1. Initial species concentrations. They will be read in an array *ya* with dimension neqn. neqn is fixed in header file dropcl.for.

There are 30 gas phase species (in ppbv) and 30 aqueous phase species(in mol/L). All concentrations start with y<number1-7> at the beginning of the line.

Lines start with y1-y4 are gas phase species concentrations.

Lines start with y5-y8 are aqueous phase species concentrations.

2. Parameters needed in the simulation. These parameters are global variables which are passed in common blocks as declared in dropcl.for. *aqueous, gas* and *coupling* are flags used in test runs to create results for pure gas phase or pure aqueous phase scenarios.

Visualize species evolution with time from output files:

Gtx is used to graph the results. Contact Tom Kuczmarski in GCR about gtx. The procedures are:

1. Open 'newgtx' on GCR Division's UNIX network.
2. In the command window, type:
   (1) Define a 2-D array to hold the data:
   <2-D variable name> = readascii('<filename>')
   (2) Define x values, the time:
   x = reform(<2-D variable name> (0,*))
   (3) Define individual species:
   <specie name 1> = reform(<2-D variable name> (<index number>,*))
   Change the Dim 1 Coord Variable field in the pop-up window for this variable to <x>
   (4) Define more species of interest as described in (3)
   ...

The file to read can be either aqout.aq or aqout.gas. These output files have a four line special header at the beginning of the file for gtx to recognize the format of the following data. There is one number in each line:

2	--- column major
2	--- Two dimensions
<number of columns>	--- 32 for aqout.gas and 33 for aqout.aq
<number of rows>	--- *iters* (var read from input file) + 1

3. After defining all species according to their index in *ya*, click on 'Plot Control' in variable pop-up window, then click on 'plot' in plot control window.

References

Calvert, J.G., Lazrus, A., Kok, G.L., Heikes, B.G., Walega, J.G., Lind, J. and Cantrell, C.A., 1985, Chemical mechanisms of acid generation in the troposphere, *Nature* **317**, 27-35.

Lelieveld, J. and P.J. Crutzen (1990) Influences of cloud photochemical processes on tropospheric ozone. *Nature*, **343**, 227-233

Lelieveld, J. and P.J. Crutzen (1991) The role of clouds in tropospheric photochemistry. *J. Atmos. Chem.*, **12**, 229-267.

Pandis, S.N. and J.H. Seinfeld (1989) Sensitivity analysis of a chemical mechanism for aqueous-phase atmospheric chemistry. *J. Geophys. Res.*, **94** (D1), 1105-1126.

Appendix 1

Sample Input File AQINP

```
c EXAMPLE AQINP INPUT FILE FOR CLOUD9.FOR
c
c Example No. 1 with just gas phase rate constants
c The ordering of the input is as follows:
c
c *** Initial Gas Phase Concentrations: ya's (PPB)
c  1 o3   2 o1d   3 o2   4 o   5 no2   6 no  7 h2o2  8 oh
c  9 hcho 10 ho2   11 co   12 h2   13 ch3ooh 14 no3   15 hno3  16 n2o5
c 17 xm   18 h2o   19 ch4  20 ch3o2 21 co2   22 hco2h 23 so2   24 h2so4
c 25 hno2 26 ch3no2 27 hcl  28 nh3   29 ch3oh  30 ch3coh
c **** Initial Aqueous Phase Concentrations: ya's (mol/L)
c 31 niii 32 nv    33 civ  34 h2o2t 35 hchot  36 hcooht 37 hclt 38 ho2t
c 39 nh4t 40 clt   41 chso3t 42 siv  43 svi    44 so5t   45 oha  46 o3a
c 47 o2a  48 h2oa  49 ohm  50 co3m  51 dummyh  52 no2a   53 no3a 54 ch3no2a
c 55 prod 56 ch3o2a 57 ch3ooha 58 ch3oha 59 ch3coha 60 noa  61 clohm


c  fe3p   mn2p   h2ol

c ____________________________________________________________________
c
c ya, initial value ordering:
c
c    1     2     3     4     5     6     7     8
c    9     10    11    12    13    14    15    16
c    17    18    19    20    21    22    23    24
c    25    26    27    28    29    30
c    31    32          33          34          35          36          37          3-
8
c    3940          41          42          43          44          45          4-
6
c    4748          49          50          51          52          53          5-
4
c    5556          57          58          59          60          61

c ---------------------------------------------------------------------
y1 1.50e+1 1.0e-30 0.19e+9 1.0e-06  0.70e-2 1.000e-4 0.60e0 3.39e-5
y2 0.200e0 6.50e-3 5.00e+1 1.0e-30  0.750e0 4.000e-6 0.55e0 1.0e-30
y3 1.0e+09 1.0e-30 1.0e-30 0.02000  340.e+3 0.0070e0 0.98e0 1.0e-30
```

```
y4 4.00e-4 0.600e0 0.500e0 0.600e0  0.800e0 1.000e-4
y5 0.00000 2.00e-6 11.9e-6 0.00000  0.00000 0.000000 8.0e-6 0.00000
y6 2.00e-6 0.00000 0.00000 0.00000  8.00e-6 0.000000 0.0000 0.00000
y7 0.00000 0.00000 6.78e-10 0.00000  14.7e-6 0.00000  0.0000 0.00000
y8 0.00000 0.00000 0.00000 0.00000  0.00000 0.00000  0.0000
ch 4.00e-7 2.00e-7 8.00e-6
```

```
c
c
c *** Temperature(degrees Kelvin)
c
temp    285.
c
c *** Cloud Water Content (L water/L air)
c
wl      4.e-7
c
c *** Cloud Droplet Radius (cm)
c
rad     10.e-4
c
c *** Mean Free Air Path (cm)
c
xmfp    0.065e-4
c
c *** Species Diffusivity (cm/s) Assumed constant for all species.
c
diff    0.1
c
c *** Ideal Gas Constant (L atm/mol K)
c
c gasc    0.082058  it's a parameter now, in dropcl.for
c
c *** Pressure (atmospheres)
c
pres    1.0
c
c *** Initial Time for start of problem (sec)
```

```
c
xo      0.0
c
c *** Time step (sec)
c
xstep   900.00
c
c *** Number of Iterations for total problem
c
iters   97
c
c *** Flags for gas,aqueous phase calculation and the coupling.
c *** 0 for off, 1 for on
c
gas     1
aque    1
coup    1
end
```